Magnetic Resonance Imaging of synovitis without the use of intravenous gadolinium

Carole Burnett

Submitted in accordance with the requirements for the degree of
Doctor of Philosophy

The University of Leeds

School of Medicine

July 2015

Intellectual Property and Publication Statements

The candidate confirms that the work submitted is her own and that appropriate credit has been given where reference has been made to the work of others.

This copy has been supplied on the understanding that it is copyright material and that no quotation from the thesis may be published without proper acknowledgement.

All images included in this thesis have been produced by Carole Burnett except those given reference to (Figure 2-8, Figure 2-10, Figure 2-13, Figure 4-8 and Figure 4-9).

The right of Carole Burnett to be identified as Author of this work has been asserted by her in accordance with the Copyright, Designs and Patents Act 1988.

Acknowledgements

There are many people that I would like to thank for their help and support given to me during this thesis. Firstly I would like to thank my supervisors, Dr Anne-Maree Keenan, Professor Anthony Redmond, Dr John Ridgway and Dr Richard Hodgson. Without their continued support I would not have completed this journey.

My sincerest thanks go to Professor Philip Conaghan, Mr Ramakrishnan Venkatesh, Stephen Draycott, Dr Andrew Barr and Dr Raja Bin Raja Mohammed without whom I would not have recruited patients for the COSMOS study. Their patience and support is greatly acknowledged.

During this process I have been very lucky to work with medical physicists that have helped me obtain a greater understanding of the complex phenomenon that is MRI. Thank you to Dr Peter Wright, Dr Steven Tanner and Dr John Biglands for all of your help and allowing a radiographer to gain a small insight into the world of medical physics. Dr Philip O'Connor and Dr Andrew Grainger provided invaluable radiological support for this project and for which I am very grateful. I cannot thank Rob Evans, Jacqueline Dunkerley and Anna Rathbone enough for their radiographic support through this process. The complexities of information technology were made simpler thanks to the work of Ged Connolly-Thompson. Thank you to all the staff of the LMBRU and Chapel Allerton Hospital for your kind support. Thank you Mr Ramakrishnan Venkatesh and Laura Horton for three of the images used in Chapter 2. I would like to say a big thank you to Dr Heidi Siddle and Robbie for keeping me sane and on the straight and narrow (a difficult task, I know). Thank you to Dr Faye Barnett for proof reading my work. I am forever in the debt of the patients of Chapel Allerton Hospital who gave up their time to participate in the COSMOS study. Funding was provided by the National Institute of Health Research to undertake a PhD under the clinical academic training programme (CAT CDRF 1-005.)

I would like to thank my Mum and Dad for being there and having faith in me. And finally thank you to my husband, Michael, for his unending patience and support. I could not have done this without you.

=^..^= =^..^= =^..^=

List of presentations arising from this thesis

Oral presentations

Burnett, **C.** Grainger, A.J, Redmond, A.C and Hodgson R.J. Magnetisation Transfer Contrast Imaging of Synovitis. NIHR BRC/BRU training camp. June 2011

Burnett, **C.** The use of multi-parametric non contrast MRI to identify synovitis in patients with osteoarthritis of the knee. NIHR Mentor meeting. Leeds, United Kingdom. January 2014.

Burnett, C, Redmond, A.C, Keenan, A.M, Grainger, A.J, Ridgway, J.P and Hodgson R.J. The use of multi-parametric non contrast MRI to identify synovitis in patients with osteoarthritis of the knee. NIHR BRU trainee's event. Manchester, United Kingdom. September 2014.

Poster presentations

C.Burnett, Grainger, A.J, Redmond, A.C and Hodgson R.J. Magnetisation Transfer Contrast Imaging of Synovitis. International Society of Magnetic Resonance Medicine, Montreal. May 2011.

C.Burnett, Grainger, A.J, Redmond, A.C and Hodgson R.J. Magnetisation Transfer Contrast Imaging of Synovitis. European League Against Rheumatism. London. United Kingdom. June 2012.

C.Burnett, Grainger, A.J, Redmond, A.C and Hodgson R.J. Magnetisation Transfer Contrast Imaging of Synovitis. NIHR annual training meeting. Leeds. United Kingdom. September 2012.

C.Burnett. The use of multi-parametric non contrast MRI to identify synovitis in patients with osteoarthritis of the knee. NIHR Mentor meeting. Leeds, United Kingdom. January 2014

Burnett, C, Redmond, A.C, Keenan, A.M, Grainger, A.J, Ridgway, J.P and Hodgson R.J. The use of multi-parametric non contrast MRI to identify synovitis in patients with osteoarthritis of the knee. European Society of Skeletal Radiology, Rija, Latvia. 2014.

Burnett, C, Redmond, A.C, Keenan, A.M, Grainger, A.J, Ridgway, J.P and Hodgson R.J. The use of multi-parametric non contrast MRI to identify synovitis in patients with osteoarthritis of the knee. European League Against Rheumatism, Rome, Italy. 2014.

Burnett, C, Redmond, A.C, Keenan, A.M, Grainger, A.J, Ridgway, J.P and Hodgson R.J. The use of multi-parametric non contrast MRI to identify synovitis in patients with osteoarthritis of the knee. International Society of Skeletal Radiology, Edinburgh, Scotland. 2014.

Abstract

Synovitis is an important feature in arthritis and is commonly visualised using contrast enhanced magnetic resonance imaging (MRI). Currently, the reference standard for assessing synovitis is gadolinium enhanced MRI which requires an intravenous injection and carries significant potential risks such as nephrogenic systemic fibrosis. Removing the necessity for using gadolinium will reduce these risks and result in greater patient acceptance of MRI investigation of synovitis.

The aims of this thesis were to investigate the use of MRI imaging sequences and include them in a novel non-contrast MRI protocol, The COSMOS protocol (contrast-obviated MRI scanning of synovitis) to identify synovitis in the knees of patients with osteoarthritis.

Potential sequences, both qualitative and quantitative, that could be included in the COSMOS protocol were identified initially through (i) a comprehensive review of the literature and (ii) review of historic images within a large research centre. The sequences were then trialled, optimised and then assessed on a large cohort of patients with knee osteoarthritis in order to determine the protocol's suitability to identify synovitis without contrast.

The results of the new COSMOS protocol show that it is feasible and practical to delineate synovitis in the knee using MRI without the use of intravenous gadolinium contrast. The characteristics of the tissues within the knee can be measured using magnetisation transfer ratio and T1 values to provide empirical differentiation of structures. The identification of a distinct range in T1 values for synovitis provided data that was exploited to produce a further inversion recovery sequence that was optimised to supress synovitis in patients with knee osteoarthritis (OA).

While further work is required to validate the COSMOS protocol, this thesis has demonstrated that it is possible to image synovitis without intravenous gadolinium contrast agents in a cohort of patients with a clinical diagnosis of OA knee.

Contents

List of Tables

List of Figures

List of Equations

List of Abbreviations

2D ……. 2 dimensional
3D ……. 3 dimensional
ACL ….. Anterior cruciate ligament
ACR ….. American College of Rheumatologists
ADC ……. Apparent diffusion coefficient
B_1 …..RF field
B_0 …..Main magnetic field
BLOKS …… Boston Leeds OA knee score
BML …… Bone marrow lesion
BOLD imaging….. Blood oxygen level dependent imaging
C …… Celsius
CE-MRI…… Contrast enhanced MRI
CI …… Confidence interval
CSF …… Cerebrospinal fluid
COSMOS ….. Contrast obviated MR scanning of synovitis
CT ….. Computerised tomography
DALY's …… Daily adjusted life years
DESS…… Dual echo steady state
DICOM ….. Digital imaging and communication
DMARD ….. Disease modifying anti-rheumatic drugs
DNA …… Deoxyribonucleic acid
DTA ……. Diffusion tensor anisotropy
DTI …… Diffusion tensor imaging
DWI …… Diffusion weighted imaging
eGFR …… Estimated glomerular filtration rate
ETL …… Echo train length
FA ….. Flip angle
FDG ….. 18F- fluoro-deoxy-D-glucose
FID….. Free induction decay
FIESTA….. Fast imaging employing steady-state acquisition
FISP ….. Fast imaging with steady precession
FLASH ..... Fast Low Angle Shot
FLAIR….. Fluid attenuated inversion recovery

fs …… fat saturation
GAGs …… Glycosaminoglycans
GBCA ……. Gadolinium based contrast agent
GBCAs …… Gadolinium based contrast agents
GE ….. Gradient Echo
HFP …… Hoffa's fat pad
Hz …… Hertz
IACON …… Inflammatory arthritis disease continuum study
ICC ……. Intra-class correlation
IEC ….. Commission Electrotechnique Internationale
IR ……. Inversion recovery
IV ……. Intravenous
JPEG….. Joint Photographic Experts Group
KL …… Kellgren and Lawrence
KOSS …… Knee OA scoring system
LMBRU ……Leeds Musculoskeletal Biomedical Research Unit
M….. Net magnetisation
M_0 …… Net magnetisation at equilibrium
M_{xy} ….. Transverse magnetisation
M_z …… Longitudinal magnetisation
MCP…… Metacarpo-phalangeal joints
MEDIC ……Multiple-echo data image combination
mm …… millimetre
MOAKS ……. MRI OA knee score
MRI ……Magnetic Resonance Imaging
ms….. millisecond
MT …… Magnetisation transfer
mT/m …..millitesla per metre
MTR …… Magnetic transfer ratio
NC-MRI ……Non contrast MRI
NHS ….. National Health Service
NICE …… National Institute for Health and Care Excellence
NIHR….. National Institute of Health Research
N_p …… Phase encoding steps
NSA ……. Number of signal averages
NSAIDs….. Nonsteroidal Anti-inflammatories Drugs

NSF ……Nephrogenic Systemic Fibrosis
OA ……Osteoarthritis
PA …… Popliteal artery
PACS ……Picture archiving and communications system
PAT ……. Patella
PCL ….. Posterior cruciate ligament
PD ……. Proton density
PET …… Positron emission tomography
QM …… Quadriceps muscle
QT …… Quadriceps tendon
RA …… Rheumatoid arthritis
RAMRIS ……RA MRI scoring system
REC ….. Research ethics committee
RF….. Radio frequency
ROI …… Region of interest
RS-EPI …… Readout segmented EPI
SAR …… Specific absorption rate
SD …… Standard deviation
SEE …… Standard error of estimate
SEM ….. Standard error measurement
SF ….. Synovial fluid
SNR …… Signal to noise ratio
SPAIR …… Spectral adiabatic inversion recovery
SPECT ….. Single positron emission computerised tomography
SPGR ……. Spoiled gradient recall echo
SPP …… Suprapatellar pouch
SPSS …… Statistical package for the social sciences
SS-EPI …… Single shot echo planar imaging
STIR ……Short Tau Inversion Recovery
T2w fs …… T2 weighted fat saturation
T …..Tesla
t …..Time
^{99m}Tc …… metastable Technetium
TE ….. Time to echo
TI ….. Inversion time
TIB …… Tibia

TOF ……. Time of flight
TR …..Repetition time
TSE ….. Turbo spin echo
UK ….. United Kingdom
US ….. Ultrasound
VIBE….. Volume Interpolated Breath-hold Examination
ω_0 ……. Larmor frequency
WIP ….. Works in progress
Wkg^{-1} …… watts per kilogramme
WORMS …… Whole organ magnetic resonance imaging scores
γ …… gyromagnetic ratio
z…... Main magnetic axis

Chapter 1 Introduction

1.1 Overview

Osteoarthritis (OA) is the commonest form of arthritis affecting over 8.5 million people in the United Kingdom (UK) [1] and an estimated 17 million people are expected to be living with OA by 2030 [2] . As many as 36 million working days are thought to be lost in the United Kingdom each year, costing an estimated £3.2 million [3, 4].

Knee osteoarthritis is particularly prevalent: Arthritis Research UK reported [5] that more than 6 million people in the UK have a knee affected by OA and that the individual and societal burden of this is considerable [6]. The direct cost to the NHS in 2001 for the disease process of knee OA was estimated to be £620.5 million for the UK alone [6].

OA has been historically thought to be a mechanical degenerative disease but advances in imaging tools, in particular magnetic resonance imaging (MRI) [7] have brought a better understanding of the disease process. Of note imaging has identified the importance of synovitis and this is now an important biomarker of the disease [8-10].

The current reference standard for imaging synovitis is gadolinium contrast enhanced MRI. Unfortunately the contrast used in MRI can disassociate from the gadolinium binding chelate and has been linked to the fatal disease Nephrogenic Systemic Fibrosis (NSF) [11] in patients with poor renal function. The administration of intravenous gadolinium during the MRI examination also turns a non-invasive imaging technique into an invasive one. If it were possible to image synovitis in the knees of patients with OA without the use of intravenous gadolinium, it would be possible to:

1. Include patients for imaging regardless of their renal function
2. Remove all other possible side effects associated with the contrast agent e.g. allergic reactions
3. Scan more than one joint at each examination
4. Increase patient tolerance of the examination
5. Reduce the examination time and cost
6. Allow for the non-contrast imaging of synovitis to be applied to all joints in the research and clinical environment
7. Use MRI as a biomarker in longitudinal assessment of disease progression or response to treatment.

Importantly, it would be a more patient friendly protocol, allowing those who are needle phobic or have poor venous access to be scanned.

MRI pulse sequences have evolved since the inception of the technique, with specialised techniques being developed to either exaggerate the appearance of a tissue type or to supress it. Novel techniques have been used in neuro imaging to characterise tissue types and assess vascularisation. Whilst some of these techniques are common practice in neuro imaging, their use in musculoskeletal imaging has been limited. Exploration of combinations of these techniques in multiparametric imaging protocols may allow synovitis to be imaged without contrast agents in MRI.

1.2 Thesis aims and hypothesis

The hypothesis explored within this thesis is:

'MRI can detect with high sensitivity, synovitis in the knee of patients with OA without the use of intravenous gadolinium based contrast agents.'

This thesis explored the literature to provide a current knowledge of current MRI techniques and attempts to image synovitis without the use of contrast agents in MRI. Data within the Leeds Musculoskeletal Biomedical Research Unit (LMBRU) was examined to identify potential candidate sequences that may allow for synovitis to be employed in the new non-contrast protocol. Once the protocol had been developed and optimised, the COSMOS (contrast obviated MR scanning of synovitis) protocol was acquired in patients with OA of the knee and compared to the reference standard of post gadolinium contrast Volume Interpolated Breath-hold Examination (VIBE) imaging.

1.3 Structure of the thesis

The structure of this thesis is outlined below, together with a summary of each chapter.

Chapter 2 Literature review

A thorough review of the literature was undertaken within this chapter and focuses on two key topics:

i) The knee and ii) imaging of osteoarthritis

Within the section dedicated to the knee, basic anatomy of the joint is described with particular emphasis on the synovium.

In the imaging of arthritis section, comparison is made with all imaging modalities that are available to provide diagnostic images of the osteoarthritic knee. Emphasis is placed on MRI, the imaging technique of choice for this thesis, with a revision section of basic principles and an introduction to potentially novel techniques that may be utilised within this piece of work.

Chapter 3 Appraisal of MRI techniques based on the literature review and existing data held within the LMBRU

This chapter reviews existing data within the LMBRU to identify any possible candidate MRI sequences for the non-contrast MRI protocol to image synovitis in the knee with MRI. Assessment of the strength and weaknesses of potential sequences was performed resulting in a set of core sequences to be incorporated in the COSMOS protocol.

Chapter 4 Optimisation of the COSMOS non-contrast MRI protocol

This chapter describes how potential candidate MRI sequences derived from Chapter 3 were refined with the aim of optimising each in order to develop a non-contrast scanning protocol that could be used in the main COSMOS study for imaging synovitis in patients with knee OA.

The protocol developed was assessed for acquisition timing, generating appropriate tissue weightings and coil selection.

Chapter 5 The COSMOS study

Chapter 5 describes the COSMOS study which examined the quality, sensitivity, specificity and reliability of the new COSMOS protocol. A pilot study was carried out prior to commencing the main study to ensure that no technical issues had been overlooked. The process, the results and modifications resulting from the pilot study are described at the beginning of this chapter.

The major portion of the chapter is dedicated to the main COSMOS study. Descriptions of the methods, results and conclusions are presented in detail in this chapter.

Chapter 6 Diffusion weighted imaging of synovitis in the knee in patients with OA

Chapter 6 explores diffusion weighted imaging to visualise synovitis on non-contrast MRI scans. A separate chapter is dedicated to this technique to describe the modifications that were required in order to allow for a work in progress sequence developed by Siemens® Healthcare to be adapted for use in musculoskeletal imaging.

A proof of concept study was performed to explore whether the use of diffusion weighted imaging was feasible in the knee. The concept, methods, results and possible future directions of this imaging technique are described and debated in this chapter.

Chapter 7 Inversion recovery imaging of synovitis in the knee in patients with OA

As a result of the findings from the main COSMOS study, an additional chapter has been included in this thesis. Some unexpected results obtained from Chapter 5 led to a proof of concept study being performed with the final 20 patients of the COSMOS study in order to explore the use of the inversion recovery sequence in imaging synovitis. The methodology and results obtained from this arm of the study are described alongside possible future directions for this technique.

Chapter 8 Discussion and future directions

In the final chapter of this thesis a summary of the work is provided. Results, conclusions, limitations and discussions arising from the preceding chapters are described.

Possible future directions for components of the COSMOS study are discussed as well as additional future projects, that if completed may allow for non-contrast MRI of synovitis within OA to be translated into the clinical environment.

Chapter 2 Literature review

2.1 Introduction

A literature review has been carried out to explore and define the subject matter of this thesis. The review will consist of:

- The knee joint: Anatomy and pathological involvement with OA
- The definition of synovitis and its contribution to the osteoarthritic disease process
- The impact of OA both on the individual and society
- Various imaging techniques available to image osteoarthritic joints
- As MRI is the basis of this thesis, a description of the principles used to acquire MR images, the basics of MRI physics and the physics behind sequences that were potentially suitable
- An examination of contrast MRI scanning, the current reference standard for imaging synovitis in the knee
- A review of previous studies that have attempted to use non-contrast MRI scanning
- Methods for measuring the quantity of synovitis in the knee joint on the MRI scans

2.2 The knee

The knee is a large complex joint of the lower limb and is classified as a synovial hinge joint. The knee joint (Figure 2-1,Figure 2-2 and Figure 2-3) allows for articulation of the femoral condyles, the medial and lateral tibial plateau and the gliding of the patella with the distal femur [12]. The joint allows for flexion extension internal and external rotation of the lower limb. It

is an important joint as it allows for movement of the individual in the vertical and horizontal planes.

Bones	Ligaments	Muscles	Soft tissue structures
Femur	Medial collateral	Rectus Femoris	Medial meniscus
Tibia	Lateral collateral	Vastus Intermedius	Lateral meniscus
Fibula	Anterior cruciate	Vastus Medialis	Articular cartilage
Patella	Posterior cruciate	Vastus Lateralis	Quadriceps tendon
	Ligament of Humphrey	Semimembranosus	Patellar tendon
	Ligament of Wrisberg	Semitendinosus	Synovial capsule
		Biceps Femoris	Bursae
		Gastrocnemius	Nerves
		Soleus	Arteries
			Veins

Table 2-1 Components of the knee joint

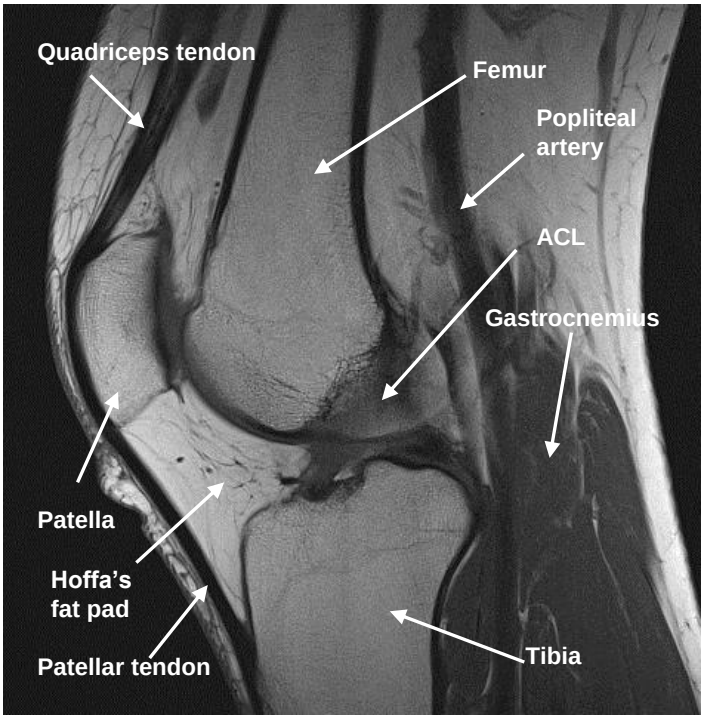

Figure 2-1 Sagittal T1 turbo spin echo (TSE) MRI scan of a normal knee joint

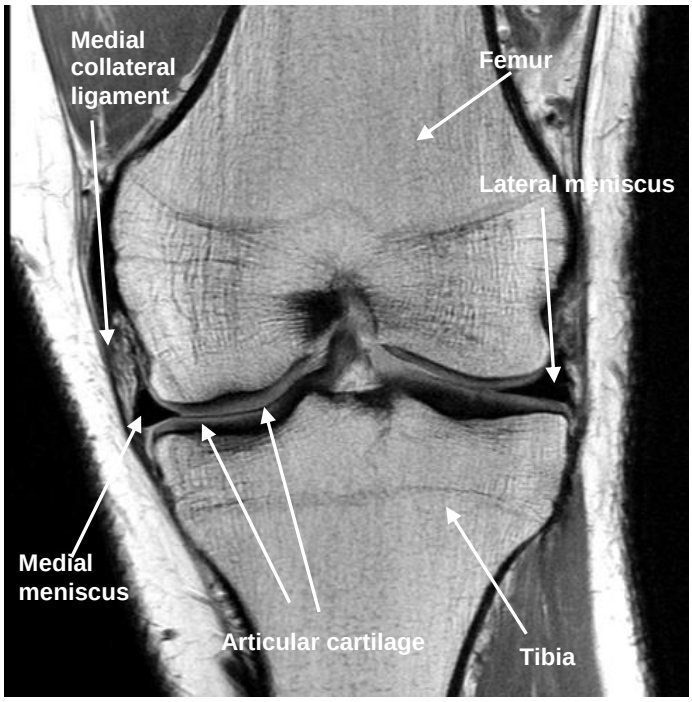

Figure 2-2 Coronal T1 TSE MRI scan of a normal knee joint

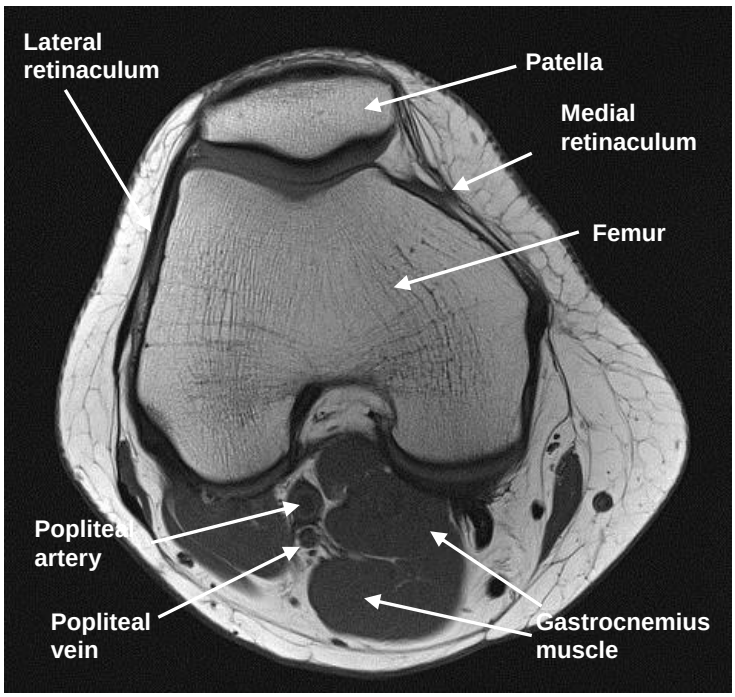

Figure 2-3 Axial T1 TSE MRI scan of a normal knee joint

The individual components of the knee have specific and combined function. The bones are weight bearing, allow for stabilisation of the joint and

attachment of ligaments and tendons. Articular cartilage covers the articular ends of the bones which provide cushioning and a smooth surface for the bones to articulate on. Articular cartilage is formed from collagen fibres and chondrocytes and covers the articular surfaces of bones of the diarthrodial joints. It is made of hyaline cartilage, contains collagen and has no blood or nerve supply. It distributes weight and decreases friction within the joint.

In between the articular surfaces of the femur and tibia lie the menisci. The menisci are semi-circular discs of cartilage that distribute the forces throughout the knee. Damage or disruption to the congruity of these structures, prevents smooth movement of the bones of the joint.

The ligaments provide stability of the joint in both the lateral and antero-posterior directions. The range of extension and flexion are regulated by the physical limitation of the ligaments. The muscles provide strength and work antagonistically with each other to provide movement of the joint.

The joint capsule is formed of two layers: the fibrous outer layer and the inner synovium. The synovium forms the deepest layer of the joint capsule and secretes synovial fluid to lubricate and nourish the joint. Cells within the synovium also remove any intra-articular debris. Inflammation of the synovium is known as synovitis: Imaging of synovitis within the knee of patients with osteoarthritis is the central component of this thesis. The synovium covers all non-articular surfaces of the knee including the intra-articular ligaments and tendons. There are five connected synovial partitions within the knee joint [13]. These are:

Central portion (Figure 2-4): The anterior attachment of the synovium is the patellar articular borders. It then extends below the vastus medialis and lateralis and attaches to the shaft of the femur. Hoffa's fat pad displaces the synovium posteriorly from the patellar tendon. Lateral folds of synovium from the patella extend inferiorly and attach anterior to the anterior cruciate ligament on the intercondylar fossa and lateral to the posterior cruciate ligament [13]. It then extends medially and laterally covering the anterior surfaces of the cruciate ligaments [14]. The medial and lateral folds of the synovium follow the capsule and extend inferiorly from the femoral articular surfaces to the meniscal attachments.

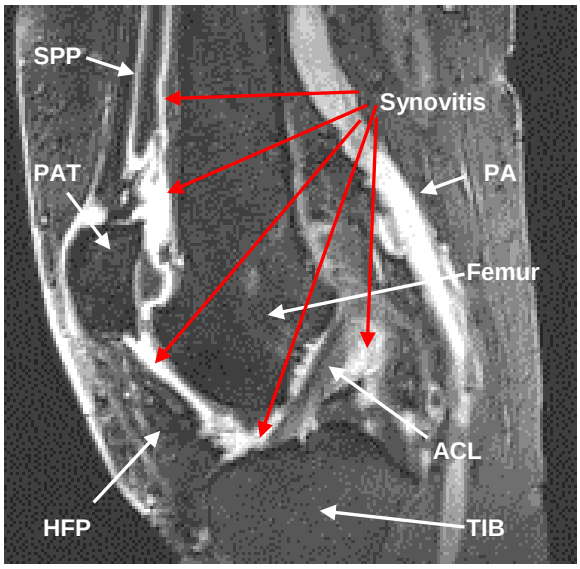

Figure 2-4 Sagittal post contrast SPGR MR subtraction image of the knee showing the synovium: central portion.

SPP = Supra patella pouch. PAT = patella, HFP = Hoffa's fat pad, SF = Synovial fluid, PA = Popliteal artery, ACL = Anterior cruciate ligament, TIB = Tibia

Suprapatellar pouch (Figure 2-5): The synovium extends from the superior pole of the patella and forms a pouch between the quadriceps tendon and femur.

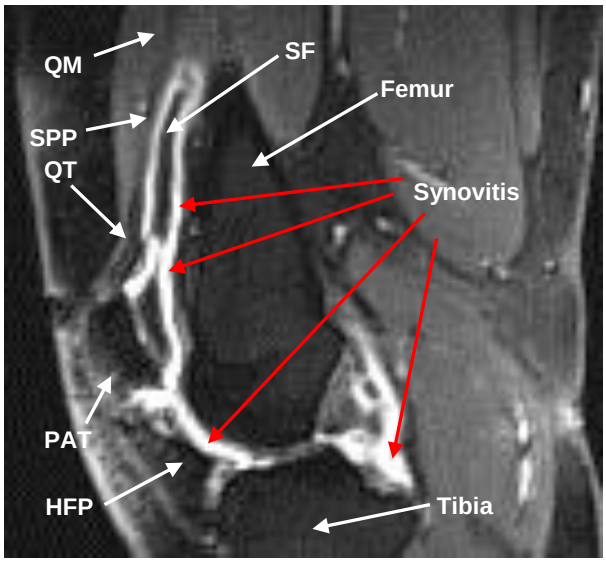

Figure 2-5 Sagittal post contrast MRI SPGR subtraction image of a knee showing the suprapatellar pouch synovial distribution

QM = Quadriceps muscle. SPP = Suprapatella pouch. QT = Quadriceps tendon, PAT = patella, HFP = Hoffa's fat pad, SF = Synovial fluid,

Posterior femoral recess: The synovial membrane extends posteriorly from the femur and two recesses are formed between the femoral condyles and the medial and lateral heads of the gastrocnemius muscle.

Sub-popliteus recess (Figure 2-6): Posterior to the lateral meniscus and anterior to the popliteus muscle lies a small pocket of synovium.

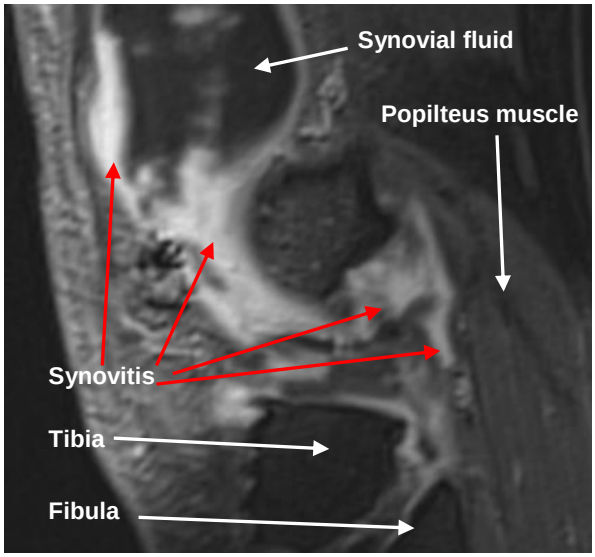

Figure 2-6 Sagittal post contrast MRI SPGR subtraction image of the knee showing the synovium: Sub-popliteus recess

Superior to the posterior third of the medial meniscus: whilst not seen in every individual, this pocket of synovium can be identified on arthroscopy (Figure 2-7) [13].

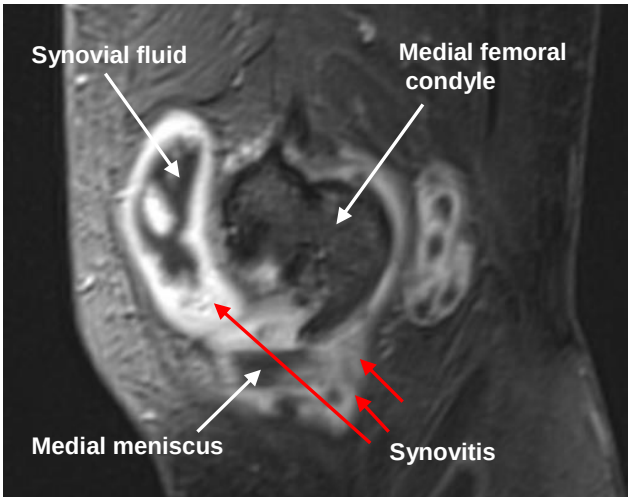

Figure 2-7 Sagittal post contrast SPGR subtraction image showing the synovium: Posterior to medial meniscus

The joint of the knee is divided into three compartments: medial, lateral and patellofemoral. Each compartment is responsible for load bearing depending on the movement being made. All compartments are liable to structural damage and can be involved in the osteoarthritic process.

2.3 Osteoarthritis of the knee

Musculoskeletal conditions are the single most common cause of chronic disability [15]. Measured in terms of disability adjusted life years (DALYs), OA is the fourth most frequent predicted cause of health problems worldwide in women and the eighth in men [16]. In 2000 almost 80,000 knee and hip replacements were performed for OA costing £450 million [1].

OA is the commonest form of arthritic disease [17]. It commonly affects weight bearing joints [18]. Lawrence et al in 2008 estimated that 27 million American adults suffered from OA, an increase of 6 million from 1995 [19]. Reginster reported in 2002 that between 1.3 and 1.75 million people in England and Wales had OA and 6 million new diagnoses of OA were being made annually in France [20]. It is estimated that 17 million people in the UK (twice the number in 2012) will be living with OA by 2030 [2]. With OA being associated with the aging population [21] the prevalence is likely to increase.

In the United Kingdom in 2008 a paper commissioned by Arthritis Research UK reported that more than 6 million people have a knee joint affected by OA [5, 22]. In 2006/7 62,000 knee replacements were performed in England and Wales and of these 94% were due to OA [5]. A recent paper by Culliford et al in 2015, applied a new modelling technique based on increased body mass index and calculated that by 2035 the estimated number of total knee replacements could be as high as 1,219,362 [23].

The cost of treatment for OA in the United Kingdom was assessed by Chen et al in 2012. They estimated that the cost for the treatment of OA of the knee in terms of both direct and indirect costs. Indirect cost for Disability Living Allowance in 2001 for those claiming the allowance due to OA was £2.41 billion. Whilst it may appear strange that a paper comments on data which is 11 years old, the author mentions the disappointment of a more recent paper by Dame Black in 2008 [24] which did not provide a breakdown of costs resulting in the exact contribution of OA to the United Kingdom remaining undefined. The findings of Chen for direct costs associated with OA knee treatment are summarised in Table 2-2 [6, 25].

Intervention	Cost
Topical Non Steroid Anti-inflammatories (NSAIDS)	£8.5 million
Oral Non Steroid Anti-inflammatories	£25 million
Iatrogenic events related to NSAIDS	£56.9 - £124.4 million
Proton Pump Inhibitor prescription	£11.6 million
Arthroscopic lavage and debridement	£25 million
Primary total knee replacements	£426 million

Table 2-2 Direct costs incurred by osteoarthritis of the knee for the United Kingdom in 2001 [6]

The impact of OA on the individual is considerable and can be life changing, affecting both their work and social life. In 1999/2000 in the UK, 36 million working days were lost due to OA at an estimated loss in production of £3.2 billion [1]. Wilkie et al in 2014, reported that 25% of participants in a study in

England terminated their working careers early [26] due to the effects of OA. Seventy-nine percent of those affected by OA have reported that they have had to reduce their activity resulting in a detrimental effect on their independence and social lives [1]. Everyday activities such as shopping or meeting up with friends become a challenge. Mobility at home presents problems such as going up and down stairs or rising from a seated position [27]. In the OA Nation report 2012, 36% of the respondents to a survey said that OA had affected their emotional well-being whilst over half stated that OA has had a large impact on their daily lives [1]. The loss of independence and inability to participate in activities can result in patients suffering from depression and therefore add an additional burden to the health services through medication and treatment [28, 29]

The knee is a common site for OA and has a substantial impact. In a recent study, Kingsbury et al reported that the knee joint was the most common joint affected by OA [30]. Alarmingly, almost one quarter of those who present to their General Practitioners with knee OA have had to stop work due to the OA [26].

Traditionally OA has been seen as a disease which centres around the loss of articular cartilage [31]. Recent research however, indicates OA is not a simple wear and tear disease process but rather a complex combination of signs and symptoms affecting not just the bones of the joints [32]. The roles of other structures of the joint (ligaments and cartilage) and systemic influences such as deoxyribonucleic acid (DNA) are being investigated [32]. There are a number of risk factors which have been associated with knee OA [32]:

Ethnicity: Whilst the prevalence of OA of the knee in different ethnic groups has been reported to show differences [33], the results must be carefully interrogated to assess whether this is true. A number of studies have shown that there is a difference in the prevalence of OA knee in non-Caucasian and Caucasian women [33-37]. African American, Jamaican and Chinese women have been shown to have a higher prevalence of knee OA than in Caucasian women [34-36] whilst Eskimos have a lower incidence [38]. However the reporting of the statistics from these papers (e.g. lack of definitive statistical results [35]) and the comparison of very different socio-economic groups, lifestyles, occupations, available diets and the exposure to

available medical services, makes one feel sceptical and questions what the true results are.

Gender: The prevalence of knee OA is higher in the female population when compared to their male counterpart [39]. Srikanth et al reported that the incidence of knee OA was significantly higher in women and interestingly more severe than any other form of OA [40]. As OA is a multi-factorial disease, other risk factors may contribute to this result, such as hormonal and weight influences, but the over-riding incidence of OA of the knee is higher in the female population [40, 41].

Age: Age is the greatest risk factor in the development of OA. It has been shown that the frequency can increase by as much as 60% when two similar populations of under 44 and over 65 years of age are compared [42]. Felson et al found that radiographically diagnosed OA knee in the age group 63 to 70 years was 27%. This increased to 44% in the over 80 year olds [43].

Hormonal status: Studies have been carried out that demonstrate that oestrogen is a protective factor in developing OA [39, 44]. Postmenopausal women are at a higher risk of OA and while the use of the oral contraceptive pill has been shown to have an unlikely effect on the development of OA [45], there does not appear to be any correlation between hysterectomy and the onset of OA [39].

Genetics: The role of genetics has been associated with the development of OA. A study of female twins in 1996 showed that genetic factors may account for 40-60% of disease development [46]. However in 1996 Wright et al suggested that genetics played a smaller role in knee OA when compared to hip and hand OA [47]. Genetic mutations resulting in collagen defects has been investigated to explain familiar expression of the disease [48].

Obesity: Body habitus has a correlative relationship with OA and often present together as comorbidities. Obesity increases the risk and progression of the disease by increased joint loading, loss of functionality and therefore reduced physical activity [49]. The spiral of pain, lack of functionality and increased weight gain compound the progression of knee OA.

Occupational factors: Jobs that involve repeated kneeling or crouching put extra mechanical strain on the knee joint, particularly the patellofemoral joint, and increase the risk of OA [50]. These include teaching and nursing as well as steel erecting, electrical maintenance, roofing and other construction work [51]. The increased degeneration of this joint produces inflammatory changes that perpetuate the degenerative process.

Sports participation: Sport participation, especially those that induce a mechanical load on knee joints e.g. road running have been reported to exacerbate the incidence of OA of the knee joint [52]. Professional and elite athletes who undertake high impact sports without major injury are at increased risk of the development of knee OA [53].

A combination of these factors predisposes an individual to the possibility of developing OA.

2.3.1 Clinical presentation of osteoarthritis of the knee

Pain is the most common feature of OA knee. This increases with activity and subsides with rest. Night pain is commonly reported in advanced disease, waking the patient from sleep. The main cause of pain in the arthritic joint remains a mystery. Articular cartilage does not possess neurones whilst other structures of the knee have nociceptive fibres [54]. Nociceptive fibres respond to damage to a particular part of the body and are normally time limited. There are notable exceptions to the time limitation of duration of pain and these include arthritis [55]. Whether this is due to a centrally driven pain response or a local causation is a question outside of the remit of this thesis.

Local causation of pain has been further investigated with the prevalence of newer imaging techniques. The debate as to what causes pain within the arthritic knee has focused on the presence of bone marrow lesions [56] but new evidence shows that synovitis is also responsible [54, 57].

Pain is a subjective measure and is variable between individuals. Whilst validated tools can be used to assess pain [58], discrepancies between pain

scores and imaging findings occur [59]. The lack of correlation with imaging features of OA and pain levels has been reported [59].

Stiffness may occur in the morning and other arthritidies should be excluded to ensure that a correct diagnosis is determined. Typically stiffness is experienced for a period of minutes rather than hours, as experienced with inflammatory disease e.g. rheumatoid arthritis. Depending on the structures of the knee involved in the disease process different activities may increase pain. Standing for prolonged periods, climbing down stairs, walking for either a long duration or distance may exaggerate the pain suffered. Common activities such as kneeling, bending down and rising from a chair may be difficult [1].

The variable presentation of pain in the knee joint may depend on the structures that are involved [54, 57, 59-62]:

- Osteophyte formation on one or multiple bones
- Tears of the menisci
- Tears of the anterior cruciate ligament
- Patellofemoral degeneration
- Joint effusion
- Synovitis
- Inflammation of the iliotibial band
- Bursae
- Baker's cyst

Tenderness of the joint can be variable and the presence of one area of pain does not necessarily give the diagnosis of OA. It is important to note that individual pathology of just one of the above will cause the patient pain.

The alignment of the knees may be affected. There may be valgus alignment if the lateral compartment of the knee is involved and varus if the medial compartment is involved [63]. Because the mechanical process of walking is altered this mal-alignment may give secondary pain in the ankles, spine and hips.

Physical assessment of the knee may show the following signs [21, 64, 65]:

- Swollen joint due to a joint effusion
- Irregular bone margins
- Laxity of the joint ligaments
- Poor quadriceps bulk and functionality
- Reduced movement
- Crepitus

While OA is a progressive disease, the prognosis for each individual is highly variable. It is not known what exaggerates symptoms or the demise of the joint or minimises the patients' disability from the disease.

2.3.2 Diagnosis of osteoarthritis of the knee

Diagnosis of OA is normally made on the history given by the patient and clinical examination. Whilst tests can be used to confirm the diagnosis, early disease maybe missed if used in isolation from a patient's history.

In 2014, the National Institute for Health and Care Excellence (NICE) published criteria for diagnosing OA [3]. Whilst not joint specific, the criteria stated that OA should be diagnosed clinically without investigations if a patient:

- Is 45 years old or over
- Has activity related joint pain
- Has no morning joint related stiffness or morning stiffness that lasts no longer than 30 minutes.

The American College of Rheumatology (ACR) criteria for diagnosing OA of the knee joint includes a diagnostic path that includes criteria based on clinical and other investigations. The criteria are presented in Table 2-3.

Clinical criteria	Clinical and investigation criteria
• Knee pain for most days of prior month • Crepitus on active joint motion • Morning stiffness ≤ 30 minutes in duration • Age ≥ 38 years	• Knee pain for most days of prior month • Osteophytes at joint margin (radiograph)
• Knee pain for most days of prior month • Crepitus on active joint motion • Bony enlargement of the knee on examination	• Knee pain for most days of prior month • Synovial fluid typical of OA (laboratory) • Morning stiffness ≤ 30 minutes • Crepitus on active joint movement
• Knee pain for most days of prior month • Age ≥ 38 years • Bony enlargement of the knee on examination	• Knee pain for most days of prior month • Age ≥ 40 years • Morning stiffness ≤ 30 minutes • Crepitus on active joint movement

Table 2-3 American College of Rheumatology criteria for OA of the knee [33]

2.4 The role of synovitis in osteoarthritis

2.4.1 Definition of synovitis

As described previously, the synovium is the structure which covers the diarthrodial joints, tendon sheaths and bursae [66]. The normal synovium allows for movement of structures adjacent to it. The synovium also produces synovial fluid which allows for lubrication of the joint.

Synovitis is defined as inflammation of the synovial membrane [67]. The normal synovium is composed of one to four layers of cells, is well vascularised and has a nerve supply [8]. Histology of synovial tissue taken from OA knee joints have shown hyperplasia of the lining cell layer with accompanying infiltration of lymphocytes and monocytes in the sub-lining layers [68]. The process of inflammation within the OA affected joint is not really understood [69]. Synovial biopsies taken from OA knee patients

undergoing arthroscopy have shown the following differences compared to the normal synovium [69] Figure 2-8:

- Increased vascularity
- Thickening of the lining
- Inflammatory cell infiltration

The changes demonstrated ranged from marked hyperplasia to fibrotic infiltration of the synovium [70]. Whilst it is recognised that patients with rheumatoid arthritis (RA) display more synovial involvement than those with OA, two patients in Haraoui et al study displayed features of synovitis that was indistinguishable from RA [70]. The effect of synovitis within an osteoarthritic joint may be confusing. While reports have shown that painful osteoarthritic joints show no synovitis and conversely may be present in joints that are not considered to have OA [67] it has been shown that up to 50% of patients presenting with OA demonstrate synovitis on MRI or arthroscopy [71].

On MRI scans synovitis is defined as thickening and enhancement of the synovium after the administration of intra-venous contrast agents [72]. Synovitis has been used as a biomarker to indicate the surrogate inflammatory burden of the disease [73].

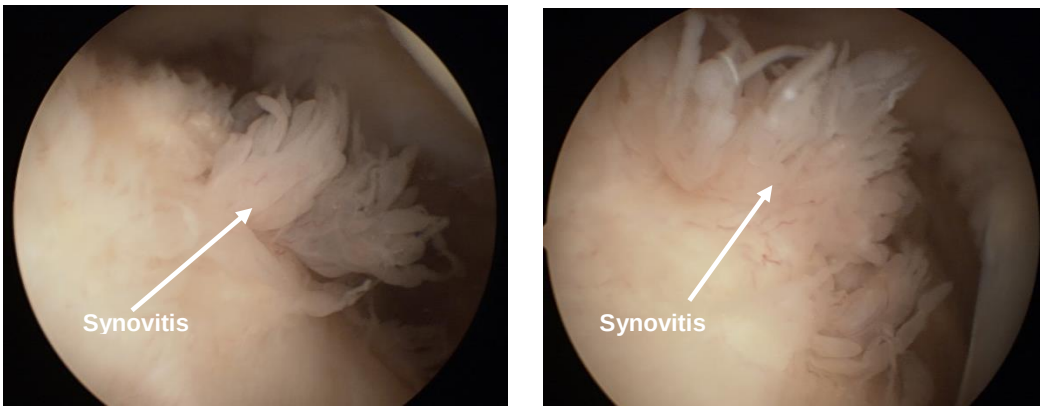

Figure 2-8 Synovitis of the knee joint as viewed via arthroscopy

Images curtesy of Mr. R Venkatesh (Leeds Teaching Hospital NHS Trust)

2.4.2 Role of synovitis in OA

Recent research has focused on the role of synovitis in OA. Historically OA was thought to be just a disease of the bone and cartilage, but with modern imaging techniques the entire disease process can be reviewed. Absolute diagnosis of synovitis is still made by the invasive procedure of biopsy: however, given the pain and potential complications, this is rarely undertaken clinically. The advent of high resolution ultrasound and MRI allows us to visualise the interaction of all structures in the disease process. Imaging of patients in both early and late presentation of OA, have shown synovitis to be present.

Pellitier et al [71] raises an important question regarding the involvement of synovitis in OA. It remains unclear whether synovitis is an innocent bystander or is involved with the structural changes of the disease. And whether synovial inflammation is only relevant during the flare of the disease or does it contribute to the disease process on an ongoing basis?

Disease activity and the association of inflammation in joints affected by OA has been the subject of many studies with conflicting outcomes [9, 10, 74-81]. In 2013 Felson et al hypothesised that the disease of OA is purely mechanical in origin and inflammation is a consequence of pathomechanics that may contribute to further joint damage in later disease [80]. This conclusion, whilst interesting and thought provoking, does not reflect the complete body of published work regarding the role of synovitis in OA. The author however admits that ‘This is not a systematic review but rather draws from selected research findings to make certain points’ [80]. A degree of bias must therefore be inferred.

Conversely, Sellam and Berenbaum conclude that synovitis is a pivotal factor in the pathogenesis of OA [75]. In a review of 116 papers published up to December 2009 the authors conclude that whilst synovitis is not a prerequisite for the development of OA, it is involved in the breakdown of cartilage and thus in the progression of the disease [75].

Recent treatments for the management of OA have included those that have been used to treat RA for many years. The rationale for this regime is that OA is an inflammatory disease and disease modifying drugs such as methotrexate can reduce the inflammatory component of OA and therefore

reduce the destructive element of synovitis. These treatments for OA are in their infancy and future research is required.

Long standing synovial inflammation can lead to fibrosis of the structure which results in stiffness and poor function of the affected joint [68]. This is due to the loss of elasticity of the synovium and the change in biomechanical stresses at the joint [68].

2.5 Imaging of osteoarthritis

2.5.1 Introduction

Radiographic techniques have long been used to assess joint pathology including OA [82]. Conventional X-rays were the initial imaging technique utilised and continue to be the most requested technique [83]. Advances in modern imaging techniques have increased the number of imaging modalities available to assess the musculoskeletal system and increase our knowledge of the disease process [84] including the impact of OA [85-87] .

2.5.2 X-rays

X-rays (plain films or radiographs) have been used to image joints to assess their disease status with regard to arthritis [88]. X-rays are readily available and cheap to produce. However the technique has disadvantages as it requires the use of ionising radiation, shows the anatomy as a projection two dimensional image and primarily images bony anatomy. Despite this X-rays are still the first line of imaging investigation used to evaluate a degenerative joint [83].

X-rays only show quite major changes to the bony structures of the joint and disruption to the joint space and are not sensitive to early alterations to bone structure and changes to the composition of bone tissue (Figure 2-9) [89].

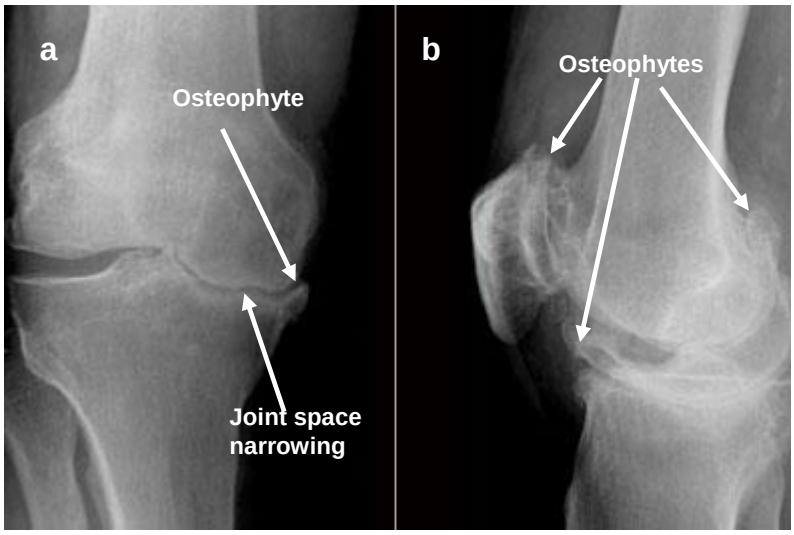

Figure 2-9 X-rays of advanced OA in a knee joint
(a) AP view (b) Lateral view showing osteophyte formation and joint space narrowing

In the knee, an X-ray derived scoring system has been produced to evaluate the degree of joint involvement in the OA disease process. The Kellgren and Lawrence (KL) scoring system was described in 1957 [90] and is still in use today. This system describes the bony morphology and degree of joint involvement in OA.

In the knee four grades are described to show severity of the disease:

Grade 1: Doubtful narrowing of joint space and possible osteophytic lipping

Grade 2: Definite osteophytes, definite narrowing of joint space

Grade 3: Moderate multiple osteophytes, definite narrowing of joints space, some sclerosis and possible deformity of bone contour

Grade 4: Large osteophytes, marked narrowing of joint space, severe sclerosis and definite deformity of bone contour

Advanced changes in the bone and bone marrow structure (osteochondral lesions) can be identified on X-rays but only when their size is such that they are probably symptomatic to the patient.

Despite X-rays having major limitations in their diagnostic sensitivity and specificity, they continue to be the most common radiological diagnostic tool requested both at initial diagnosis and longitudinal follow up of disease progression and response to treatment [91].

Kellgren and Lawrence's scoring system is unable to identify early changes to the bones such as bone marrow lesions (BMLs) which have been identified to show early disease and can be prognostic to disease development [89].

As we learn more about osteoarthritis, it is becoming clearer that this disease is a complicated process involving all structures of the joint. It is therefore necessary to identify an imaging modality that can demonstrate the involvement of all joint tissues and not just bone.

2.5.3 Computerised Tomography and Radionuclide Imaging

Whilst not routinely or commonly used in OA, there are other specialised techniques that can be used to image OA. The sensitivity and specificity of the techniques may not be equivalent to other established imaging techniques related to OA, but their problem solving capacity may be of use in specific cases.

2.5.3.1 Computerised Tomography

Computerised Tomography (CT) is an imaging modality that uses ionising radiation to produce axial cross-sectional images that show good bone detail but limited soft tissue information. Images are produced by an X-ray source and detector being rotated around the patient in order to generate information that can be reconstructed into a two dimensional image. The image produced represents the differences in attenuation of the X-ray beam by anatomical structures.

Unenhanced CT scanning of synovitis is not appropriate due to the poor soft tissue contrast produced by the imaging technique [67]. The administration of an intravenous contrast agent can enhance the soft tissue images and delineate blood flow to anatomical structures such as synovitis and can show areas of inflammation. This is a relatively quick, cheap technique and is widely available [67]. However, the radiation burden to the patient is considerably high especially in the trunk area. This is of particular concern to younger patients who may have numerous scans during their lifetime and precludes this technique from being used in longitudinal research studies.

Advances in technology have allowed for reduction in radiation dose and thinner slices to be acquired with multiple rather than single detectors [92]. Dual energy CT scanning has allowed for differentiation of anatomical structures using two different energy sources to produce two different X-ray spectra. This has limited application currently in musculoskeletal imaging but has been used to differentiate gout crystals from bone [93] and delineate tendons in the hand [94].

To increase the sensitivity of depicting synovitis within the area examined, the acquired axial images can be reconstructed to demonstrate the joint in the various anatomical planes using appropriate software. Advances in computing have enabled the development of new image reconstruction software which is commercially available that results in minimisation of the artefact due to metal implants and can be used to provide information which may be missed using other imaging techniques in a joint that has been replaced [95].

A recent study looking at synovial imaging in patients with RA utilising contrast enhanced CT scanning has shown that synovitis is visible using a bone masking technique [96]. However, despite the greater patient acceptance of this method compared to MRI, the use of high doses of iodinated contrast agent and ionising radiation, poor soft tissue delineation and the inability to demonstrate bone marrow lesions limits the clinical use of this technique currently.

2.5.3.2 Radionuclide Imaging

Radionuclide imaging methods including Single Photon Emission Computerised Tomography (SPECT) and Positron Emission Tomography (PET) are invasive radiographic techniques that involve the injection of radioactive physiological tracers into the body that are targeted to specific organs. This technique demonstrates physiological and metabolic processes rather than anatomy [97]. The addition of a radioactive element to a biological marker can be injected into a patient, then traced and imaged using equipment which has a high capital and revenue cost and which is not commonly available in the clinical environment. The radiation burden to the patient is high but these techniques can be helpful as a problem solver, for example in distinguishing inflammation from infection.

There are a limited number of studies using radionuclide imaging to investigate OA. The majority are concerned with bone marrow abnormalities rather than soft tissue pathology [98, 99]. Studies looking into synovial evaluation in patients with RA have been completed but there are currently a limited number of studies that have examined patients with OA. White blood cells and immunoglobulins labelled with ^{99m}Tc have been observed to detect synovitis in patients with OA but further evaluation of these techniques is required [100].

PET demonstrates metabolic activity in tissues using injected radioactive labelled metabolites. Commonly,18F- fluoro-deoxy-D-glucose (FDG) is used in the clinical environment and can demonstrate glucose metabolism within a structure reflecting inflammation, infection or malignancy [101]. PET imaging has been used in a small number of studies to evaluate OA [102, 103]. Despite the low resolution of the PET images, increased uptake of 18F-FDG was seen in joints that were affected by OA however the delineation of the individual anatomical structures within the joint was limited.

Hybrid PET-CT and PET-MR scanners are relatively new in the clinical environment and have the ability to show anatomy overlaid with maps depicting physiological metabolism. The ability of combining the low resolution physiological PET images with higher resolved CT and MRI anatomical images would allow for more accurate localisation of the increased metabolic activity [104]. However, cost implications and availability of these techniques have resulted in limiting their use to oncology imaging.

2.5.4 Ultrasound

High resolution ultrasound is an imaging technique that visualises soft tissue structures of the body without the use of ionising radiation. It is a widely available imaging modality and is relatively cheap to provide. Advances in hardware technology have increased the size of the field of view that can be imaged and provide the ability to record and detect blood flow within structures. However, this imaging technique only shows soft tissue structures and blood flow and resultant image appearance can be highly operator dependent. Although used widely as a diagnostic tool in the hospital environment for assessing musculoskeletal pathology, it is not used routinely to image OA. Due to the lack of specificity in imaging OA with ultrasound, subtle changes associated with early disease may be missed by the inexperienced operator [105]. Reproducible scanning and scoring of synovitis at identical locations on consecutive visits is difficult even for an experienced practitioner [67].

Doppler ultrasound imaging was first introduced to image cardiac scans in the 1980's [106]. Doppler imaging allows for the assessment of synovial vascularity [107]. Conventional Doppler imaging is suitable for imaging fast flowing blood in large vessels. Power Doppler is more sensitive to flow but not does not differentiate blood flow direction or velocity, however it is able to detect edges well, particularly in small vessels [108]. Doppler ultrasound has been used as a disease diagnostic tool and has been used to determine the response to drug therapy in patients with RA [109, 110].The detection of synovitis by Doppler ultrasound in OA has been investigated to a lesser extent but the results correlating disease as assessed using ultrasound with histology have been favourable [107]. Figure 2-10 shows a Doppler ultrasound image depicting synovitis within the suprapatellar pouch of the knee posterior to the quadriceps tendon. The red dot on the image in the area of synovitis shows increased Doppler flow suggestive of active inflammation.

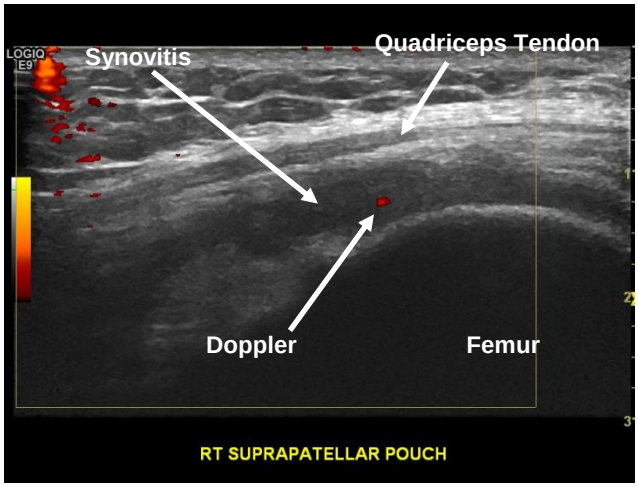

Figure 2-10 Longitudinal ultrasound image of the knee
showing synovitis within the suprapatellar pouch, posterior to the quadriceps tendon.

The red dot within the synovitis (labelled) represents Doppler flow within the structure, indicating an active inflammatory process.
(Image courtesy of Laura H Horton, Leeds Teaching Hospitals NHS Trust)

Unfortunately, the quality of ultrasound images is dependent on the body habitus of the patient and joint size [111]. Ultrasound is absorbed and reflected by some structures such as bone, and will therefore have limited value in scanning some joints. Larger patients or joints result in poorer quality images as the ultrasound waves are only able to penetrate a certain depth. Superficial structures or small joints can produce good quality anatomical detail but this is not the case for all anatomical structures.

Ultrasound only images soft tissue and bone surface abnormalities. The integrity of the bone components of the joint cannot be visualised with this technique unlike other imaging techniques available, thus providing an incomplete picture of the joint involvement of disease.

Whilst the scan is relatively quick and can be repeated, reproducing an identical scan is very difficult and will vary between different operators. The interpretation of the images by another operator at a later date may also lead to variability of assessment.

2.5.5 Magnetic resonance imaging

Magnetic resonance imaging is a technique which allows for good soft tissue visualisation of most structures of the body [112]. The necessity to delineate different structures is paramount in the accurate imaging of arthritic joints to aid diagnosis and monitor response to treatment. MRI is a non-invasive imaging technique that produces detailed images that show both anatomical and pathological features. A comparison of MRI and other imaging techniques are listed in Table 2-4.

	X-ray	Ultrasound	MRI	CT/PET
Advantages	1.Cheap 2.Easily accessible in all hospitals 3.Quick 4.Patient acceptable 5.Reproducible 6.Not operator dependent	1.Does not utilise ionising radiation 2.Accessible in most hospitals 3. Patient acceptable. 4.Shows soft tissue structures 5.Doppler can show vascularity of structures 6.Relatively cheap	1. 3 dimensional imaging of most structures of the body with good soft tissue contrast 2.Does not utilise ionising radiation 3.Able to characterise tissue types 4.Not operator dependent 5.Able to quantify tissue volumes 6.Able to image all joints	1.Good bone information 2. Physiological information 3. Bone masking software
Disadvantages	1.Utilises ionising radiation 2.Does not show soft tissue structures	1.Operator dependent 2.Unable to demonstrate bone marrow oedema 3.Unable to image large joints	1.Relatively expensive 2.Certain patient groups are unable to have a MRI scan due to certain medical implants 3.Can be claustrophobic 4.Relatively long examination 5.Lack of availability 6.May require intravenous contrast agents 7.Patients may not fit in the scanner	1.Poor soft tissue delineation 2.High radiation dose 3.Poor availability 4.Relatively high cost

Table 2-4 Table summarising the advantages and disadvantages of imaging techniques

The major advantages of MRI scanning are that it does not utilise ionising radiation, produces three dimensional images without restriction of image orientation, has the ability to quantify the ‘quality’ of tissue types and is not operator dependent. In the imaging of osteoarthritis, MRI is able to demonstrate all structures associated with the disease in the affected joint [113]. In Figure 2-11 a coronal T1 TSE MR image shows a normal knee joint. Compare this with Figure 2-12, a coronal T1 TSE MRI scan of an osteoarthritic knee demonstrating reduction in joint space, degenerative lateral collateral ligaments and osteophyte formation.
MRI is sensitive and specific in identifying both early and chronic changes associated with osteoarthritis [113]. Unlike ultrasound, MRI is able to image any joint regardless of size [87].

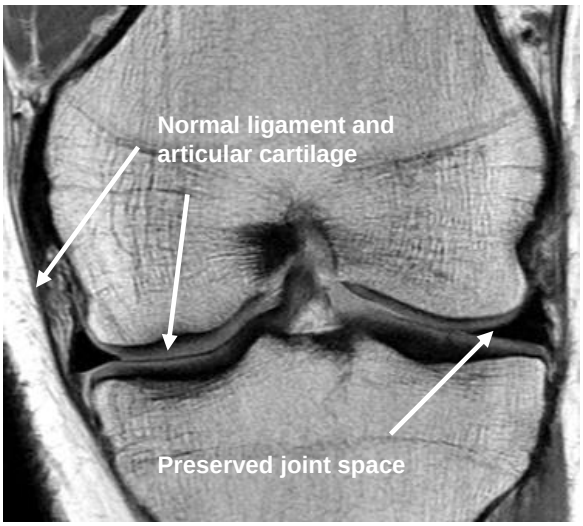

Figure 2-11 Coronal T1 TSE MRI scan of a normal knee

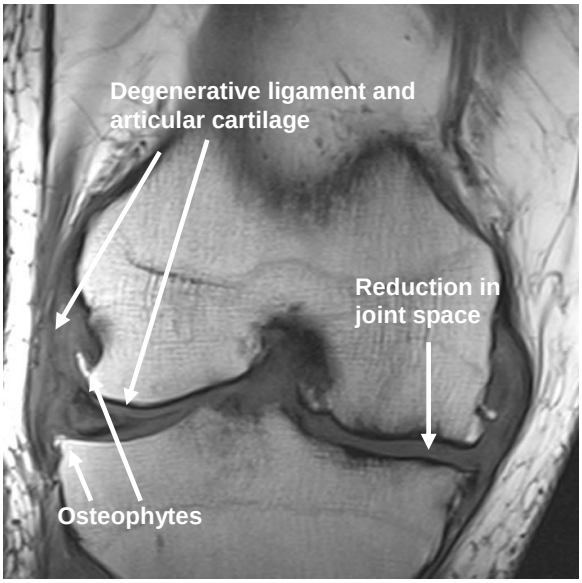

Figure 2-12 Coronal T1 TSE MRI scan of OA knee
demonstrating reduction in the medial joint space, osteophyte formation and the degenerative lateral collateral ligament.

2.5.5.1 Magnetic resonance imaging: Basic principles

In order to describe the principles of the MRI signal, the imaging characteristics and the generation of the resulting image, a brief overview is included below.

Whilst not specifically a literature review, this section will be referred to throughout this thesis and will prevent the duplication of information. A more complete and rigorous description of MRI is found in references [114-116].

A brief outline of pertinent pulse sequences to this thesis will be given in order to give the examiner a basic understanding of the techniques employed in this body of research. A more detailed description of diffusion weighted and inversion recovery imaging is given in Chapters 7 and 8.

2.5.5.2 The MRI system

The field strengths available for routine clinical scanning systems are between 0.2 and 3 Tesla (T) [117]. The majority of commercially available MRI scanners comprise of a superconducting magnet to produce the magnetic field. The patient lies parallel to the main magnetic field (B_0) with the body part of interest that is being scanned in the isocentre of the magnet, the most homogenous part of the magnetic field.

A superconducting MRI scanner is comprised of three electromagnetic components: a set of main electromagnetic coils, three gradient electromagnetic coils and an integral radiofrequency (RF) transmit coil (Figure 2-13) [31].

The gradient and RF components within the scanner produce additional magnetic fields to the static field that when turned on produce spatially encoded signals to obtain an image.

There are three reference axes which are conventionally used to describe the directions of the magnetic fields in a horizontal bore superconducting system [116]:

- z: parallel to the main field direction (B_0)
- x: left right direction
- y: posteroanterior

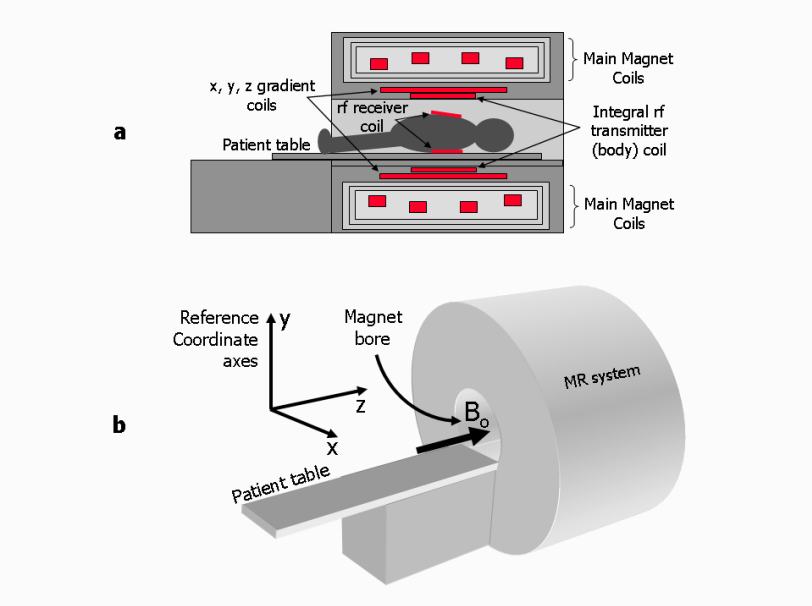

Figure 2-13 The MR system components.
a) Diagram showing the relative locations of the main magnet coils, x, y, and z gradient coils, integral radio frequency transmitter body coil and radiofrequency receiver coils. b) Typical arrangement for a cylindrical bore MR system showing the magnet bore and the reference coordinate axes with the static B_o field direction along the horizontal z axis. [114] (page2)

The gradient coils within the scanner can be turned on and off quickly producing a magnetic field gradient along the direction of B_0 that has a variable strength depending on the position along the x, y or z direction corresponding to the gradient coil utilised. Application of a magnetic field gradient allows spatial visualisation and encoding of the MR signal. Stronger and more rapidly switched gradients allow for higher spatial resolution or permit faster scanning [115]. Selection of the gradient coils is dependent on the orientation of the imaging slice or volume selected by the MR system operator according to the anatomy of interest.

The signals from the patient that constitute the information of the patient's tissues are produced as a result of radiofrequency pulses (RF). These pulses are generated by a dedicated transmitter coil that surrounds the body part of interest that is being scanned or more usually from the integral body coil of the scanner. These have smaller amplitude than the other magnetic fields produced but oscillate at a characteristic radiofrequency dependent on the field strength of the main magnetic field. This RF field is sometimes called the B_1 field. Receiver coils are used to collect the signal produced from this

process (sometimes this is the same coil that is used to transmit the RF [transmit/receive coils]).

2.5.5.3 Production of a MRI signal

The signal normally used to generate MR images originates from the nucleus of hydrogen atoms within a structure and their interaction with the pulse sequence used to obtain the image. As hydrogen is present in both water and lipids, and these elements are common in the human body, hydrogen MRI is used to image the human body.

The hydrogen nucleus has an innate property that demonstrates a nuclear spin which produces a small magnetic field. Every hydrogen nucleus present has an intrinsic property called a nuclear spin that causes a small magnetic field. The magnetic field produced is called a magnetic moment. If the body of tissue is not influenced by a strong external magnet field, these moments are in a random orientation. However, if an external magnetic field is applied, the magnetic moments tend to align themselves either with or opposed to, the magnetic field. The moments distribute themselves so they slightly favour alignment with the magnetic field, and this excess of hydrogen nuclei (protons) results in a net magnetisation (*M*). This excess is very small constituting a few parts per million.

The greater the external magnetic field (B_0) the bigger the discrepancy between those protons aligned and anti-aligned, and therefore the greater the size of the net magnetisation. When the net magnetisation is at equilibrium it is given the symbol M_0 (Figure 2-14).

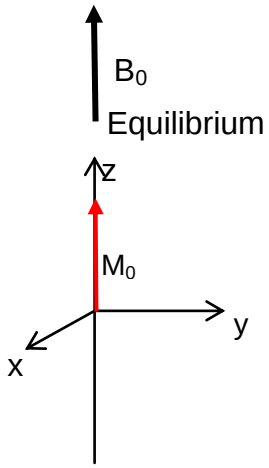

Figure 2-14 When the net magnetisation (M_0) is at equilibrium it is aligned with the external magnetic field, along the z axis.

To produce a MR signal from the net magnetisation, a radiofrequency pulse must be generated to deliver energy to the protons. The RF pulse must be defined at a specific resonant frequency, known as the Larmor frequency, ω_0, which is determined by the Larmor equation (Equation 2-1):

$$\omega_0=\gamma B_0$$

Equation 2-1: The Larmor equation

B_0 = magnetic field strength and γ = gyromagnetic ratio

As the RF pulse has caused the net magnetisation to form an angle with the x axis, it can be divided into two components: M_z (longitudinal) and M_{xy} (transverse) (Figure 2-15). RF pulses that apply energy to the protons to move the net magnetisation away from the equilibrium are called *excitation pulses*.

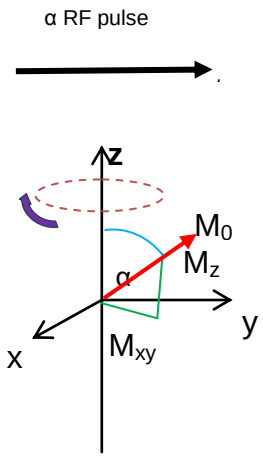

Figure 2-15 When the RF pulse is applied to the net magnetisation, an angle is formed between it and the z axis, flip angle (α).
This rotates around the z axis in the direction of the arrow.
The net magnetisation can be split into two components, Mz and Mxy.
The MR signal is produced by the rotating Mxy component. t= time.

If an excitation pulse is applied with a value of 90°, the net magnetisation is able to rotate 90° from the z axis into the xy (transverse) plane. This process results in no component of magnetisation remaining along the z axis, and the protons are said to be '*saturated*' (Figure 2-16). When applied, the 90° RF pulse produces the greatest amount of transverse magnetisation and MR signal, and is employed to generate the initial signal for a spin echo based pulse sequence.

When the RF pulse is turned on the net magnetisation moves away from B_0 and rotates around it (precession). The larger the amount of energy applied in the form of the RF pulse, the larger the angle the net magnetisation makes with the z axis (B_0). When the angle of precession has been achieved, the RF pulse is turned off and this is known as the flip angle. Pre-defined flip angles of less than 90° are represented by *α* or by the specific flip angle selected. The transverse component of M (M_{xy}) is responsible for generating the MR signal. When a flip angle is chosen that is less than 90° a proportion of the net magnetisation is left along the z axis for a single pulse. Low flip angles produce smaller amount of signal when compared to the signal

produced as a result of 90° flip angle, but the smaller excitation pulses can be repeated rapidly. Excitation pulses with a small flip angle are utilised in gradient echo imaging to produce MR signal to regulate the amount of magnetisation that is transferred between the z axis and the xy plane in fast acquisition applications.

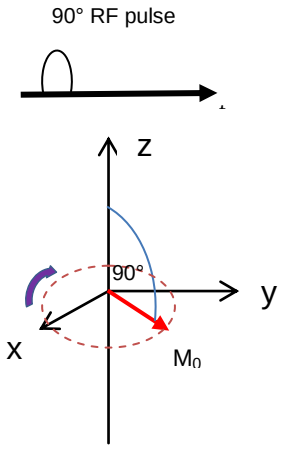

Figure 2-16 When the net magnetisation lies completely in the xy (transverse) plane, the maximum MR signal is detectable.
The RF pulse has a value of 90° and can be referred to as the saturation pulse.

2.5.5.4 MR signal characteristics

After the RF pulse has been removed, the net magnetisation immediately starts to return to its original state; relaxation. There are two processes that relate to the two transverse and longitudinal elements:

1. T1 is the longitudinal relaxation time (measured in milliseconds, ms) and is a measure of the time taken for the protons to redistribute to the original energy states (the time for the net magnetisation to return to its equilibrium) with the z axis (longitudinal axis). An alternative name is spin lattice relaxation as it refers to the time for the ‘spins’ to give back their energy to the lattice in order for them to reach their equilibrium state. It is

an exponential process with a time constant T1. The shorter the time constant, the quicker the relaxation process is.

2. T2 or spin-spin relaxation is the time constant (measured in ms) which characterises the rate at which the transverse magnetisation vector decays towards zero. After the application of the RF pulse, all of the magnetic moments rotate coherently. They all point to the same direction in the xy plane and the angle of direction is known as the '*phase angle'*. When all the moments are coherent with each other they are said to be '*in-phase'*. However they lose their coherence over time and spread out so that they no longer rotate with each other. The net sum of magnetisation is reduced and consequently the measured net magnetisation is also reduced. They are then said to be '*out of-phase'*. There are two reasons for the protons to become incoherent with each other: The fluctuation of the Larmor frequency of the individual proton and local variations in the applied magnetic field. Fluctuations of the Larmor frequency result in decay of the transverse magnetisation. This is an exponential process and has a time constant, T2. This combined with the effects of variation within the applied magnetic field is called T2* relaxation. This influences the rate of decay when measuring a free induction decay (FID) (oscillating magnetic field that gradually decays) signal. T2* is an exponential process with a time constant T2*.

Both processes occur simultaneously in the human body, but T2 relaxation is normally a faster process: the signal decays before equilibrium has been reached.

Structures of the body have different signal characteristics which allow them to be visualised on MRI scans and be differentiated from each other and pathology. Optimised visualisation of structures is important to allow for accurate identification of normal and abnormal structures.

For example, in fluid imaging the spin-spin interaction between the hydrogen molecules is minimal due to the paucity and distance between them. The dephasing of the molecules occurs at a slower rate in fluids when compared

to those within other structures. Hydrogen has a higher natural frequency in water when compared to structures which are solid. The Larmor frequency of hydrogen in water is greater than that of hydrogen on its own. Fluids have long T1 and T2 MRI characteristics. The majority of water found in the body is bound to a protein molecule. The binding of the protein to the hydrogen molecule reduces the movement frequencies of them thus resulting in becoming closer to the Larmor frequency. This makes energy exchange more favourable and results in the shortening of the T1 value meaning that proteinaceous fluids appear brighter than water.

The process by which an MR image is produced is described below:

2.5.5.4.1 Slice selection

The selection of a slice (slice selection) is achieved by applying a gradient magnetic field at the same time as the transmitted RF excitation pulse. The pulse is not a single frequency but is composed of a small range of frequencies, which is called the transmit bandwidth of the RF pulse. The frequency of the RF pulse corresponds to the Larmor frequency at a chosen point along the applied gradient. This results in resonance only occurring in protons along a plane that cuts through the point at right angles to the gradient direction, thus defining a slice of tissue. The orientation of the slice is dependent on the direction of the applied gradient. The thickness of the selected slice is a result of the combination of the RF pulse bandwidth and the steepness of the gradient.

2.5.5.4.2 Phase encoding

After the slice selection is achieved a phase encoding gradient is applied for a selected period of time. This results in the protons rotating at different frequencies dependent on their relative position along the gradient: An increase in the magnetic field due to the gradient causes the protons to acquire results in a higher frequency of precession, whilst a decrease in the magnetic field causes the protons to acquire a lower precessional frequency. Therefore, the protons are continuously changing their relative phase dependent on their position along the gradient. When the gradient is switched

off, the protons will have changed their relative phase by an amount dependent on their position along the gradient. This process is called *phase encoding* and the direction of the applied gradient is called the *phase encoding direction*.

2.5.5.4.3 Frequency encoding

Frequency encoding occurs after the phase encoding gradient has been applied. The frequency encoding gradient is applied at right angles to this causing the protons to rotate at different frequencies dependent on their position along the gradient. In comparison to the phase encoding gradient, the frequency encoding gradient is applied for a greater duration and simultaneously the signal is measured or sampled. The signal is made up of a range of frequencies (bandwidth) corresponding to the Larmor frequencies of the proton magnetic moments at their different positions along the gradient. This process is called *frequency encoding* and the direction of the applied gradient is called the *frequency encoding direction*.

2.5.5.4.4 Image reconstruction

The frequency encoded signal is analysed by a mathematical tool called ‘Fourier transformation’ that converts the time dependent MR signal into its different frequency components. The amplitude of the frequency components can be allocated to a location along the frequency encoding gradient to ascertain the relative signal at each location. The range of frequencies over the field of view of the image is called the receiver bandwidth and is dependent of the slope or amplitude of the frequency encoding gradient. Data from a specific phase encoding step cannot be decoded by the Fourier transformation as the single phase change has no time component. In order to introduce a time component a number of signal echoes are generated by repeating slice selection, phase encoding and frequency encoding, keeping the same slice and frequency gradients but altering the amount of phase encoding every time. For each phase encoding step, the signal is measured and digitised. The time between each repetition is called the repetition time (TR). When all the signals for a selected number of phase encoding steps have been acquired, they can be decoded by Fourier transformation.

2.5.5.4.5 Imaging parameters

The repetition time (TR), measured in ms, is a parameter that can be set by the operator. The time of the sequence acquisition and the contrast of the image are dependent on the value of TR.

The length of the scan and the spatial resolution of the image is also dependent on the quantity of pixels in the phase encoding direction of the reconstructed image and is dependent on the number of phase encoding steps (N_p) (Equation 2-2):

$$\text{MR scan acquisition time} = TR \times N_p$$

Equation 2-2: Equation to calculate MRI scan acquisition time

The image matrix is comprised of the frequency and phase encoding matrices and represents pixels of the reconstructed data. It not only controls the final image size but also defines how the raw data is stored. The system for raw data storage in the matrix is called *k-space* and will not be described in the scope of this thesis. The acquisition time for a scan is proportional to the phase encoding matrix.

2.5.5.4.6 Image contrast

Contrast of MR images are dependent on a number of parameters and the type of pulse sequence employed. For spin echo and fast spin echo sequences, the main contributors to the contrast of the sequence are the TR and echo time (TE). For T2 imaging the use of long TR and TE values is required, and for T1 imaging, short TR and TE values are used. Intermediate or proton density imaging uses a long TR and a short TE

In spoiled gradient echo imaging the flip angle, TR and TE have the greatest effect on the contrast weighting of a scan however the choice of flip angle depends on the chosen TR.

In T1 spin echo imaging, the selection of a short T1 determines that tissues with a long T1 will recover less than those with a short T1. Tissues that have recovered slower will have a smaller longitudinal magnetisation before the next RF pulse resulting in a smaller transverse magnetisation after the RF pulse. The short TE restricts the influence of the different T2 decay rates.

In proton density imaging, the selection of a long TR allows for recovery of the z magnetisation for the majority of tissues reducing the effect of T1 relaxation time differences. The 90° excitation pulse results in transferring a similar amount of signal into the xy plane for all of the tissues. A short TE restricts the amount of T2 decay for any tissue at any time. The resultant signal is high from all tissues with little differences between them. The main influence of the signal amplitude is the equilibrium magnetisation of the tissue.

The factors that influence the contrast in gradient echo imaging will be described in more detail in the gradient echo section of this chapter (2.5.5.4.8).

There are two main MRI pulse sequences which other specialised MR sequences are modified from and based on. These are: spin echo and gradient echo sequences.

2.5.5.4.7 Spin echo MRI sequence

Spin echo sequences are produced by applying a 180° RF pulse after the initial 90° excitation pulse. T2 relaxation induced de-phasing is a random irreversible process; the additional de-phasing caused by the static magnetic field inhomogeneities is potentially reversible. The application of a 180° RF pulse changes the sign of the relative phase in the xy plane; negative becomes positive and vice versa. All the spins come back into phase resulting in the FID to reach a maximum at TE, the echo time. In order to reverse the de-phasing produced by field non-uniformity, the 180°must be applied at a time of T/2. The signal that re-phases after the application of the 180° RF refocusing pulse is called a *spin echo*.

Fast spin echo sequences are a spin echo with the addition of even multiple spaced refocusing pulses to form an echo train. The extra echoes allow for acquisition of multiple lines of data i.e. to have different phase encodings for every echo in order to speed up data acquisition. The time between each

successive echo is called the echo spacing and is a fixed value. The echo train length is the number of echoes in the spin echo train. Acquisition times for fast spin echo imaging are therefore much shorter and are calculated by Equation 2-3:

$$\text{Scan acquisition time} = \frac{TR \times N_{pe} \times NSA}{ETL}$$

Equation 2-3 Equation to calculate the scan acquisition time of a fast spin echo sequence

TR = repetition time, N_{pe}= Number of phase encodings,
NSA = Number of signal averages, ETL = Echo train length

After the application of the 90° pulse in spin echo sequences, a 180° refocusing pulse is applied to 'flip' the direction of the magnetisation in the xy plane through 180°. The 180° pulse is used to reverse the loss of coherence (individual magnetic moments rotating together) caused by any inhomogeneities in the magnetic field.

2.5.5.4.8 Gradient echo MRI sequence

In gradient echo imaging the use of a smaller flip angle means that a shorter TR can be used, resulting in shorter acquisition times. The echo is produced by the de-phasing and re-phasing of the MR signal by an imaging gradient. In gradient echo imaging, the effects of magnetic field inhomogeneities are not compensated for, therefore the MR signal is affected by T_2* and not T_2. Because of this, shorter TE's are used.

There are two main types of gradient echo pulse sequences that are of particular importance in this thesis: Spoiled gradient echo (FLASH®, Siemens) and Double Echo Steady State (DESS®, Siemens). In FLASH sequences, any potential existing transverse magnetisation generated by each RF pulse is destroyed after it has been sampled preventing this from contributing or interfering to the signal during the following TR. This is

achieved by spoiling or dephasing the signal with a spoiler gradient at the end of each TR period or by RF spoiling [115].

Parameters for FLASH imaging allow for quick acquisition times to be achieved (one minute or longer depending on what is required by the operator) and can be used to image the body part in question dynamically whilst giving or after the administration of gadolinium.

Steady state generated echo techniques do not destroy the signal after sampling, but allow it to carry over into the next TR. This results in the generation of a new signal [Free Induction Decay (FID) component] and refocused signal in each successive TR. The imaging gradients can be used to control these signals by dephasing and rephrasing them at appropriate times. Manufacturers have developed a range of steady state sequences that emphasise the dephased components. For Siemens these include FISP (FID component) and PSIF (refocused echo component) and True FISP (all components combined). DESS is a hybrid technique that is available on Siemens platforms that separately refocuses the FID and spin echo components, and then combines the resultant image data into a single image. This results in a heavily weighted T2 image, but retains the signal from short T2 tissues, without potential artefacts formed when using True FISP [118]. In the final image, the combined two components give high resolution images with strong T2 weighting. Water excitation can be added to the scan and is currently being used in the ‘Osteoarthritis Initiative’ project to assess cartilage morphology [119].

2.5.5.4.9 Inversion recovery

Inversion recovery imaging is a type of MR imaging technique that allows for the ‘inversion’ or suppression of the signal of a tissue type from the image by selecting an appropriate inversion time.

The 180° pulses are also utilised to prepare the net magnetisation before the application of an inversion pulse. This ‘inverts’ the net magnetisation to be anti-aligned with the z axis resulting in a non-detectable signal inverting or suppressing the signal as used in the inversion recovery sequences

STIR imaging produces a sequence that demonstrates the fluid as hyperintense when compared to other structures imaged. STIR imaging is

commonly employed to suppress fat signal in a non-homogenous field where spectral fat suppression provides non-uniform results [120].

However, the inversion time may be altered to suppress or null any T1 time specified. The most appropriate inversion time to be selected is 70% of the chosen T1 of the tissue to be nulled [116]. Care must be taken in interpreting the images as any tissue with the selected T1 will be suppressed.

Fluid attenuated inversion recovery (FLAIR) imaging is another example of an inversion recovery technique which has been optimised to nullify the long T1 signal from cerebral spinal fluid (CSF) in brain imaging. This technique has been used routinely in clinical practice to increase the sensitivity of multiple sclerosis plaques in the brain and spinal cord [121].

Inversion recovery sequences can incorporate more than one TI time by applying more than one 180° inversion pulse and therefore null more than one type of tissue. Extensive research using this technique has allowed for greater sensitivity in detecting plaques in multiple sclerosis imaging [122].

2.5.5.4.10 T1 mapping

T1 mapping or relaxometry provides quantitative MRI data based on the T1 relaxation time constant. Each tissue type has a range of T1 values which is dependent on field strength [123-125]. Relaxation times can be used as a biomarker to identify normal and abnormal tissues [126]. Measurement of T1 values for normal and pathological tissue can be made in-vivo using inversion recovery sequences or variable flip angle spoiled gradient echo techniques [115].

The ‘reference standard’ for measuring T1 is the inversion recovery technique [127]. Inversion recovery measuring of T1 is a very long procedure. A series of multiple inversion recovery sequences using variable inversion times, with a TR of at least five times the longest inversion time is utilised to ensure there is adequate time for longitudinal recovery. Regions of interest are plotted onto the individual images for each inversion time and the readings are plotted onto a ‘fit model’ to calculate T1 values. This technique would not be practical in the clinical environment due to the possibility of patient movement and the lack of patient acceptability.

Variable flip angle spoiled gradient echo imaging can also be performed to calculate T1 values for tissues. This procedure is quicker than the inversion recovery process but is influenced by an inhomogeneous magnetic field and coil selection. A series of spoiled gradient echo images with a selected flip angle values are acquired with identical geometry. Signal intensities recorded in corresponding region of interest (ROIs) on each separate flip angle are then plotted into an exponential model to fit the data and calculate the T1 value. Figure 2-17 shows an example of measured signal intensities from a series of variable flip angle data sets plotted onto an exponential fit model. The model can calculate the T1 provided the TR value has been included in the equation (T1 calculated as 1426ms in this example).

flip angle	S(measured)
5	154
10	154
15	124
20	102
25	82
30	78
T1	1426

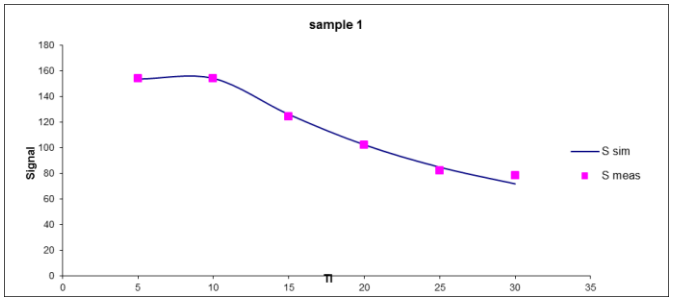

Figure 2-17 Example of T1 exponential fitting for a TR of 11ms.
S sim is simulated T1 fit and S meas is measured intensities from flip angle data.

T1 measurements can be represented in an image format where pixels are assigned the T1 value with a representative colour scale for each value [128]. This allows for a quick assessment of the T1 measurements without the use of complicated, time consuming manipulation of the data (Figure 2-18).

Molecules of hydrogen in fat display a procession which is nearly equal to the Larmor frequency and therefore decrease the T1 of these structures. Fat is hyperintense on T1 and T2 Turbo Spin Echo (TSE) imaging.

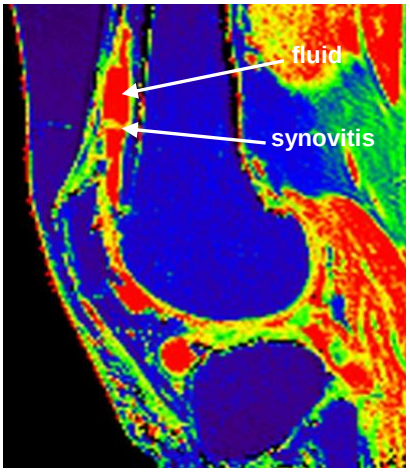

Figure 2-18 Sagittal T1 map of the knee joint of a patient with OA knee showing synovitis and synovial effusion.
Areas depicted by a blue colour delineate structures with small T1 values (~350ms) and areas of red are those are of higher T1 values (>1400ms)

2.5.5.4.11 Fat suppression

The suppression of fat signal may increase the conspicuity of certain anatomical and pathological structures especially after the administration of gadolinium [129]. In MRI there are various techniques that can be employed to achieve this: Spectral fat saturation, water excitation, Dixon, Spectrally Adiabatic Inversion Recovery (SPAIR) and Short Tau Inversion Recovery (STIR). These techniques are based on the different relaxation properties (STIR) of the off resonance frequencies (chemical shift) of the tissues (Dixon and water excitation, spectral fat saturation and SPAIR) [130].

The advantages and disadvantages of these techniques are presented in Table 2-5 [130].

Fat saturation technique	Advantages	Disadvantages
Dixon	• Insensitive to B_1 and B_0 inhomogeneities. • 4 contrasts for 1 acquisition	• Increases minimal TR
Spectral fat saturation	• Tissue contrast is not affected	• Sensitive to B_1 and B_0 inhomogeneities. • Additional preparation pulse increases minimal TR and acquisition time
Water excitation	• Reduced sensitivity to B_1 inhomogeneities	• Increased minimum TR, TE and acquisition time
SPAIR	• Insensitive to B_1 inhomogeneities • Tissue contrast not affected	• Increased minimum TR or reduced number of slices
STIR	• Insensitive to B_1 inhomogeneities	• Additional inversion pulse increases minimal TR and acquisition time or reduces number of slices acquired. • Tissue contrast is affected

Table 2-5 Advantages and disadvantages of different MRI fat saturation techniques [130]

2.5.5.4.12 Dixon Technique

Dixon imaging is a sequence that allows for fat and water imaging to be performed in a magnetic field that may not be homogenous [131]. Historically Dixon imaging was used for low field imaging when fat saturation was not possible due to the proximity of the fat and water peaks to each other [132]. Recently Dixon imaging technique has become popular and is used in clinical MRI as a reliable method of producing homogenous water or fat sensitive images [133].

Dixon imaging is a consequence of slightly different Larmor frequencies of tissues. Signal in or out of phase depends on the echo time for the gradient echo used. Each sequence produces the following images: In phase, out of phase, water, fat and combined images. The in phase image is the sum of the fat and water signal and the out of phase image is the difference between them [132]. To produce the water only image these two images are added together and the subtraction of the out of phase image from the in phase image results in the fat only image [115] (Figure 2-19).

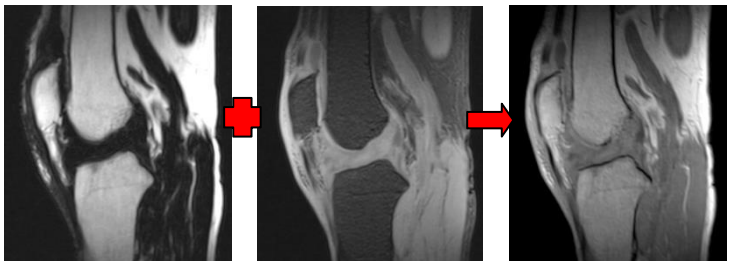

(a) Fat + Water = In phase

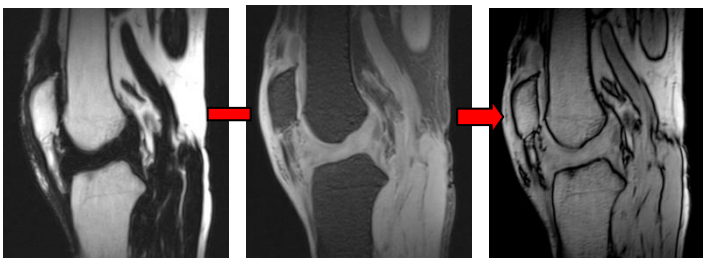

(b) Fat – Water = Out of phase

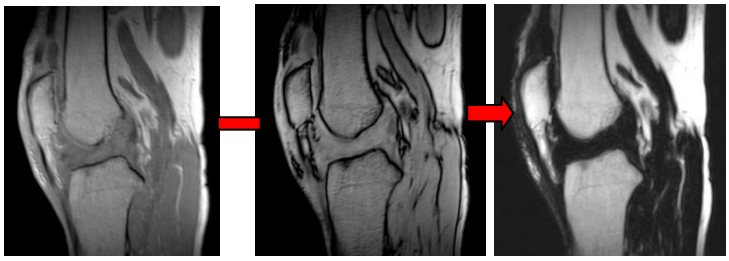

(c) In phase - Out of phase = Fat

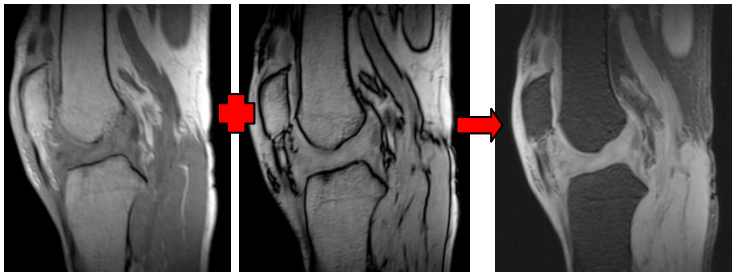

(d) In phase + Out of phase = Water

Figure 2-19 Dixon imaging as demonstrated in a knee MRI scan

(a) In phase sequence (b) Out of phase sequence (c) Fat sequence (d) Water sequence

2.5.5.4.13 Magnetisation Transfer

Magnetisation Transfer (MT) is a MRI technique that has been widely used historically in imaging of the neurological system where it increases the contrast on T1 and Time Of Flight (TOF) images allowing for greater sensitivity in pathology detection, and supressing the signal observed from the brain parenchyma tissue [134] .

MT is a technique that can be applied to certain pulse sequences to increase the contrast of the images.

MT is similar to frequency selective fat suppression in that a RF pulse is applied off resonance to suppress signal from tissues with wide ranges of Larmor frequencies related to the high macromolecule content of the tissue.

MT is used to supress protein-bound water: there are two groups of protons, those that are bound and those that are free. The restricted or bound proteins are not seen on normal imaging but they can influence the image by the exchange of energy between the two groups. This results in the magnetisation from the bound group moving to the free protons reducing the signal seen.

MT imaging can be either difference or more quantitatively using Magnetisation Transfer Ratio (MTR) images. Difference MT images demonstrate the calculated difference between the two images for each voxel and MTR images show the relative change in signal for each voxel [135].

The inherent nature of this technique results in effects that can be desirable or prohibitive in use [115]:

- Increased radio frequency power deposition
- Necessity to increase the TR and hence the scan time
- Fat becomes more conspicuous
- Increased contrast by reducing signal in some tissues

2.5.5.4.14 Diffusion Weighted Imaging

Diffusion Weighted Imaging (DWI) was first used in the brain to distinguish between infarct and reversible ischaemia following a stroke [136]. DWI measures the movement of free water molecules within a structure. High diffusion values are seen in healthy tissue where water has the ability to move freely and low values in insulted tissue, where the movement of water has been restricted for example caused by cell swelling. Different 'normal Apparent Diffusion Coefficients (ADC) values' have been applied to different organs and tissues depending on the structure of the tissue types.

Diffusion weighted imaging relies on the ability of the water molecule to move (Brownian motion). In a pure liquid, the molecules are able to move freely in any direction (isotropic movement). In tissue, the movement is restricted due to cell barriers. The water molecules therefore show a preferred path of movement dependent on the barriers. It has been proposed that diffusion within a joint effusion is restricted due to the organisation of cellular structures within the synovial fluid [137].

DWI measures the movement of free water molecules within a structure. High diffusion values are seen in fluid where water has the ability to move freely. On ADC images the fluid is hyperintense when compared to other structures of the knee (Figure 2-20).

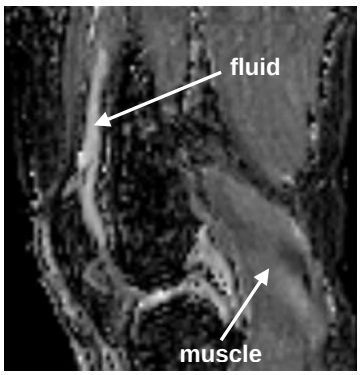

Figure 2-20 Sagittal ADC image of a DWI image of the knee joint in a patient with osteoarthritis of the knee.

Free moving water molecules with an unrestricted diffusion is shown as hyperintense signal in a synovial joint effusion in the suprapatellar pouch as labelled.

DWI has recently been applied to other organs and pathologies to determine the possibility of disease involvement, particularly cancer in the prostate,

breast, lymph nodes, liver and kidney. Axial single shot echo planar imaging (SS-EPI) has been used to produce ADC images for these structures. Rapid acquisitions ‘freeze’ tissue motion that would otherwise interfere with the measurement of diffusion. SS-EPI has its limitations in that it is very sensitive to tissue susceptibility differences thus producing gross artefacts at tissue interfaces such as bone and air. This is particularly problematic when imaging the posterior fossa of the brain, where there is a high bone and air burden due to the petrous bones and air in sinuses. The artefacts are greatly accentuated at higher field strength magnets such as 3T. Data sets commonly have poor resolution due to the decay of the transverse magnetization (average imaging matrix would be 128 x128). Greater resolution would be ineffective due to rapid signal decay. Alternative imaging sequences have been investigated to reduce these artefacts and allow for imaging to be performed in other planes rather than the axial one to demonstrate pathology within the inner ear (cholesteatomas). As the knee joint has large bones within the joint, the use of SS-EPI would be problematic producing artefactual images due to susceptibility artefacts caused by tissue boundaries that would preclude any diagnostic value.

2.5.5.5 Imaging of synovitis with conventional MR pulse sequences

Conventional T2 weighted imaging shows fluid as a hyperintense signal but this can be hard to distinguish from synovitis depending on the imaging sequence viewed. This can result in either over or under estimation of synovitis [54] as the fluid and synovitis are scored as one. In spite of the lack of ability to clearly differentiate synovitis from effusion, these techniques are still used in 2014 by Wang et al and Atukorala et al to determine the quantity of synovitis within a knee [138, 139].

Despite DESS being sensitive to flow artefact, it has been used to image the musculoskeletal system [140], in particular the articular cartilage of the knee joint [141].

Some sequences can be used to increase the conspicuity of fluid (STIR, T2 TSE and DESS) whilst others can suppress the signal such as cerebrospinal fluid (CSF) by Fluid Attenuation Inversion Recovery (FLAIR).

Fluid sensitive sequences including T2 fat saturated spin echo [142] and DESS imaging [143] have been shown to be useful in the detection of synovitis. The assumption that the inflamed synovium will have a greater fluid content and hence display the same imaging characteristics as fluid is the rationale for this approach. The literature contains a body of examples and validation of conventional sequences that show fluid on MRI scans as hyperintense signal on T2 weighted images [144, 145].

MRI characteristics of tissue are dependent on the T1 and T2 of the tissue. For example:

- Fluids have long T1 (1500ms - 2000ms) and long T2 values (700ms -1200ms)
- Water based tissue structures have medium T1 (400ms - 1200ms) and lower T2 values (40ms – 200ms)
- Fat based tissue structures have short T1 (100ms - 150ms) and short T2 values (10ms - 100ms)

The knowledge of these characteristics allows for suitable pulse sequences to be selected with appropriate scan parameters (TR, TE, Flip angles) which are chosen to allow for optimal contrast of the structures. Parameter choice also determines the scan time and resolution of the image and these can be manipulated to reduce movement artefact and decrease voxel size. The choice of pulse types such as spin echo, fast spin echo or spoiled or steady state gradient echo also affects the ability to visualise different tissue types [115]. Gradient echo sequences allows for 3D rapid imaging with T1 weighting when using short TR and TE’s [146]. Spin echo or fast spin echo imaging produce high resolution anatomical imaging for pathology assessment [147].These high resolution anatomical images can be used as masks or ‘maps’ for other sequences can be overlaid.

Some pathologies are best delineated using specific tailored sequences. For example, bone marrow oedema is clearly seen on DESS, MTR, proton density fat saturated (PD fs) , T1 mapping and T1 TSE sequences (as annotated on Figure 2-21) but is not as conspicuous on the T2 TSE sequences (Figure 2-21). The degree of the pathology can be accentuated or reduced by sequence selection.

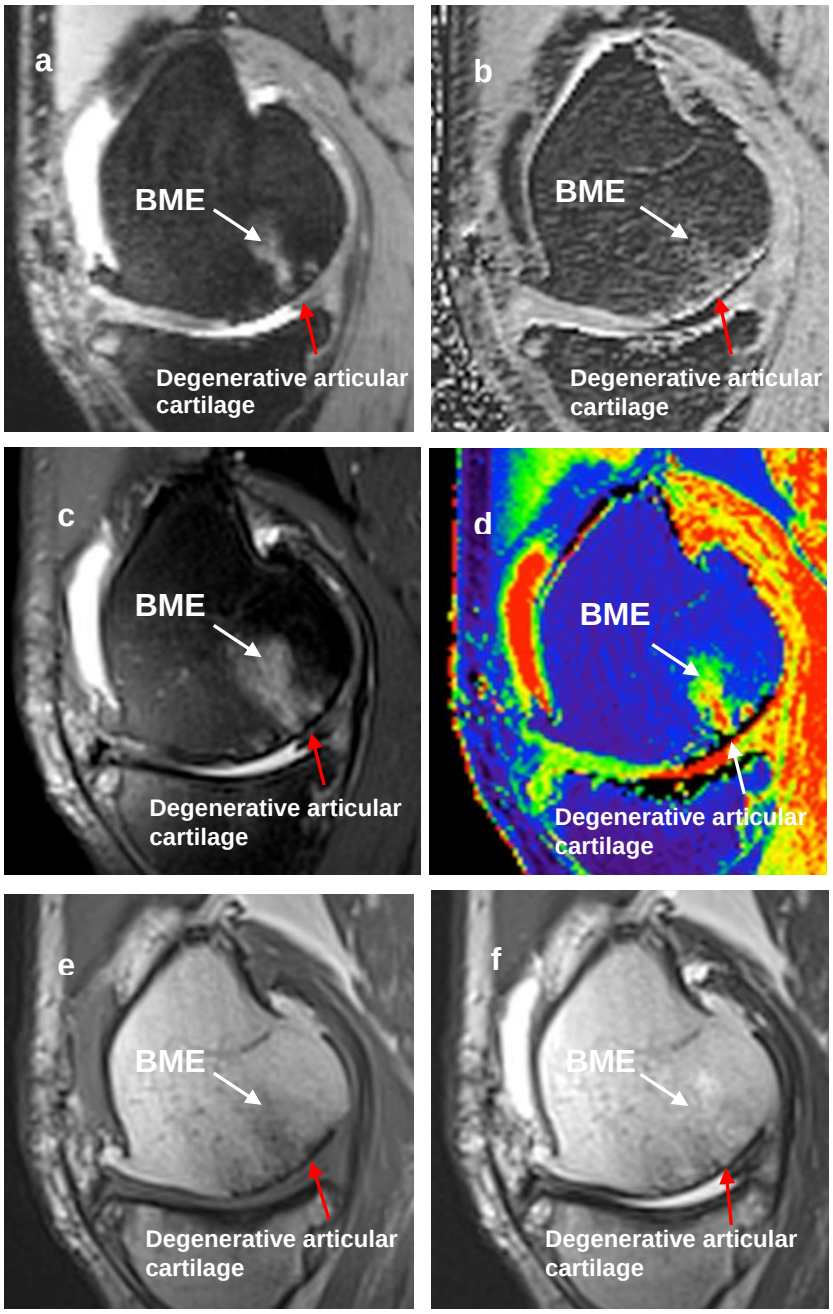

Figure 2-21 The importance of selecting the appropriate pulse sequence for detecting pathology.

Images showing degenerative articular cartilage in the knee with associated bone marrow oedema (BME) (a) DESS (b) MTR (c) PD fs (d) T1 mapping (e) T1 TSE (f) T2 TSE

Care must be taken when interpreting images without the full knowledge of anatomy as well as the physics involved with MRI. Artefacts that appear on some images can resemble pathology, for example magic angle effect results

in significantly increased signal intensity in tendons when aligned at around 55° to the direction of the main magnetic field [148-150]. This is caused by changes in the dipolar interactions between hydrogen protons which are loosely bound around collagen fibres. The resultant increase in T2 relaxation time causes focal increased signal on images that have a short echo time and can be mistaken for pathology such as tears [149, 151].

Fat planes exist between structures of the body and can be used to identify the limits of a structure. Whilst this may not be that significant in visualising large structures that have a known position, it may help in identifying those that have a varied position such as synovitis. Bone, articular cartilage, menisci and muscles have known anatomical positions and can be identified with a combination of anatomy knowledge and conventional MRI sequences. Synovitis however may or may not be present anywhere within the joint and is not uniform in position or volume from one patient to another or even in the same individual.

2.5.5.6 Quantitative imaging

2.5.5.6.1 Introduction

MRI is able to perform reproducible measurements using specially designed pulse sequences to produce images that provide quantitative data rather than qualitative or anatomical data. Quantification of tissue types by MRI allows identification of normal and abnormal tissue types [124]. Quantification of tissue composition and viability can aid in the detection of early pathology that is subtle and unidentifiable on conventional MR images. Longitudinal serial imaging using these methods can show the response to treatment or be used as a biomarker of disease progression.

2.5.5.6.2 Magnetisation Transfer

MT techniques have recently been implemented in musculoskeletal imaging for example in the assessment of articular cartilage [152]. The interactions of MT with different tissue types have been documented in the literature [153].

Not all tissues are affected by MT; tissues of the knee and their interaction and sensitivity with MT are summarised in Table 2-6.

Tissues that show MT effect	Tissues that do not show MT effect
Subcutaneous fat	Skeletal muscle
Bone marrow	Hyaline cartilage
Synovial Fluid	Tendons
Fast flowing blood	Menisci
	Ligaments
	Joint effusion
	Skin

Table 2-6 Structures of the knee joint and their interaction with the magnetisation transfer pulse [153]

Water only exhibits MT if it interacts closely with intracellular or extracellular macromolecules such as collagen [154]. Therefore, if synovitis represents cellular infiltration or fibrotic tissue rather than free water it might be expected to exhibit MT. Furthermore, simple measurements such as the MTR could allow quantification of such changes [123].

Because fluid within the knee joint is not free fluid, the effect of MT on the fluid is varied depending on the amount of proteinaceous matter within it. In Figure 2-22a, the image with MT, the area of synovitis is harder to visualise as the joint effusion has proteinaceous particles in it when compared to that without MT (Figure 2-22b). On the MT difference and MTR images, areas of fluid are able to be visualised from other structures but the effect of MT on the proteinaceous synovial fluid is not reflected in the MTR measurements.

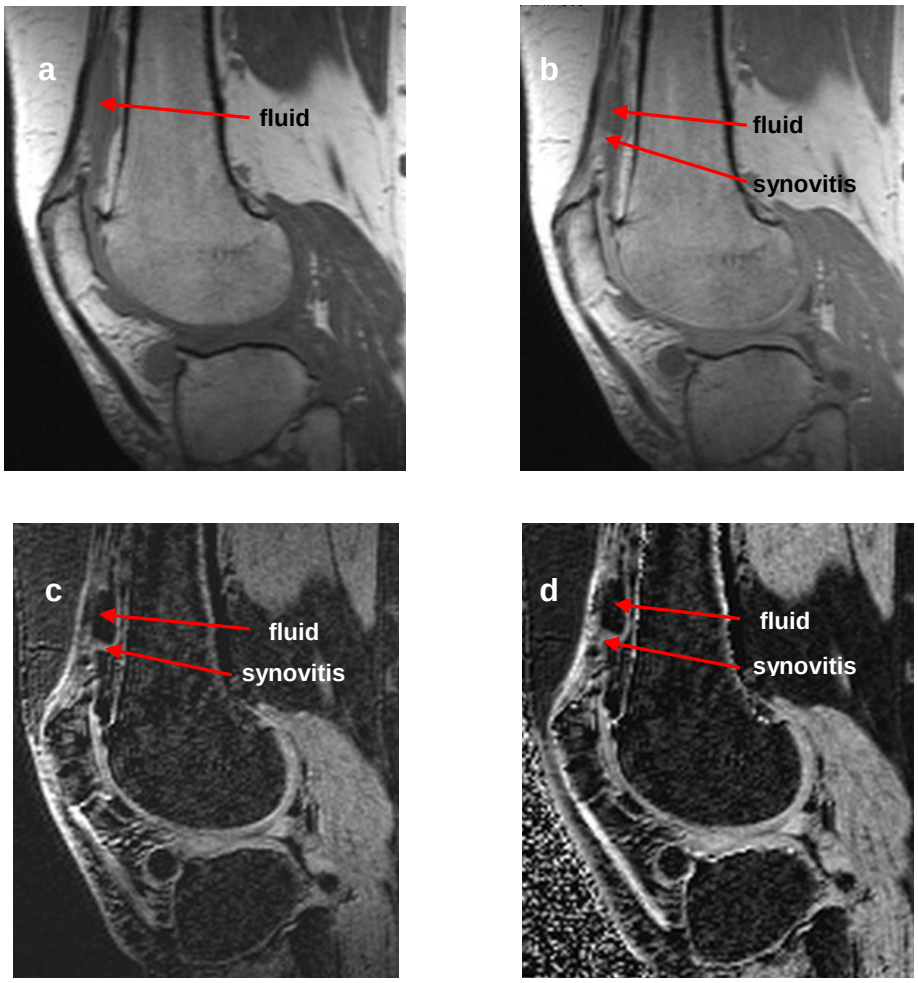

Figure 2-22 Sagittal MT images of the knee of a patient with osteoarthritis.

A synovial effusion is demonstrated in the suprapatellar pouch with synovitis surrounding it as labelled on the images: (a) SPGR + MT, (b) SPGR – MT, (c) MT difference, (d) MTR
SPGR = spoiled gradient recall echo

2.5.5.6.3 T1 mapping

Whilst the literature includes many papers recording T1 values for tissues of the body at 1.5T, the data from 3T scanning is scarce. Gold et al [118] published the first values for T1 and T2 times at 3T for musculoskeletal tissue in 2004 in vivo. This paper has been cited as the definitive record for these values. However, the sample size was small (n=5), the population scanned were young (27 – 38 years of age) and a transmit/receive coil was used.

More recently in 2011, Jordan et al from the same group published a second paper [119] in which the T1 values did not agree with those published in 2004

(Table 2-7). There were multiple steps in their methodology which may account for the discrepancies in both these studies:

1. Not selecting the same type of coil for both groups: The choice of a transmit/receive coil for volunteers and a receive only coil for the known validation samples.
2. Different validation samples for each study.
3. The lack of recording of temperature at the time of the experiments T1 measurements varies with temperature. Whilst it is assumed that the temperature is constant for both studies it has not been made explicit.
4. The choice of pulse sequence used.
5. The inappropriate choice of TR resulting in incomplete tissue relaxation.
6. Validation of results by scanning different individuals on the different MR field strengths resulting in comparison of two different subjects.

Stanisz et al in 2005 measured the T1 relaxation times of various organs of the body including skeletal muscle [123]. The limitations of this study included:

1. Small sample size (n=3)
2. Only in-vitro samples measured
3. The lack of description as to which muscle the samples were taken from
4. The demographics of the population of the samples
5. Measurements of T1 values made at 37°C

The summary of the results from these three studies are tabulated in Table 2-7.

	Gold et al [124] In vivo	Stanisz et al [123] In vitro	Jordan et al [125] In vivo
Cartilage (ms) (SD)	1240 ± 107	*	1015.6 ± 71.1
Muscle (ms) (SD)	1420 ± 91.7	1412 ± 13	1255.9 ± 57.9
Subcutaneous fat (ms) (SD)	288 ± 8.42	*	403.8 ± 17.7
Bone marrow (ms) (SD)	288 ± 5.27	*	381.2 ± 8.0
Synovial fluid (ms) (SD)	2850 ± 279	*	2564.7 ± 269.7

Table 2-7 Comparison of published T1 values for structures of the knee at 3T

The limited and conflicting results for T1 measurements within the literature of structures the knee warrants further work in this area to be performed and this is further confirmed by the lack of T1 data relating to synovitis.

Interestingly a paper was published in 2013 (after the commencement of the COSMOS study) by Ma et al in Nature [155] that hypothesised that tissue within the brain in each individual, had unique MRI quantitative characteristics which could be used as a ‘MRI fingerprint’. Ma proposed that a ‘MRI fingerprint’ could be acquired in the same acquisition time as a qualitative scan and be used as biomarker able to detect significant changes in tissues at a cellular level within the brain. The use of unique MRI tissue characteristics of the tissue within an individual may render qualitative scanning redundant when the results could be achieved using pattern recognising algorithms reducing measurement errors incurred by the observer and therefore increasing accuracy of disease identification. If this is possible in the brain then it should hold true with other structures of the body, such as the knee, providing appropriate parameters and algorithms have been selected.

2.5.5.7 Contrast enhanced MRI

2.5.5.7.1 Introduction

The main aim of the work described in this thesis is to develop MRI based techniques to replace the use of gadolinium based contrast agents to image synovitis in patients with OA of the knee. Chelated gadolinium is injected intravenously and results in shortening of the T1 of structures in which it accumulates in [156]. This is achieved by the resonance of the electron in the gadolinium chelate matching the Larmor frequency, which increases the rate of transfer of energy to the lattice thus shortening the T1 relaxation time.

Gadolinium enhanced MRI has been employed in many studies to assess the inflammatory processes (synovitis) in RA [157, 158]. Whilst the use of gadolinium has proved useful it is toxic and the association with the disease of nephrogenic systemic fibrosis (NSF) [159] in renal compromised patients has motivated alternative MRI techniques to be sought.

2.5.5.7.2 Contrast enhanced MRI of synovitis

Whilst non contrast MRI scanning has the capability to identify anatomical structures, it is limited in its sensitivity in differentiating subtle biomarkers of disease. Numerous studies have been undertaken to improve the sensitivity and specificity of this imaging modality in assessing patients with arthritis [160-162]. The administration of an intravenous contrast agent is common practice to help aid in the distinction of pathological markers from anatomical structures.

Contrast enhanced MRI (CE-MRI) is a well validated imaging tool able to demonstrate synovitis within the joints of patients with RA [163-167] . Whilst this technique is widely used to assess the joints of patients suffering from RA, it is not commonly used to study patients with OA.

Imaging of RA with contrast MRI is an essential tool for assessing synovitis within the knee and wrist joints [168]. Conversely, imaging of patients suffering with OA by MRI is not common in current clinical practice [169]. Inflammatory tissue such as synovitis appears as hyperintense signal (Figure 2-23). Studies looking at the involvement of synovitis involving the OA knee

joint and CE-MRI have been published whilst papers describing other joints such as the hand, spine and shoulder are limited or absent [169].

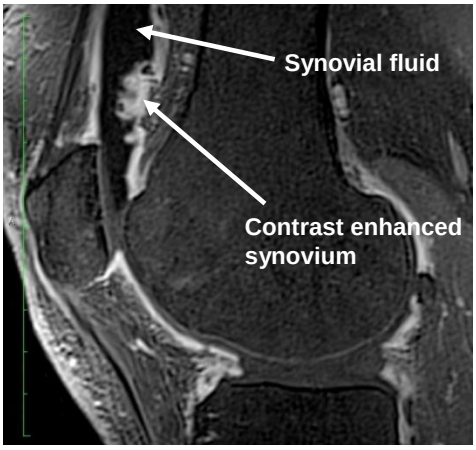

Figure 2-23 T1 sagittal gadolinium contrast enhanced MRI scan of an osteoarthritic knee.
The hyperintense signal on the images demonstrates synovitis within in the knee joint as annotated on the image.

Chelated gadolinium is the base of the majority of contrast agents used in MRI. Intravenous (IV) contrast agents can be used in conjunction with MRI scanning to delineate areas of inflammation within the human body. Gadolinium is a rare earth metal found in the periodic table at position 64. Gadolinium has paramagnetic properties and affects the T1 weighting of the water signal in the tissues. Binding gadolinium to a chelate decreases the toxicity of the metal to an acceptable level. There are numerous commercially available gadolinium contrast agents. These include:

- Dotarem® / Artirem® (Gd-DOTA)
- Magnevist® (Gd-DTPA)
- Omniscan® (Gd-DTPA-BMA)
- Eovist® (Gd-EOB-DTPA)
- ProHance® (Gd-HP-DO3A)
- Multihance® (Gd-BOPTA)

Choosing a particular MRI contrast agent is based on factors including: the half-life of the agent within the body, the excretion route from the body, cost and availability.

Each agent is slightly different due to the mechanism of binding of the gadolinium to the chelate. This allows for different excretion rates and routes and visualisation of different tissues or pathologies. Because of the bindings, each agent has a different rate of disassociation of the gadolinium ion and the chelate [159]. Some contrast agents disassociate more easily than others. Disassociation of the gadolinium ion can result in failure to excrete the gadolinium by the body and therefore potentially have a harmful effect on the patient. Decreased excretion rates of gadolinium can lead to NSF in patients with poor renal function [170]. NSF is a disease causing fibrosis of the skin and internal organs. It can lead to contractures, immobility and sometimes death [171]. NSF was first recognised in the United States of America in 1997. In 2006 a study in Austria linked NSF to gadolinium exposure [172]. Gadolinium has been found in the skin of patients suffering from NSF [173].

Gadolinium contrast agents are predominantly excreted by the kidneys. In patients with renal impairment, the total body clearance of gadolinium is considerably slower when compared to the norm. The time for clearance increases from 1.3 hours in healthy volunteers to 34.3 hours in patients on haemodialysis and up to 52.7 hours in patients on peritoneal dialysis [174].

Debate still ensues with regards to the potential number of patients that could potentially be exposed to NSF due to poor renal function. Davenport et al in 2015 reports uncertainty of risk in patients with an estimated glomerular filtration rate (eGFR) of less than 45ml/min/1.73m^2 but if there is a risk, it is greatest in patients with an eGFR lower than 30ml/min/1.73m^2 [175]. Conversely, Kanda et al in 2014 and McDonald et al in 2015 report that gadolinium has been found in brains of patients at post mortem who had previously had normal eGFR's [176, 177]. Whilst this may be the case, the results of these two studies should be considered carefully as all of the patients examined in these studies had been investigated for primary or secondary brain tumours and had therapeutic intervention (chemotherapy or direct radiotherapy to the brain) and therefore the blood / brain barrier would not be intact allowing for gadolinium to cross and accumulate there. Thus the

hypothesis that abnormal eGFR's do not influence the incidence of NSF is questionable.

Bjorkengren et al in 1990 [178] identified that the administration of IV gadolinium may be useful in detecting synovitis in symptomatic patients with acute RA. Since then, use of CE-MRI to image synovitis in patients with RA has been well documented and validated [179-181].

Whilst enhancing synovium is a sign of synovitis, normal synovium that is present may also enhance on MRI scans after the administration of contrast due to the normal vascularisation of the structure. Boegård et al conducted a study in 1996 in an attempt to demonstrate normal synovial enhancement of the knee. Ten healthy volunteers were imaged to determine the amount of enhancement of synovium in asymptomatic subjects [182]. The selection of subjects in Boegård et al study were of an age where degenerative changes of the knee may be expected (40 – 61 years of age). Patients were included in the study did not report pain and were not suffering from OA however no radiological procedure was performed to assess if there was any sub-clinical degeneration within the knee joint. Unsurprisingly the study demonstrated some mild non-uniform enhancement in all joint compartments of all study participants as well as degenerative pathology within the knee (torn menisci, articular cartilage lesions and a Baker's cyst). It is fair to suggest that the population studied by Boegård et al may not be normal healthy knees but are normal knees of that age group. Thus the demonstration of normal enhancement of the healthy synovium may not have been achieved in this study. Despite this, the study demonstrates that healthy synovium in asymptomatic patients does enhance and it is therefore important to appreciate the normal variances that occur in order to prevent over diagnosis of synovitis [183]. The degree of enhancement *and* the thickness of the enhancing synovium are markers which determine whether the images acquired depict pathological enhancement [163] and hence clinical importance.

The lack of literature relating to contrast administration and the timing of image acquisition in patients with OA has resulted in referring to studies relating to contrast enhanced MRI of the knee in patients with RA, presuming that the different arthritic disease processes affect the synovium in similar ways.

The importance of contrast agent use in visualising synovitis has been documented and the importance of timing of imaging post contrast has been debated in the literature. Imaging too soon after the administration of contrast will underestimate the amount of synovitis present [184] and imaging too late may conversely overestimate [185]. By imaging too quickly, there is the possibility that the contrast agent has not had adequate time to reach the vasculature of the synovium. By imaging too late, there is the possibility that the contrast agent may have had time to diffuse from the synovium into the synovial fluid (Figure 2-24).

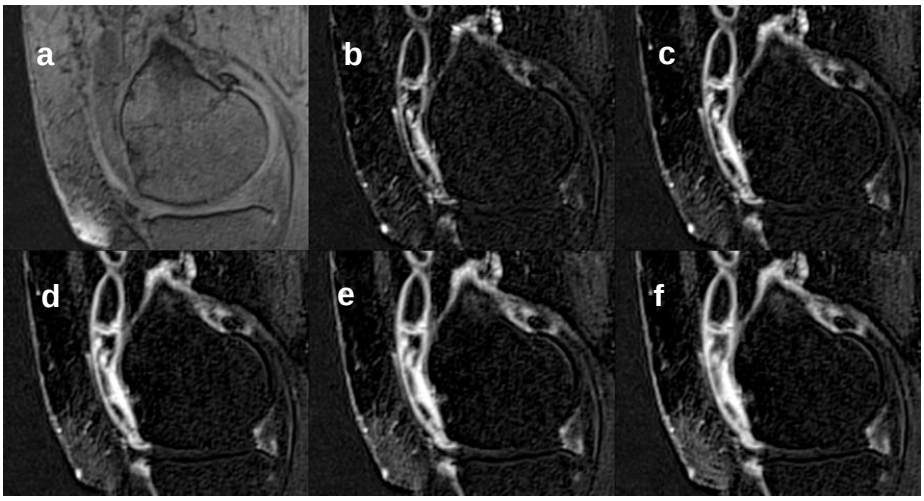

Figure 2-24 Sagittal SPGR pre and post gadolinium images of the medial compartment of a knee in a patient with osteoarthritis.
The images show the amount of enhancement at different timings post intravenous gadolinium administration. The variation in synovial volume visualised increases with time: (a) pre contrast, (b) 1.50 minutes, (c) 3.40 minutes, (d) 5.30 minutes, (e) 7.20 minutes, (f) 8.70 minutes.

Two studies have been undertaken to explore the importance of timing of imaging post contrast administration to maximise the conspicuity of synovitis and minimize that of the synovial effusion in patients with RA [186-188]. Whilst both studies show some agreement with each other, there are disparities between them. These are outlined in Table 2-8.

	Østergaard et al 2001 [188]	Yamato et al 2005 [186]
Number of patients studied	5 patients	17 knees 13 patients 2 healthy volunteers
Age range	43 – 81 years (mean 65 years)	Patients 39 to 68 years Volunteers not disclosed
Duration of knee symptoms	4 – 12 years Mean 9 years	Not recorded
Current medication	1 x methotrexate 1 x auranofin 3 x oral prednisolone 3 non-steroidal anti-rheumatic drugs	Not recorded
Study conclusion of appropriate time for imaging to commence after the administration of intravenous gadolinium	After 2.5 minutes and before 10 minutes	Optimal enhancement at 4.2 minutes

Table 2-8 Comparison of two studies assessing the timing of imaging post gadolinium [186, 188]

Østergaard and Klarlund [188] who are commonly cited with regards to the timings of scanning post contrast, used subjects that were being treated using the disease modifying drug; methotrexate. Methotrexate was shown to decrease significantly the volume of synovitis after the commencement of treatment (mean score 1.92 versus 0.14 at 12 weeks versus 24 weeks, $p<0.0001$) using the RA MRI scoring system (RAMRIS) scoring tool in a study researching its effect on the volume of synovitis in patients with hand RA by the same author in 2011 [189].

The question has to be asked as to whether the data from Østergaard and Klarlund's study is a true reflection of the physiology of contrast enhancement in patients with RA due to the probable effect of the disease modifying medications the subjects were taking? [188]

2.5.5.8 Non contrast enhanced MRI of arthritis

MRI is more sensitive than X-rays in detecting the destructive changes to joints in RA [190]. As noted previously, the conventionally accepted MR imaging approach requires the administration of intravenous contrast agents which is associated with cost and risk [191]. As a result, evaluations of MRI techniques that do not require the use of contrast agents have been performed to assess whether the omission of contrast agents alter the sensitivity and specificity of disease diagnosis and progression. Several techniques have been assessed to evaluate the ability of using conventional imaging and specialised pulse sequences in isolation, with varying degrees of success. A summary of the findings of these studies is presented in Table 2-9.

Authors	Patients	Sequence and plane	Scoring	Results
Hill et al [54]	20 Knee OA	Sagittal T2 fs v Sagittal T1 fs CE	Semi-quantitative. Grade 0 to 3 1 site	Non CE MRI underestimated synovial thickness in 6 cases and overestimated in 1 case when compared to CE MRI
Roemer et al [192]	50 Knee OA	Sagittal PD fs v Sagittal T1 fs CE	Semi-quantitative. Grade 0 to 3 At 6 sites	Fair to moderate agreement between non CE and CE MRI Hoffa's fat pad signal alteration showed high sensitivity (86-97%) but low specificity (10 to 38%)
Roemer et al [193]	111 Knee OA	Axial PD fs v Sagittal and axial T1 fs CE	Semi-quantitative. Grade 0 to 3 at 11 sites	Synovitis present in the majority of knee joints regardless of the presence of an effusion. Non CE unable to distinguish between synovial thickening and joint effusion

Table 2-9 Summary of non-contrast enhanced MRI studies assessing synovitis in patients with osteoarthritis of the knee.
The MRI sequences, synovial measurement tools are tabulated alongside a synopsis of the results of the study [169]
Contrast enhanced (CE)

As early as 1992, studies were performed to assess the possibility of using non-contrast enhanced conventional spin echo MR imaging to distinguish synovitis from effusion in the knee of patients with RA [194]. From 1051 scans reviewed, 550 patients demonstrated a synovial effusion and 12 of these showed thickened synovium. The imaging results were compared to biopsy results which confirmed that 10 out of the 12 had synovitis. This early study proved that it was possible to distinguish thickened synovium from fluid but a limitation was the absence of a negative diagnosis of synovitis in the patients that did not demonstrate a joint effusion on the MRI scan. In 2008, prompted by the advent of NSF, non-contrast enhanced (NC-MRI) was revisited to assess the possibility of imaging synovitis with MRI without intravenous contrast agents [142].Conventional sequences were again used to image the knee joints of patients affected by OA. T1 in and out of phase gradient echo images and T2 gradient echo images were used to examine 27 patients with a diagnosis of OA affecting the knee joint, through the patella region. Whilst this study concluded that again there was evidence that non enhanced MRI scanning can accurately assess the degree of synovial thickening in the major compartments of the knee joint, there was no correlation with a validated technique of synovium assessment; either with enhanced MRI scanning or biopsy. However, a reliability study using inter-reader correlation coefficient readings for two independent readers found good agreement ($r=0.82 – 0.92$. $p<0.0001$) [193].

An alternative method to assess the presence of synovitis used conventional spin echo MRI sequences to assess the agreement of signal alteration in Hoffa’s fat pad on unenhanced and enhanced contrast images [192]. This study relies on the hypothesis that the amount of synovitis demonstrated within Hoffa’s fat pad is representative of, and responds to, that of the whole knee joint. Conventional sagittal T1 spin echo pre and post contrast, and proton density fat saturated (in three planes) sequences were acquired. The study concluded that the unenhanced images showed high sensitivity (80-100%) but low specificity (25-36%) when assessing active inflammation within Hoffa’s fat pad on proton density fat saturated images [195]. The low reported specificity in this study could be due to two reasons: poor discrimination between low grade synovitis on the post contrast images and the appearance of normal synovium enhancement. Scoring synovitis on a single midline slice does not fully represent the synovial burden of the knee. The improvement of image contrast can be obtained by using MT contrast in

conjunction with compatible MRI sequences [196]. Whilst MT has significant benefits, the time penalty and increased heat deposition are limitations when compared to fat saturated images.

Østergaard et al in 2009 used conventional T1 spin echo pre and post gadolinium with STIR images to scan the hand and wrist joints of patients with RA (n=40 high field MRI, n = 45 low field MRI) [156]. This two centre study used three different scanners (manufacturers: Philips, Siemens and Esaote) with field strengths of 1.5, 1.0 and 0.2T and three different scanning protocols. In the attempt to compare like with like, the low field, 0.2T results will not be discussed in this report. The results from Østergaard's study showed that the removal of contrast agent did not affect the ability to detect bone erosions or bone marrow oedema (sensitivity 0.71- 0.95, specificity 0.84 - 0.96) but significantly affected the detection of synovitis (sensitivity 0.86 – 0.93, specificity 0.31 – 0.79) when compared to the reference standard of post contrast gadolinium imaging.

More recently, novel MRI scanning techniques have been used to assess the feasibility of imaging synovitis without contrast agents. The use of a double inversion recovery sequence was explored to examine the possibility of using it in a clinical environment and the results were compared with post contrast imaging [197]. Synovial fluid signal was suppressed from the joint effusion allowing for synovium to be identified. Unfortunately due to the length of the sequence repetition time required, (TR =8000ms), to image the structures with the longest T1 (synovial fluid T1 = 3620ms) the sequence is impractical. The TR is directly proportional to the scan time and lengthens the scan time, increasing the possibility of patient movement and intolerance rates. Although the protocol can theoretically scan 25 slices (3mm thick 0.3 mm gap: coverage 25.5 cm) in two minutes 20 seconds, the inversion time (TI) was only corrected for one slice to produce optimal tissue suppression. Therefore the scan would need to be repeated for every slice required: 25 slices required = 25 x 80 seconds = 33.3 minutes.

Fast Imaging Employing Steady-state Acquisition (FIESTA) imaging was investigated to see whether it could be used as an indicator of synovitis [198]. The detection rate was 57% with no indication of sensitivity or specificity of the technique. However there was no attempt to differentiate synovitis from the synovial fluid.

Diffusion tensor imaging (DTI) had been used previously to image the structure of ordered biological tissue. DTI measures the diffusion of water molecules in vivo and provides microstructural information of the tissues imaged [199, 200]. Because of the restriction of movement of water molecules due to cell membranes or other structures, water molecules exhibit preferential diffusion in some directions. The directional movement is called diffusion anisotropy (DTA). This can be used to assess tissue organisation at a microscopic level. DTI and DTA allow detection of an abnormality when it cannot be seen on conventional MRI [201]. Agarwal et al assessed its use in imaging synovium. Imaging changes were correlated with levels of inflammatory cytokines in the synovial fluid [137]. The study showed that DTI and DTA imaging can differentiate between normal and inflamed synovium as shown by the presence of inflammatory cytokines.

Whilst conventional imaging sequences and standalone novel techniques have not been entirely successful in imaging synovitis without contrast agents, there are clearly merits to some of each technique. The work of this thesis will utilise and combine multiple MRI sequences to determine if it is possible to image synovitis without the use of contrast agents.

2.6 Quantifying synovitis on MR images

2.6.1 Quantitative segmentation

The possibility of measuring reproducible finite volumes of synovitis is the holy grail of synovitis imaging. This would allow for comparison of the disease activity in relation to diagnosis and treatment. Many techniques have been proposed and assessed [202-205]. Whilst a validated scoring system is routinely used in scoring wrist joints in RA [187, 206-208] there is not an accepted method for measuring synovial pathology in the joints of patients with OA.

There are two fundamental methods for segmenting synovitis; automated and manual. Automated techniques are quicker and manual techniques are very time consuming and observer dependent.

2.6.1.1 Automated segmentation

Automated segmentation relies on the absolute value of pixel intensity after the administration of IV contrast agents and the degree of uptake by tissues. The pixel value can be selected to optimize the images and a ‘threshold’ applied to the image to visualise the tissue of interest [209]. Different methods for selecting the ‘threshold’ have been applied in studies to determine the most reliable method [188, 209, 210]. These include: setting a percentage enhancement [209]; signal intensity relative to muscle tissue signal [211] or interactively defined by seed placement in a specified area of values [212].

The percentage enhancement technique is the commonest method used to assess synovitis in patients with RA. Whilst this technique selects the areas of greatest uptake, care must be taken to ensure that the enhancing vascular structures are not included. Because this technique relies on the signal intensity of a pixel, good uniform fat saturation is required. Fat gives a high signal on T1 weighted MR images and this may be within the range of values that the automated software will pick up. This may be minimised by using subtraction images but if there is miss registration between the pre and post contrast images it may not resolve this issue. Dedicated software is required to perform this task and appropriate training is required for the operator. Automated segmentation has been demonstrated to take between ten and fifteen minutes to perform in one study [213].

2.6.1.2 Manual segmentation

Manual segmentation is a very time consuming subjective method of calculating synovial volume. The average time required to use this method in one patient is 60 minutes [213] but it can take as long as two hours depending on the volume of synovitis present [187]. By virtue of the nature of this method, it is not as accurate as an automated technique. This is due to:

- The observer's ability to detect the differences in pixel intensity
- The inaccuracy of drawing around structures by manual tracing with a computer mouse
- The quantity and complexity of volume of synovitis that has to be assessed

There is not the requirement to produce bespoke software but this technique requires extensive training of the operator in pattern recognition and interpretation to allow for accurate measurements of synovial volumes to be carried out. The greatest hindrance associated with this technique is the lack of dexterity of both the operator and tools, and the accuracy of region placement for explicit demarcation of synovitis from other structures within the knee. Drawing a manual area of interest with a mouse around a small area is difficult despite the lack of training. Even with experienced observers, inter-observer reproducibility has only been demonstrated to be about 5% for manual segmentation in the knee [205].

Automated segmentation is a technique that allows for identification of synovitis from other structures of the knee by applying a threshold pixel value by which every pixel with a value above or below this value is removed or kept in the image. This technique however does not allow for distinction between synovitis and blood vessels, for example, only purely on the value of the defined pixel threshold. When compared to automated threshold segmentation of synovitis, manual segmentation is more accurate in that the trained operator does have the advantage over the automated technique in identifying inhomogeneity of fat saturation and presence of vessels, and can preclude them from the segmented volume.

2.6.2 Scoring of synovitis on MR images

In order to simplify and increase the accuracy in measuring synovial volume within the knee joint, alternative methods have been proposed. Semi-quantitative scoring to assess synovitis in specific areas of the knee has been adopted to provide a representation of the disease burden. These are based on features in specific areas of the joint that are believed to be important in the classification of disease severity [214]. Bone marrow lesions,

cartilage integrity, ligaments and synovitis have been used to produce a reliable scoring system. For the purpose of this review, synovitis will only be discussed. Whilst the entire volume of synovitis will not be measured these techniques give a representation of the disease process within the joint.

There have been a number of iterative developments of semi-quantitative scoring tools. These are:

- Whole Organ Magnetic Resonance Imaging Score (WORMS) 2004 [215]
- Knee Osteoarthritis Scoring System (KOSS) 2005 [216]
- Boston-Leeds Osteoarthritis Knee Score (BLOKS) 2008 [203]
- MRI Osteoarthritis Knee Score (MOAKS) 2011 [214]

A summary of the scoring tools are documented in Table 2-10. While all of these tools have their merits, none of them provide a practical method of globally scoring the knee joint to provide a whole joint volume of synovial burden.

Semi-quantitative measuring tool	Synovitis scoring criteria	Inter-reader agreement	Intra-reader agreement
BLOKS [203]	Size of signal change in Hoffa's fat pad: 0 = normal 1 = mild 2 = moderate 3 = severe	Weighted kappa (95% CI) 0.62 (0.05-1.00)	N/A
KOSS [216]	Synovial thickening scored as present or absent on sagittal T1 SPGR images.	ICC (95% CI) = 0.74 (0.58 to 0.85) Weighted kappa = 0.69	ICC (95% CI) = 0.81 (0.69 to 0.89) Weighted kappa = 0.77
WORMS [215]	Scoring scale 0 to 3. Combined effusion and synovitis score for the estimated maximum distention of the synovial cavity. 1 = < 33% 2 = 33 to 66 % 3 = > 66%	ICC = 0.74	N/A
MOAKS [214]	On a non-defined sagittal PD/T2 fs image one single score for hyperintensity within Hoffa's fat pad 0 = normal 1 = mild 2 = moderate 3 = severe On a non-defined sagittal PD/T2 fs image one single score for effusion renamed effusion/synovitis	Hoffa synovitis: ICC (95%) = 0.70 (0.47 to 0.93) Weighted kappa 0.75 Effusion / synovitis: ICC (95%) = 0.72 (0.52 to 0.92) Weighted kappa = 0.70	Hoffa synovitis: ICC (95%) = 0.42 (0.14 to 0.70) Weighted kappa 0.55 Effusion/ synovitis: ICC (95%) = 0.90 (0.78 to 1.00) Weighted kappa = 0.90

Table 2-10 Comparison of 3 different semi-quantitative synovitis scoring methods for non-contrast MRI assessment of synovitis within an OA knee.

Guermazi et al in 2011 described a method to assess the whole knee joint in patients with OA of the knee [202]. The representation of the synovial burden is dependent on the area of the knee joint that is assessed. Roemer et al in 2010 described the commonest areas of synovitis present in the knee joint [193]. In 111 knees, the frequency (%) of synovitis was recorded in selected compartments of the knee. The study acquired images in two planes; sagittal and axial. Image acquisition commenced three minutes following the administration of intravenous contrast agent. Each scan took four minutes to

obtain resulting in the images being acquired between three and 11 minutes post contrast administration. Whilst the images were acquired in line with published recommended timings [188] the disparity of timings between the two data sets (sagittal and axial) may over or under emphasize the degree of synovitis present. The grade and definition of synovitis was defined is presented in Table 2-11.

Grade	Definition
0	Physiological enhancement and no synovial thickening
1	< 2mm (equivocal synovial thickness)
2	≥ 2- 4 mm (moderate synovitis)
3	> 4 mm (severe synovitis)

Table 2-11 Definition of grade of severity of synovitis on post contrast MRI images of OA knees utilised in a study conducted by Guermazi et al [202].

The findings of the anatomical distribution and severity of synovitis disease in patients with knee OA as described by Guermazi et al are summarised in Figure 2-25 and Figure 2-26.

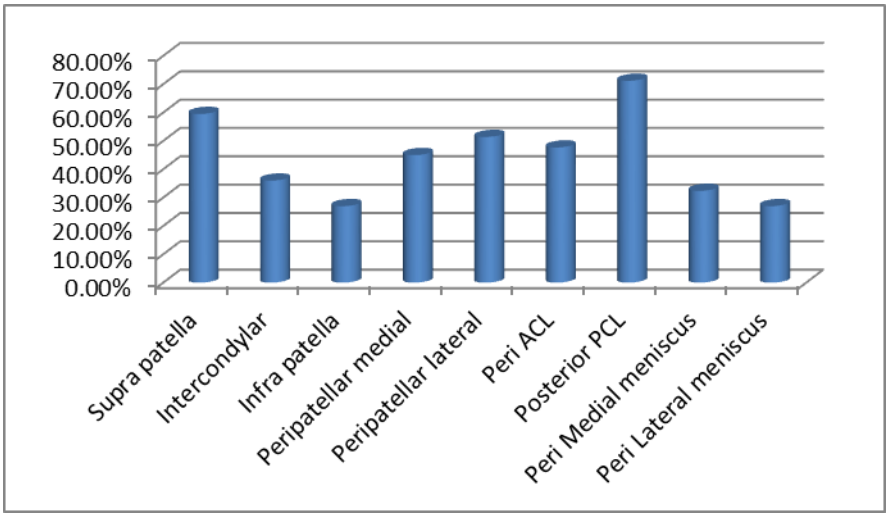

Figure 2-25 Anatomical distribution of synovitis in the knee joint of patients with osteoarthritis.

The graph is a visual representation of a table of results described by Guermazi et al in 2011 [202]

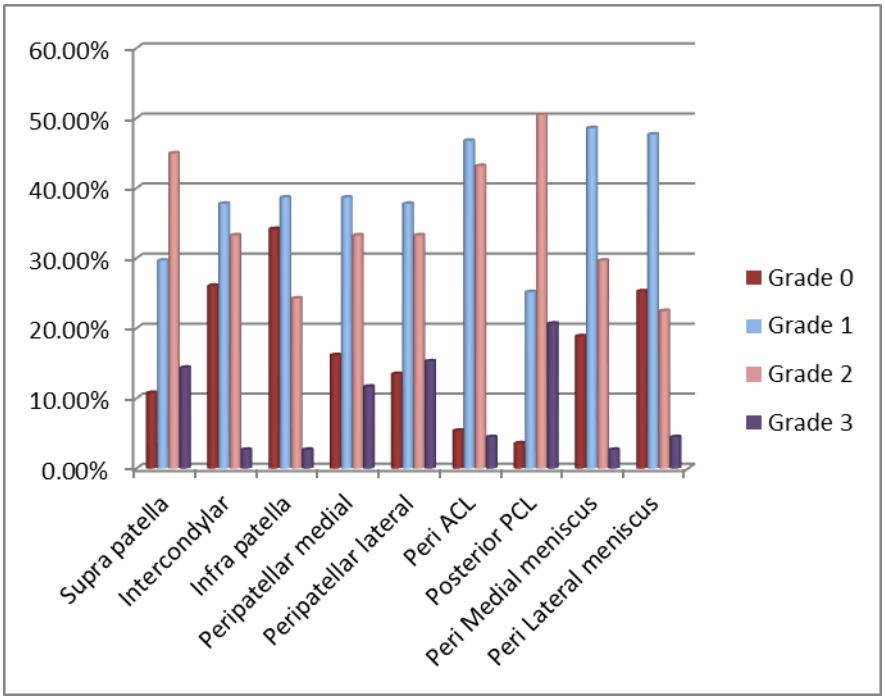

Figure 2-26 Severity of synovitis by anatomical area of the knee joint of patients with osteoarthritis.

The graph is a visual representation of a table of results described by Guermazi et al in 2011 [202]

In order to minimise the complexity of semi-quantitative synovitis scoring systems, Guermazi et al used the findings by Roemer et al to develop a reproducible scoring mechanism. Eleven anatomical sites were selected to measure the severity of synovitis. They were those identified by Roemer plus two additional areas: adjacent to loose bodies and within Bakers cysts if present [202]. The measurement of synovitis is explained in detail but raises two issues. Firstly, the plane used to image the knee in this study is not localised to the lateral femoral condyle as is done in normal practice. Instead the medial femoral condyle was used thus producing an image of the mid patella and ACL on one slice which is not routinely seen in clinical imaging.

In the second instance the use of the ACL as an anatomical landmark to assess synovitis is questionable. Hill et al demonstrated that ACL integrity is low in patients with OA and therefore this landmark may not be visible in some patients being assessed [217].

Despite these limitations, the scoring system produced by Guermazi et al scoring system gives a representative global assessment of synovitis in the knee joint as all compartments of the joint are assessed and scored. Other studies have looked at the presence and severity of synovitis but only measure in selected locations of the knee joint and may not give a true reflection of the disease burden. Rhodes et al proposed a semi quantitative scoring system concentrating on the parapatellar area of the knee [204]. One site posterior to the femoral condyle was also assessed but the supra patellar, infra patellar and Hoffa's fat pad were completely ignored. The absence of synovitis in the patella area does not preclude the presence of synovitis in other areas of the knee [193].

2.7 Summary

OA is the most common musculoskeletal disease that has a large socio-economic burden on society and the knee joint is the most commonly affected joint. The debilitating outcome of this disease results in a substantial impact not only to the individual, but society in general. Our understanding of the disease process has changed recently, moving from a bone centric disease to one of an inflammatory whole joint process. Recent advances in

medical imaging have provided the opportunity to identify stages in the disease process providing a better understanding of the driving forces and tissue involvement. As a result, synovitis has been seen to be a biomarker and accelerator of the degenerative process of OA. As demonstrated in this chapter, there has been a distinct lack of studies looking at the involvement of synovitis in the knee in patients with OA. Those studies that have been carried out looking at the knee both in OA and RA conventionally utilise IV gadolinium contrast agents to assess the synovial volume within the knee joint.

Adapting the validated technique of MRI to visualise synovitis without the need for intravenous contrast agents would allow for greater and safer access to clinical imaging of the disease, whilst providing the potential for new methods to monitor disease progression.

Analysis of non-contrast MRI scans using simple reproducible and time efficient scoring systems would improve the acceptance of non-contrast MRI of OA in the clinical environment.

The following chapters of this thesis will explore the potential techniques that can image synovitis without the use of IV contrast agents and correlate these with the current validated ‘reference standard’ techniques involving the use of contrast enhanced MRI.

Chapter 3 Retrospective analysis of existing MRI data held in LMBRU

3.1 Introduction

The NIHR funded LMBRU Imaging Unit was opened in 2009 as a research centre devoted to the assessment and treatment of musculoskeletal conditions, with a particular emphasis on arthritis. The unit has dedicated imaging facilities (3 Tesla MRI scanner and high resolution ultrasound), which have been used to evaluate the involvement of the arthritic disease process in joints and assess response to treatments. Since 2009, 34 research studies have been undertaken in the unit using the MRI scanner to image the joints of patients with musculoskeletal conditions. As a result of this, the LMBRU has a large existing database of research-specific MRI scans of pathology associated with arthritis at various stages of the disease process.

3.2 Aims and objectives

The aim of this chapter was to review LMBRU MRI data to explore potential MRI sequences to provide an initial framework for imaging synovitis in patients with osteoarthritis without the use of contrast agents.

3.3 Methods

In order to identfy potential MR sequences, a review of existing data acquired at the LMBRU was performed. Possible candidate sequences for non-contrast MRI (NC-MRI) of synovitis were assessed and strengths and

weakness explored to ascertain whether any of the sequences were potentially suitable for imaging synovitis. These sequences included:

3.3.1 Those sensitive to fluid and hence potentially sensitive to synovitis

3.3.3 Magnetisation transfer contrast

3.3.4 Quantitative T1 mapping sequences

3.3.2 Quantitative T2 mapping sequences

3.3.5 The Dixon imaging technique

This chapter will describe the overview, method, results, discussion and a review of findings for each candidate sequence, followed by an overarching summary.

3.3.1 Fluid sensitive sequences

3.3.1.1 Introduction

MRI sequences demonstrating high signal from fluid have commonly been used to identify effusions and oedema within structures associated with inflammatory processes [143, 218, 219]. Studies have been performed previously to explore the potential for replacing the use of intravenous contrast agents to visualise synovitis with fluid sensitive sequences [142, 220] and other studies have suggested that a fluid sensitive sequence could be of use to visualise synovitis within the knee [8, 18, 120, 220, 221].

3.3.1.2 Method

A review of the archived data within the unit was performed to assess which fluid sensitive sequence was the most sensitive and specific for visualising synovitis. Although the knee was the target joint in the final study (Chapter 5) LMBRU imaging studies involving patients with OA of the knee was limited. Only one study had been performed within the unit involving patients with OA

knee (n = 24 patients), to assess the response of bone marrow lesions in the knee to intra-articular steroid injections.

Conversely, the number of studies in the LMBRU involving patients with RA is much greater. There have been six large studies of the hand in RA involving in excess of 400 patients with multiple MR imaging visits and these were chosen to assess the sensitivity of fluid sensitive imaging sequences in the imaging of synovitis. The data within the unit represents a comprehensive range of disease presentation and severity.

The justification for using the hand data of RA patients was:

- Synovitis is present in both rheumatoid and osteoarthritic joints and presumed to have similar imaging characteristics in both large and small joints
- The volume of hand data available would provide a large enough cohort of scans (n = 58) to assess the suitability of sequences to image synovitis
- The conspicuity of fluid would be less in the small joints of the hand and therefore if the sequence could identify fluid within small joints the process would be transferable to larger joints e.g. the knee.

A retrospective assessment was undertaken on 58 hand and wrist scans performed on patients with RA. All of the data sets were anonymised and a mid-volume slice reviewed for the presence or absence of synovitis in the hand or wrist. Post contrast images were used as a reference standard in the absence of a gold standard of histology.

In order to explore the sensitivity and specificity of each image sequence in identifying synovitis, the non-contrast images were randomly reviewed prior to the post contrast data sets and scored using the RAMRIS scoring reference image atlas to confirm the presence or absence of synovitis [222]. The images were scored over a period of a week to help minimise the bias associated with the viewer recognising matching data sets. The sequences reviewed were all coronal views:

- T2 weighted turbo spin echo fat saturated (T2w fs) metacarpo-phalangeal joints (MCPs) (TR 4390ms, TE 77ms) Scan time 3.54 minutes
- T2w fs wrist (TR 4390ms, TE 77ms) Scan time 3.54 minutes
- STIR whole hand (TR 4450ms, TE 83ms, TI 220ms) Scan time 3.57 minutes
- DESS whole hand (TR 14ms, TE 5ms, FA 25 degrees.) Scan time 3.43 minutes
- Post contrast Volume Interpolated Breath-hold Examination (VIBE) whole hand (TR 12ms, TE 3ms, FA 30 degrees) Scan time 4.25 minutes acquired at 5.04 minutes after the commencement of the administration of gadolinium (i.e. 9.29 minutes)

The presence or absence of synovitis demonstrated on the images was scored by an experienced observer using a binary tool, one = present, 0 = absent on the matched images. The sensitivity and specificity of the imaging sequences to identify synovitis within the hand and wrist joints on MRI using non-contrast MRI and post gadolinium sequences are presented in Table 3-1.

3.3.1.3 Results

Although both the DESS and VIBE data sets were acquired in a 3D volume, the 3D data sets were reconstructed to produce 2D images matching the location and slice thickness of the 2D sequences (STIR and T2w fs) to allow for direct comparison of the different data sets.

Of the 58 scans, 51 showed synovitis on the post contrast VIBE images. Without the validation of the diagnosis of synovitis by histology, the reference standard was taken to be enhancement of synovitis on post contrast gadolinium VIBE MR imaging.

Sequence	Sensitivity	Specificity
Coronal DESS hand and wrist scan	96%	71%
Coronal T2w fs metacarpal scan	25.6%	12.5%
Coronal T2w fs wrist scan	47.2%	100%
Coronal STIR hand and wrist scan	38.8%	100%

Table 3-1 The sensitivity and specificity of scoring hand and wrist MRI scans of 58 patients with RA for the presence of synovitis using non-contrast sequences, scored against the VIBE post-contrast scans as the reference standard.

3.3.1.4 Discussion

Hyperintense structures demonstrated on the post contrast gadolinium VIBE images were considered to represent synovitis. However, the timing of the VIBE acquisition of the images assessed was nearly ten minutes after the administration of gadolinium. As discussed in the literature review, although the scan was acquired within the recommended ten minutes post gadolinium injection [188], the possibility of synovial fluid enhancement is high at this time point. This raises the question as to whether the enhancing tissue represents only synovitis or a combination of synovial fluid and synovitis.

As no gold standard or alternative reference standard of histology is available, the hyperintense signal on the post contrast gadolinium images was taken to represent only synovitis and the non-contrast images were compared to these to assess the presence or absence of synovitis. However, this reference standard may not be perfect and synovial fluid that has had gadolinium diffuse into it may contribute to some of the hyperintensity seen on the post contrast images thus overestimating the volume of synovitis present.

Of the data reviewed, the DESS images correlated best with the post contrast VIBE images for the detection of synovitis (sensitivity 96%, specificity 71%) (Figure 3-1). Possible reasons for the DESS scoring higher sensitivity than the T2w fs images are:

- Potential non-uniformity of fat saturation on the T2w fs, despite scanning the hand and wrist in 2 separate acquisitions and providing for the anatomy of interest to be in the isocentre of the magnet when scanned (the most homogenous part of the magnetic field).
- That the patient moved their hand from the original position removing it from the isocentre of the MRI
- That the patient moved during the scan resulting in movement artefact on the images reducing the visual quality of the images.
- Reduction of visualisation of vascular structures on the DESS allowing for greater conspicuity of the synovitis present.

The results of the scoring of the DESS images compared favourably to the results from Østergaard et al in assessing synovitis using both STIR and T2w fs images [156], who reported sensitivity 90%, specificity 49% in the MCP area, and sensitivity 87%, specificity 42% in the wrist [156].

The imaging of the MCPs and wrist using a T2w fs sequence required two separate acquisitions to be obtained. This was in an attempt to place the anatomical part of interest in the most homogenous portion of the magnetic field to facilitate a uniform fat saturation of the scanned images. Each T2w fs sequence took nearly four minutes to obtain, resulting in a total of eight minutes scanning to image the entire hand. The DESS scan also took four minutes to acquire and needed only one acquisition to cover the entire hand and wrist. The DESS scan was shown to be more sensitive to imaging synovitis in the hand and wrist in approximately half the time for T2w fs imaging. There is decreased visualisation of vessels on DESS images when compared to T2w fs or STIR images minimising the possibility of mistaking vessels for synovitis and thus increasing the specificity for imaging synovitis. The decrease in specificity in DESS imaging when compared to T2w fs imaging is probably due to the inability to differentiate between fluid and synovitis.

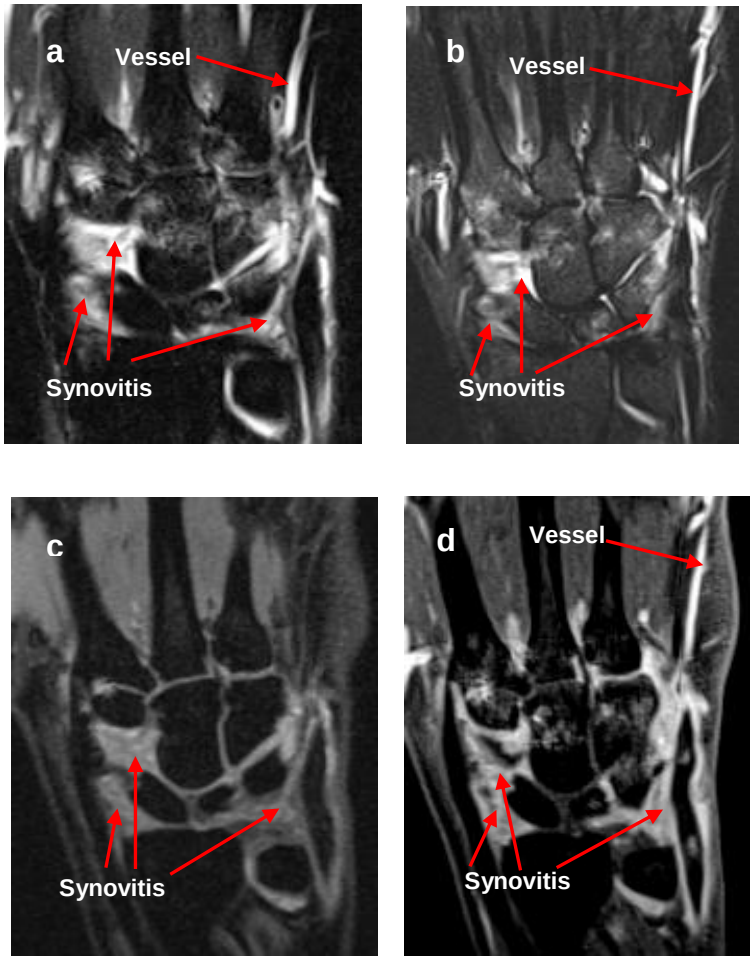

Figure 3-1 Coronal wrist images of a patient with rheumatoid arthritis demonstrating synovitis.

(a) T2 weighted fat saturated, (b) STIR, (c) DESS, (d) VIBE post contrast.
Both synovitis and vessels appear as hyperintense structures on the images above (as labelled)

3.3.1.5 Summary of findings: fluid sensitive sequences

As a result of these findings, it was decided to incorporate the DESS sequence into the first iteration of the non-contrast protocol as:

- DESS is a 3D sequence allowing for high resolution thin imaging with isotropic voxels that can be reconstructed into any plane
- When scoring for the presence or absence of synovitis the DESS results compared well with the literature.

- The uniformity of the fat saturation on the T2w fs images varied considerably. The probability of non-homogenous fat saturation on the T2w fs images could increase when imaging the knee as a larger field of view is required and the knee will not be in the isocentre of the magnet.
- T2w fs and STIR images are 2D sequences unlike the 3D DESS.
- STIR images have a uniform fat suppression but have a low SNR and resolution when compared to the DESS and T2w fs images
- DESS imaging takes approximately half the time to acquire when compared to the T2w fs scans

3.3.2 Magnetisation Transfer

3.3.2.1 Introduction

Magnetisation Transfer (MT) is a technique that can be applied to certain pulse sequences to increase the contrast of the images. Previous work performed by the candidate [223] has shown that it was possible to identify synovitis on SPGR difference images calculated from images with and without MT (Figure 3-2).

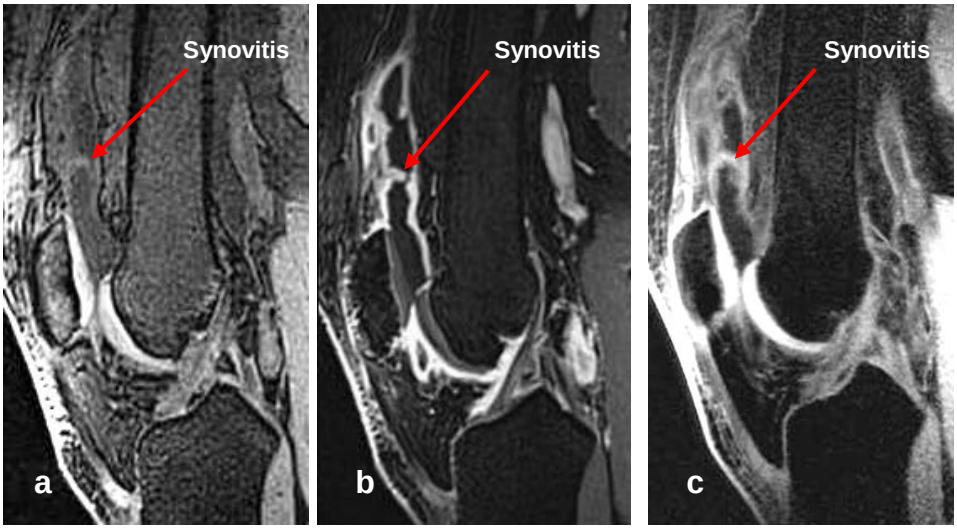

Figure 3-2 Sagittal knee MRI scans of a patient with osteoarthritis

(a) Unenhanced VIBE image (b) Enhanced VIBE image (c) MT difference image. The presence of synovitis on the unenhanced VIBE image (a) is difficult to visualise due to the similarity of signal characteristics with other tissues on this image. On the MT difference image (c) the synovitis is clearer due the differences of the interactions of tissues with the MT pulse.

3.3.2.2 Method

A pilot study was performed to assess the agreement between SPGR MTR images and post contrast VIBE images. Existing MRI data of twenty patients diagnosed with arthritis (OA n=15, RA n=5) affecting the knee were reviewed. The demographics of this cohort are described in Table 3-2.

	Gender	Age	Disease
Patient 1	Female	70	OA
Patient 2	Female	75	OA
Patient 3	Male	72	OA
Patient 4	Male	61	OA
Patient 5	Female	53	RA
Patient 6	Male	58	OA
Patient 7	Female	43	RA
Patient 8	Male	59	RA
Patient 9	Female	45	RA
Patient 10	Male	62	RA
Patient 11	Female	68	OA
Patient 12	Female	74	OA
Patient 13	Female	82	OA
Patient 14	Male	65	OA
Patient 15	Female	76	OA
Patient 16	Female	75	OA
Patient 17	Female	57	OA
Patient 18	Male	49	OA
Patient 19	Female	63	OA
Patient 20	Female	66	OA

Table 3-2 Demographics of the patients with MTR data that was scored to assess agreement of the presence of synovitis when compared to post gadolinium contrast images

2D sagittal SPGR images with and without MT (TR 450ms, TE 2.5ms, flip angle 30 degrees) and a matching 3D sagittal water-excited VIBE scan (TR 9.3ms, TE 4.9ms, flip angle 30 degrees) following the administration of intravenous gadolinium contrast agent were assessed. The MT pulse utilised was a Gaussian pulse and 500 degree flip angle with an offset frequency of 1950Hz and duration of 9984 micro seconds.

Subtraction of the SPGR images ± MT was performed to produce a MT difference image, where the SPGR image without MT is subtracted from the SPGR image with MT using algorithms built in to the MRI scanner. A midline image through the body of the patella was selected as the optimal slice for the radiologists to assess the volume of synovitis in an attempt to provide the greatest amount of synovitis on one single image i.e. suprapatellar pouch, Hoffa's fat pad and infrapatellar pouch. An example of the image used can be seen in Figure 3-2. A single representative slice was chosen as it would be impractical to segment and score the entire data set in a timely fashion due to the volume of data acquired.

Two consultant radiologists independently segmented and measured the synovial volume on the anonymised images. The unenhanced MT difference data results were compared to the post contrast VIBE images to assess whether there was agreement between the two imaging techniques when identifying synovitis on the MRI scans. The images were scored using a semi-quantitative method to assess the severity of the synovitis, where 0 = no synovitis is present, 1 = a synovial thickness less than 2mm and 2 = a synovial thickness of greater than 2 mm and less than 4mm, and 3 = a synovial thickness of greater than 4mm in the suprapatellar and infrapatellar pouches and the thickness of the synovitis measured 1cm above the pole of the patella. These scores were combined to give a total score for synovial burden in the knee.

The approach used to determine the suitability of MT for the COSMOS protocol was comparison and assessment of consistency of the results obtained from MT and post gadolinium imaging, rather than the accuracy of the technique when compared to post gadolinium imaging as an absolute benchmark. The rationale for the approach is that the gold standard for absolute synovitis measurement is histology and that synovial volume measured on post gadolinium imaging is known to vary over time, thus precluding its use as an absolute imaging gold standard. The consistency of measurement of synovitis between observers and techniques was considered the method of choice for assessing agreement [85, 224] between the two imaging techniques.

In addition to the MT difference imaging, a second use of the MT images is the ability to calculate MTR. MTR can be calculated from MT and images without MT (as described in the Chapter 3) (Equation 3-1). The quantitative

measurements obtained can be used to characterise the characteristics of tissues as an alternative method to T1 and T2 mapping.

$$MTR = (M_0 - M_{MT})/M_0$$

Equation 3-1 MTR equation

Where M_0 is the signal from the image without MT and M_{MT} is the signal from the image with MT.

Three sets of existing data were used to calculate preliminary MTR results by a single observer using sagittal knee SPGR images with and without MT of patients with a clinical diagnosis of OA. ROIs of approximately 5mm^2 were located on post gadolinium images and then copied to the raw ±MT images that were required to calculate the MTR values, to ensure structures such as the synovitis were matched to the reference image to allow for accurate identification.

3.3.2.3 Statistical analysis

(a) Comparison of results from a single observer for measuring the volume of synovitis on MT difference and post gadolinium contrast MR images.

In order to investigate the level of consistency between the volume of synovitis measurements of the knee using two imaging techniques, the conventional reference standard of post gadolinium imaging and the novel technique of MT difference images made by a single observer, Pearson's correlation coefficient was used to test for agreement. A paired t-test was then performed to see if there was a systematic difference between the different measurement techniques for measuring the volume of synovitis (in mm^3).

Analysis of the acquired data for all elements in the MTR section was performed using Statistical Package for the Social Sciences (SPSS version 21.0) and data for both imaging techniques was tested and showed normal distribution.

(b) Comparison of results from a single observer of MT difference and post gadolinium contrast using a semi quantitative scoring system.

Comparison was made between the amount of synovitis measured on MR images of the knee using a semi quantitative scoring tool to see if there was a difference between the scores made by one observer measured on the post gadolinium images and MT difference images.

Spearman's correlation coefficient was used to measure agreement between the two sets of semi quantitative measurements of synovitis on MR images and Wilcoxon's signed rank test was performed to see if there was a systematic difference between the semi quantitative measurements obtained from the post gadolinium and MT difference images.

The error of the results was then determined using a standard error measurement (SEM) calculation Equation 3-2.

$$\text{SEM} = \text{SD}\sqrt{1 - r}$$

Equation 3-2 Standard error measurement equation. [225]

SD = standard deviation of the test and r = reliability of the test

(c) Comparison of results from two observers measuring synovitis on post gadolinium images of the knee using a semi quantitative scoring system.

To assess the accuracy of two independent observers using a semi quantitative scoring tool to measure synovitis on post gadolinium images in the knees of patients with OA, Spearman's rho correlation coefficient was used, with a Wilcoxon signed rank test and calculation of the standard error of the measurement.

(d) Comparison of results from two observers measuring synovitis on MT difference images of the knee using a semi quantitative scoring system.

Similarly, assessing the accuracy of two independent observers using a semi quantitative scoring tool to measure synovitis on MT difference images in the OA knees of patients was assessed using a Spearman's rho, Wilcoxon signed rank test and standard error measurement.

3.3.2.4 Results

(a) The results of a single observer comparing the synovitis volume measured on MT difference and post gadolinium contrast MR images.

The mean value for synovitis volume measurements on the MT difference images was = 2.85mm^3 (SD =1.46) and for the post gadolinium images mean = 1.82mm^3 (SD = 1.68)

Pearson's correlation showed a high agreement between the volume of synovitis measured on the MT difference and post gadolinium images (r = 0.896, p < 0.0001). However, a systematic difference was demonstrated between the two synovitis volume measurements (t = -6.21, p < 0.0001), with the volume of synovitis measured on the MT difference images larger than that of the post gadolinium images (2.85mm^3, SD =1.46 compared to 1.82mm^3, SD = 1.68 respectively). A graphical representation of the results is shown in Figure 3-3.

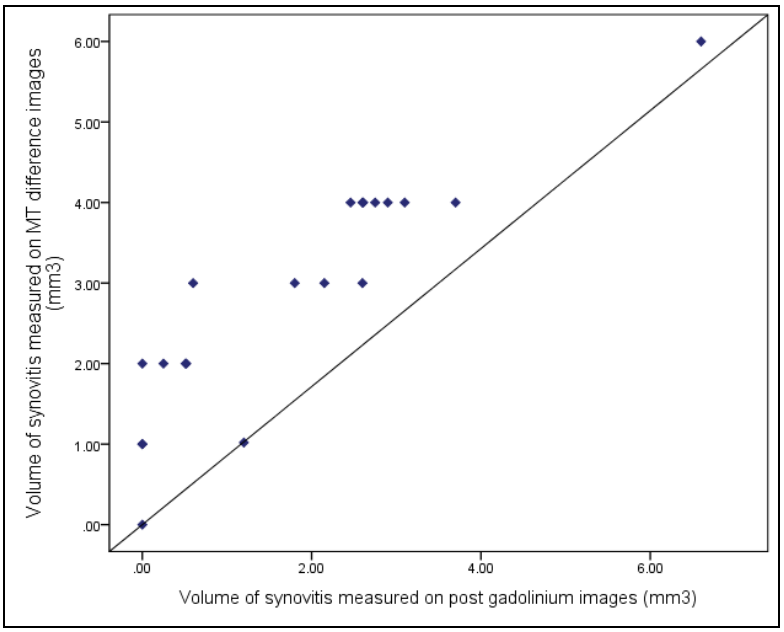

Figure 3-3 Scatter plot showing results from a single observer for measuring gadolinium enhanced and MT images for assessing synovial volumes in knee MRI scans in patients with OA knee.

A line of identity is plotted on the graph. The overestimation of synovitis on the MT difference images when compared to that scored on the post gadolinium images can be seen.

(b) The results from a single observer of comparing semi quantitative scoring of MT difference and post gadolinium contrast images.

The median values for synovitis semi quantitative measurements on the MT difference images was = 2.00, IQR = 2.00 and for the post gadolinium images, Median = 2.00, IQR = 1.75.

Spearman's rho correlation showed agreement between the semi quantitative scoring of synovitis measured on the MT difference and post gadolinium images (ρ= 0.565 and p = 0.009). No systematic difference was demonstrated by the Wilcoxon signed ranked test (z= -0.162 and p= 0.871). The error associated with the measurement was considerable SEM=0.574 (95% CI = ±1.148).

(c) The results comparing two observers measuring synovitis on post gadolinium images of the knee using a semi quantitative scoring system.

The median semi quantitative score for observer 1 was 3.0 with an IQR = 3.0 and for observer 2, a median of 2.0 with an IQR = 1.75. A box and whisker plot demonstrates these results in Figure 3-4.

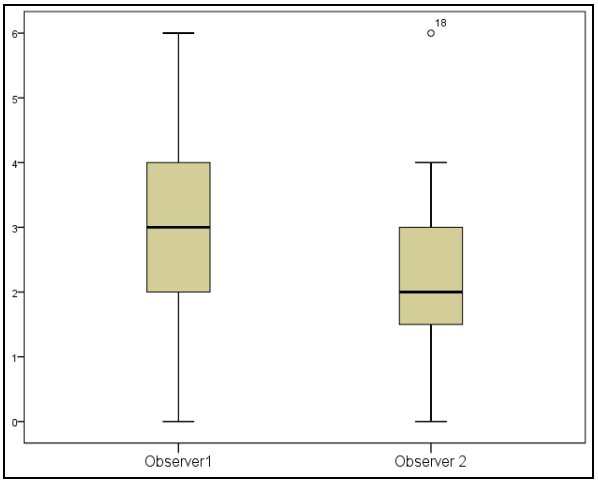

Figure 3-4 Box and whisker plot showing median and IQR values comparing the results of two observers for semi quantitative scoring of synovitis on post gadolinium VIBE images in patients with OA knee

Point 18 shows an outlier in the post gadolinium semi quantitative scoring results for observer 2.

There was a high correlation between the observers (ρ = 0.934, p<0.0001). There was also a systematic difference between the two observers, with observer 1 over scoring on the post gadolinium images when compared to the more experienced observer 2 (z = 3.357, p = 0.001). The error associated with the measurement was low SEM=0.257 (95% CI = ±0.514).

(d) The results from comparison of two observers measuring synovitis on MT difference images of the knee using a semi quantitative scoring system.

The median semi quantitative score for observer 1 was 2.0 with an IQR =2.0 and for observer 2, a median of 3.0 with an IQR = 3.0. Figure 3-5 demonstrates these results as a box and whisker plot.

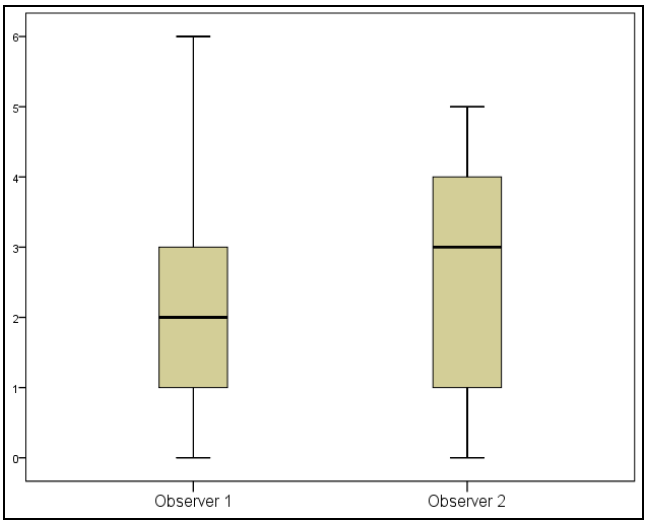

Figure 3-5 Box and whisker plot of median and IQR values showing the comparison of the results for two observers using a semi quantitative scoring system to measure synovitis on MT difference images in patients with OA of the knee.

Once again there was high agreement between both observers (ρ=0.776, p<0.0001) in measuring the synovitis volume on the novel non-contrast enhanced MT images. There was a trend towards a systematic difference between the two observers, with observer 2 over scoring on the MT difference images when compared to the radiologist who has more experience in looking at MT images, observer 1. This difference did not however reach statistical significance (z=1.734, p=0.083). The error associated with the measurement was considerable (SEM=0.548), indicating

that for a score of 3, a second measurement could be within the range of 2 to 4 (95% CI = ±1.096).

The preliminary MTR results for structures of the knee (synovitis, medial head of the gastrocnemius muscle and synovial fluid) measured from three patients with arthritis are presented in Table 3-3.

	Patient 1	Patient 2	Patient 3	Mean (SD)
Synovitis	0.36	0.30	0.36	0.34 (0.03)
Muscle	0.41	0.41	0.45	0.42 (0.02)
Synovial fluid	0.18	0.18	0.30	0.22 (0.07)

Table 3-3 Table showing preliminary MTR results from three patients, with a diagnosis of OA knee, within synovitis, the medial head of the gastrocnemius muscle and synovial fluid.

3.3.2.5 Discussion

Scoring the MT difference images for the presence or absence of synovitis in patients with a diagnosis of OA knee appears to be feasible. The delineation of synovitis is easier in areas of the knee where a fluid collection or fat are in close proximity to the synovitic tissue. The difference in the image contrast of the structures allows for identification of the synovitis, as can be seen on Figure 3-2c. Conversely, in areas where synovitis is in close proximity to a structure with similar MT characteristics, this makes the differentiation harder (for example in the posterolateral corner of the knee where synovitis may be close to the popliteus muscle).

Without the gold standard of histology being available against which to compare the imaging results, consistency of measurement was assessed for post gadolinium imaging and MT difference imaging. Volumetric measurements of synovitis involvement within the knee were made using both imaging techniques by one observer and semi quantitative assessment made by two observers.

For clarity, observer 1 is a radiologist with extensive experience in assessing and scoring novel MR imaging techniques. Observer 2 is a radiologist who has greater clinical experience than observer 1 but is not as familiar with scoring novel MR imaging techniques.

Intra-observer agreement for assessing synovitis volume in mm^3 on the post gadolinium and MT difference images was good though it can be seen that observer 1 over scored on MT difference the images when compared to the results obtained from the post gadolinium images. This could be as a result of the lack of clarity between the boundaries of the synovitis with other structures in the knee or as a genuine belief that the volume of synovitis was greater on the non-contrast imaging.

Using a semi quantitative scoring tool, observer 1 also demonstrated good agreement in findings between the post gadolinium contrast images and those obtained from the novel MT difference pulse sequence. The error measurement was considerable for the semi quantitative measurements recorded by observer 1. This may be a true reflection of the results obtained, but may be due to the small quantity of data assessed and the limited range of scores utilised in the scoring tool.

Unsurprisingly, the use of semi quantitative scoring in measuring synovitis resulted in very good inter-observer agreement when performed on the post gadolinium images with which both radiologists were familiar. It can be seen however, that observer 1 had a larger range of values and overestimated the severity of synovitis when compared to observer 2. Observer 2 is a more experienced clinical radiologist than observer 1 and this inequality may affect the results obtained.

In the MT difference image study, inter-observer agreement was lower than that for post gadolinium contrast enhanced images using the semi quantitative scoring tool. When compared to observer 1, observer 2 overestimated the volume of synovitis on the MT difference images. The most probable reason for this variation in results obtained from the two observers was the inexperience of observer 2 at looking at and scoring MT scans when compared to observer 1. Whilst observer 1 is a more experienced radiologist than observer 2, MT difference images of the knee are not used routinely in the clinical environment for assessing any knee pathology therefore limiting the possible experience to a research environment. As with all image interpretation, there is a learning curve when

looking at and scoring new image sequences, whether they are novel or conventional, and this may have been reflected in the results of the observers with different experiences in reporting MT imaging. The discrepancy in the results achieved was thought not to necessitate precluding MT imaging from the COSMOS protocol. The technique appeared to be promising and with extra training of the second radiologist and the development of further experience, it was felt that the agreement between could be improved to a point where the technique might be feasible for the prospective COSMOS study.

MTR images allow for quantification of tissue types that could potentially be used in conjunction with or replacing T1 imaging. MTR is a potentially more robust measurement tool, as the technique is not reliant on coil type (transmit/receive or receive only) and B_1 field homogeneity. The field strength of the MR scanner does influence the readings obtained however, and care must be taken if comparing results from different scanners.

There are no reference MTR values in the literature for patients with OA knee at 3T for any of the structures measured. There are however, documented measurements of MTR expressed as a percentage in the gastrocnemius of healthy volunteers of 33.1% (SD 2.1%) (equivalent to a MTR of 0.331) by Sinclair et al [226] using Quantitative Magnetisation Transfer (a variation of MTR imaging using multiple acquisitions with distinct offset frequencies). There is a difference between the published data and that measured in the pilot study, but the different technique and demographics of the groups (Sinclair et al's study healthy volunteers with a mean age of 33.6 years as opposed to the COSMOS pilot study patients with OA of the knee with a mean age of 65.4 years) could account for the disparity in the results.

Whilst there are possible issues of identifying synovitis from muscle in close proximity using the MT difference technique, there may be scope for utilising MTR imaging to aid in differentiation between them. If there is a distinct range of values for muscle and synovitis, it may be possible to perform the separation of the structures on a quantitative basis rather than just a visual one.

There are no published data for the normal values of MTR in musculoskeletal structures in the healthy population or in patients with OA knee, but a continuation of this work in a larger study population may provide a data base for MTR measurements of tissue structures for patients with OA knee.

3.3.2.6 Summary of findings: Magnetisation transfer contrast

The potential for magnetisation transfer imaging sequences to allow for imaging of synovitis with MRI without contrast agents appears promising. Not only does the technique produce an image that can be visually interpreted, a second set of images can be calculated to produce quantifiable data. Although the process of producing the images requires two image acquisitions, the potential was thought to be significant enough for MT to be included in the non-contrast COSMOS MRI protocol.

3.3.3 T1 mapping sequence

3.3.3.1 Introduction

Anatomical structures have a defined range of T1 values that relate to certain characteristics of the tissues.T1 mapping has been used therefore to measure the characteristics of tissue, as described in the literature review. The relaxometry of tissue changes with pathology and the use of resulting T1 maps can, for instance, increase the detection of multiple sclerosis plaques in the brain [227].

A comprehensive review of the literature indicates that T1 maps have not previously been used within the knee joint to identify one piece of anatomy from another by employing empirical T1 values. It was hypothesised that utilising T1 mapping in the imaging of the knee for the detection of synovitis without contrast agents may allow for increased sensitivity for differentiating synovitis from other structures, and may therefore be useful as a biomarker to monitor response to therapies.

3.3.3.2 Method

Using the existing MRI scans within the Unit, T1 measurements of anatomical structures of the knee were measured in 11 knee sagittal MRI scans using a series of images acquired using multiple flip angles. The demographics of the patients are shown in Table 3-4. The MRI sequence

used to generate the base data required to calculate the T1 maps was a sagittal Fast Low Angle Shot (FLASH) gradient echo, TR 8ms, TE 3.6ms, FA 3 and 17 degrees. Parametric pixel by pixel T1 maps can be calculated using specialised software either on the MRI scanner or on a dedicated workstation and a colour scale can be allocated to display the different ranges of T1 values. This allows for a quick visual interpretation of the range of values for an anatomical structure. A T1 map was generated inline using MAP IT® software (Siemens Medical, Erlangen). An example of a T1 map in a patient with OA knee is given in Figure 3-6. Structures with high T1 values (>2500ms) are represented by red pixels (e.g. synovial fluid and blood within the popliteal artery). Structures with lower T1 values (~300ms) such as subcutaneous fat and bone marrow are represented by a blue colour.

	Gender	Age	Disease
Patient 1	Female	70	OA
Patient 2	Female	75	OA
Patient 3	Male	72	OA
Patient 4	Male	61	OA
Patient 5	Female	53	RA
Patient 6	Male	58	OA
Patient 7	Female	43	RA
Patient 8	Male	59	RA
Patient 9	Female	45	RA
Patient 10	Male	62	RA
Patient 11	Female	68	OA

Table 3-4 Demographics of the patients from the existing data base held in the LMBRU to assess the imaging parameters for T1 mapping

Validation of the calculated T1 measurements generated by the scanner software was achieved by comparing these to the results obtained from a bespoke T1 calculating software tool (P.J. Wright 2010) written in Matlab®.T1 values were calculated on a voxel by voxel basis and the results were presented in the form of T1 maps.

Regions of interest (ROIs) of approximately 5mm^2 were used to measure the T1 values of the gastrocnemius muscle, synovial fluid and synovitis (if present). Multiple measurements were taken on different slices to compensate for B_1 field in-homogeneities and possible fluctuations of measurements due to variations of calculated T1 readings within patient to patient. The number of measurements made in each structure is provided in Table 3-5.

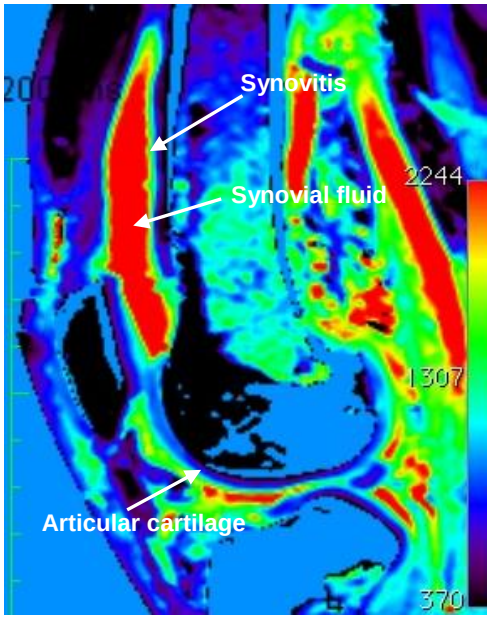

Figure 3-6 Sagittal T1 mapping image of a knee in a patient with osteoarthritis.

A synovial effusion is visualised in the suprapatellar pouch. Fluid is shown a red pixel colour. Synovitis surrounds the synovial effusion and has a different T1 value than synovial fluid and therefore is represented by another colour. The articular cartilage is clearly visualised on the femoral condyle as labelled. The scale attached to the image show the colour attributed to the T1 values measured in ms (fluid over 2224ms, fat approximately 350ms).

Tissue Type	Number of measurements
Synovium	1408
Muscle	704
Synovial Fluid	352

Table 3-5 Number of T1 measurements made within structures of the knee joint in 11 patients.
Multiple measurements were made to compensate for possible magnetic field and patient variations

There is limited data published on T1 values of the knee and that which is published is of normal healthy subjects. In order to explore the comparability of the T1 measurements obtained from the LMBRU T1 mapping sequence with those from normal subjects in the literature, two control volunteers were also scanned [124]. Both volunteers were female, aged 45 and 56 years of age.

To ensure that the T1 measurements acquired from the historical data and volunteers were not a reflection of the pathology of the individuals imaged, the existing T1 protocol was assessed for accuracy and was used to measure calibrated gel samples of known T1 values.

The T1 mapping variable flip angle sequence that had been used to acquire the existing data in the LMBRU, (TR 8ms, TE 3.6ms, flip angles 3 and 17 degrees) was used to scan six test tubes from the Eurospin® MRI test tool. A range of T1 values were chosen to assess the measurement accuracy across a range of short and long T1 values. The T1 values chosen reflect the range that would be expected to be seen within tissues of the knee joint (~350ms for fat and ~1800ms for muscle and synovitis) as described in the literature [124].

3.3.3.3 Analysis

In order to compare the T1 values between the 11 patients, the two volunteers and the literature, T1 values were compared for the synovium, muscle and synovial fluid. Given the small numbers and limited data available for the literature, formal statistical analysis was not appropriate. Descriptive statistics are presented.

3.3.3.4 Results

The results of the T1 measurements made from the existing data and volunteers are presented in Table 3-6 with the values from the literature tabulated for comparison.

Tissue Type	Mean measured T1 on existing data in OA and RA knees (ms) (SD)	Mean measured T1 on healthy volunteers (ms) (SD)	T1 from literature (ms) (SD)
Synovium	1821.8 (358)	Not available	Not available
Muscle	1155.5 (359)	932.5 (88)	1420 (38) [124]
Synovial Fluid	3659.9 (523.4)	3068.0 (522)	3620 (320) [124]

Table 3-6 Comparison of T1 measurements of structures of the knee from existing data of 11 patients with arthritis, measurements from the two volunteers and published results from the literature [124] .

Visual depiction of the T1 measurements (mean values with two standard deviations) from muscle and synovial fluid from the patients, volunteers and literature are shown in Figure 3-7 and Figure 3-8.

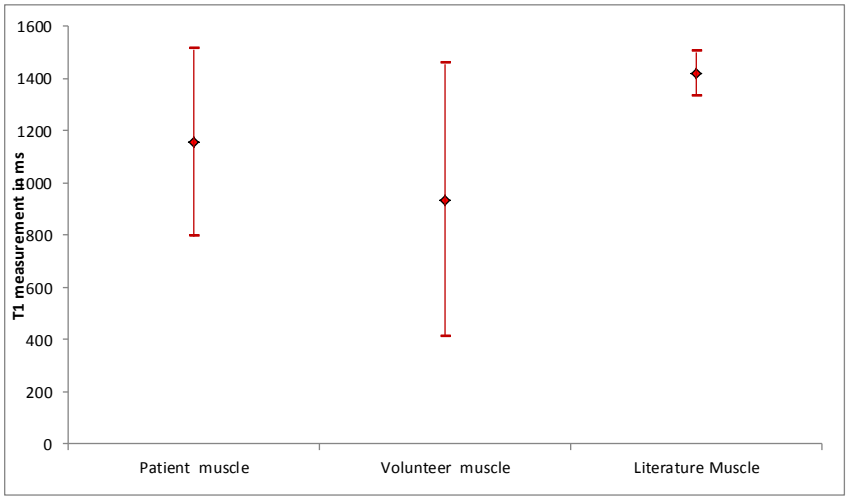

Figure 3-7 Comparison of mean T1 measurements of muscle
measured from data held within the LMBRU in patients with RA and OA affecting the knee, two volunteers and the published literature. Mean T1 values with two standard deviations are shown.

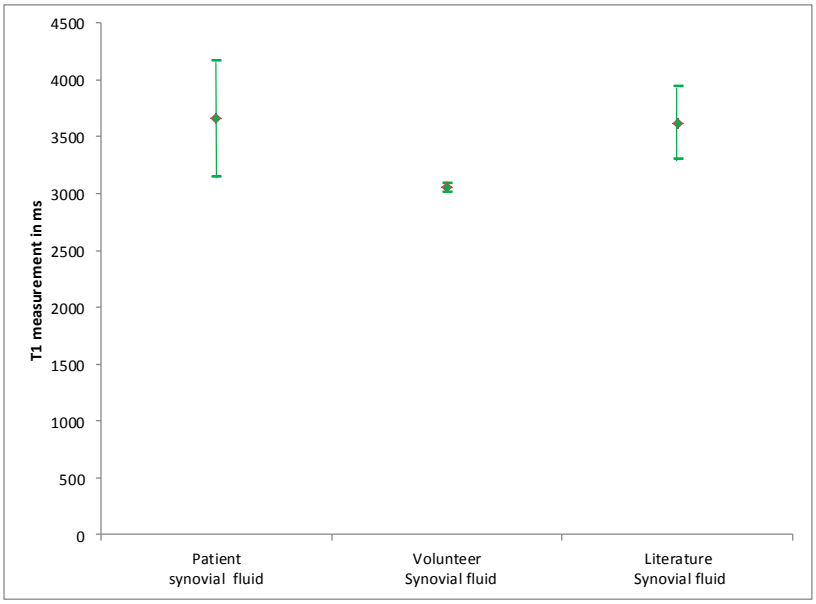

Figure 3-8 Comparison of mean T1 measurements of synovial fluid
measured from data held within the LMBRU in patients with RA and OA affecting the knee, two volunteers and the published literature. Mean T1 values with two standard deviations are shown.

Data acquired to validate the existing T1 protocol from samples of known T1 values of the Eurospin® test tool are tabulated in Table 3-7.

The mean T1 measurements made (except for test tube two) were all lower than the published lowest expected value. The mean recorded value for test tube two was higher than the highest expected value.

	Measured T1 values at 21 °C (ms) (SD)	Calibrated T1 values (ms) (SD)
Tube 2	402.1 (10.0)	374 (27)
Tube 5	486.5 (19.4)	551 (31)
Tube 10	621.9 (25.4)	878 (31)
Tube 14	1549.4 (36.5)	1323 (72)
Tube 15	1338.6 (29.1)	1532 (56)
Tube 17	1155.7 (31.5)	1656 (63)

Table 3-7 Comparison of T1 values recorded using the historic LMBRU T1 protocol when scanning the known sample values from the Eurospin® test tool

3.3.3.5 Discussion

The T1 maps calculated showed visual separation of the tissues of interest even though the empirical calculated T1 values did not agree with the literature (Table 3-6). Comparison of T1 measurements of structures of the knee from existing data of 11 patients with arthritis and measurements from the two volunteers did not agree with published results from the literature [124]. Although the results of the T1 readings showed a trend which was comparable to the published data, the lack of agreement was disappointing. Despite measuring ‘normal’ tissue as well as ‘pathology’, the empirical T1

values obtained from the LMBRU archive and two new acquisitions from healthy controls did not agree closely with the published data. However, the discrepancies of the calculated T1 values from data held within the LMBRU still allowed for identification of structures within the knee due to the relative differences in the T1 values of the structures despite the lack of agreement with the literature.

Comparison of the historical data and that measured on the two healthy volunteers did not agree with the values recorded in the literature [124]. The T1 measurement pulse sequence used by Gold et al (Look-Locker method inversion recovery) was different from that used within the LMBRU and may have contributed to some of the difference in the compared values. However since Gold published this paper in 2004, his group has published a subsequent paper in 2011 contradicting the values reported in the original paper [125].

In addition to the in vivo data not agreeing with the literature, the results obtained from the Eurospin® test tool and the historic T1 mapping protocol did not agree with the known calibrated gel samples. This could be due to:

1. Inappropriate flip angle selection of the gradient echo sequence used to produce the data to calculate the T1 maps.
2. The possible effects on the quality of the data caused by the coil selection. Transmit/receive coils can be prone to inhomogeneous B_1 magnetic field across the coil.
3. In clinical scanning it is common practice to apply a filter to the MR image to improve the visual appearance of the images. Whilst in the clinical environment there are no detrimental effects to the images, there is a possibility they could affect the underlying raw data.

As T1 mapping was thought to be potentially a theoretically important sequence in the final non-contrast MRI protocol, it was decided to investigate the possible reasons for the disagreement of the calculated and published values. If a reproducible protocol could be devised and optimised, the T1 mapping sequence could allow for calculation of T1 values that were comparable to the published data and be able to measure the T1 of synovitis

and other structures of the knee accurately. Validation of the T1 protocol against calibrated T1 values suggested that the existing T1 mapping protocol does not provide accurate T1 values across the wide range of values potentially expected to be seen in the knee. This was an unexpected finding which resulted in a large piece of prospective work being undertaken in order to produce a reliable T1 measuring protocol. Details of this work are set out fully in the sequence optimisation chapter (Chapter 4). The unexpected finding that the existing T1 protocol was not fully optimised has implications for using the existing LMBRU data as a source of reference data that could be used to benchmark tissue values.

3.3.3.6 Summary of findings: T1 mapping sequences

Despite the unexpected results obtained from the T1 measurements from the existing data set, volunteers and Eurospin® test tool, the potential of the T1 mapping sequences could not be ignored. The decision was made to devote a significant amount of time if necessary, to the evaluation and optimisation of a reproducible T1 mapping protocol which could be included in the non-contrast MRI COSMOS protocol for imaging synovitis.

3.3.4 T2 mapping sequences

3.3.4.1 Introduction

Alternative methods to T1 mapping to quantify the quality of tissue include T2 mapping, which has been used in prostate imaging to identify normal prostate from pathological tissue [228] and patellar articular cartilage imaging to assess the quality of the tissue [229] and provide complimentary information regarding the degeneration of articular cartilage [230-232]. There are published data reporting the T2 values within body tissues that can be used to compare the images from the LMBRU using the same methods [124] .

3.3.4.2 Method

Within the LMBRU there is an archive of data acquired using T2 quantification sequences, and these were reviewed to validate the T2 values of structures within the knee joint against the published literature. Eleven sets of MR scans from patients with a clinical diagnosis of arthritis were evaluated to assess the accuracy of T2 values of structures of the knee. The demographics of the patients are described in Table 3-4.

The multi-echo spin echo MR technique was employed to generate the images for the calculation of the T2 maps. The parameters of the sequence were: TR 2,500ms, TE 11.1, 22.2, 33.3, 44.4, 55.5, 66.6 and 77.7ms, acquisition time four minutes.

Multiple measurements were taken to accommodate for the variations caused by non-uniformity in the RF field and possible heterogeneity of T2 values within structures. As described previously for the T1 mapping, T2 calculations were also made from new acquisitions obtained from two healthy volunteers to act as a control. The demographics of the volunteers were female n = 2, aged 47 and 54 years. The number of measurements is presented in Table 3-8.

Tissue Type	Number of measurements
Synovitis	1408
Muscle	704
Bone Marrow	704
Subcutaneous fat	704

Table 3-8 Number of measurements taken for T2 measurements of structures within the knee joint in 10 patients with arthritis of the knee from historic data held in the LMBRU.

As with the T1 mapping protocol, the scanner software is capable of calculating a pixel by pixel parametric T2 map displayed using a colour scale,

from a multi-slice multi-echo sequence. A choice of appropriate colour scale is made from the existing colour scale library within the OsiriX® software that allows for optimum delineation of structures within the knee. An example of a T2 map of a patient with osteoarthritis of the knee is shown in Figure 3-9 with a colour of red attributed to structures of around 1,000ms and green to those of around 400ms. Anatomical structures such as the posterior cruciate ligament (PCL) can be seen on the images as signal void due to the short T2 of the structure (as labelled on Figure 3-9) and synovial effusion can be identified on the image due to the long T2 characteristic of the fluid. The remaining anatomical detail is hard to identify as there is a limited sliding range of the signal returned by the other structures within a narrow range.

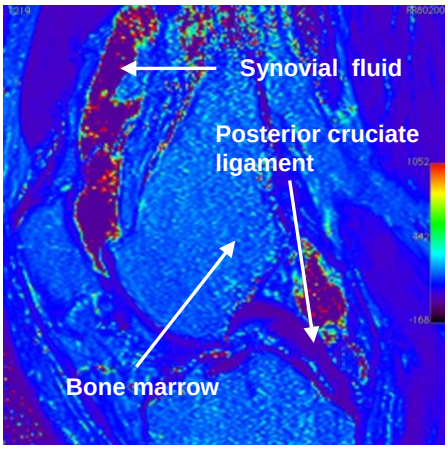

Figure 3-9 Sagittal T2 image of a knee joint of a patient with osteoarthritis

The scale of colour is depicted on the image with a red colour representing ~1000ms, green ~400ms and blue very short T2 values < 100ms.The T2 map shows a synovial effusion within the suprapatellar pouch. The delineation of synovitis can be seen around the synovial effusion. The resolution of the image is poor resulting in a pixelated image.

3.3.4.3 Analysis

Similar to the approach to our analysis of T1 values, the T2 values were compared for the 11 patients, the two volunteers and the literature, T2 values were compared for synovitis, muscle, bone marrow and subcutaneous fat. Given the small numbers and limited data available for the literature, formal

statistical analysis was again not appropriate. Descriptive statistics are presented.

3.3.4.4 Results

As with the T1 measurements, the T2 measurements differed from those published in the literature. A comparison of T2 values calculated from data from the LMBRU, volunteers and that of the literature is presented Table 3-9.

Tissue Type	Mean measured T2 on archived data (ms) (SD)	Mean measured T2 on volunteers (ms) (SD)	T2 values from literature (ms) (SD)
Synovitis	290.3 (121)	x	x
Muscle	51.6 (69)	43.8 (7)	31.7 (1.90) [124]
Bone Marrow	202.2 (46)	180.7 (34)	133 (6.14) [124]
Subcutaneous fat	193.4 (34)	169.6 (28)	133(4.43) [124]

Table 3-9 Comparison of the mean and standard deviation of T2 measurements of structures of the knee measured on existing LMBRU data from ten patients with arthritis, two volunteers and results published in the literature.

The results from Table 3-9 are depicted graphically in Figure 3-10, Figure 3-11 and Figure 3-12.

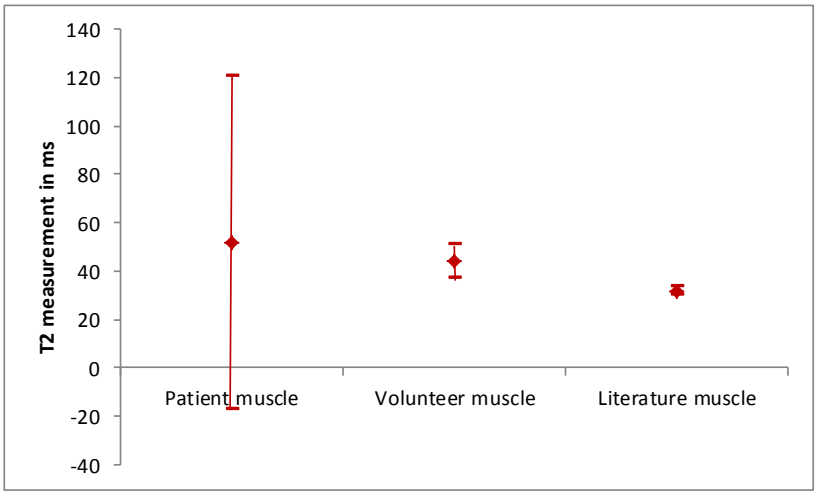

Figure 3-10 Comparison of mean T2 values with two standard deviations measured in the medial head of the gastrocnemius muscle
in patients with arthritis of the knee, two healthy volunteers and published data from the literature

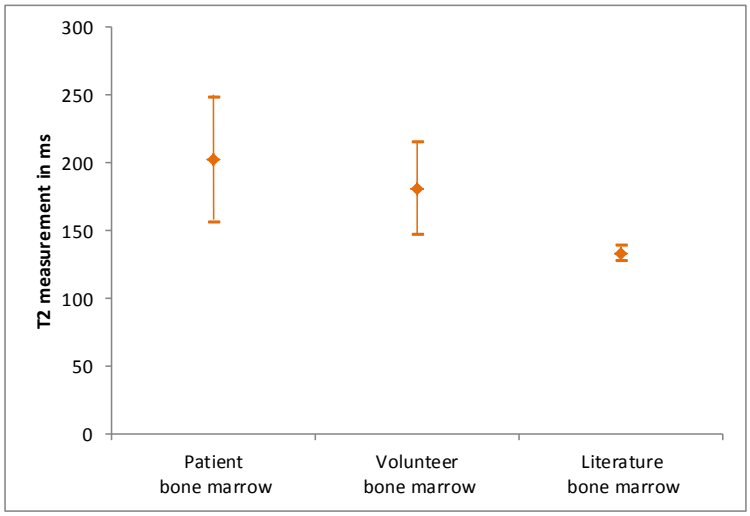

Figure 3-11 Comparison of mean T2 values with two standard deviations measured in bone marrow of the femoral epiphysis
in patients with arthritis of the knee, two healthy volunteers and published data from the literature

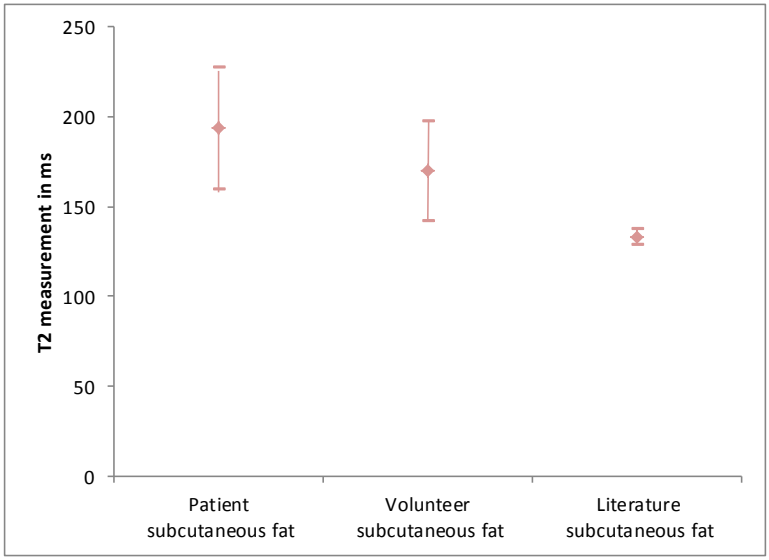

Figure 3-12 Comparison of mean T2 values with two standard deviations measured in subcutaneous fat
in patients with arthritis of the knee, two healthy volunteers and published data from the literature

3.3.4.5 Discussion

The overall trend for the T2 values is similar to that in the published literature but with higher relative values. The measured T2 values for both the archived existing data and the two volunteers were higher than that recorded in the literature. This may be due to stimulated echo components to the second and subsequent echoes. Stimulated echoes generated from imperfect refocusing pulse slice profiles can result in significant distortion of echoes in multi-echo sequences. This results in signal enhancement [233]. However the most probable reason for the non-agreement is the limited selection of TE's used in the sequences. With the maximum TE selected as 77.7ms, the possibility that structures with long TEs will not have an accurate and precise T2 value and do not agree with the literature.

Further reflection on the selected parameters for the T2 protocol reveals a small range of TE values and those that were selected are best suitable for shorter T2 values and not the range that would be expected within the knee.

In addition to the readings measured not agreeing with the literature, a large overlap in values of different tissues was observed bringing into question whether T2 imaging could add anything to the imaging of synovitis without the use of contrast agents.

Unlike the trend in results seen in the T1 mapping pilot study, there is a large overlap in values for measurements of the tissues measured, especially for synovitis which would render this technique inappropriate regardless of the imaging parameters selected.

As a consequence of the poor agreement of the measurements from the existing data and the literature it was decided not to explore the possibility of including a T2 mapping sequence in the non-contrast COSMOS MRI protocol in Chapter 5. It was considered not to be an efficient use of time to perform an in-depth exploration of the non-agreement seen in the results from T2 mapping and therefore excluded from the final COSMOS non-contrast protocol.

3.3.4.6 Summary of findings: T2 mapping sequences

It was decided not to include the T2 mapping sequences into the COSMOS protocol. If required to aid imaging muscle tissue, further optimisation could be done on the T2 mapping sequence.

3.3.5 Dixon imaging

3.3.5.1 Introduction

Some structures of the knee lie in close proximity to each other and have similar signal characteristics, resulting in difficulty in identifying one from another. If it were possible to use MRI sequences in combination it may be possible to visualise separating structures and tissue borders. Multiparametric combined MR imaging may aid in the identification of synovitis from other structures.

3.3.5.2 Method

As described previously for T1, T2 and MTR sequences, previous studies within the LMBRU have utilised the Dixon technique in the imaging protocol. As explained in the literature review, one imaging sequence using the Dixon technique produces four sets of images: in phase, out of phase, fat and water images.

Archived MRI data with in the LMBRU contained 24 Dixon knee scans of patients with a clinical diagnosis of osteoarthritis. The Dixon technique is described in depth in the literature review, section 2.5.5.4.12.

3.3.5.3 Results

Images from the Dixon sequences were reviewed using OsiriX® viewing software. The four different sets of images produced by the Dixon sequence provide different tissue-weighted scans and therefore different information. The water sequence provides an image where anatomical structures such as articular cartilage, muscle and fluid are clearly demonstrated. The 'frond like' indentations into Hoffa's fat pad in Figure 3-13 can be identified, but the tissue type causing this cannot be determined solely on this image.

Chemical shift artefact can be seen on the out of phase images, Figure 3-13b, a characteristic that can be used to define fat/water interfaces. The muscles, superior synovial pouch and areas of fat are clearly defined by the dark line around them. Again the fronds of tissue indenting Hoffa's fat pad are identified although what this represents is unclear.

On the fat image Figure 3-13c, there is poor differentiation of fluid from articular cartilage and possible synovial tissue. On its own, this image appears therefore to have little value in eliminating the use of contrast agents but by using the appropriate software tools, multiparametric images can be used by fusing sequences together.

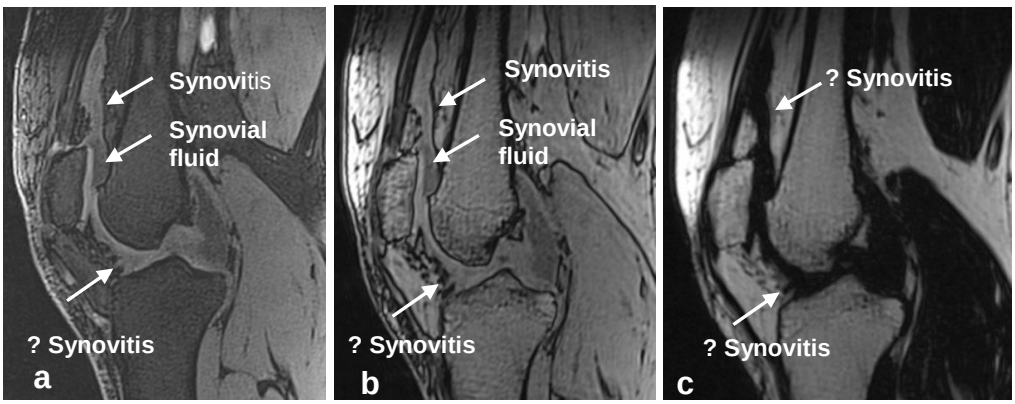

Figure 3-13 Sagittal Dixon MR images of a patient with OA of the knee.

(a) Water image, (b) out of phase image, (c) fat image.
Boundaries between structures can be identified on the water (a) and out of phase (b) images as labelled on the scans. On the fat image (c), the differentiation between the fluid and the synovium is difficult to discern.

Fat images from the Dixon sequence were superimposed onto the proton density fat saturated images in order to ascertain whether this would improve the visual conspicuity of synovitis. The geometrical imaging parameters for the Dixon (voxel dimensions 1 x1 x 1 mm) and the proton density fat saturated (voxel dimensions 0.4 x 0.4 x 3 mm) sequences did not match, which complicated the processing, but although the fat images did not match the proton density fat saturated images exactly, slice for slice and voxel for voxel, it was possible to register the sequences to each other using the OsiriX® software to produce sample images that could be reviewed. An example is shown in Figure 3-14. In Figure 3-14a, a sagittal proton density fat saturated image is shown, as would be conventionally displayed. Signal from fluid is hyperintense and the fat signal has been supressed and is displayed as an intermediate signal (as labelled). Anatomical structures such as the ACL and PCL are clearly seen on this image. There are however, two areas of intermediate signal sitting in Hoffa's fat pad anterior and inferior to the femur, which could represent fat or another type of soft tissue e.g. synovitis, as labelled on the image. When the fat image is fused with the PD fs image, tissue with a fat content is shown as red or yellow in signal as shown in Figure 3-14b. By combining the two images, it can be seen that the two areas of intermediate signal within Hoffa's fat pad, now display different imaging characteristics. The superior area now displays a red colour and the inferior area maintains the intermediate signal. It can be inferred therefore, that the

superior area is fat and the inferior one not. Confirmation that the lower area is indeed synovitis can be validated by comparing this image with the post contrast VIBE scan.

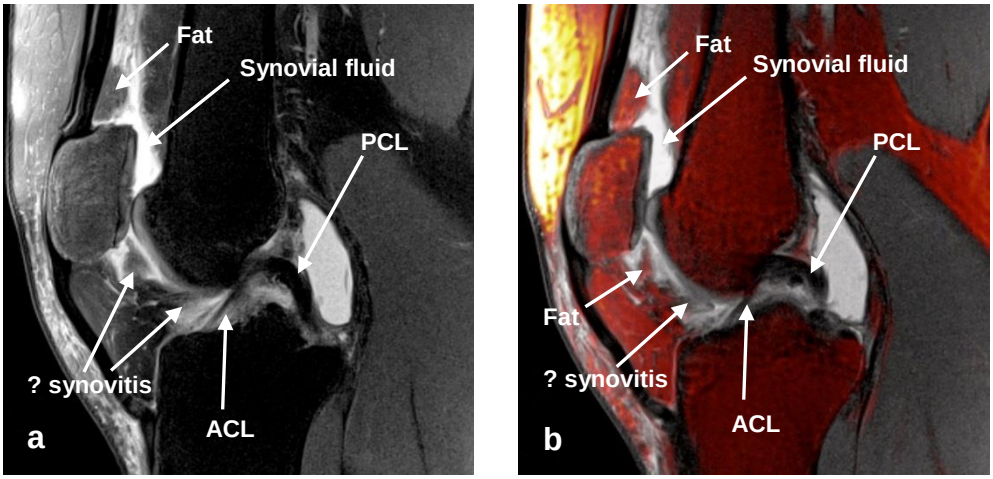

Figure 3-14 Sagittal proton density images in a patient with OA of the knee.

(a) Proton density fat saturated image viewed in the conventional mode.
(b) Proton density fat saturated image with fat from a Dixon VIBE image fused together.

Further uses of the addition of fat to a second MRI sequence are shown in Figure 3-15. In Figure 3-15a, a conventional PD fs MRI scan is shown of the medial compartment of the knee. Fluid is demonstrated as hyperintense signal and fat as intermediate signal. A band of synovium can be seen within the synovial effusion as labelled on the image. In Figure 3-15b, the same image has been manipulated by inverting the grey scale so that fluid is now visualised as hypointense signal, and fat from a Dixon scan has been fused with this. Tissue containing fat is now represented by a pink or yellow coloured pixel. The band of synovium can be clearly seen against the hypointense synovial fluid and the difference in visual conspicuity achieved by the multiparametric image, allows for the articular cartilage to be seen as more defined structure when compared to the conventional display (Figure 3-15a). Within the posterior medial meniscus, disruption of its internal structure can be seen on both sets of images (Figure 3-15a and Figure 3-15b) demonstrating degenerative tears within the meniscus.

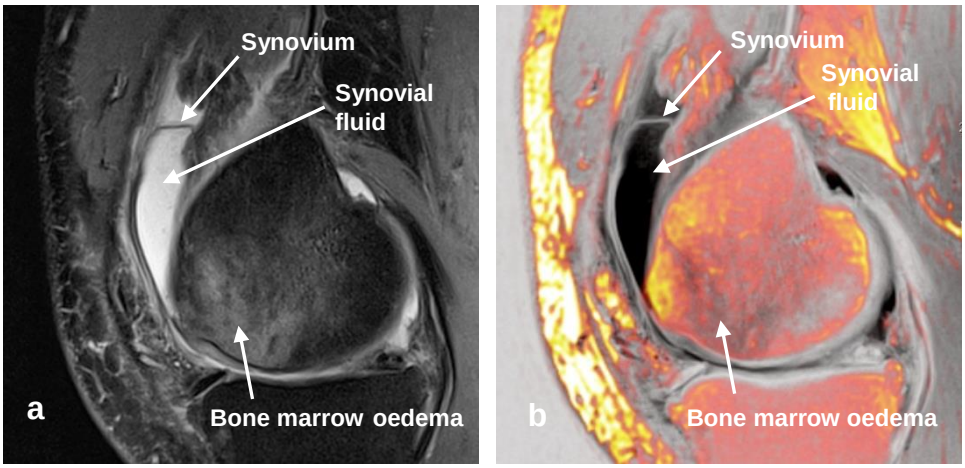

Figure 3-15 Sagittal proton density fat saturated MR images of the medial component of the knee from a patient with a diagnosis of OA of the knee.

Image (a) is a PD fs image displayed in the conventional viewing mode. Image (b) the proton density fat saturated scan has had the grey scale inverted, so that fluid is now black, and fat from the Dixon fused image shows as pink or yellow in colour. In images (a) and (b), the synovium can be seen clearly against the background of the joint effusion.

3.3.5.4 Discussion

Dixon imaging has been used to assess fat content in the structures such as the liver, heart and bone and has been used for clinical evaluation to identify and measure fat fractions [234-236]. The potential for discriminating and identifying fat from other structures in the knee appears to be feasible with the use of the fat image from the Dixon scan. Despite the differences in the geometric resolution of the scans, the OsiriX® software was able to identify similarities between the Dixon and PD fs images sufficient to allow for them to be registered and combined. Images can be manipulated in a very short time to produce multiparametric images that can be reviewed and stored.

Within the OsiriX® programme, a pixel colour scale was assigned to tissues with fat content on the fused images. The summation of fat with the PD fs images appears to be able to distinguish areas of fat from structures that are

not and could potentially be synovitis (Figure 3-14b). Inversion of the grey scale provides the viewer with a different perspective of the data and structures may appear clearer than when seen on the conventional greyscale non-inverted images.

Within the cohort of patients used to assess the Dixon technique, only PD fs images were acquired and the exploration of fusing the fat with alternative sequences was not possible. It may be that another sequence type, MT or T1 TSE, with a different tissue weighting may yield a greater conspicuity of synovial tissue from other structures than PD fs.

Further investigation into the potential of parametric imaging with the Dixon sequence is justified based on these initial results. If it is possible to ensure that the geometric imaging parameters of all the sequences in the COSMOS protocol are identical, it would allow for more accurate multiparametric images to be produced that can be validated with the post contrast imaging sequences. At this stage it was envisioned that the COSMOS protocol would comprise of more than one tissue weighting, and the potential of fusing the fat only images to another sequence was considered likely to provide extra information to allow for imaging synovitis without contrast.

3.3.5.5 Summary of findings: Dixon imaging

Despite the limited number of patients that were assessed and the imaging sequences having different voxel sizes, the Dixon technique appeared to provide an alternative method for visualising structures of the knee when fused with the PD fs sequence. The ability to potentially demonstrate fat planes between structures may allow for greater specificity in determining the synovitic volume in the knee. The Dixon scan which can produce four image contrasts for one acquisition was acquired in a time of 1.26 minutes. In order to explore the further potential of the Dixon sequence it was selected for inclusion in the non-contrast COSMOS MRI protocol.

3.4 Conclusion

Reviewing the data held within the LMBRU proved to be an interesting and valuable experience. As well as looking at the images and the potential that each sequence may have if included into the COSMOS protocol, the scrutinising of imaging parameters from previous MRI studies revealed inconsistencies and highlighted lessons that could be learned.

Evaluation of the existing data did not reveal a sequence that could be directly transferred from the existing protocol database into the potential COSMOS study. The review did however identify sequences that showed potential and that warranted further optimisation.

(i) Of the fluid sensitive images reviewed form the existing data, the DESS images showed excellent sensitivity and good specificity in identifying synovitis when compared to other sequences. In addition to this, DESS had added benefits of providing a high resolution 3D image in a time that is approximately half that of T2w fs sequences

(ii) T1 mapping sequences are able to provide anatomical and quantitative information relating to the characteristics of the tissues imaged. Despite the empirical values measured from the existing database not matching those from the literature as closely as would have been preferred, the potential of this sequence was such that it was placed into the COSMOS non contrast MR protocol for further evaluation and optimisation.

(iii) Gradient imaging with and without MT allow for the calculation of quantitative images (MTR) that if used in conjunction with the MT difference and T1 mapping images, may add extra information in identifying synovitis on non-contrast MRI images. Scoring of synovitis on MT difference images from the existing data held

within the LMBRU, has been shown to be feasible and when compared to the reference standard of post gadolinium contrast images, appears to provide comparable results. It was therefore decided to include these sequences into the COSMOS protocol for further evaluation and optimisation.

In conclusion, as a result of work performed exploring the potential of sequences from the existing data held within the LMBRU, the following sequences were chosen to be included into the COSMOS protocol to augment the conventional MRI sequences in imaging synovitis without the use of intravenous contrast agents:

- DESS as the fluid sensitive sequence
- T1 mapping after the investigation and validation of correct flip angle selection
- MT and MTR imaging
- Dixon VIBE sequence

Further evaluation and optimisation of these sequences is described in the following chapter.

Chapter 4 Quantitative MRI sequences optimisation

4.1 Introduction

In order to produce a reproducible, artefact free, non-contrast MRI scanning protocol to image synovitis, potential candidate MR sequences have been identified in Chapter 3: once identified, the sequences need to be optimised. The processes by which the quantitative MRI sequences were optimised are described in this chapter, with attention to imaging parameters and coil configurations, with the final objective being to compile a MR protocol that requires no intravenous gadolinium contrast to visualise synovitis in knees of patients with a clinical diagnosis of OA.

4.2 Aims and objective

This chapter describes the optimisation process in order to compile an MR imaging protocol of conventional MR sequences and novel techniques to image synovitis in patients with OA of the knee. The strategy to optimise images was focused around (i) existing images from patients from existing LMBRU studies and (ii) the use of test phantoms comprised of bottles filled with aqueous copper sulphate supplied by manufacturer of the MRI scanner; the geometry of each sequence was assessed against the phantom.

MRI sequences were then optimised, with attention to imaging parameters and coil configurations, with the final objective being to compile a MR protocol that requires no intravenous gadolinium contrast to visualise synovitis.

4.3 Methods

Optimised imaging parameters for conventional sequences such as DESS and TSE imaging were taken from existing studies in the LMBRU and do not form part of this thesis.

Based on the results of the literature review and assessment of existing data, a draft MR imaging protocol was developed utilising potential candidate pulse sequences that were thought to be the most sensitive to the visualisation of synovitis without the aid of intravenous contrast agents. The sequences were developed and optimised using phantoms to produce a protocol that is reproducible and provides results that are in line with published data where applicable.

Possible candidate sequences and equipment configurations that were optimised for their inclusion in the non-contrast MRI protocol were:

4.3.1 Magnetisation transfer contrast with SPGR or MEDIC sequences.

4.3.2 Quantitative T1 mapping sequences

4.3.3 Coil selection and configuration

Diffusion weighted imaging and inversion recovery techniques have been assigned to separate chapters at the end of this thesis (Chapters 7 and 8) as they were not initially thought to be contenders for the COSMOS non-contrast MRI protocol and were only developed and assessed as a direct result of this research.

Once again, this chapter presents an overview, description of the methods, results and discussion for each candidate sequence. A conclusion is presented at the end of the chapter.

4.3.1 Magnetisation Transfer

4.3.1.1 Introduction

As described in the literature review, magnetisation transfer has been used to increase the contrast in MRI images [153]. MT is a technique that uses a RF pulse applied off resonance to suppress signal from tissues with wide ranges of Larmor frequencies in structures with a large pool of bound protons.

MT is used to supress protein-bound water: there are two groups of protons, those that are bound and those that are free. The restricted or bound proteins are not seen on normal imaging but they can influence the image by the exchange of energy between the two groups. This results in the magnetisation from the bound group moving to the free protons reducing the signal seen.

Whilst MT can increase the visualisation of specific tissue types, not all MR sequences are compatible with MT due to the constraints of the pulse sequence.

Specific absorption rates (SAR's) measure the quantity of exposure of RF deposited to the patient [115]. Specific absorption rates increase with the addition of MT to a pulse sequence. SAR is measured in watts per kilogram and is calculated on the weight of the patient entered into the scanner at the beginning of an examination. The greater the strength of the magnetic field, the larger the SAR implications [237]. Modern scanners allow for the operator to work at two levels of SAR: normal and first level (the latter dependent on confirmation form the operator before it is applied). Safe operating levels have been set to minimise the amount of increased body temperature to be no more than 1°C at first level (IEC 60601-2-33). In practical terms this is the same as $4Wkg^{-1}$ over 6 minutes [238]. SAR has the following relationships with these variables [115]:

- Increases with the square of Larmor frequency
- Increases with the square of the flip angle
- Increases with the patient size
- Increases with the number of RF pulses deposited in a selected time

Which in practice have an effect on the following:

- The type of coil used for transmission
- The value of TR selected
- The number of slices selected
- The chosen value for the refocussing flip angle
- The addition of ‘add ons’ to a pulse sequence
- The type of MR sequence selected

As well as pulse selection constraints, MT can have effects that prohibit from being used or require the protocol parameters to be such that the sequence will run regardless of the weight of the patient. If this is not achieved, it would result in the probability that the imaging parameters may need to be altered from patient to patient preventing the use of the results obtained to be included in the study.

The longer the MT pulse the more effect is produced but this also increases the SAR. The effects and consequences of SAR increase with larger field strength magnets. At 1.5 Tesla imaging, SAR does not play a practical role in MR scanning (with the exception of paediatric imaging). At 3 Tesla imaging, SAR interactions are frequent and necessitate alterations to the approach to scanning techniques e.g. the use of concatenated group scanning.

4.3.1.2 Aim

The aim of this section of work is to identify an appropriate pulse sequence to which MT can be added to in order to image synovitis without intravenous contrast agents:

(a) In a patient acceptable time
(b) Producing a scan volume that allows for coverage of the knee joint
(c) Without any artefacts distorting the image
(d) Without SAR implications preventing the running of the sequence
(e) Without altering the sequence parameters from one participant to another.

4.3.1.3 Method

Work described in this section is based on previous work performed by the candidate who explored the potential for MT imaging to quantify and specify the type of bone marrow oedema within the knee joint of patients with arthritis [239, 240]. In these papers, 2D spoiled gradient echo sequences with and without a MT pulse were acquired alongside post gadolinium 3D spoiled gradient echo with fat suppression images. Initial assessment of the scans showed that synovitis was also demonstrated on the MT difference images as well as the areas of bone marrow oedema (Figure 4-1).

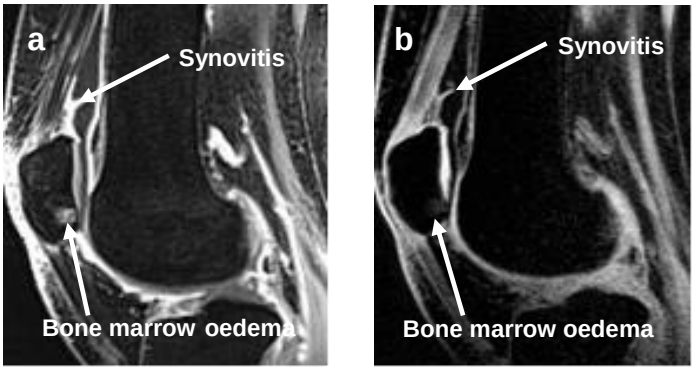

Figure 4-1 Sagittal Knee MRI scans in a patient with osteoarthritis. (a) Post IV contrast 3D VIBE scan (b) 2D SPGR MT difference scan [240]. Synovitis within the suprapatellar pouch is identified on both scans as labelled on the images. The protocol was developed to assess bone marrow oedema in the knee. An area of bone marrow oedema is seen in the lower pole of the patella as shown on the images.

The initial 2D SPGR MT sequences used to study bone marrow oedema had the following imaging parameters (Table 4-1):

Parameter	Value
TR (ms)	450
TE (ms)	17
Flip angle (degree)	30
Voxel size (mm)	0.7 x 0.5 x 3.0
Slice thickness (mm)	3
Slice distance factor (%)	20
Number of slices	16
Acquisition time (minutes)	1.55

Table 4-1 Parameters for the sagittal 2D SPGR ± MT MRI sequences used in a previous study [240] used for bone marrow oedema assessment

The MT pulse utilised was a Gaussian pulse and 500 degree flip angle with an offset frequency of 1950Hz and duration of 9984 micro seconds.

Whilst the presence or absence of synovitis could be identified on this pilot study, there were a number of limitations with the sequence:

- The limited amount of tissue covered by the scanning volume
- The large dimensions of the voxel size
- The inability for the MT images to ‘match’ the T1 mapping and post gadolinium images in location or geometry

The ability to scan the entire knee joint required the scanning volume to be increased: more slices will have to be added to the existing scanning protocol or the slice thickness and distance factor increased. As inflamed synovium has been classified as synovitis when it is over 2 mm in thickness [202], increasing the thickness of slice or increasing the gap to over 2mm could affect the amount of synovitis detected on the images due to partial volume effect [241]. It was therefore not clinically viable to increase these parameters so an alternative solution was sought.

Building on this work, it was essential to explore alternative methods of scanning the entire knee volume in an acceptable time in order to demonstrate the amount of synovitis present within the knee. It was decided to assess the feasibility and impact of 3D imaging for producing diagnostic MT images. 3D imaging allows for thin contiguous slices to be imaged [118] resulting in isotropic voxels with a high signal to noise ratio, acquired in an acceptable time. When combined with fat imaging techniques, conventional 3D imaging was already incorporated into the initial non contrast MRI scanning protocol (3D VIBE pre and post gadolinium sequences). It would therefore seem appropriate to match the geometry of the VIBE sequences with the MT images to allow for direct comparison of images.

A 3D SPGR ± MT sequence was prepared on the MRI scanner with the imaging parameters presented in Table 4-2. The protocol was assessed on a water phantom to ensure that:

- The geometric location exactly matched that of the other non-contrast sequences
- There were no obvious artefacts
- There were no issues regarding the specific absorption rate when MT pulse had been combined in vitro with a 3D sequence

The acquisition coils (small flex coils) were selected as for the other non-contrast sequences and the variables that needed to be optimised were:

- The TR value to be selected
- The number of slices required
- The value of the excitation pulse

In order for the MT sequence to be matched to the other 3D sequences, the geometry of the other 3D sequences was inputted into the imaging parameters of the 3D MT SPGR scan: thus the number of slices was pre-determined by the other sequences.

As described in Chapter 2, MT has its disadvantages when added to a pulse sequence: when added it is necessary to increase the radio frequency power deposition and the TR and therefore the scan time. Because it is imperative for the imaging parameters to remain constant for the SPGR ± MT for every patient regardless of weight or body dimensions, it was necessary to select a TR and flip angle that would not need to be adjusted.

The choice of a flip angle of 15 degrees was selected based on previous work undertaken in the LMBRU, the TOCRA study, a clinical trial to explore response to Tocilizumab in patients with RA. Images from this study were used as a reference source of images that had previously been validated to image synovitis in the knee.

Assessment of the SAR calculation was performed using a range of TR values. The aim was to find the smallest TR value that would allow for the number of slices desired to be scanned, that did not result in exceeding a SAR value of 100%, thus preventing the manipulation of scan parameters from patient to patient. This was achieved by scanning a water phantom with

the same coil configuration as for the other sequences. Fifteen SPGR scans with MT starting with a TR of 15ms rising to 30ms were performed using an inputted body weight of 70 kg into the scanner. Measurements were taken of the SAR calculated by the scanner for each value of TR.

Whilst SPGR imaging ± MT has been explored, there are other MRI sequences which have been shown to demonstrate the anatomy of articular joints better than SPGR [242] however the use of MT in combination with these to produce quantifiable data has not been investigated. Multiple-echo data image combination (MEDIC) is a sequence which has been shown to give good anatomical definition of the joints [243] and is compatible with MT. MEDIC is a heavily T2* weighted spoiled gradient echo sequence with multiple echoes. MEDIC has a relatively high signal to noise ratio (SNR) and has been useful in imaging articular cartilage [244].

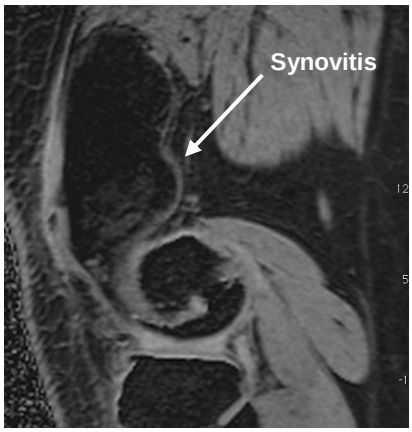

Figure 4-2 Sagittal SPGR MTR image of a patient with osteoarthritis of the knee.

A synovial effusion surrounded by synovitis is present on the image.

Comparison of the SPGR images ± MT with MEDIC images ± MT was performed to assess which sequence would be appropriate for adding to the protocol. Image acquisitions were performed on a quality control phantom and a volunteer who had a known Baker's cyst present

The parameters for SPGR and MEDIC sequences with and without MT are presented in Table 4-2.

Imaging parameter	Medic 3D MT	Initial MT 3D SPGR
TR (ms)	702	22
TE (ms)	17	2.46
Flip angle (degree)	30	15
Voxel size (mm)	0.8 x 0.8 x4.0	0.8 x 0.8 x 0.8
Slice thickness (mm)	4	0.8
Slice distance factor (%)	10	0
Number of slices	30	144
Acquisition time (minutes)	6.35	3.52

Table 4-2 Parameters for 2D MEDIC MT and initial 3D MT SPGR MRI sequences for assessing synovitis without intravenous contrast agents.

4.3.1.4 Results

Scanning the knee was feasible using the MEDIC sequence with and without the addition of MT. The sequences took six and a half minutes each equating to 13 minutes for the total MTR calculating protocol to be acquired. The MEDIC sequence provided images with high SNR. There was good delineation of structures within the knee joint; especially the articular cartilage, a tissue that has been imaged with the MEDIC sequence with results published in the literature [243, 244]. Unfortunately an artefact was demonstrated on the sagittal MEDIC image within an area of fluid (Baker's cyst) which could be construed to be synovitis as seen in Figure 4-3. The artefact is probably as a result of the subtraction used in the MEDIC sequence construction, resulting in a high signal artefact in areas of fluid where there is movement of the fluid during the acquisition. This does not have a detrimental effect on visualising images for anatomy that does not move, but could lead to overestimation in the volume of synovitis within a joint if there is a large enough fluid collection to produce it.

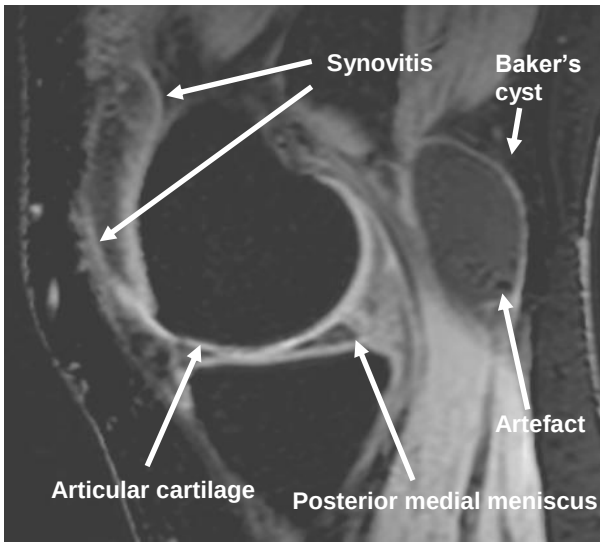

Figure 4-3 Sagittal MEDIC MR image of the knee in a patient with osteoarthritis.

The image shows a fluid filled Baker's cyst surrounded by synovitis. Within the hypointense signal area of fluid within the Baker's cyst are artefacts of the pulse sequence which mimics the appearance of synovitis within it.

It is possible and practical for the 2D SPGR sequence with and without MT to be used in the imaging of the knee in a relatively short acquisition time. However, the relatively thick, non- isotropic voxels present similar limitations as those associated with the MEDIC sequence. The slices are not thin enough to prevent partial volume from occurring and therefore affect the amount of synovitis from being measured accurately.

A 3D SPGR sequence with and without MT is achievable in an acquisition time that is acceptable to the patient, provides a large enough scanning volume to image the knee without any significant artefact on the images.

A 3D SPGR volume was chosen to allow for thin contiguous images to be produced, that could be matched with the post contrast gadolinium images to allow for direct comparison on the images. Unfortunately the 3D images had a lower SNR when compared to the original 2D MT protocol as a result of the thinner slice thickness. However the advantages of having a 3D isotropic high resolution volume outweighed the slight reduction in SNR.

The results from experimentation of TR values and SAR readings demonstrated that only those sequences with a TR of 28ms or more allowed the protocol to run without resulting in a SAR of over 100%. A value of 28ms was therefore selected for the TR as it is the shortest permissible and therefore results in the quickest scan acquisition time.

4.3.1.5 Discussion

MT has been shown to demonstrate both visually (MT difference imaging) and quantitatively (MTR measurements) synovitis within the knee joints of patients with a diagnosis of arthritis. The ability of adding on this technique to pulse sequences is limited and results in consequences which may preclude it from being used in a clinical study (for example SAR restrictions).

The benefits of using a T1 weighted gradient echo based sequence with MT would allow for relatively thin images to be acquired in a relatively short acquisition time and allow for quantitative measurements to be made. Work previously performed by the candidate had shown the compatibility of MT and the clinical practicality when used in conjunction with the SPGR sequence. There is however an alternative sequence that could potentially be used and has been used previously to image the knee, the MEDIC sequence. The MEDIC sequence has been used to demonstrate and measure the volume of articular cartilage [243, 245].

The geometry for both the 2D SPGR with and without MT and the MEDIC sequence were not the most favourable for imaging synovitis within the knee of patients with a clinical diagnosis of OA. The geometry was such that the slice thickness was too thick for both pulse sequences (4mm for the MEDIC and 3mm for the 2D SPGR). The thickness of the slices could prevent accurate measurement of the volume of synovitis due to partial volume.

If the MEDIC sequence were to be modified in order to maintain the scanning volume dimensions and reducing the slice thickness would result in a significant increase in acquisition scanning time which was currently six and a half minutes, as the TR would need to be increased (as scanning time is proportional to the TR) which would prevent this sequence from being used

in a clinical cohort. In addition to this and despite being proven to produce high resolution articular cartilage images in the knee joint [140], the artefact observed on the sagittal MEDIC image (Figure 4-3) precluded MEDIC from being a sequence to be included into the final COSMOS non-contrast study.

The volume coverage of the 2D SPGR sequences was inadequate to cover the whole of the knee: 16 slices of 3mm in approximately two minutes. To increase the number of slices to be of a number that is required to cover the whole knee would result in the increase of TR or result in multiple concatenations to compensate for this modification. Both solutions would increase the scanning time considerably increasing the possibility of the patient moving and marring the resultant images.

An alternative to the 2D SPGR sequence is a 3D SPGR technique with and without MT. By scanning a volume, the high resolution (less than 1mm) isotropic voxels can be acquired in a reasonable acquisition time (four minutes per sequence). The 3D technique with a suitably selected TR, will allow for the entire knee to be imaged using contiguous thin slices. An additional benefit of using a 3D technique is the increased signal to noise ratio which compensates for the decrease resulting from thinner slices. The ability of acquiring a 3D data volume provided another advantage in that the images can be matched to the exact location and geometrical parameters of the other sequences within the COSMOS protocol.

The minimum TR for the 3D SPGR sequence to run without producing any SAR issues with the shortest acquisition time was 28ms.

There is limited data available on MTR values measured within the knee joint to which the MTR values measured with this protocol can be validated against. However, the same principles applied to the optimisation of the T1 mapping protocol were used, in that all imaging filters were removed to prevent them affecting the MTR quantitative results.

Unfortunately, unlike T1 measuring, there are no phantoms of known value to compare and validate any results acquired, so therefore any results obtained must be taken to be correct.

4.3.1.6 Conclusion: MT imaging

Despite the advantage of increased SNR in the MEDIC sequence, the ability to produce quantifiable data in an acceptable time with minimum artefact resulted in the 3D SPGR sequences with and without MT to be selected for the COSMOS scanning protocol.

4.3.2 T1 measurements

4.3.2.1 Introduction

The potential use of a quantitative MRI sequence that can measure the characteristics of synovial tissue in addition to the volume would add to the clinical relevance of MRI scanning. Not only could the geometric volume be measured and compared at subsequent visits to assess the response to treatment, but an objective measurement to understand what is happening at an organ level to the tissue involved, could provide an important biomarker that could be used to assess the response of the tissue to disease modifying drugs.

4.3.2.2 Aim

The aim of this section of the thesis is to identify and optimise appropriate imaging parameters for a T1 mapping sequence that will allow synovitis to be visualised (with an approximate T1 value of 1400ms) and is able to measure T1 values for other structures of the knee in patients with a clinical diagnosis of OA knee in an acquisition time that patients are able to tolerate.

4.3.2.3 Method

Two approaches were used to explore the creation of and evaluation of a T1 protocol that could be used within the COSMOS study: In the first instance data from existing patients images held within the LMBRU were reassessed to confirm that the existing T1 protocol was not appropriate to use in the COSMOS study; then when the protocol had been proven to be unsuitable, we further optimised and validated the new sequence using phantoms. T1 quantitative data and the scanning protocol used to acquire those images of the knee joint in patients with arthritis held within the LMBRU from the TOCRA and OA knee studies were appraised to confirm previously measured T1 values of structures of the knee. The demographics of this patient cohort are presented in Table 4-3.

	Gender	Age	Disease
Patient 1	Female	70	OA
Patient 2	Female	75	OA
Patient 3	Male	72	OA
Patient 4	Male	61	OA
Patient 5	Female	53	RA
Patient 6	Male	58	OA
Patient 7	Female	43	RA
Patient 8	Male	59	RA
Patient 9	Female	45	RA
Patient 10	Male	62	RA
Patient 11	Female	68	OA

Table 4-3 Demographics of existing data of patients that were imaged using the T1 mapping sequence, held within the LMBRU that were reassessed to confirm the T1 values of structures within the knee.

The protocol that was used to acquire the T1 images held in the data bank of the LMBRU was sagittal Fast Low Angle Shot (FLASH) gradient echo sequences with imaging parameters of TR 8ms, TE 3.6ms, FA 3 and 17 degrees.

Confirmation of the T1 values measured in Chapter 3 of the medial head of the gastrocnemius muscle and synovial fluid of the patients detailed in Table 4-3 was performed using the same technique as detailed in 3.3.3.2. Assessment of the appropriateness of the flip angle selection (3° and 17°) in the existing T1 mapping sequence was performed by employing a bespoke computer programme in Matlab® written by Dr P J Wright. A retrospective simulation was carried out to calculate the optimum flip angles required to image a target value T1 of 1400ms with the following; TR of 8ms and flip angles of 3° and 17° (as were the imaging parameters for the T1 mapping used in the historical data collection). Five hundred simulations per flip angle were calculated. 1% noise was added to the simulation to replicate the T1 calculation as would be seen in a MR image [126].

Once confirmation that the inappropriate selection of imaging parameters was proven by the simulation to image structures with an expected T1 value of approximately 1400ms, a range of experiments were performed in an attempt to produce a T1 mapping protocol that could produce accurate T1 values. The existing imaging protocol was modified and optimised primarily concentrating on the following: flip angle selection, the addition of image filters to the raw data and coil selection.

Test gels of known values from the Eurospin® phantom which reflected the expected range of T1 values to be measured within the knee joint, and had been calibrated for use on a 3T scanner were used to assess and validate the T1 measurements.

Obtaining optimal accuracy of the T1 mapping protocol requires accurate selection of the pulse sequence parameters [246]. It has been previously suggested that the use of two flip angles is sufficient for acquiring and calculating T1 values [247] and this principle was adopted for the compilation of the T1 mapping sequence (Figure 4-4).

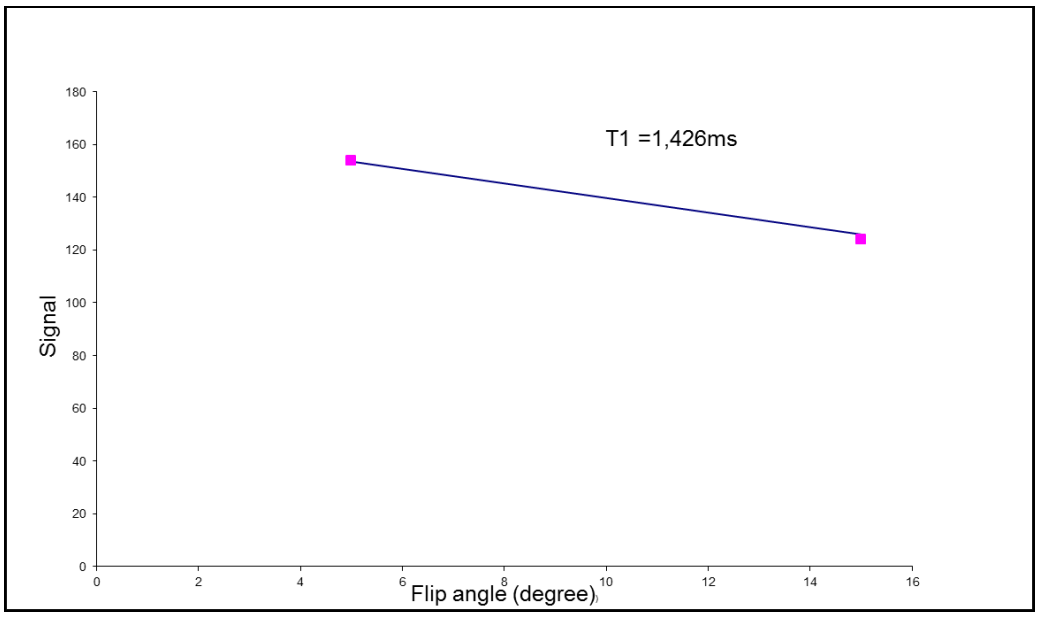

Figure 4-4 Graph showing a T1 calculation using two flip angles (5° and 15°) in a SPGR sequence.
The use of two flip angles produces a straight line graph and calculates the T1 value as 1426ms.

However, the use of three or more flip angles has been recommended to increase the accuracy of T1 fitting [248]. Tofts advocates the use of at least three flip angles be used when measuring a large range of T1 values [249] (Figure 4-5). It has been demonstrated that inaccuracies occur in the calculation of T1 values at 3T due to flip angle errors [249].

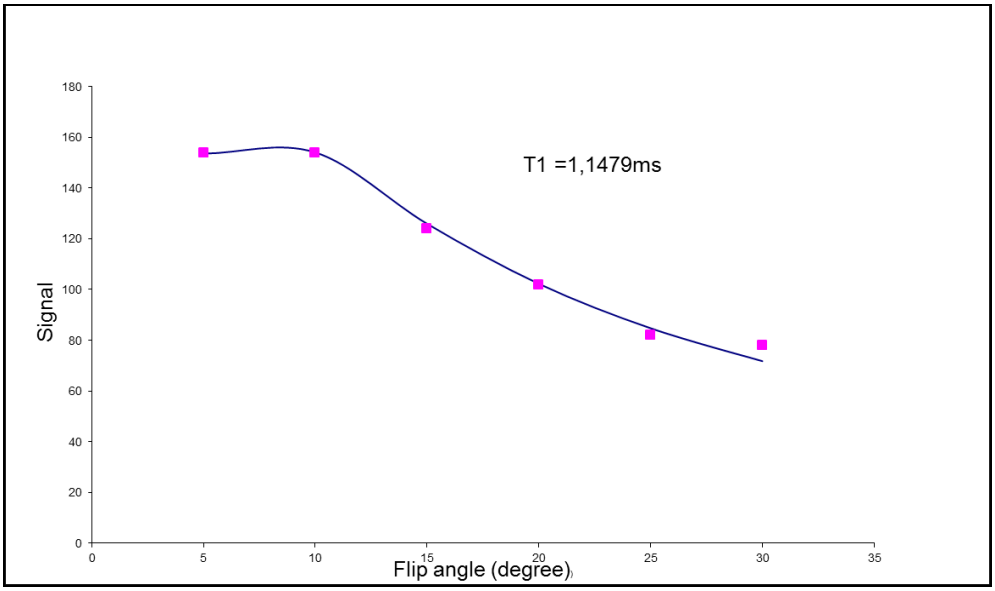

Figure 4-5 Graph showing T1 calculation using five flip angles (5°, 10°, 15°, 20° and 25°).
By increasing the number of flip angles used to calculate the T1 value, the graph approaches the exponential shape and a more accurate T1 value is calculated. In this example the calculated T1 value of 1479ms as compared to 1426ms in Figure 4-4.

The existing T1 protocol used the minimum number of two flip angles to calculate the T1 maps which were not optimised for structures of an expected T1 value of 1400ms. In addition to modifying the selection of flip angles to allow for the measurement of structures with a T1 of 1400ms it was also decided to increase the number of flip angles used in an attempt to increase the accuracy of the fitting of the curve and therefore the validity of T1 calculations [246, 249].

The use of two flip angles in the T1 mapping sequences results in the calculated T1 calculations and measurements are only reliable for the optimised target T1 value and therefore unable to accommodate values at either end of the spectrum of T1 values.

By increasing the number of flip angles there will be a reduction in the error in readings of tissues with a range of T1 value, e.g. fluid (long T1 value, ~3000ms), bone marrow (short T1 value, ~400ms) and the target tissue (intermediate T1 value, ~1400ms) within the knee joint.

Therefore the number of flip angles used to calculate the T1 measurements was increased from two to seven to allow for the ability of calculating relatively accurate T1 values of the structures of the knee.

The values of flip angles initially selected for the new T1 protocol were 5, 10, 15, 20, 25, 30 and 50 degrees. However due to the design of the spoiled gradient echo pulse sequence used for the T1 mapping, only flip angles under 27 degrees can be used as the sequence 'clips' the data at this point resulting in the same T1 values measured for tissues with 'long' T1 values regardless of the increase in flip angle value and the true T1 value of the tissue. Therefore the use of five flip angles below 27° (of 5°, 10°, 15°, 20° and 25°) were selected for the new T1 mapping protocol

Eurospin® test gel filled object test tubes, of known T1 values were used to validate the new T1 protocol. The test objects were scanned in the reference standard of the head coil initially to ensure that any readings produced were as accurate as possible and not affected by the coil selection.

In an attempt to negate any possible B_1 effects, a B_1 correction sequence was incorporated into the new T1 mapping protocol. Accuracy of the T1 values is vulnerable and can be affected by B_1 errors. The main mechanisms involved with these errors are:

- Inaccurate setting of the flip angle in the prescan procedure
- The dielectric resonance at 3T causing the RF field to be higher near the centre of the object when compared to its periphery
- RF transmission coils producing an ununiformed field

The inclusion of a B_1 prescan sequence to be run immediately prior to the multiple gradient echo sequences of different flip angles was included to ascertain whether the inclusion of a correction map may be of help to produce accurate T1 readings by compensating for variations in the B_1 field.

Siemens MRI scanners have the ability to allow users to apply and add image filters and correction factors to imaging sequences. These include: 2D distortion correction, 3D distortion correction, phase stabilisation, smooth,

phase partial Fourier and slice partial Fourier. These are useful in many situations by decreasing scan acquisition time and subjectively 'improving' the image but the addition of these may affect the data in such a way that it renders any quantitative measurements made from them meaningless. In order to omit any potential effects that any filters may have on the quantitative images, the T1 mapping sequences were repeated with the omission of all image filters.

In addition to appropriate selection of imaging parameters, the homogeneity of the B_0 field and stability of the imaging system is essential for accurate reproducible quantitative measurements. In order to monitor the stability of the imaging environment, a robust quality control programme should be included to predict or identify any potential faults.

4.3.2.4 Analysis

The T1 maps were assessed visually and T1 values measured. Mean and standard deviation for T1 values of the medial head of the gastrocnemius muscle and synovial fluid of existing data held within the LMBRU were measured using OsiriX® software. These values were plotted alongside those found in the literature for comparison and are displayed graphically.

The appropriateness of the imaging parameters selected of the existing LMBRU T1 mapping protocol for imaging structures with a value of approximately 1400ms were appraised: mean and standard deviations for the simulated T1 values using the original imaging parameters were measured using a bespoke simulator built in Matlab® by Dr P.J. Wright. Colour graphical representations of the results are presented in addition to the empirical values.

4.3.2.5 Results

T1 measurements for muscle and synovial fluid, as measured in Chapter 3, were confirmed by recalculation and the results compared to the literature (Table 4-4).

Tissue Type	Mean measured T1 on existing data in OA and RA knees as measured in Chapter 3	Repeated mean measured T1 values on existing data in OA and RA knees	T1 from literature
Muscle (ms) (SD)	1155.5 (359)	1162.5 (339)	1420 (38) [124]
Synovial Fluid (ms) (SD)	3659.9 (523.4)	3669.4 (518.3)	3620 (320) [124]

Table 4-4 T1 values measured from the cohort of knee patients held with the LMBRU to confirm values previously measured in Chapter 3 compared to those published in the literature.

Graphical representation of the test re test measurements of T1 values for muscle and synovial fluid from existing data from patients within the LMBRU are shown in Figure 4-6 and Figure 4-7.

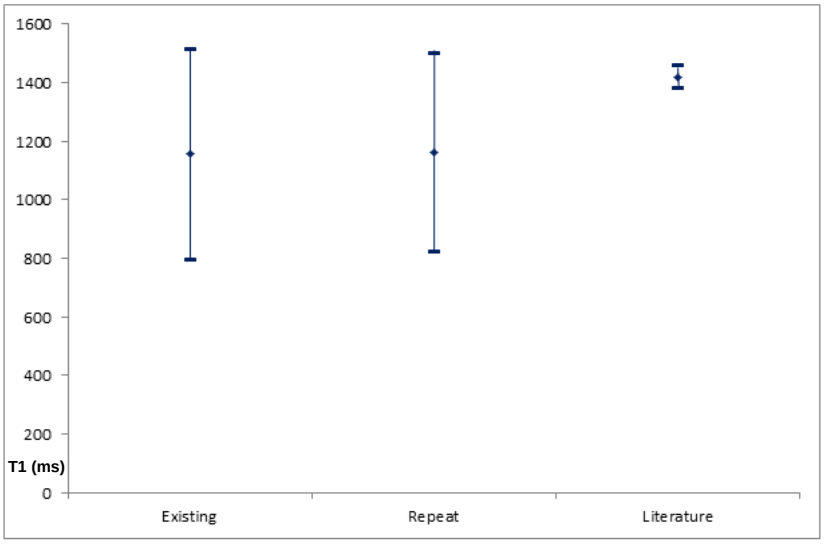

Figure 4-6 Comparison of mean T1 values with two standard deviations for measurements made of the gastrocnemius muscle from data within the LMBRU and the literature.

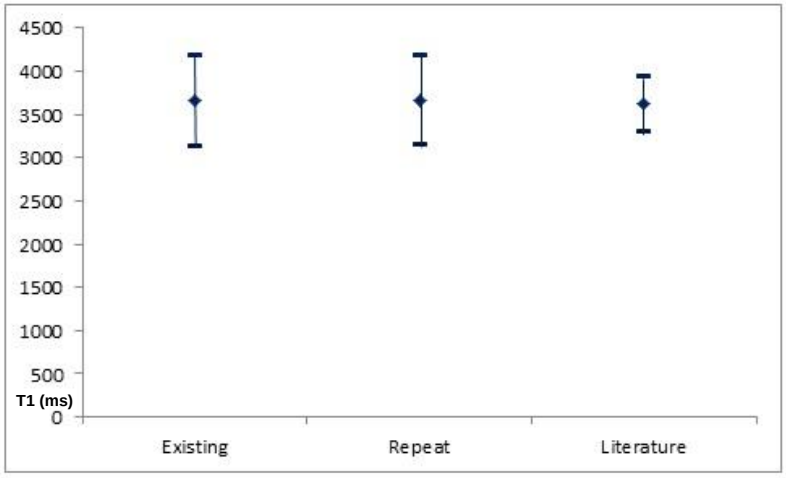

Figure 4-7 Comparison of mean T1 values with two standard deviations for measurements made of synovial fluid from data within the LMBRU and the literature.

Confirmation of inappropriate flip angle selection in the existing T1 mapping sequence was explored by inputting the imaging parameters into a computer simulator. The results of the T1 calculations calculated from the computer

simulation using the existing T1 protocol demonstrated that the selected flip angles of 3° and 17° were inappropriate for imaging tissues with an expected T1 value of 1,400ms. Figure 4-8 shows the mean T1 values calculated and Figure 4-9 the standard deviation of the simulated values.

In Figure 4-8 the colour scale represents T1 values measured in ms with dark blue representing a value of 0ms and dark red representing 3,800ms. The scale range results as a fact that the combination of the two flip angles was incorrect for calculating a T1 of 1400ms, and the simulator was unable to fit them, thus resulting in apparently very high T1 values. The target value of a T1 of 1400ms is represented by pale blue and can be identified on the plot by the white asterisks. The diagonal of dark blue pixels representing a T1 value of 0ms is due to the fact that you are unable to calculate a value of T1 with two identical flip angle values. The plot explicitly shows T1 values but is inherently showing error due the inappropriate selection of flip angles.

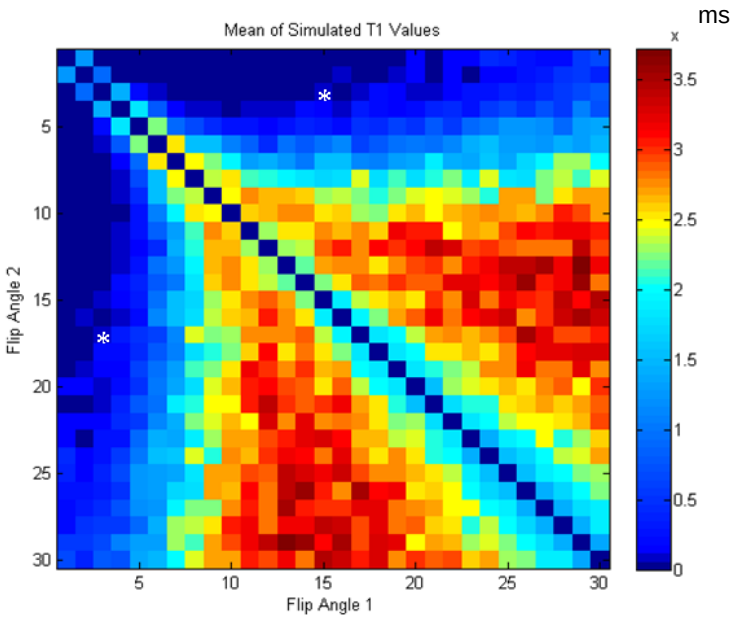

Figure 4-8 Plot showing mean simulated T1 values

The scan parameters used were: TR = 8ms Target T1 = 1400ms. Added noise = 1%
The colour scale is mean T1 values measured in ms.

ms

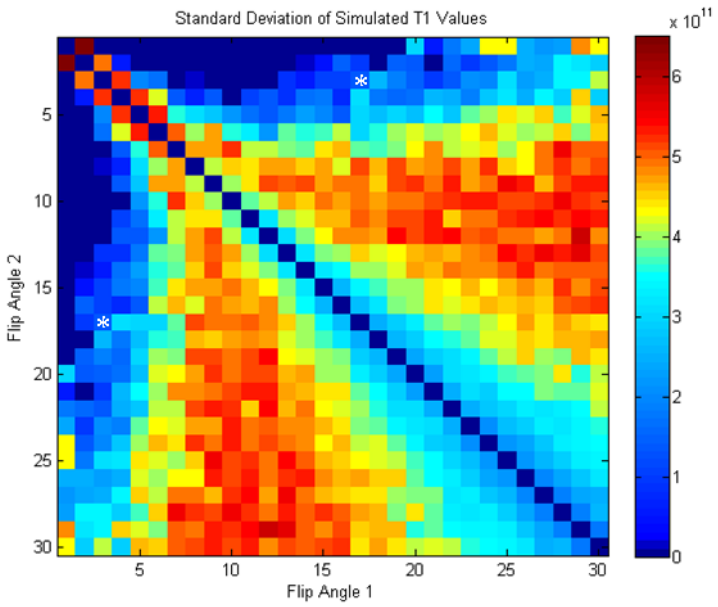

Figure 4-9 Standard deviation of simulated T1 values

The scan parameters used were: TR = 8ms Target T1 = 1400ms. Added noise = 1%
The colour scale is standard deviation of T1 values measured in ms.

The results of the simulation showed that the most accurate mean T1 = 1539ms would be for flip angles of 2 and 11 degrees. The smallest standard deviation in T1 = 951ms for flip angles of 2 and 10 degrees with mean T1 of 1567ms. The T1 and standard deviation for flip angles of 3 and 13 = 9.64E+09 +/- 1.35E+11. This confirms that the chosen flip angles used in the existing LMBRU T1 mapping sequences (3° and 17°) were not optimised for a T1 of approximately 1400ms.

The new T1 protocol using five flip angles (5°, 10°, 15°, 20° and 25°) produced initial T1 measurements that were disappointing when compared to the values published in the literature. Whilst the T1 values calculated from the test phantoms were closer to the expected values than those achieved using the existing protocol, there was still a disparity between them (Table 4-5).

	Tube 1	Tube 2	Tube 4	Tube 5	Tube 7	Tube 8	Tube 10	Tube 14	Tube 15	Tube 17	Tube 18
Expected (ms) (SD)	235 (17)	374 (27)	572 (41)	551 (31)	770 (66)	773 (66)	878 (72)	1323 (157)	1532 (56)	1656 (63)	1805 (139)
Measured (ms) (SD)	236 (13)	314 (30)	622 (35)	624 (37)	754 (74)	766 (50)	914 (60)	1185 (89)	1686 (63)	1604 (56)	2074 (92)
Previous T1 protocol (ms) (SD)	x	402.1 (43)	x	486.5 (43)	x	x	621.9 (65)	1549.4 (103)	1338.6 (65)	1155.7 (72)	x

Table 4-5 Results of calculated meanT1 values from new T1 protocol with image filters included in the protocol measured on eleven phantoms with known T1 values measured in the head coil.

Key: x: Calculation not measured either due to number of sample tubes used in the experiment or slice position not possible.

The data displayed in Table 4-5 of T1 values measured using a T1 protocol that incorporated imaging filters is presented graphically in Figure 4-10.

The graphical depiction of the results demonstrates that the T1 protocol with image filters is not accurate for measuring structures with a T1 value of over 400ms.

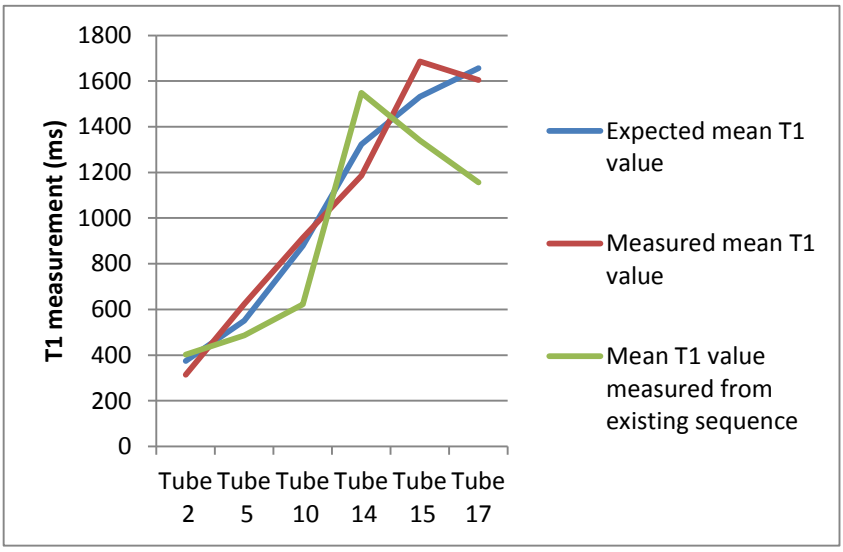

Figure 4-10 Comparison of the mean T1 values measured using the new T1 protocol with image filters

included in the protocol with those measured using the existing T1 protocol and the expected values calculated by the manufacturer of the test phantom. Measurements were taken using data acquired using the reference standard of the head coil.

However, when the image filters (for example image distortion correction filters) were removed from the sequence the T1 values calculated reflected those expected as calibrated by the manufacturer of the phantom as shown in Table 4-6.

	Tube 2	Tube 4	Tube 5	Tube 8	Tube 10	Tube 14	Tube 15	Tube 17
Expected (ms) (SD)	374 (27)	572 (41)	551 (31)	773 (66)	878 (72)	1323 (157)	1532 (56)	1656 (63)
Measured (ms) (SD)	324 (36)	500 (53)	528 (41)	770 (56)	900 (64)	1200 (98)	1560 (46)	1650 (56)
Previous T1 protocol (ms) (SD)	402.1 (43)	x	486.5 (43)	x	621.9 (65)	1549.4 (103)	1338.6 (65)	1155.7 (72)

Table 4-6 Results of T1 values from new T1 protocol without image filters included in the protocol measured on eleven known gel phantoms from the Eurospin® test tool scanned in the head coil.

Key: x: T1 value not measured either due to number of sample tubes used in the experiment or slice position not possible.

A graphical representation of the mean T1 values measured without image filters included in the protocol is presented in Figure 4-11. This shows that the new T1 scanning protocol is appropriate for imaging structures with a range of T1 values (400ms to 1600ms) and compares well with the expected values provided by the manufacturer of the test phantoms.

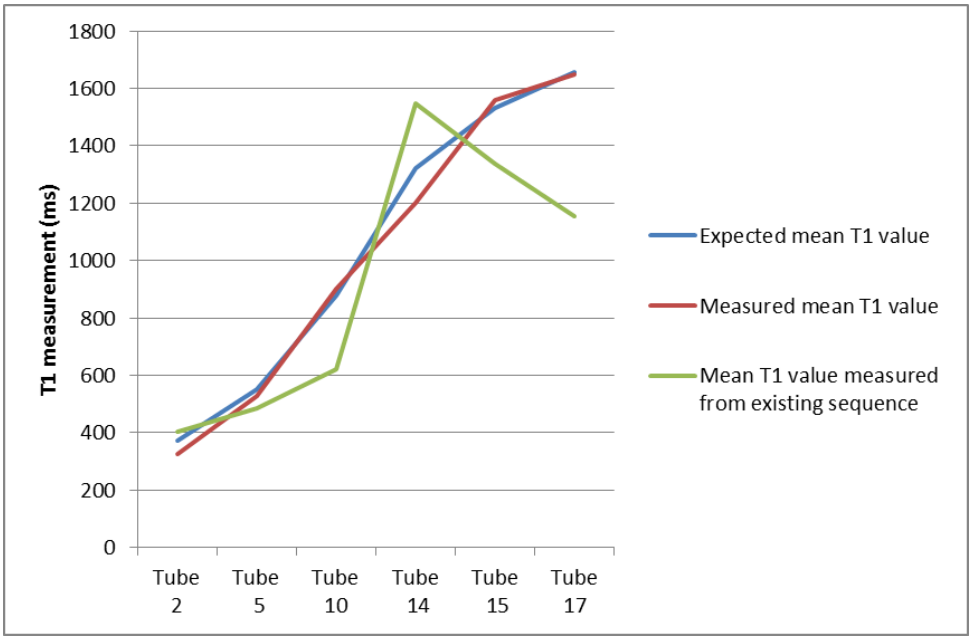

Figure 4-11 Comparison of the mean T1 values measured using the new T1 protocol without image filters

included into the protocol with those measured using the existing T1 protocol and the expected values calculated by the manufacturer of the test phantom. Measurements were taken using data acquired using the reference standard of the head coil.

Unfortunately, the B_1 correction map was ineffective in minimising inaccuracies of T1 measurements by compensating for any possible B_1 inhomogeneities as it was discovered at a later date that this sequence was only compatible with a specific bespoke T1 mapping protocol and unable to be used with any other sequence.

4.3.2.6 Discussion

Comparison of the T1 values between those measured on existing data held within the LMBRU, healthy volunteers and the literature, demonstrated inconsistencies between the values. Whilst it may have been expected between the LMBRU patient cohort and the literature the discrepancies between the healthy volunteers and the published data were unforeseen.

The demographics of the patient cohort were very different than that of the literature in both age and disease status. Values recorded in the literature were obtained on young healthy individuals whilst the LMBRU data was acquired from older individuals with a diagnosis of OA or RA involving the knee joint. In retrospect this was to be expected as the effects of the arthritic process in the knee joint will affect the characteristics of the tissues involved: For example atrophy of the muscles and degeneration of the articular cartilage resulting in different T1 values when compared to normal tissue. This is only a hypothesis as there have been no published studies documenting this.

Comparison of the healthy volunteer measurements with the literature also demonstrated variations of the T1 values measured. The healthy volunteers used, had different demographics when compared to that of the literature, but the volunteers were healthy and had no history of trauma or pathology of the knee joint.

In order to further test the existing protocol in vivo, an additional cohort of volunteers could have been scanned to provide an age and sex matched comparison identical to the literature. However, the COSMOS study had only ethical approval to scan a limited number of volunteers and the limit had been reached. There was though an alternative method available to provide the definitive result which was not dependent on possible variations of T1 values measured in vivo. The ability to use the existing and any subsequent T1 mapping protocols to scan test objects of known T1 values would be able to give the empirical and definitive result.

The results of the phantom scanning and computer simulation of the existing T1 protocol confirmed the inappropriate imaging parameters to produce accurate T1 readings of structures with an expected T1 value of 1400ms (the expected approximate T1 of synovitis).

The increase in accuracy of fit for T1 measuring has been shown to increase with the increased number of flip angles used within the protocol. Increasing the number of flip angles and using a larger range of flip angle values, allows for measurements of structures with a spectrum of T1 values. This however results in an acquisition time penalty as each flip angle has to be acquired separately thus increasing the T1 protocol from approximately 10 minutes to

over 20. This has the potential for increasing the risk of patient movement during the T1 mapping protocol and probable artefacts on the T1 maps rendering the data unusable.

Despite the possible disadvantages that would result if the number of flip angles were increased the potential benefits of acquiring accurate T1 values outweighed these. In theory, it would have been feasible to use the existing T1 protocol to visualise the structures of the knee, as the T1 values demonstrated on the images were such that structures could be visually differentiated from one another. If however, definite quantitative empirical values were required and were to have the potential to be used as a biomarker in disease identification or response to treatment, an accurate reproducible T1 protocol is required. Furthermore, if the T1 mapping protocol were seen to be of use in knee joints with OA, the possibility of translating this protocol to other joints and types of arthritis would require accurate quantitative measurements in addition to subjective visual differentiation of tissues.

Further optimisation of the new protocol was achieved by removing all of the filters from the imaging parameters. Whilst these may be appropriate in clinical scanning to improve the subjective quality of the images, the unknown affect they have on quantitative data acquired appears to affect the accuracy of values calculated.

Inhomogeneities of the B1 field may still have an effect on the T1 values calculated as it has not been possible to incorporate a B1 correction map within the protocol. However, the effects of this have been minimised as much as can be practicable by selecting an appropriate coil to scan the knee, as described in section 4.3.3.

A T1 protocol has been optimised for imaging the structures of the knee focussing on an optimised T1 of 1400ms, that which is expected of synovitis. The inclusion of multiple flip angles into the T1 mapping protocol will allow for the T1 values to be measured of other structures of the knee simultaneously to synovitis, which may provide extra information in either delineating structures or to be used as a biomarker of a disease.

4.3.2.7 Conclusion: T1 mapping

As a result of the experiments, a gradient echo sequence repeated with 5 different flip angles has been seen to produce the most reliable data set for T1 calculations. The flip angles selected were 5, 10, 15, 20 and 25 degrees. All prospective image filters were removed from the scanning protocol to prevent inaccuracy of signal characteristics on the quantifiable data.

4.3.3 Comparison of coil configurations

4.3.3.1 Introduction

Selection of the appropriate coil combination is essential in producing good quality diagnostic MR images [115] as well as reproducible quantitative data. The use of the smallest coil possible increases the signal to noise ratio of the MR image. Receive only coils do not have the inherent disadvantage of B_1 field inhomogeneities experienced with transmit/receive coils.

There are a number of suitable coils that can be selected to image the knee joints on a Siemens Verio® 3T scanner. These include:

1. 8 channel transmit and receive dedicated knee coil
2. 15 channel transmit and receive dedicated knee coil
3. 4 channel receive only small flex coils
4. 32 channel receive only cardiac coil

4.3.3.2 Aim

The aim of this section of the thesis is to evaluate possible MRI coils that could be used in the COSMOS study and to select the most appropriate coils for imaging the knee with a non-contrast and quantitative MRI protocol. The

coil selection must be acceptable to the patient to allow for tolerance of the COSMOS imaging protocol and provide accurate quantitative measurements.

4.3.3.3 Method

The knee joint can be imaged in a variety of MRI coils including dedicated knee joint coils which are available from the scanner manufacturer or third party vendor. However the knee joint can potentially be imaged using other generic coils providing the knee and the coil can be immobilised adequately.

There are two dedicated knee coils available for use with the Siemens 3T Verio® scanner: 8 and 15 channel transmit/receive coils. Transmit and receive coils, such as the knee coils, have inherent issues with the homogeneity of the B_1 field within them. These variances affect the B_1 field and therefore the T1 measurements across the field of view. B_1 correction maps are available to use prospectively and retrospectively on acquired data to correct for variations. However, there is no one agreed method and the process is convoluted and may not be reliable [250, 251]. The use of correction maps may not be required if the same scanner and coil configuration were used to scan the same individual on longitudinal visits. In order to remove the majority of these effects on the variations on the T1 measurements, transmit/receive coils were not used to acquire the data for this study.

Unlike transmit/receive coils, receive only coils do not have the inherent issues with uniform homogeneity of the field and B_1 correction maps are not required to calculate the flip angles across the field. Potential receive only coils available to scan the knee joint include: flex coils (small or large) and the cardiac coil.

Within the LMBRU both the small flex coil combination and the cardiac coils have been used to produce diagnostic images in the knee of patients with RA (Inflammatory Arthritis Disease Continuum, the IACON study).

The newly developed T1 mapping sequence using five flip angles was used to assess the suitability of the coils for inclusion within the study.

Six test tubes of known T1 values from the Eurospin® test tool were scanned in each coil: small flex coils, 8 channel transmit/receive knee coil and cardiac coil with the new T1 mapping sequence. The tubes selected reflected the expected range of T1 values of structures of the knee joint:

Tube 2 :347-401ms (expected fat T1 value), tube 5: 520-582ms, tube 10: 806-950ms, tube 14: 1166-1480ms, tube 15: 1476-1588ms and tube 17: 1593-1719ms (expected muscle and synovitis T1 value).

In addition to these the head coil was also used to scan the test tools, even though it was not suitable for scanning a knee, as it is a validated coil for producing T1 values, particularly with the Eurospin® test tool.

T1 maps for each tube and each coil were generated using OsiriX® software. The maps were calculated five times to average any variations in generated values. Mean values for the T1 measurements are reported.

4.3.3.4 Analysis

The use of inferential statistics was not possible to perform in order to compare the agreement of T1 measurements calculated by the new T1 protocol with the known values of the test phantoms. This was due to the lack of the complete data set being available relating to the manufactures data and only the mean and standard deviation of T1 values were available.

Comparison was made of the T1 values measured of the six test phantoms acquired with the head coil (reference standard), 8 channel knee coil, cardiac coil and the small flex coils. This was achieved by calculating T1 maps using OsiriX® software and then calculating the mean values with two standard deviations for each combination.

Comparison was made between the T1 values measured with each coil and the expected value of the test phantom. The difference between the values calculated and the manufacturer's data values was assessed by calculating the standard error of estimate (SEE) for each coil.

4.3.3.5 Results

T1 values were measured on the generated T1 maps for each coil and test tool sample. Sample pictures obtained of calculated T1 maps using OsiriX® acquired with the reference standard, head receive only coil and the 8 channel knee transmit/receive coil are shown in Figure 4-12. The mean and standard deviation of T1 values are shown on the images.

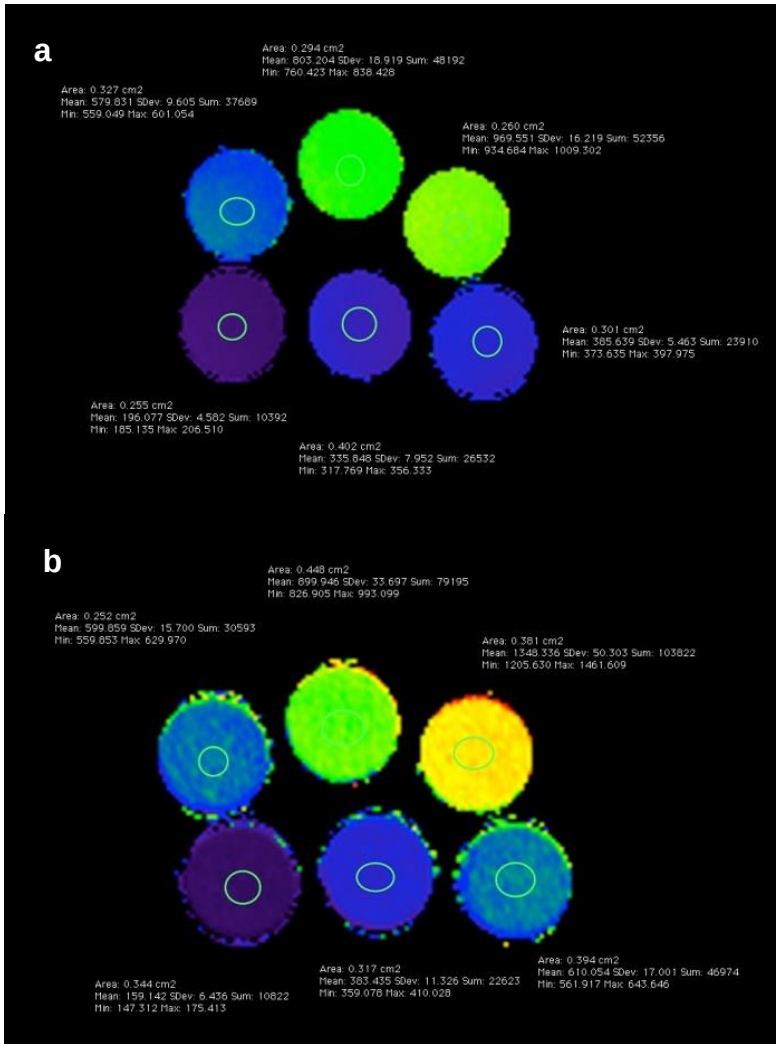

Figure 4-12 Comparison of T1 maps obtained with the new T1 protocol on two coils (a) 8 channel knee coil (b) head coil.
ROI's show the differences in empirical values for T1 values measurement imaged on the 8 channel knee coil and head coil.

The results of the mean T1 values with standard deviation for the new T1 mapping sequence measured on each coil are tabulated in Table 4-7.

Tube 2 374ms (SD 27)	Tube 5 551ms (SD 31)	Tube 10 878ms (SD 72)	Tube14 1323ms (SD 157)	Tube15 1532ms (SD 56)	Tube 17 1656ms (SD63)
HEAD COIL 345ms (SD150)	**HEAD COIL** 516ms (SD113)	**HEAD COIL** 864ms (SD95)	**HEAD COIL** 1298ms (SD97)	**HEAD COIL** 1498ms (SD87)	**HEAD COIL** 1627ms (SD83)
SMALL FLEX COIL 313ms (SD172)	**SMALL FLEX COIL** 540ms (SD178)	**SMALL FLEX COIL** 905ms (SD65)	**SMALL FLEX COIL** 1313ms (SD63)	**SMALL FLEX COIL** 1564ms (SD76)	**SMALL FLEX COIL** 1615ms (SD65)
CARDIAC COIL 335ms (SD28)	**CARDIAC COIL** 515ms (SD22)	**CARDIAC COIL** 882ms (SD22)	**CARDIAC COIL** 1282ms (SD20)	**CARDIAC COIL** 1485ms (SD21)	**CARDIAC COIL** 1600ms (SD21)
8 CHANNEL KNEE COIL 432ms (SD57)	**CHANNEL KNEE COIL** 426ms (SD69)	**8 CHANNEL KNEE COIL** 547ms (SD70)	**8 CHANNEL KNEE COIL** 1593ms (SD246)	**8 CHANNEL KNEE COIL** 1433ms (SD198)	**8 CHANNEL KNEE COIL** 1139ms (SD140)

Table 4-7 Mean T1 values calculated with the new T1 mapping protocol acquired on gel samples of known T1 values on a variety of MR coils at 3T.

The results using the new T1 protocol demonstrate that the mean T1 values measured from the head, small flex and cardiac coil are similar to those produced by the manufacturer of the test phantom whilst those measured with the 8 channel knee coil do not reflect the expected values (Figure 4-13).

Calculating the standard error of the estimate for the T1 values measured on each coil demonstrated that the small flex coil displayed the least variation or results when compared to the expected values (Table 4-8).

	R squared	Standard error of the estimate
Head coil	0.971	118.92ms
Small flex coil	0.976	97.32ms
Cardiac coil	0.975	110.04ms
8 channel knee coil	0.615	388.41ms

Table 4-8 Comparison of the results for the standard error of estimates for the T1 values measured on different coils using the new T1 mapping protocol on data acquired from phantoms with known T1 values.

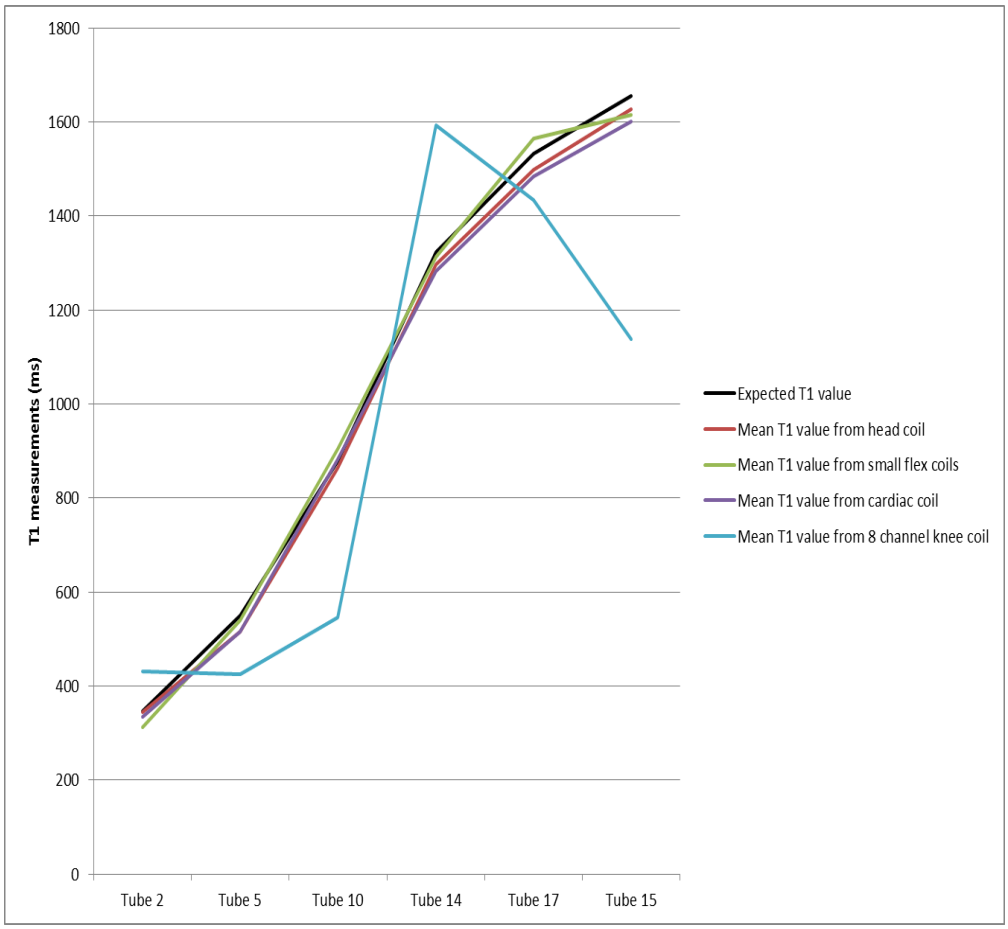

Figure 4-13 Graphical representation of mean T1 values measured over a range of T1 values (350ms to 1620ms) from four different coils, head, small flex, cardiac and 8 channel knee coil, alongside the expected values calculated by the manufacturer.

4.3.3.6 Discussion

Of all the coils tested with the new T1 protocol the only coil that did not produce T1 values in line with the expected values, was the dedicated 8 channel knee coil. The cardiac, head and small flex coils produced results across the range of T1 values tested, which were comparable to those provided by the manufacturer (Table 4-7 and Figure 4-13). The reference standard head coil was obviously rejected as a possible coil for use with the

COSMOS study due to the inability of scanning a knee with it. However, the results acquired with this coil provided reference values for the T1 protocol used with the Verio® system allowing for comparison and ensure validity of the results produced by the other coils.

Despite being manufactured to allow for good immobilisation of the patient and optimum knee imaging, the 8 channel knee coil was not judged to be suitable for use in the COSMOS study. The dedicated 8 channel transmit/ receive knee coil was rejected as a potential candidate for coil selection in the COSMOS protocol due to the inhomogeneity of the B_1 field across the coil affecting the accuracy and reproducibility of T1 measurements. T1 values acquired using the knee coil to scan the test phantoms did not reflect the expected results as documented by the manufacturer. The knee coil was unable to produce accurate T1 values even at a 'specific value' thus preventing its use when examining a small range of T1 values, low (300ms) for example. In addition to the inaccuracy of the T1 values produced, the dedicated 8 channel knee coil presents another possible limitation due to the physical dimensions of the coil. The internal circumference of the coil may prevent some patients from being scanned due to the size of their leg, in particular the quadriceps, and prohibit the coil from being closed.

The cardiac coil was a potential candidate for coil selection but the practical limitations of patient positioning, immobilisation and siting the coil in the isocentre of the magnetic field rendered it impractical. The main practical issues involving the cardiac coil were:

- The practical limitations of getting the knee joint into the coil and getting the patient comfortable.
- The physical components of the cardiac coil are such that is impossible to place off centre to the scanner allowing for placement of the other knee joint.
- The length of the connector cables are such that it can only be placed in a very limited range of positions on the table resulting in the legs of the patient having to be bent up when they first get onto the scanner. Whilst this can be rectified when the scanning table is at its

operational height, it is a possible rate limiting factor in patient recruitment if they are unable to bend and lift their legs to a position to allow for the table to be raised.

The T1 values measured using this coil reflected the expected values documented by the test tool manufacturer and could be used to provide accurate data. However the practicalities of using this coil deemed it inappropriate as a first choice of coil for the COSMOS study.

The small flex coils gave the best results for suitability of use in the COSMOS study. The T1 measurements obtained from the test phantoms scanned with the small flex coils resulted in values which were comparable with the manufacturer's data both for low and high values. The flex coil showed the smallest error of estimation (97.32ms) when compared to the expected reference value. The use of the two small flex coils provided a practical solution for imaging the knees of patients in that they were comfortable and allowed the knee to be placed into the isocentre of the magnetic field. Patient recruitment would not be limited to the size of the knee as a very large range of knee dimensions can be accommodated with the flex coil selection when compared to the dedicated knee coil. This would allow for a representative sample to be included into the COSMOS study allowing for an accurate patient cohort to be included. Velcro straps, pads and sand bags provided adequate immobilisation of the leg in the small flex coils.

4.3.3.7 Conclusion: Coil selection

The imaging coils selected to image patients with OA knee in the COSMOS study were the two small flex receive only coils.

4.3.4 Conclusion

It has been possible to optimise the MT and T1 quantitative MR sequences to produce a protocol that allows for quantitative images to be produced in an acceptable acquisition time for patients with a coil combination which will allow for the majority of knees to be imaged regardless of size. The selection of a receive only coil will minimise the effects of any B1 inhomogeneities.

The imaging parameters have been selected to be such that there should not be necessary to alter them on a patient to patient basis thus providing comparison of images from patients with identical imaging parameters. Thus any differences perceived on the images will be due to pathology and not the imaging environment.

Sagittal SPGR sequences with and without MT, T1 mapping sequences utilising 5°,10°,15°, 20° and 25° scanned using the two small flex coils were included into the non-contrast COSMOS protocol. The imaging parameters are presented in Table 4-9.

	TR (ms)	TE (ms)	Averages	Bandwidth (Hz/pixel)	Flip angle	MT	Scan Time
3D SPGR + MT	28	2.46	1	540	15°	On	3.50 minutes
3D SPGR - MT	28	2.46	1	540	15°	Off	3.50 minutes
3D T1 map 5°	11	2.46	1	540	5°	Off	1.55 minutes
3D T1 map 10°	11	2.46	1	540	10°	Off	1.55 minutes
3D T1 map 15°	11	2.46	1	540	15°	Off	1.55 minutes
3D T1 map 20°	11	2.46	1	540	20°	Off	1.55 minutes
3D T1 map 25°	11	2.46	1	540	25°	Off	1.55 minutes

Table 4-9 Imaging parameters for the optimised quantitative MR sequences for inclusion in the COSMOS non-contrast protocol using two small flex coils

Chapter 5 COSMOS study

5.1 Introduction

The underpinning aim of this thesis was to develop an inexpensive, patient friendly procedure to measure synovitis that would offer an alternative to MRI contrast enhanced scanning. Following initial identification of candidate sequences reported in Chapters 3 and 4, this chapter describes (i) an initial pilot study (n=10) which further refined the COSMOS protocol in terms of practical application and sequence parameters and (ii) the application of the modified COSMOS protocol to a large OA patient cohort (n=91).

5.2 Formulation of the COSMOS protocol

The aim of Chapters 3 and 4 were to identify possible candidate sequences to be included in COSMOS. Each sequence has its strengths and weaknesses in potentially identifying different types of tissue and the selection of the MRI sequences was performed to maximise tissue differentiation potential in the shortest acquisition time. The initial 11 sequences selected and the potential benefit of each are presented in Table 5-1.

MRI pulse sequence name	Potential differentiation of tissues
Sagittal 2D T2 TSE	Fluid vs Synovitis vs extra articular tissues
Sagittal 2D T1 TSE	Anatomical boundaries, blood products
Sagittal 2D Proton density fat sat	Fluid vs Synovitis vs extra articular tissues
Sagittal 3D SPGR + MT	Synovitis vs fluid To be used in the calculation of the MT difference images To be used in the calculation of MTR images
Sagittal 3D SPGR - MT	Synovitis vs fluid To be used in the calculation of the MT difference images To be used in the calculation of MTR image
Sagittal 3D DIXON VIBE	Fat vs other tissue types
Sagittal 3D DESS	Fluid vs Synovitis vs extra articular tissues
B1 map	Potential for adjusting of field inhomogeneities
Sagittal 3D T1 GE mapping sequences	Synovitis vs muscle Calculation of T1 maps
Sagittal 3D VIBE pre contrast	Ability to use as mask for post contrast VIBE subtraction
Five Sagittal 3D VIBE post contrast sequences	Delineation of inflammation

Table 5-1 Sequences from the initial COSMOS protocol.
The potential benefit for each sequence in terms of tissue differentiation is also provided

5.3 COSMOS pilot study

5.3.1 Aims and objectives

The primary aim of the pilot study was to evaluate the proposed non-contrast COSMOS MRI protocol in a small clinical cohort of patients with knee OA. This was an important process in the study to ensure, to the best of the ability of the candidate, to provide a data set at the completion of the study that would be without error and be able to be used as a reference group for further studies. The main areas that were to be explored and modified if required were:

(a) Determine patient acceptability of the protocol

(b) Ensuring high image quality, free from artefact

(c) Stability of the quantitative sequences

(d) Ability to discriminate different tissue types in an OA knee population

5.3.2 Method

Patients with OA of the knee were recruited from the orthopaedic and rheumatology departments of the Leeds Teaching Hospital NHS Trust for both the pilot and the main COSMOS studies. Following ethical approval (REC number 12/YH/0238, RR12/10208), potential participants were approached with information regarding the study and to ascertain that they met the inclusion criteria (Table 5-2) and were screened to ensure it was *safe* to have an MRI scan. Patients that were having the administration of intravenous gadolinium based contrast agent (GBCA) as part of the study first had an eGFR blood test performed within a month before the MRI scan. This was performed to ensure that the renal function of the patients was adequate to excrete the administered gadolinium minimising the risk of exposing them to NSF [252]. Patients with an eGFR greater than 40

mls/min/1.73m^2 were able to have the gadolinium contrast agent if they agreed to this and did not have a previous allergic history, an exclusion criteria for IV gadolinium described in the ethics application.

Inclusion criteria	Exclusion criteria
Over 18 years of age	Contraindication to Magnetic Resonance Imaging
Consultant diagnosed osteoarthritis of the knee	Diagnosis of another type of arthritis
	Unable to provide consent
	Contraindication to intravenous gadolinium for contrast enhanced scanning
	eGFR < 40 mL/min/1.73m^2 for contrast scanning
	Previous history of anaphylactic reaction for contrast scanning
	Previous hospitalisation due to asthma for contrast scanning

Table 5-2 Inclusion and exclusion criteria for patients in the COSMOS study

The first ten patients recruited were included in the pilot study. The demographics of the patients and scan protocol performed are presented in Table 5-3.

	Gender	Age	Scan Protocol	Contrast	Comment
COSMOS patient 1	Female	50	Pilot COSMOS	No	No gadolinium administered
COSMOS patient 2	Female	52	Pilot COSMOS	No	No gadolinium administered
COSMOS patient 3	Male	44	Pilot COSMOS	No	No gadolinium administered
COSMOS patient 4	Male	64	Pilot COSMOS	No	Reproducibility of MT and T1 scans performed. No contrast given
COSMOS patient 5	Female	44	Pilot COSMOS	No	Patient unable to tolerate scan. Scan abandoned
COSMOS patient 6	Female	46	Pilot COSMOS	Yes	
COSMOS patient 7	Male	58	Pilot COSMOS	Yes	
COSMOS patient 8	Male	52	Pilot COSMOS	Yes	
COSMOS patient 9	Male	76	Pilot COSMOS	Yes	
COSMOS patient 10	Female	50	Pilot COSMOS	Yes	

Table 5-3 Demographics of the first ten patients and scanning protocol performed in the COSMOS pilot study

Data from the COSMOS pilot study was analysed and scrutinised to identify any issues with the protocol in order to streamline the main COSMOS study. Testing of the COSMOS protocol had been performed on phantoms and volunteers, but the true test of patient acceptability and appropriate selection of imaging parameters is to apply the protocol to a small clinical cohort.

The first three patients of the COSMOS pilot study had the non-enhanced COSMOS protocol performed on them without acquiring the post contrast comparative VIBE sequences.

Previously, the non-contrast MRI protocol had been checked on five healthy volunteers to assess scan coverage and possible SAR implications; however as this may not be representative of those with OA knee it was thought to be prudent to assess these prior to the main study. For this reason, it was deemed best practice not to expose the first three patients to an invasive procedure and to perform COSMOS protocol without the use of contrast agents. If no contraindications were apparent, subsequent patients were considered for the administration of intravenous gadolinium if they consented to this.

The initial COSMOS scanning protocol is detailed in Table 5-4.

Imaging plane and sequence	TR (ms)	TE (ms)	FA degrees	Voxel size	Acquisition time
2D sagittal T2 TSE	5000	70	*	0.8 x 0.8 x 2 mm	3.02 minutes
2D sagittal T1 TSE	908	10	*	0.8 x 0.8 x 2 mm	3.07 minutes
2D sagittal PD fs	5840	42	*	0.8 x 0.8 x 2 mm	5.05 minutes
3D sagittal SPGR with MT	22	2.46	15°	0.8 x 0.8 x 0.8 mm	3.52 minutes
3D sagittal SPGR without MT	22	2.46	15°	0.8 x 0.8 x 0.8 mm	3.52 minutes
3D sagittal VIBE Dixon	10	2.45 / 3.68	10°	0.8 x 0.8 x 0.8 mm	1.53 minutes
3D sagittal DESS	14	5	25°	0.8 x 0.8 x 0.8 mm	2.28 minutes
Axial B1 map	1000	14 / 14	90°, 120°, 60°, 135°, 45°	3.9 x 3.9 x 10 mm	1.09 minutes
Sagittal T1 mapping sequences comprising of:					
3D T1 map 5°	11	2.46	5°	0.8 x 0.8 x 5mm	1.55 minutes
3D T1 map 10 °	11	2.46	10°	0.8 x 0.8 x 5mm	1.55 minutes
3D T1 map 15°	11	2.46	15°	0.8 x 0.8 x 5mm	1.55 minutes
3D T1 map 20°	11	2.46	20°	0.8 x 0.8 x 5mm	1.55 minutes
3D T1 map 25°	11	2.46	25°	0.8 x 0.8 x 5mm	1.55 minutes
Sagittal 3D WE VIBE Pre gadolinium	9.8	4.9	30°	0.8 x 0.8 x 0.8 mm	1.50 minutes
Sagittal 3D WE VIBE Post GBCA X 5 phases At 0 minutes 1.50 minutes 3.40 minutes 5.30 minutes 7.20 minutes	9.8	4.9	30°	0.8 x 0.8 x 0.8 mm	1.50 minutes per sequence

Table 5-4 Sequences and key imaging parameters used for the first ten COSMOS patients

Those that were having GBCA administered were cannulated with a blue venflon in the median cubital fossa under aseptic conditions.

Patients were scanned on the LMBRU Siemens Verio® 3T MRI scanner. Two receive-only small flex coils were placed around the knee using sand bags and Velcro® straps to secure them in place and immobilise the leg. The knee of interest was placed as close as possible to the isocentre of the magnet without causing the patient any discomfort.

If gadolinium was administered, the venflon was connected to a MRI compatible pump injector (Spectris Solaris®, Medrad) loaded with GBCA (Dotarem®, Gadoteric acid 279.32 mg/ml, Guerbet©, Roissy, France) and normal saline (0.9%w/v) flush. A pump injector was chosen to administer the GBCA to allow for consistency in delivery rate for each patient.

The patient was given an emergency alarm to activate if they wished to terminate the procedure, and headphones to minimise the scanner noise.

Sagittal scans were localised and performed through the affected knee. The scanning volumes were copied to each other to ensure that the location of the acquired slices would match.

At the appropriate timing within the scan protocol, GBCA was administered to the patient at a rate of 2mls per second with a dose calculated based on their body weight, but with a maximum of 20mls administered. This resulted in the commencement of contrast enhanced sequence acquisition at 0, 1.50, 3.40, 5.30 and 7.20 minutes after the administration of the GBCA. 50mls of saline was given after the gadolinium to flush the system ensuring that the complete dose had been administered.

In respect of image analysis and review for the COSMOS study, the images were reviewed and post processing was performed on an independent workstation using OsiriX® software (version 4.0 64 bit, Pixmeo, Geneva).

In order to ascertain the stability of the scanning environment for quantitative T1 and MTR measurements using the selected coils and new MRI sequences in vivo, patient number four only had repeated SPGR with and without MT and one of the T1 mapping sequences (flip angle 5°) performed on them. Each scanning sequence was repeated six times at the same location within the knee, within the medial head of the gastrocnemius, (i.e. six

acquisitions of the T1 mapping sequence of 5° and six acquisitions of the SPGR with MT and without MT equating to one hour scanning time). A pragmatic approach was taken in selecting the number of repetitions of the scans as the maximum amount of data was desired in an acceptable scanning time that could be tolerated by the patient. Fifty measurements of signal intensities were made using ROIs of approximately $5mm^2$ of each sequence at the same location in the medial head of the gastrocnemius muscle to assess the reproducibility of the sequence.

In the patients that had the complete T1 mapping protocol and the SPGR sequences with and without MT, T1 maps were calculated and MTR images generated. From these images MTR and T1 measurements were made in the medial head of the gastrocnemius, bone marrow of the femoral epiphysis, subcutaneous fat, articular cartilage, synovial fluid and synovitis if present. Sixty ROIs of $5mm^2$ from each quantitative method and tissue type were made.

5.3.3 Analysis

Patient acceptability was assessed by an informal, unstructured interview with particular emphasis on their comfort and length of duration of the scan.

All of the images were visually inspected to ensure that they were of diagnostic quality, had no patient movement artefact or any other artefacts on the images that may mar interpretation or calculation of quantitative measurements on the T1 and MTR scans.

Stability of the quantitative sequences from patient four, T1 and MT, were assessed by calculating the mean values and standard deviation for the six readings using Statistical Package for the Social Sciences (SPSS version 21.0). The mean values (with two standard deviations) were plotted graphically. Due to the small amount of data assessed, the use of inferential statistics was not appropriate.

T1 maps and MTR images were generated using OsiriX® software. Mean values for muscle, bone marrow, subcutaneous fat, articular cartilage,

synovial fluid and synovitis were measured and recorded. Sixty ROI measurements were made of each tissue type.

5.3.4 Results

(a) Patient acceptability

A summary of the patient demographics, scan protocol, whether contrast was administered and the ability for the patient to tolerate the scan are presented in Table 5-3.

Of the ten patients that commenced the COSMOS pilot study, nine completed the scan. Unfortunately, one patient had quite severe OA of the lumbar spine and despite trying to make her as comfortable as possible she was unable to lie still long enough to complete the examination. Five patients had intravenous gadolinium administered and five patients had a non-contrast enhanced scan, one of whom was the patient who was unable to tolerate the complete scan.

(b) Quality of images

All of the images acquired were visually inspected to assess the diagnostic quality of them. Particular attention was paid to assessing for the presence of artefacts, either due to patient movement or those attributed to the technique. The T1 and MT images from three patients demonstrated artefact on them and will be discussed further in section 5.3.5.

(c) Stability of the quantitative sequences

Signal intensity values measured from the gastrocnemius muscle on the SPGR sequences with and without MT to assess stability showed a mean value of 983 (SD 10.86) for MT and a mean value of 1004.17 (SD 9.77) for

those without MT. The individual results of the stability of the MT scans and the MTR value calculated from them are tabulated in Table 5-5.

	MT	No MT	MTR
Reading 1	993	1014	0.02
Reading 2	988	1003	0.01
Reading 3	977	1000	0.02
Reading 4	996	1018	0.02
Reading 5	975	996	0.02
Reading 6	969	994	0.02
Mean (SD)	983 (10.86)	1004 (9.77)	0.02 (0.004)

Table 5-5 Table showing the signal intensity readings for the SPGR scans ± MT repeated six times in the medial head of the gastrocnemius muscle in a single patient to explore the reproducibility of the sequence in vivo. The MTR values calculated as a result of the readings are also shown in the table.

Reproducibility stability for T1 measurements showed a homogenous set of results with a mean of 1218.3ms (SD 1.17ms) calculated for the six measurements. The individual T1 readings are displayed in Table 5-6.

	T1 (ms)
Reading 1	1230
Reading 2	1230
Reading 3	1220
Reading 4	1220
Reading 5	1210
Reading 6	1200
Mean (SD)	1218.3 (1.17)

Table 5-6 Table showing the mean T1 measurements for six repeated T1 scans in the medial head of the gastrocnemius muscle of a single patient to explore the stability and reproducibility of the sequence in vivo.

(d) Ability to discriminate tissue types

MTR and T1 readings were made of anatomical structures within the knee. Sixty ROI measurements of $5mm^2$ were made of each structure for each patient. Measurements were taken in the medial head of the gastrocnemius muscle, bone marrow of the femoral epiphysis, subcutaneous fat, articular cartilage of the femur and synovitis and synovial fluid if present. Measurements were taken in the middle of the coil configuration to prevent anomalies in readings due to variations in the B_1 field. Care was taken to measure areas of bone marrow without bone marrow oedema and normal articular cartilage. Comparison of the T1 and MTR scans with other sequences was performed to select normal bone marrow and articular cartilage if there was any uncertainty.

T1 measurements were made in all anatomical areas of the knee in eight patients (due to one patient abandoning the scan before the imaging could be performed and one patient having the reproducibility protocol only performed) and MTR calculations derived in all ten patients. The results of these are presented in Table 5-7 and Table 5-8.

	Muscle (ms)	Synovitis (ms)	Bone Marrow (ms)	Subcutaneous Fat (ms)	Articular cartilage (ms)	Synovial fluid (ms)
COSMOS patient 1 (SD)	1640 (278)	1808 (621)	*	*	*	*
COSMOS patient 2 (SD)	1867 (258)	1738 (312)	408 (65)	422 (42)	1215 (111)	3607 (635)
COSMOS patient 3 (SD)	2189 (306)	1086 (442)	343 (43)	435 (40)	837 (170)	3080 (603)
COSMOS patient 4 (SD)	1508 (87)	1095 (303)	367 (37)	512 (16)	786 (134)	2716 (1520)
COSMOS patient 5 (SD)	*	*	*	*	*	*
COSMOS patient 6 (SD)	1571 (144)	987 (213)	431 (16)	394 (17)	966 (194)	2592 (414)
COSMOS patient 7 (SD)	1655 (207)	993 (210)	337 (25)	510 (33)	953 (151)	2751 (717)
COSMOS patient 8 (SD)	1574 (178)	952 (192)	402 (28)	478 (23)	1375 (168)	3513 (460)
COSMOS patient 9 (SD)	1548 (193)	1045 (174)	372 (74)	476 (74)	921 (219)	2728 (961)
COSMOS patient 10 (SD)	1707 (156)	965 (136)	455 (52)	618 (65)	921 (198)	*
Mean (SD)	1697 (201)	1244 (368)	390 (42)	481 (69)	997 (198)	2998 (413)

Table 5-7 T1 measurements made of structures of the knee in the first ten patients of the COSMOS pilot study.

Graphical representation of the mean T1 values (with two standard deviations) measured in the different structures of the knee is presented in Figure 5-1.

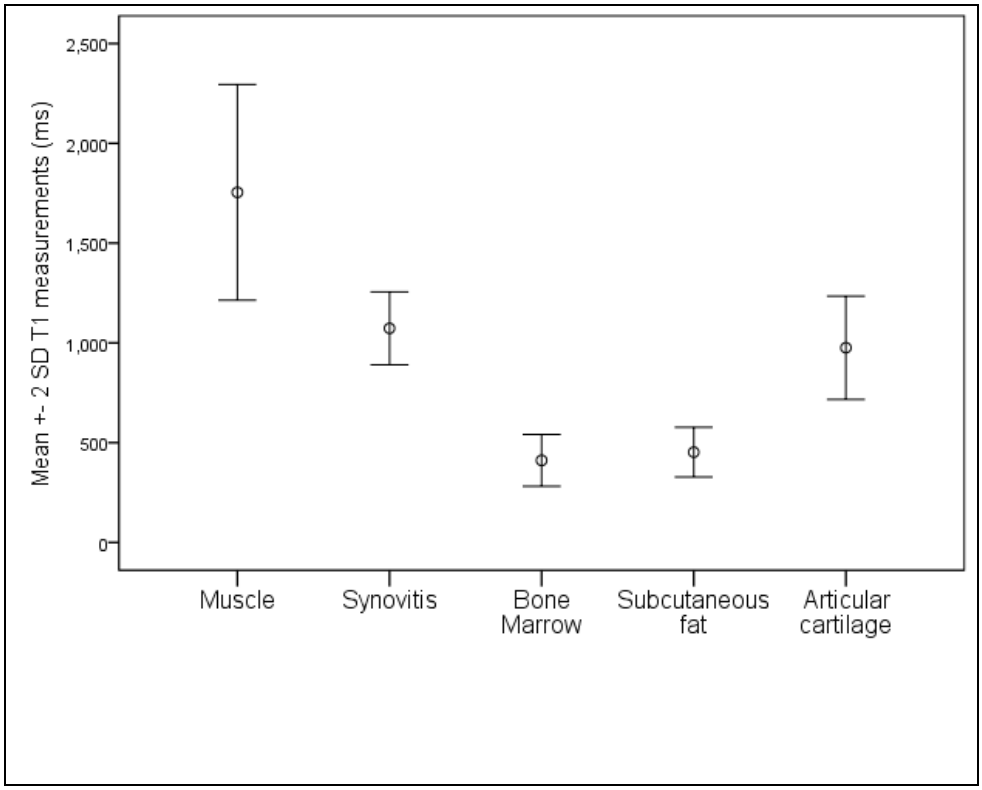

Figure 5-1 Mean T1 measurements with two standard deviations for structures of the knee in the initial ten patients of the COSMOS pilot study.

Synovial fluid has been removed from the graph as there is no overlap with this and the other structures of the knee with regards to T1 values. This allows for a smaller scale to be used on the y axis.

MTR calculations were made in all ten of the patients in the COSMOS pilot study. Measurements were made in the medial head of the gastrocnemius, bone marrow, subcutaneous fat, articular cartilage and synovitis if present. The results of the values measured for the structures of the knee are presented in Table 5-8.

	Muscle	Synovitis	Bone Marrow	Subcutaneous Fat	Articular cartilage	Synovial fluid
COSMOS patient 1 (SD)	0.38 (0.04)	0.36 (0.08)	0.01 (0.05)	0.04 (0.02)	0,45 (0.05)	*
COSMOS patient 2 (SD)	0.39 (0.05)	0.34 (0.11)	0.03 (0.05)	0.02 (0.02)	0.39 (0.07)	*
COSMOS patient 3 (SD)	0.39 (0.03)	0.34 (0.09)	0.04 (0.05)	0.04 (0.01)	0.39 (0.04)	*
COSMOS patient 4 (SD)	0.38 (0.02)	0.45 (0.08)	0.06 (0.01)	0.03 (0.01)	0.38 (0.05)	*
COSMOS patient 5 (SD)	0.39 (0.01)	0.34 (0.09)	0.09 (0.01)	0.03 (0.05)	0.40 (0.06)	*
COSMOS patient 6 (SD)	0.37 (0.02)	0.44 (0.07)	0.06 (0.01)	0.02 (0.01)	0.41 (0.06)	*
COSMOS patient 7 (SD)	0.37 (0.02)	0.28 (0.08)	0.07 (0.01)	0.03 (0.01)	0.42 (0.05)	*
COSMOS patient 8 (SD)	0.39 (0.02)	0.37 (0.01)	0.04 (0.01)	0.02 (0.01)	0.47 (0.04)	*
COSMOS patient 9 (SD)	0.36 (0.02)	0.36 (0.03)	0.08 (0.01)	0.04 (0.01)	0.38 (0.03)	*
COSMOS patient 10 (SD)	0.36 (0.01)	0.37 (0.03)	0.10 (0.01)	0.03 (0.01)	0.46 (0.02)	*
Mean (SD)	0.38 (0.01)	0.36 (0.05)	0.06 (0.03)	0.03 (0.01)	0.41 (0.03)	*

Table 5-8 MTR measurements made of structures of the knee in the first ten patients of the COSMOS pilot study

The mean MTR values measured in the different structures of the knee are graphically represented in Figure 5-2.

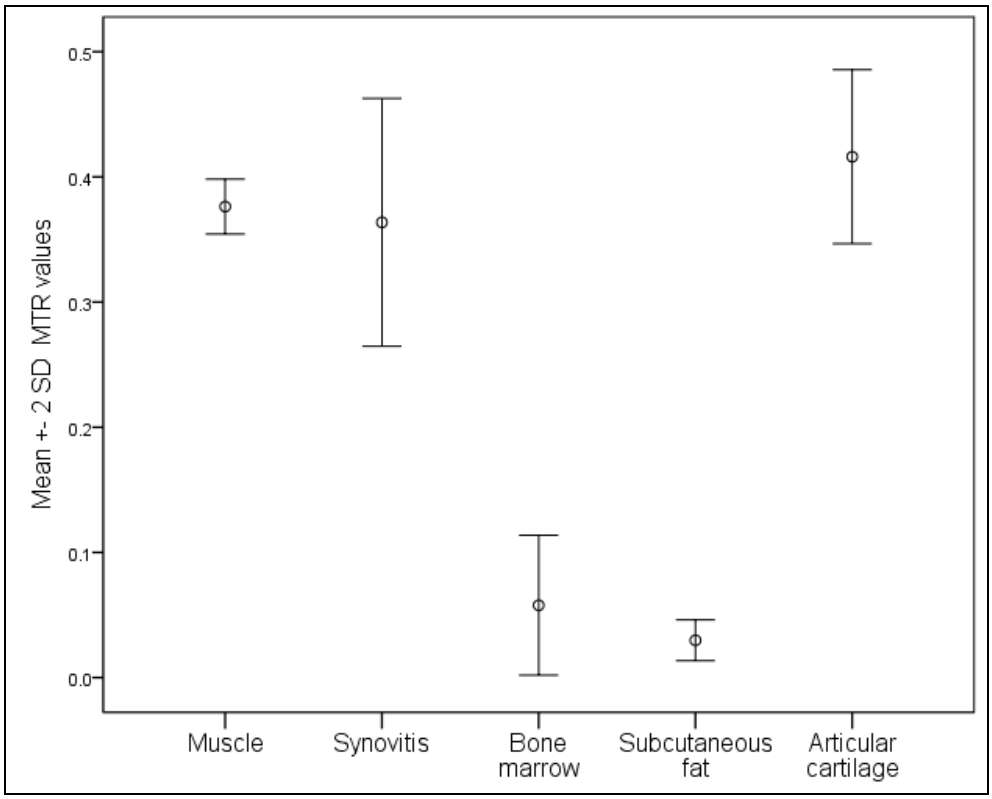

Figure 5-2 Comparison of mean MTR values with two standard deviations for structures of the knee measured in the COSMOS pilot study.

The MTR and T1 data acquired from the first ten patients were plotted against each other to see whether there was a relationship between the values of each that may aid with the differentiation of synovitis from muscle when in used in conjunction with each other (Figure 5-3). The T1 values of seven of the ten patients showed a tight range in values measured is synovitis (952ms - 1086ms). Three patients were outliers of the pilot study cohort with values of 1738ms -1808ms (Figure 5-4) recorded for synovitis.

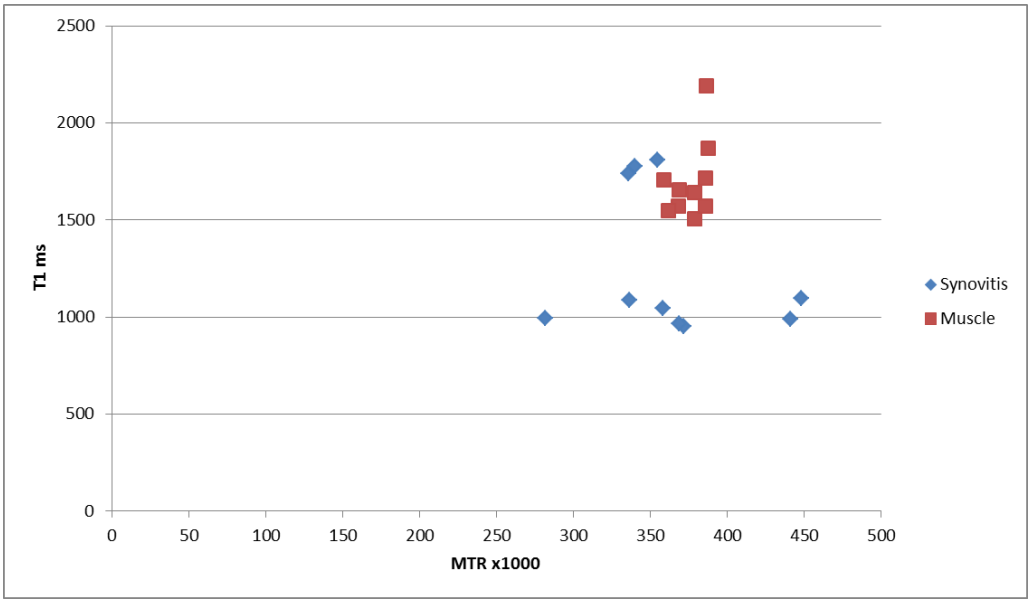

Figure 5-3 Mean T1 and MTR values (x1000) measured from the first ten patients of the COSMOS pilot study

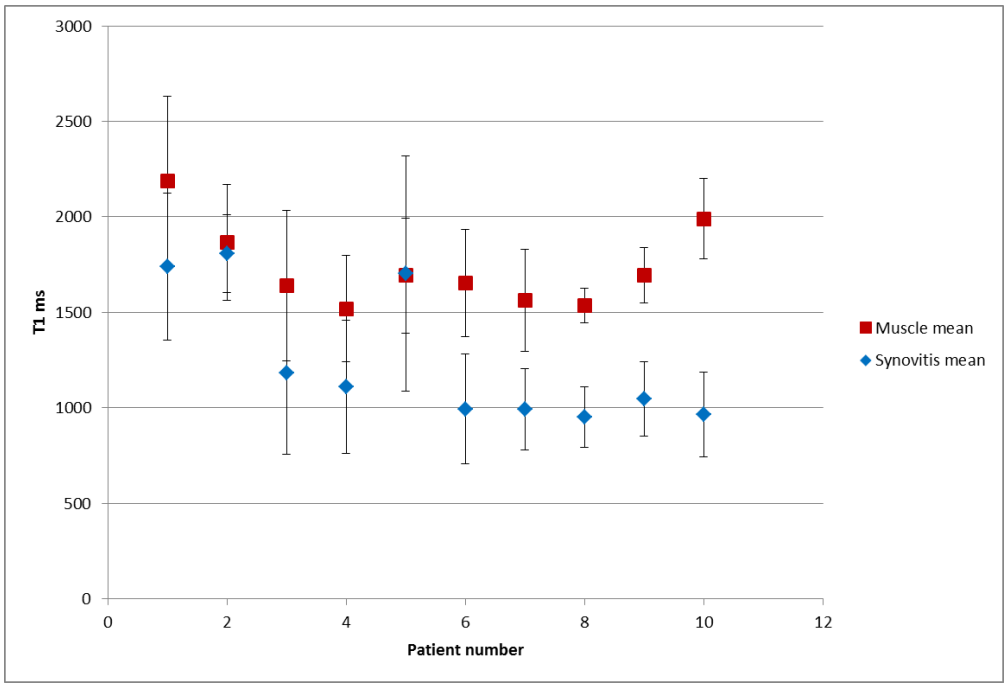

Figure 5-4 Mean T1 values with two standard deviations for synovitis and muscle from the first ten patients in the COSMOS pilot study

In order to assess the feasibility of image fusion onto different weighted scans (multiparametric imaging), fat from the Dixon sequence was used as a mask and combined with different sequences to assess whether there was an improvement in tissue type identification on the resultant images.

Unlike the data reviewed in Chapter 3 where it was only possible to produce one combination of fused images due to the limited number of sequences that had appropriate geometry in the COSMOS pilot study, it was possible to produce multiple combinations of fused sequences due to the matched geometry and locational position of the images.

In Figure 5-5 samples of multiparametric images produced from patient six of the COSMOS pilot study are shown alongside a post gadolinium VIBE image for comparison (Figure 5-5i).

Figure 5-5a, Figure 5-5b and Figure 5-5c, show PD fs images. Figure 5-5a shows a PD fs image in a conventional viewing mode with synovial fluid appearing as hyperintense signal. Figure 5-5b shows a PD fs image with fat from the Dixon scan overlaid on it, displaying fluid as hyperintense signal as is seen on the conventional viewing mode of images, whereas Figure 5-5c is a PD fs image with the grey scale inverted prior to the fusing of the fat image, showing fluid as dark signal.

The arrow on the images points to an area of potential synovitis which can be identified on all three sets of proton density images. However when Figure 5-5c is reviewed the possibility that this area is actually a combination of fluid and synovitis rather than just synovitis is raised. In this image, Figure 5-5c, the synovial fluid is shown as black signal with the synovitis seen as a structure of intermediate signal. The area indicated by the arrow appears to consist of a small synovial component and larger fluid component unlike that shown on Figure 5-5a where the area appears to be entirely comprised of synovitis.

Images shown in Figure 5-5d and Figure 5-5e are MTR images displayed in the conventional format and with fat overlaid to the processed MTR image. Visually, on the MTR image it is difficult to differentiate clearly muscle from articular cartilage but the empirical measurements are able to show differences between tissue types as demonstrated in Table 5-8 (muscle mean value 0.38 and articular cartilage mean value 0.41). If the fat image is

overlaid on the MTR image, fat planes between structures become more conspicuous allowing for better visual recognition of boundary definitions as seen in Figure 5-5e. The area of abnormality highlighted by the arrow on the MTR image Figure 5-5d is barely visible, whilst on the MTR image with fat overlaid onto it, Figure 5-5e, the differentiation of synovitis within Hoffa's fat pad becomes clearer.

Examples of additional sequences that were not available in Chapter 3 for combining with fat images are shown in Figure 5-5f (out of phase image from the Dixon sequence), Figure 5-5g (T1 TSE) and Figure 5-5h (DESS).

In Figure 5-5f, an out of phase image from a Dixon sequence is overlaid with fat from the Dixon sequence. On the combined image, signal abnormalities within Hoffa's fat pad are clearly seen but it is not possible to delineate fluid from a soft tissue component. Figure 5-5g shows an inverted grey scale T1 TSE image with fat from the Dixon sequence combined with it. Again the soft tissue abnormality in Hoffa's fat pad can be seen but its components are unable to be distinguished from one another.

A DESS scan which is fused with a MTR image to produce a multiparametric image not utilising a fat image is demonstrated in Figure 5-5h. Synovial fluid is represented by a yellow colour pixel and the resulting image appears very similar to the post gadolinium contrast image. However, when interpreting the image, the separation of fluid from synovitis is difficult but does compare well with the post gadolinium contrast image (Figure 5-5i).

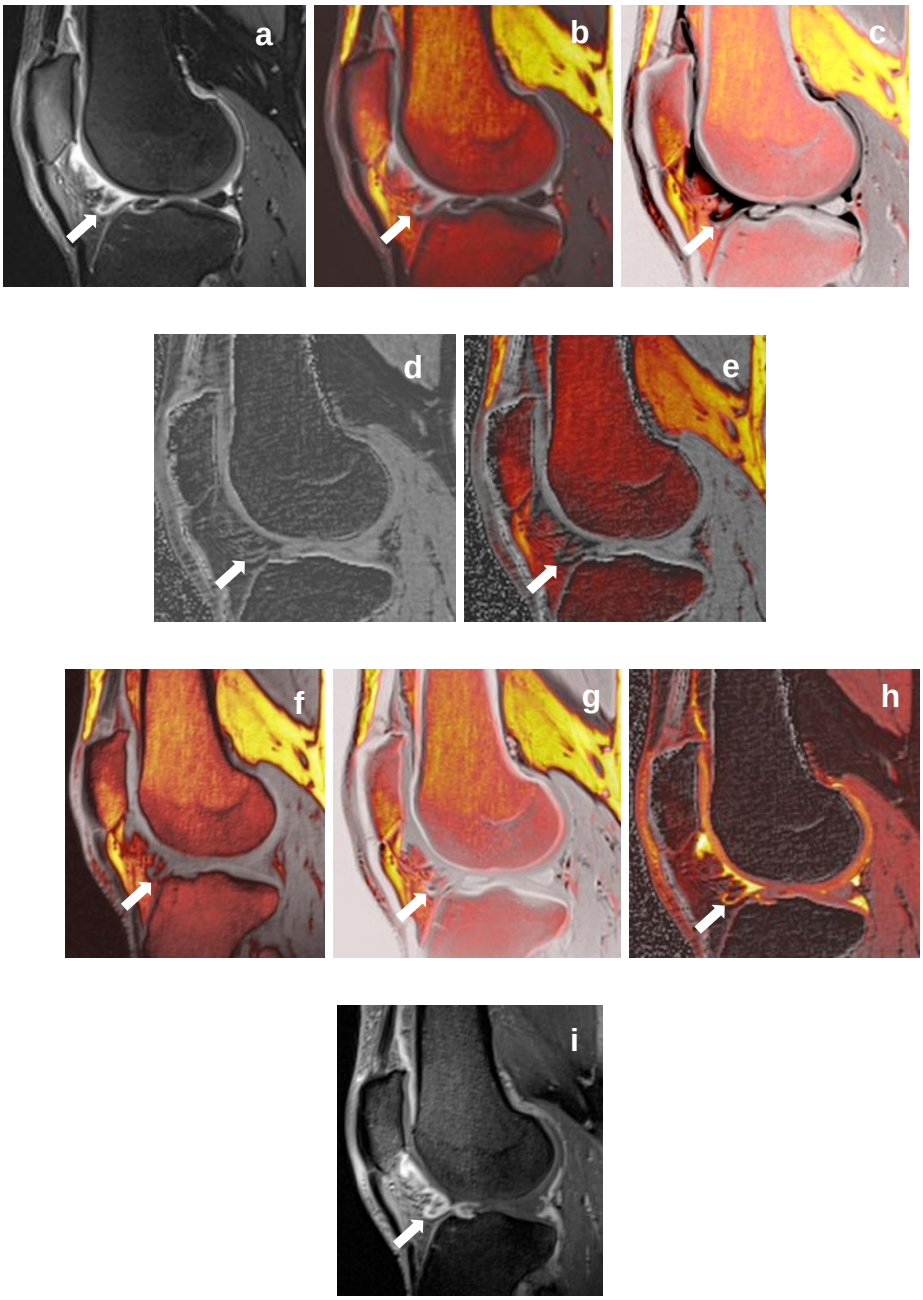

Figure 5-5 Examples of multiparametric sagittal MRI scans of a patient with OA knee with the arrow highlighting an area of potential synovitis in Hoffa's fat pad.

(a) Proton density fat sat (b) Proton density fat sat + fat (c) Proton density fat sat + fat (d) MTR (e) MTR + fat (f) Out of phase + fat (g) T1 TSE invert + fat (h) DESS + MTR (i) VIBE post gadolinium

5.3.5 Discussion

In this pilot phase it has been established that the COSMOS MRI protocol appears to provide diagnostic images sensitive to synovitis of the knee in patients with OA in an acquisition time that is acceptable for patients.

The pilot study of ten patients, nine completing the study protocol, has provided a data set for review to evaluate the imaging parameters and results produced. Careful evaluation of the first ten data sets as described in section 5.3.4 further mitigated the risk of the perpetuation of errors through the main COSMOS study.

The stability of the T1 and MTR scanning sequences in vivo was assessed and confirmed in the reproducibility portion of the pilot study. The values measured from the T1 and MTR images compared well with the values measured (MTR mean of 0.02 with a SD of 0.004 and for T1 values 1218.3ms with a SD of 1.17ms). Despite the T1 and MTR protocols being tested rigorously in phantoms, it would have been preferable to repeat this process in more patients and at different time points to ascertain stability of the protocol in vivo, but this was not practical given the time frame of the project and the number of participants granted by ethics .

Interestingly, the MTR value calculated from the results from the reproducibility test is lower than that generated from the main COSMOS study. The patient on which the reproducibility was tested on demonstrated slice wrap on the images and this affected the MTR value calculated. This was also reflected in the T1 reproducibility results.

It was not possible to validate the data acquired from the MTR images against the literature as there are no published reference MTR values for anatomical structures of the knee in patients with OA.

Assessment of the T1 values obtained from the COSMOS pilot study showed a tight range for synovitis measurement (952ms -1086ms). Three outliers demonstrated higher T1 values for synovitis when compared to the other patients in the pilot study (1738ms -1808ms). Whilst it is conceivable that these figures may reflect the true range of values seen in this population, closer examination of the data from the T1 acquisitions was performed to exclude any other potential issues that could have resulted in these results.

An extensive investigation revealed that despite vigorous testing of the COSMOS protocol on phantoms and volunteers, an underestimation of the average size of these three patients' knees had been made. The three patients that had outlying T1 values had large knees and the scanning volume of the acquisition was smaller than the knee. This resulted in slice wrap, which had caused artefact on some of the images affecting the T1 calculations.

Slice wrap results from superimposition of data from either ends of the scanning volume being *'wrapped'* into the scanning volume resulting in artefact. An example of slice wrap is shown in Figure 5-6.

Figure 5-6 Sagittal 5° SPGR T1 mapping sequence demonstrating slice wrap artefact.

Slice wrap artefact is due to the wrapping in of data into the image when the scanning volume is smaller than the object. Artefacts can mar anatomical or pathological details of a scan but can also affect quantitative calculations such as T1 and MTR measurements.

In order to prevent the artefact from occurring again and therefore producing images which are un-diagnostic, some of imaging parameters of the T1 and SPGR ± MT sequences were modified by increasing the scan volume as a result of increasing the thickness of the slices from 0.8 mm to 1mm.

The modified COSMOS scanning protocol key parameters for the T1 mapping and the SPGR ± MT are shown in Table 5-9.

Imaging plane and sequence	TR (ms)	TE (ms)	FA degrees	Voxel size	Acquisition time
3D sagittal SPGR with MT	28	2.46	15°	1 x 1x 1 mm	3.50 minutes
3D sagittal SPGR without MT	28	2.46	15°	1 x 1 x 1 mm	3.50 minutes
Sagittal T1 mapping sequences comprising of:					
3D T1 map 5°	11	2.46	5°	1 x 1 x 1 mm	3.56 minutes
3D T1 map 10 °	11	2.46	10°	1 x 1 x 1 mm	3.56 minutes
3D T1 map 15°	11	2.46	15°	1 x 1 x 1 mm	3.56 minutes
3D T1 map 20°	11	2.46	20°	1 x 1 x 1 mm	3.56 minutes
3D T1 map 25°	11	2.46	25°	1 x 1 x 1 mm	3.56 minutes

Table 5-9 Revised imaging parameters for the SPGR ± MT and T1 mapping sequence

The voxel dimensions increased due the modifications of increasing the slice thickness to 1mm and decreasing the matrix from 256 x256 to 192 x192.

A consequence of increasing the scan volume for the T1 mapping sequences was that the doubling of the acquisition scan time to four minutes per flip angle was required.

However the modification of the imaging parameters resulted in isotopic voxel dimensions, which matched those of the post gadolinium VIBE images, thus allowing for direct comparison of images and simpler registration if required. The ability of combining images which match in geometry and location allow for the possibility of performing multiparametric MR imaging of the knee and thus bring an added dimension to the assessment of synovitis in the osteoarthritic knee.

As yet there have been no published multiparametric studies in the knee with which these results can be compared. Multiparametric imaging increases the potential for identifying fluid from other structures, including synovitis, and may allow for the accurate measurement of synovial volumes where previous studies have failed.

The volume of data available from the pilot study is not sufficient to suggest that multiparametric imaging will or will not be of help in the non-contrast study, but as a proof of concept it indicates that registering and combining images from multiple sequences is feasible. Although acquisition time is increased by two minutes for the acquisition of the VIBE Dixon sequence to produce the fat images, the patient does not incur a time penalty for the images being processed as this is performed at a later time. Having established proof of concept in the pilot phase, this technique was adopted by the main COSMOS to identify which multiparametric combination or combinations may be of most help in delineating synovitis from other structures within the knee.

The inclusion of a B_1 correction map when used in conjunction with the T1 mapping images proved to be ineffective in correcting for any possible inhomogeneities of the B_1 field. The B_1 correction map was originally incorporated into a bespoke Siemens T1 mapping sequence but little documentation regarding this sequence was available at the commencement of the pilot study. Subsequently, more information regarding this sequence and compatibility with other sequences became available during the project. The B_1 correction map only works with the original bespoke Siemens T1 mapping sequence and corrections in the B_1 magnetic field using this and other T1 mapping sequences were not possible.

5.3.6 Conclusion

The COSMOS pilot study was successful in obtaining diagnostic post contrast and non-contrast images of OA knees. A non-contrast MRI pilot protocol was attempted in ten patients and achieved in nine. MRI data sets from patients with OA of the knee were acquired, which allowed for potential pitfalls to be identified, prior to imaging a larger cohort of patients. The size of the volume originally selected for the T1 mapping and SPGR ± MT was found to be inadequate and adjusted promptly to prevent the artefact from confounding the main dataset.

Experimentation with multiparametric imaging showed that the process was feasible and achievable in a relatively short post processing time. Manipulation of the images took one to two hours, depending on the number and type of image combinations selected.

5.4 The main COSMOS study

5.4.1 Aims and objectives

The aim of the COSMOS study was to apply the modified non-contrast COSMOS MRI scanning protocol in a clinical study to assess the ability of the sequences to image synovitis with MRI in patients with OA knee without the use of intra venous gadolinium. Where possible, the images obtained were compared to the reference standard of gadolinium contrast enhanced imaging to assess the ability of the non-contrast images to demonstrate synovitis in knees of patients with OA.

5.4.2 Method

Patient recruitment and inclusion criteria were that as described in the pilot study (section 5.3). Safety assessment for contrast, patient preparation and positioning was identical to that described in the pilot study (section 5.3.2). The COSMOS main study recruited an additional 91 patients, resulting in a total of 101 patients from February 2013 to July 2014. Patient demographics are presented in Table 5-10.

Gender	Mean age (years)	Range of ages (years)	Number of patients by gender	Number of contrast enhanced scans	Number of unenhanced scans	Number of patients not scanned
Female	55.7	33 – 82	45	33	11	1
Male	59.6	45 – 78	56	51	4	1

Table 5-10 Demographics of the participants of the COSMOS study. Details of the protocol and number of post gadolinium scans is included

Two consented patients did not have a MRI scan as they disclosed a contraindication on the day of the MRI scan, despite a detailed explanation of the contraindications prior to being consented. The reasons were: previous intra orbital metallic injury and a cardiac stent *in situ*, of which the manufacturer and model were unable to be confirmed.

The imaging parameters of the final optimised sagittal plane COSMOS MRI scanning protocol are presented in Table 5-11.

The methods and results of each of the non-contrast techniques from the COSMOS study, the main variables of the study are reported separately in the following sections:

5.4.3 Magnetisation Transfer imaging: MT difference and quantitative MTR maps.

5.4.4 T1 quantitative maps

5.4.5 Semi quantitative scoring of non-contrast images

Imaging plane and sequence	TR (ms)	TE (ms)	FA degrees	Voxel size	Acquisition time
2D sagittal T2 TSE	5000	69	*	1 x 1 x 2 mm	2.22 minutes
2D sagittal T1 TSE	700	10	*	1 x 1 x 2 mm	2.27 minutes
2D sagittal PD fs	5000	42	*	1 x 1 x 2 mm	3.22 minutes
3D sagittal SPGR with MT	28	2.46	15°	1 x 1 x 1 mm	3.50 minutes
3D sagittal SPGR without MT	28	2.46	15°	1 x 1 x 1 mm	3.50 minutes
3D sagittal VIBE Dixon	10	2.45 / 3.68	10°	1 x 1 x 1 mm	1.28 minutes
3D sagittal DESS	14	5	25°	1 x 1 x 1 mm	1.55 minutes
Sagittal T1 mapping sequences comprising of:					
3D T1 map 5°	11	2.46	5°	1 x 1 x 1 mm	3.56 minutes
3D T1 map 10 °	11	2.46	10°	1 x 1 x 1 mm	3.56 minutes
3D T1 map 15°	11	2.46	15°	1 x 1 x 1 mm	3.56 minutes
3D T1 map 20°	11	2.46	20°	1 x 1 x 1 mm	3.56 minutes
3D T1 map 25°	11	2.46	25°	1 x 1 x 1 mm	3.56 minutes
3D sagittal WE VIBE Pre gadolinium	9.8	4.9	30°	1 x 1 x 1 mm	1.26 minutes
3D sagittal WE VIBE Post gadolinium X 5 phases At 0 minutes 1.50 minutes 3.40 minutes 5.30 minutes 7.20 minutes	9.8	4.9	30°	1 x 1 x 1 mm	1.26 minutes per phase

Table 5-11 Key imaging parameters for the COSMOS study MRI sequences

5.4.3 Magnetisation transfer imaging

5.4.3.1 Method

Magnetisation transfer imaging was performed on ninety-three patients. The parameters for the sequences are detailed in Table 5-11. Fifty ROI measurements (5mm^2) of each tissue type were taken of each of the structures of the knee on the SPGR sequences with and without MT for each patient. The structures of the knee from which measurements were taken were: the medial head of the gastrocnemius, articular cartilage of the femoral condyle, subcutaneous fat, bone marrow and synovitis if present. Following acquisition of enhanced images the patient had intravenous GBCA administered to obtain images against which to validate the presence of the synovitis.

MT difference images were generated by subtracting pixel by pixel the image with MT from those without (M_0 - M_{MT}), where M_0 is the image without MT and M_{MT} is the image with MT. From these images, MTR images were calculated using the technique described in the literature review. 50 regions of interest (5mm^2) measurements were taken for each of the anatomical structures mentioned above.

5.4.3.2 Analysis

The scans acquired using the SPGR ± MT sequence were visually inspected for image quality to ensure they were diagnostic and were not marred by any artefacts.

Analysis of the acquired data was performed using Statistical Package for the Social Sciences (SPSS version 21.0) to calculate the mean value with 95% Confidence Interval (CI) for the MTR values for each of the main different tissue types within the knee.

5.4.3.3 Results

The images were assessed for diagnostic quality and for the presence of any artefacts. The images acquired demonstrated no visual artefacts, specifically from slice wrap that was identified on some of the images in the COSMOS pilot study.

Synovitis can be identified on MT based images. Examples of MT based images are shown in Figure 5-7, alongside the conventional sequences of DESS and post gadolinium VIBE images for comparison. The MT difference image (Figure 5-7a) demonstrates all the anatomical features of the knee that can be visualised on the DESS image (Figure 5-7e). Fluid within the synovial effusion and Baker's cyst returns a hypointense signal on the MT image and hyperintense signal on the DESS image. Delineation of the articular cartilage and the menisci is clear on both images. The fat plane interface between the synovitis and the subcutaneous fat in the anterior knee (thin arrow) on the MT difference image is seen but this is not seen on the DESS image. The MTR image displays the same results as the MT difference image. Adding fat to the MT difference image (Figure 5-7c) increases the conspicuity of the fat plane, as colour (red or yellow) is apportioned to voxels representing fatty tissue (thin arrow).

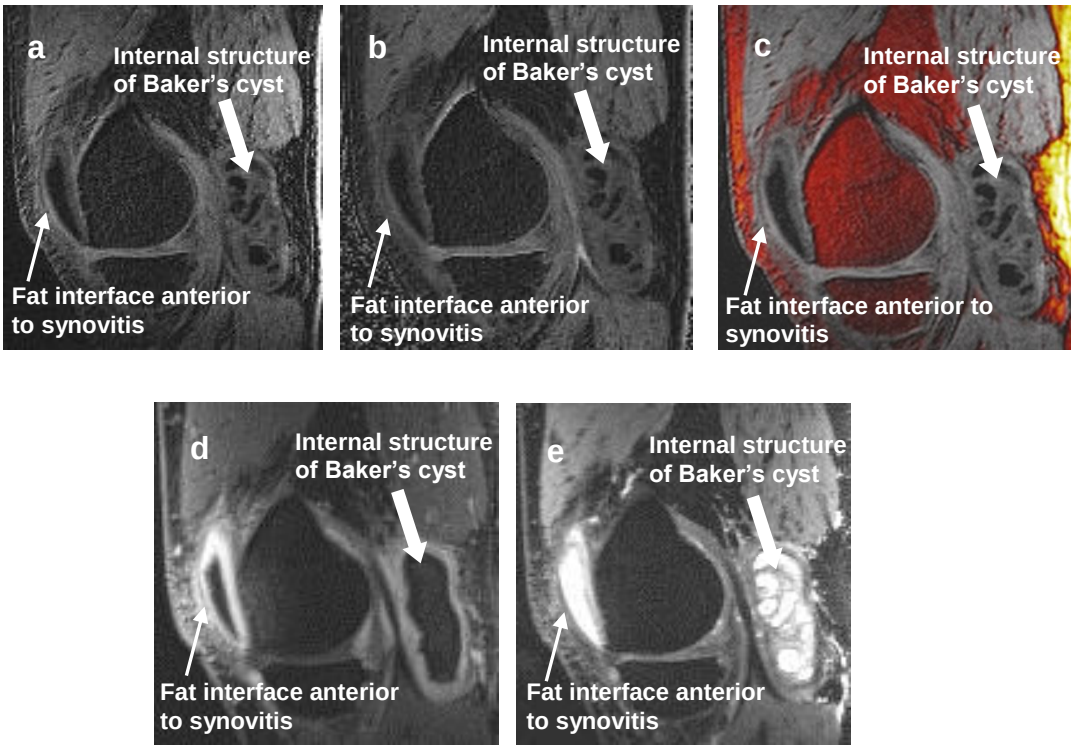

Figure 5-7 Sagittal MR images of the medial compartment of a knee in a patient diagnosed with osteoarthritis.

A synovial effusion and Baker's cyst are shown with surrounding synovitis. (a) MT difference image (b) MTR image (c) MT difference with fat overlay image (d) Post contrast gadolinium VIBE image (e) DESS image

In Figure 5-8 MT based images are compared to the reference standard of post gadolinium contrast images. Demonstrated in Figure 5-8a, is an MTR image that is able to differentiate the synovitis from other structures of the knee. The thin arrows identify areas of synovitis which are subsequently validated by the post gadolinium image, Figure 5-8c. Exploring the possibility of increasing tissue conspicuity by multiparametric imaging, a fat mask was added to the MT difference image (Figure 5-8b) allowing for the fat planes between the muscles to be seen more clearly.

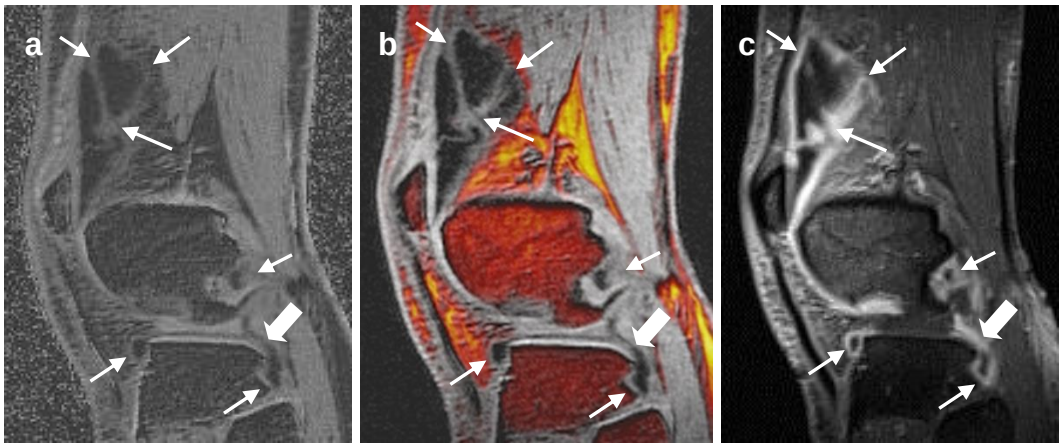

Figure 5-8 Sagittal MT and post gadolinium MRI scans of a patient with OA of the knee. (a) MTR image (b) MT difference with fat overlay (c) Post gadolinium VIBE

Fat is depicted on the MT difference image (image b) by the red, orange and yellow colour. The thin arrows point to areas of synovitis within the joint. Areas of synovitis seen on the MTR (a) and MT difference and fat images (b) are validated by the post gadolinium images (c). The thick arrow points to an area which is suggestive of being synovitis on the post gadolinium image and yet returns a signal of fluid on the MT based images.

The MTR values obtained in the COSMOS cohort are summarised in Table 5-12. MTR readings are not shown for any synovial effusions present because it was not possible to confirm the constituents of the effusion as no histology was taken. As described in the literature review pure fluid and synovial effusions display different MT effects and therefore any empirical readings would have little meaning and have no bearing on the identification of fluid within the joint.

	Synovitis	Muscle	Bone marrow	Subcutaneous fat	Articular cartilage
Mean Value (SD)	0.33 (0.05)	0.35 (0.03)	0.05 (0.02)	0.03 (0.01)	0.40 (0.04)

Table 5-12 Summary of the MTR results calculated from the COSMOS study for structures of the knee in patients with osteoarthritis

The mean MTR values measured from the COSMOS study with 95% CI are displayed graphically in Figure 5-9. This plot shows the expected difference in values from the lipid based subcutaneous fat and bone marrow, and the non-lipid based structures, synovitis, muscle and articular cartilage.

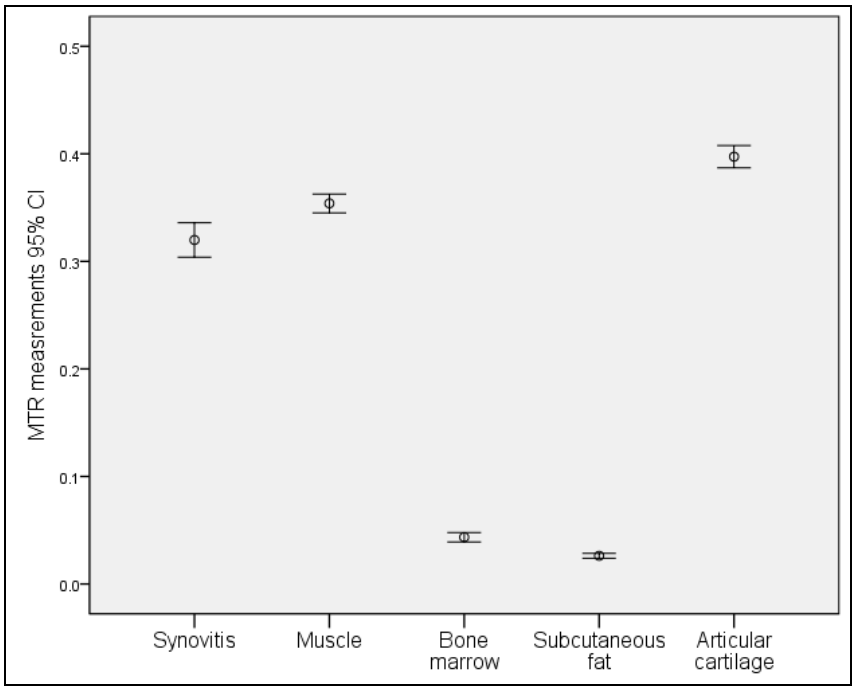

Figure 5-9 Mean MTR values with 95% confidence intervals, obtained for structures of the knee from patients with OA obtained from the COSMOS study

5.4.3.4 Discussion

Comparison of the MT based images with the post gadolinium image in Figure 5-8 it appears that the post contrast image has overestimated the volume of synovitis in the posterolateral compartment (thick arrow). On the post gadolinium image, the area highlighted by the thick arrow is suggestive to comprise totally of synovitis but on the MT images the signal is that of fluid surrounded by synovitis.

MT difference and MTR images appear to provide supplementary information to conventional MRI sequences. It is interesting that the MT based images and the DESS image show that the Baker's cyst has structure to it (thick arrow) and yet there is no suggestion of this on the post gadolinium image (Figure 5-7d). Whilst the internal structures may not be of inflammatory tissue and therefore will not enhance on the post gadolinium images, there is no suggestion of compartmentalisation of the fluid in this image.

Visually, there is little disparity between the MT difference and MTR images except for an increase in background noise on the MTR images due to the images having been calculated as a ratio. However this slight visual degradation of the image quality is outweighed by the fact that the MTR scans give an empirical value relating to the tissue characteristics measured that the MT difference images are unable to.

Comparison of MTR values obtained from the COSMOS study and the literature is difficult. The paucity of studies looking at MTR values within the musculoskeletal system and with patients with OA results in the inability to validate the results obtained. Variations in the B_1 magnetic field and MT pulse parameters can affect all MTR calculations from a single scanner that may or may not be present in another system. Comparison of values obtained from one scanner will be comparable with themselves, but a pragmatic approach must be taken when comparing results for other scanners.

Unsurprisingly, synovitis showed a relatively wide range of MTR values, 0.20 – 0.45 (mean value of 0.33). Patients scanned in the COSMOS study had different stages of disease severity and duration of disease process. Synovium and synovitis display a wide range of changes in the OA knee [8]

showing different histological appearances. Synovium within an OA knee can range from significant hyperplasia with a dense infiltration of lymphocytes and monocytes, to a thickened fibrotic structure [70]. Studies of the advanced stages of knee OA have shown that it is common for fibrin deposition and fibrosis of the synovium to occur [69]. Variation in histological appearances of the disease process will reflect in variability of MTR values. Water only exhibits MT if it interacts closely with intracellular or extracellular macromolecules [154]. Therefore, if synovium or synovitis represents cellular infiltration or fibrotic tissue rather than free water, it might be expected to exhibit MT [123]. The more inflamed the synovial tissue, the higher the MTR value would be expected.

MTR values for the medial head of the gastrocnemius muscle were within a narrower range, 0.28 – 0.40, SD 0.03 and a mean value of 0.33. This reflects a more homogenous tissue quality than synovitis, which is to be expected. Muscles of patients with OA tend to be more atrophic [253] but the structure of the muscle remains the generally the same and this is reflected in the MTR values recorded.

Bone marrow MTR measurements recorded in the COSMOS study are interesting in that there is a wide range of absolute values recorded but a relatively small standard deviation, (range 0.013 – 0.10, SD 0.015 and a mean value of 0.15). These results reflect that although only normal bone marrow was intended to be measured, there was the possibility of areas of bone marrow oedema included in some of the ROIs, despite cross referencing with other pulse sequences to minimise this. Bone marrow oedema is not simply free water but is intimately related to cells or extracellular matrix, for example by chemical exchange of protons between water and nearby collagen [254]. Areas of bone marrow oedema will display higher MTR values as a result of this. However, as the standard deviation is low, the inclusion of bone marrow with oedema in the measurements was infrequent. Graphical plotting indicated that there is one outlier in the bone marrow MTR measurements with an unusually high value, and this most probably represents an area of bone marrow oedema included in the measurements (Figure 5-9).

MTR readings for subcutaneous fat displayed a narrow range of readings with a very small standard deviation, (range 0.009 –0.057, mean value of

0.0313 and a SD 0.009). The structure of subcutaneous fat is not affected by the OA process and it might therefore be expected to return a narrow range of MTR readings. The MTR values were of a similar magnitude to those of bone marrow which is consistent with their both being lipid based.

The MTR readings for the articular cartilage show a wider range of values, (range 0.31-0.54, mean value of 0.401 and a SD 0.038). As with the bone marrow readings, it appears that despite efforts to focus on normal regions, some of the MTR measurements were obtained from unhealthy tissue as there was a wider range of results. An outlier reading of 0.541 most probably represents degenerative cartilage showing a greater effect of MT on the tissue. Care was taken to avoid abnormal areas of articular cartilage but assessing the quality of normal articular cartilage on conventional MRI sequences can be difficult. Reduction of thickness and malacia of the cartilage are obvious indicators of abnormal tissue and were avoided, but there may be changes present which are not visible on conventional imaging. The standard deviation of the results for the articular cartilage readings was higher than for bone marrow perhaps suggesting that more areas of abnormal tissue were included in the results.

The two major macromolecular constituents of articular cartilage are proteoglycans and collagen. These maintain the hydration of the cartilage and therefore its mechanical properties. Reduction of proteoglycans and loosening of the collagen framework are seen in early lesions of articular cartilage [255]. In OA, it is assumed that the articular cartilage is less resistant and the change in the collagen framework and the decrease of proteoglycans reduces osmotic pressure within the matrix reducing the ability to maintain its hydration [256]. Mechanical compression compresses the collagen fibres resulting in decreasing the distance between free water and collagen bound water increasing the effect on MT and therefore increasing the MTR.

A limitation of MTR calculations is that unfortunately the necessity for two sequence acquisitions introduces the potential for the patient to move between them, resulting in miss registration of the images for either subtracting or calculating a ratio.

5.4.3.5 Conclusion

MT difference with fat overlaid and MTR images can show the presence of synovitis within the knees of patients with OA. MT MR scanning is a relatively quick examination (eight minutes) and was tolerated well by the patients.

Empirical MTR values can be calculated for structures in the knee joint and there is a potential to use these values as a biomarker to assess disease progression or response to treatment. There is an overlapping of MTR values for synovitis, muscle and articular cartilage in patients with OA knee, which prevents this technique from being used as a diagnostic tool for synovitis in isolation from other MR sequences. When used in conjunction with other sequences however, MT and MTR imaging may be useful as a problem solver, such as that in Figure 5-8 for its role in differentiating fluid from synovitis. It has been further demonstrated that fat from the Dixon scan can be overlaid with the MT difference or MTR images, allowing for delineation of fat planes between structures.

5.4.4 T1 measurements

5.4.4.1 Method

T1 mapping sequences were acquired from 94 patients. As for the MTR data sets, the initial ten data sets were not used in the calculation of T1 values due to the necessary alterations that were made to prevent occurrence of slice wrapping. One further set of data was discarded due to artefacts on the images, probably resulting from a RF spike. As a result, 83 data sets were used to calculate the T1 values for structures of the knee. The parameters for the T1 mapping sequences used are detailed in Table 5-11.

T1 maps were calculated using OsiriX® software using all five flip angles acquired. Fifty measurements from ROIs were made on the T1 maps in the

same locations as those described in section 5.4.3.1 to calculate mean T1 values for different tissue types.

T1 values can be calculated and measured in the knee joint of patients with OA from the optimised T1 mapping sequences in vivo. Using commercially available software (OsiriX®), T1 maps can be calculated to produce colour maps with a colour apportioned on a pixel by pixel level for a specific T1 value. This allows for easy visual assessment of the T1 values within the knee. A more accurate appraisal of the distribution of T1 values can be achieved by analysing the empirical T1 values of a selected tissue from the same images by applying ROIs in the desired locations.

5.4.4.2 Analysis

Visual inspection of the images was performed to assess the diagnostic quality of the images to ensure that there were no artefacts present either due to patient movement or as a result of the imaging parameters or system issues.

Statistical analysis of the acquired data was performed using Statistical Package for the Social Sciences (SPSS version 21.0). The mean T1 values were calculated for each of the main different tissue types within the knee with a 95% CI.

5.4.4.3 Results

All images were of diagnostic quality and free from artefacts.

It is feasible to calculate T1 maps from SPGR sequences of variable flip angles of the knee joint using OsiriX® software in a very short time (less than a minute).

Figure 5-10 shows an example of a T1 map compared to a MT difference with fat image overlay and the reference standard VIBE post GBCA scan. On the T1 image, red represents structures with a high T1 (greater than 1500ms) and blue those of lower T1 values (approximately 300ms). Yellow and green

represents structures with a T1 of 1100ms to 1500ms. In Figure 5-10 a synovial effusion can be identified on all three images with synovitis surrounding it (as labelled). A band of synovitis can also be identified within the effusion itself and is shown as a yellow colour against the red of the synovial fluid on the T1 map, intermediate signal on the MT difference with fat and hyperintense on the GCBA image. An indentation seen anterior to the effusion and synovitis can be seen as red on the MT difference with fat overlay image and returns a blue colour on the T1 map indicating a lower T1 value of fat (as labelled). Whilst this area of tissue can be seen on the VIBE GBCA image as a non-enhancing structure and therefore not inflammatory, formal identification of the type of tissue it represents is not possible without histological confirmation.

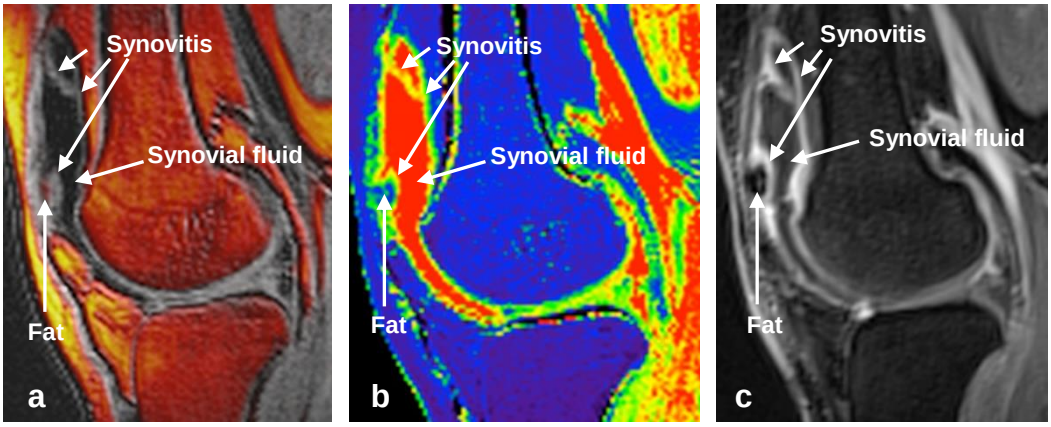

Figure 5-10 Sagittal MRI scans of a patient with OA of the knee. T1 maps are compared to MT difference image with fat overlay and post gadolinium VIBE images.

(a) MT difference image with fat overlay (b) T1 map (c) Post contrast gadolinium VIBE scan. A synovial effusion is seen in the suprapatellar pouch with synovitis surrounding it. An area of fat can be identified on the MT difference with fat overlay (a) and the T1 map image (b) anterior to this (as labelled on the image) which is unable to be clearly identified as fat on the post contrast image (c).

In addition to the synovitis visualised, the T1 maps were also able to identify bone marrow oedema on the scans. In Figure 5-11, two scans of a patient with OA knee are shown: a T1 map and post gadolinium contrast VIBE image. On the post gadolinium image irregularity of the articular joint surface is seen with areas of enhancement adjacent to them as described in the literature. Previous studies have shown that on post gadolinium contrast image sclerotic bone remained hypointense [257], and in RA that bone marrow oedema enhances [258]. Whilst BML's do not exclusively contain water, they have been shown to have an increased water content [259] and therefore a higher T1 value than the normal lipid constituent. On Figure 5-11 the bone marrow oedema is represented as green (approximately 1300ms) as compared to normal bone marrow oedema of T1 value ~350ms shown as blue.

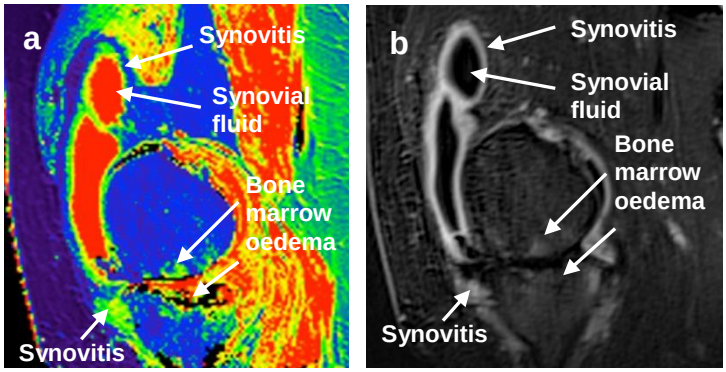

Figure 5-11 Sagittal MR images of a patient with bone marrow oedema present in the femoral condyle as a result of osteoarthritis of the knee.

(a) T1 map (b) Post gadolinium contrast VIBE image
A synovial effusion is present with synovitis surrounding it. Also visualised on the images are areas of bone marrow oedema within the femoral condyle and the tibial plateau as labelled.

From the COSMOS cohort, 83 sets of T1 maps were used to calculate the T1 values for the medial head of the gastrocnemius, articular cartilage of the femoral condyle, subcutaneous fat, bone marrow, synovial fluid and synovitis

if present *and* again subsequent to the unenhanced acquisitions, the patient received intravenous gadolinium to acquire contrast enhanced reference standard sequences against which to validate the presence of the synovitis. 50 measurements were taken from each structure using an ROI of approximately 5mm^2. The mean T1 values calculated with all five flip angles (5°,10°,15°,20° and 25°) of these structures are presented in Table 5-13 alongside the standard deviation.

	Synovitis	Muscle	Bone marrow	Subcutaneous fat	Articular cartilage	Synovial Fluid
Mean value (ms) (SD)	1005 (91)	1785 (304)	403 (65)	444 (59)	962 (125)	3915 (899)

Table 5-13 Summary of mean T1 values calculated with five flip angles (5°,10°,15°,20° and 25°) for patients for the COSMOS study for structures of the knee in patients with osteoarthritis

A graphical representation of the mean measured T1 values with 95 % CI from the COSMOS study is shown in Figure 5-12. Synovial fluid has not been plotted in Figure 5-12b as there is no overlap of readings with any other structures of the knee measured (lowest T1 value for synovial fluid is 2738ms and highest T1 value for another structure is muscle with 2638ms). By not including synovial fluid on this plot, the y axis scale can be reduced, allowing for greater visual separation of values in the lower range of T1 measurements.

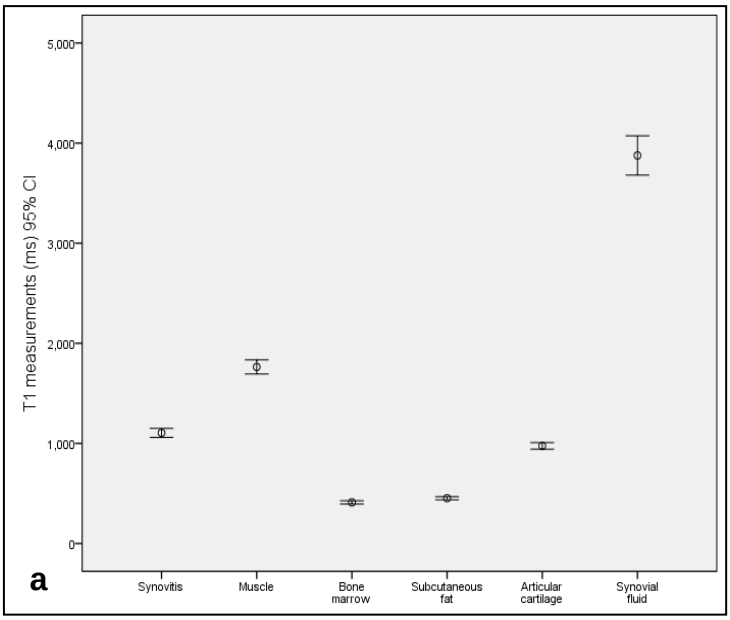

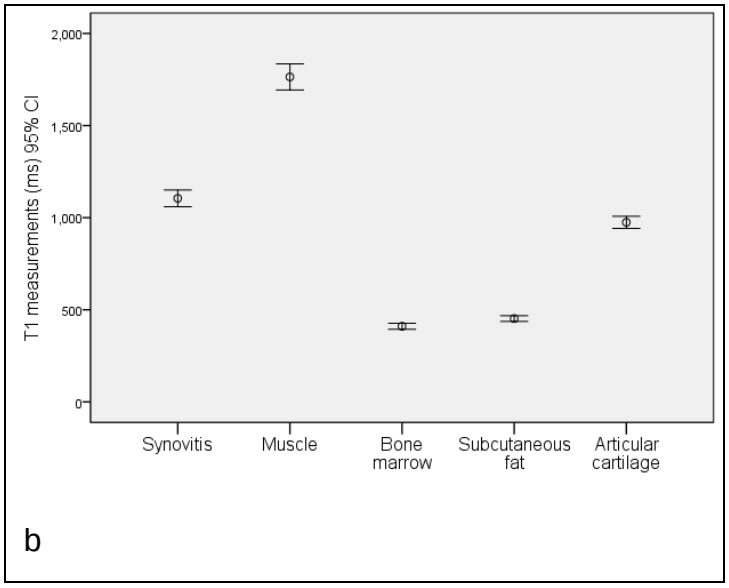

Figure 5-12 Comparison of mean T1 values with 95% confidence intervals of structures of the knee in patients with osteoarthritis obtained from the COSMOS study.

Figure 5-12a with synovial fluid included in the graph and Figure 5-12b with synovial fluid excluded from the graph to allow for greater delineation of structures with similar T1 measurements.

5.4.4.4 Discussion

T1 maps and images are able to provide complementary information regarding the disease process in patients with OA knee both visually and quantitatively. Synovitis can be identified on the T1 maps as well as other pathologies such as bone marrow oedema. In Figure 5-13 sagittal images of MT difference with fat overlay, T1 map and a post gadolinium contrast VIBE image are displayed. Synovitis can be visualised on all three images, as labelled. However the portion of synovitis anterior to the shaft of the femur is not clearly seen on the MT difference image with fat *but* is identified on the T1 map (synovitis represented by yellow/green pixels and fat as blue). Both the MT difference and T1 maps have the same resolution (1x1x1 mm) but there is clearer identification of the synovitis on the T1 maps when compared to the MT difference image. As expected and suggested in Table 5-1, the MT difference image is able to demonstrate abnormalities of the synovium superior to the posterior cruciate ligament when in close proximity to fluid which cannot be seen on the T1 image. The internal soft tissue structures within the fluid adjacent to the PCL can be seen both on the MT difference image and post gadolinium contrast image, but are not identified on the T1 map. On the T1 map, it appears that this structure is entirely composed of fluid.

Incidental to the synovitis and synovial effusion displayed on the images, an area of bone marrow oedema can be identified on all three of the sequences within the anterior femoral metaphysis. On the T1 image, the area of bone marrow oedema is shown as green, yellow and red pixels representing higher values of T1 (1100ms to 3500ms) reflecting the fluid and cellular component that has replaced the fat from the normal bone marrow (T1 ~350ms represented by blue pixels).

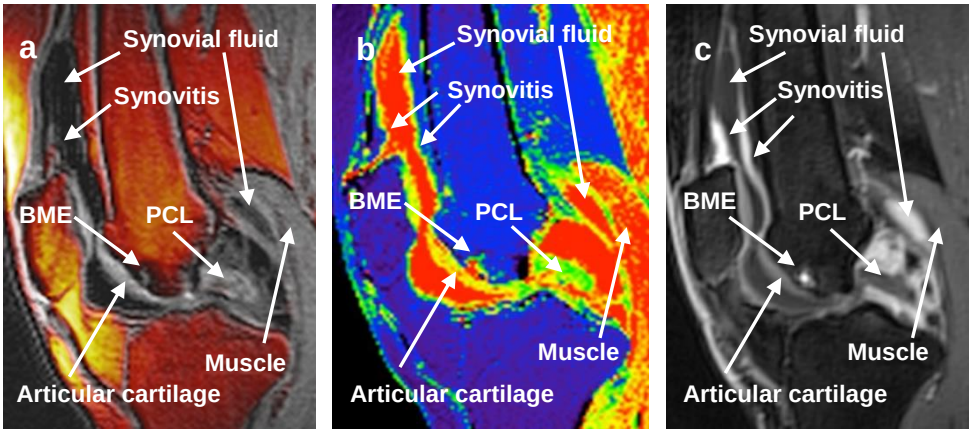

Figure 5-13 Comparison of sagittal MT difference with fat overlay, T1 map and post gadolinium VIBE MR images of a patient with osteoarthritis of the knee

(a) MT difference image with fat overlay (b) T1 map (c) post gadolinium contrast VIBE image. Synovitis, synovial effusion and an area of bone marrow oedema are identified on all three sets of images.
PCL is the posterior cruciate ligament.

T1 maps can also act as a problem solver in the detection of synovitis in the knee. In Figure 5-14, there is an area of abnormality within the suprapatellar pouch. On the MT difference with fat overlay image (Figure 5-14a), the appearances are suggestive of this area being synovitis. However, on the post gadolinium image (Figure 5-14b) there is no enhancement of this area, suggesting therefore that it could be due to avascular fibrotic synovitis. When this area is viewed on the T1 map (Figure 5-14c) however, it becomes apparent that this may not be synovium as it has structure and possibly returns fat signal. The resulting hypothesis that this may therefore be a loose body is strengthened by the appearance on the T1 TSE image (Figure 5-14d) and is confirmed on X-ray (Figure 5-15).

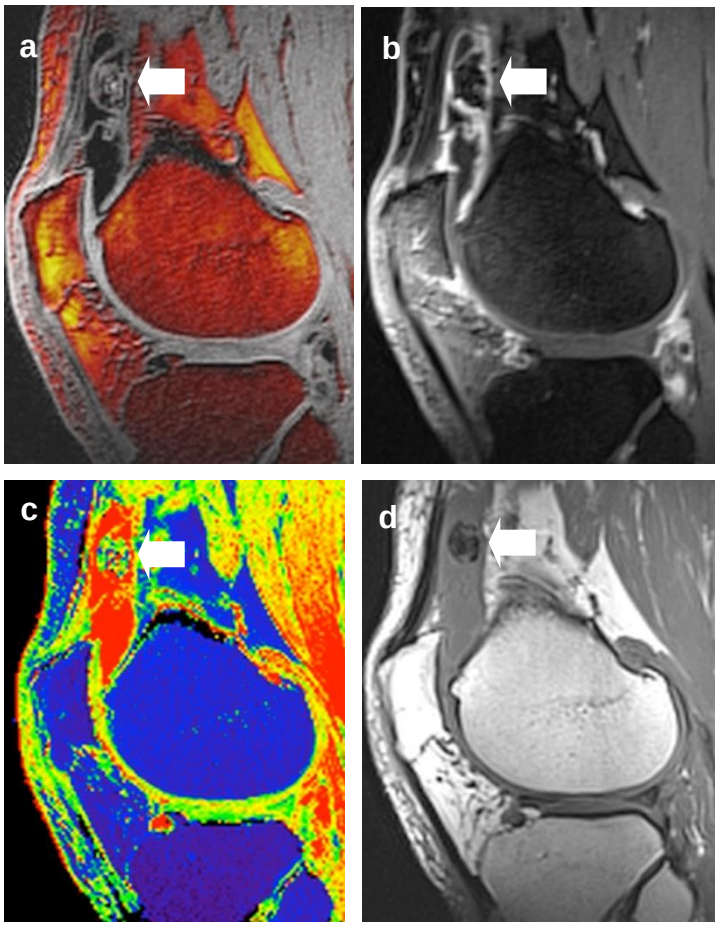

Figure 5-14 Sagittal MR images of the knee in a patient with osteoarthritis of the knee with a loose body (arrow) in the suprapatellar pouch.

(a) MTR difference and fat overlay (b) Post gadolinium contrast VIBE (c) T1 map (d) T1 TSE images

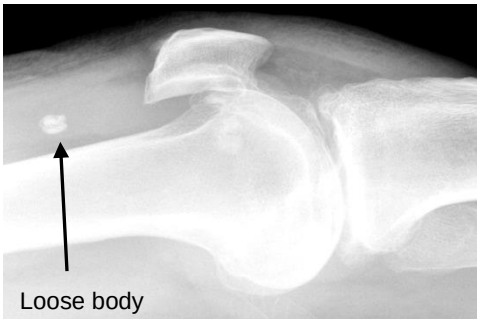

Figure 5-15 Lateral X-ray of patient in Figure 5-14 confirming the presence of a loose body in the suprapatellar pouch

The COSMOS main study has shown that it is feasible to acquire T1 SPGR data, calculate T1 maps and therefore measure T1 values using commercially available software. Acquisition time for five individual flip angle sequences takes approximately 20 minutes. As the images need to be registered to each other to enable post processing of the data, it is essential for the patient to remain in the same position with no movement. If the patient does move, there is a possibility that the T1 mapping process may calculate spurious values, which in turn may affect the diagnosis or treatment.

T1 values measured within the muscle showed a wide range of T1 values (mean of 1785ms, SD 304ms and a maximum 2638ms and minimum of 1305ms). This result likely reflects the range of quality of the muscles of the patients in this study. Studies have examined the condition of muscles in patients with OA and have shown that atrophic muscles are a common observation in this population [260]. Underuse of the affected leg and lack of appropriate exercise results in atrophy of the muscles associated with the knee joint [261]. The fatty infiltration of the muscle reduces the T1 value measured as fat has a lower T1 reading than that of muscle. There is one participant who demonstrated a ‘high’ average measurement for muscle with a T1 value of 2638ms. The reason for this is unknown. It has been shown that increased exercise increases the T1 of the muscles of the calf [262] but this is probably not the reason for this result as the patient had been lying on the scanner for approximately half an hour prior to the T1 measurements being made. T1 values of muscle have also been shown to be dependent on the presence of fibrotic tissue and the fraction of bound water [263]. With this in mind, the most probable reason for the increased T1 measurement is an increase of fluid within the muscle due to a strain. Comparison of the T1 maps with conventional imaging was not performed when selecting locations for ROI’s for measuring values in muscle. The possibility of a potential muscle strain being present was not considered.

On further exploration this spurious result was found to be from a patient that had been diagnosed with gout after participating in the COSMOS study. A diagnosis of gout had not been suspected at the time of scanning (and was an exclusion criteria) for the COSMOS study. Whether the result of the T1 measurement is as a direct result of this patient having gout is unknown.

An unexpected result of the T1 measurements was the relatively narrow range of T1 values for synovitis (mean 1073ms, SD 91ms, minimum value 849ms and maximum value 1277ms). Considering the different phases of the disease process that were imaged in the COSMOS study, ranging from the vascular active disease stage to the chronic fibrotic phase, the range of T1 values recorded for the synovitis was small. Benito et al in 2005, demonstrated that synovium in patients with early OA had a thicker lining layer with increased number of blood vessels when compared to that of late stage disease [9]. It would therefore be hypothesised that active inflamed synovitis should have a higher T1 value due to its increased vascularity and therefore fluid content when compared to fibrotic synovium. This is not reflected in the T1 measurements obtained from the COSMOS study. This result raises the question as to what happens on a cellular level to synovium throughout the disease process in OA. A limitation of the COSMOS study was that no biopsies of synovium were taken to correlate the imaging findings with the histology of the joint being examined. Even this approach may not have been definitive however as the variation of synovial inflammation is not constant within the joint and difficulties remain in ensuring comparison of the biopsy sample with the exact location imaged.

The reference standard for determining that a patient had synovitis within the knee joint was the presence of enhancing synovium on the GBCA images. ROI's were located on the post contrast images and copied onto the T1 maps to ensure that the correct area of tissue was measured. If a patient did not have gadolinium contrast (n=15), T1 measurements were not taken for the synovium. In addition to this group, ten patients that had intravenous gadolinium administered did not demonstrate enhancing synovium. Therefore 25 patients did not have the T1 of synovium measured. This group may have similar histology those included in the T1 measurement group but have had different MRI enhancement characteristics. Furthermore, T1 measurements were not made in normal synovium as it is difficult to identify precisely unenhanced synovial tissue on MRI scans. The T1 of normal synovium may be within the range of those measured in the COSMOS study and infer that the disease process of OA does not change the imaging characteristics of the synovial tissue. If the calculation of T1 values of normal synovial tissue were required, a possible method to identify the tissue would be to scan the

knee post saline arthrogram. This would distend the knee joint possibly allowing for the synovium to be identified with greater accuracy when compared to visualising it on conventional MRI sequences. However this is an invasive procedure and recruiting a large enough cohort of participants to acquire a representative T1 value of normal synovium may be difficult to achieve.

Despite the aforementioned possible limitations with the T1 measurements calculated for synovium in this study, there was thought to be enough evidence to translate these findings to an inversion recovery sequence to explore the possibility of using this to image synovitis in the knee without the need for gadolinium contrast enhanced MRI. The method and results of this piece of work exploring inversion recovery sequences are described separately in Chapter 8.

The T1 calculations for bone marrow oedema reflect the findings of the MTR measurements. The calculations of values reflect that areas of bone marrow oedema were also included into the ROIs selected to measure the T1. Bone marrow T1 values ranged from 347ms to 653ms (SD 65ms), with a mean value of 403ms. As previously described, bone marrow oedema is composed of fluid and haematological cells disrupting the normal bone marrow MRI characteristics. A higher T1 value would be expected in bone marrow oedema than that of normal bone marrow due to the fluid associated with the lesion.

The T1 values calculated for subcutaneous fat (range 347ms to 653ms, mean 444ms, SD 59ms) are similar to those of the bone marrow, which would be expected due to the lipid content of both tissues. Whilst there are no published studies specifically exploring the characteristics of subcutaneous fat around the knee joint in patients with OA knee, there appears to be a variation in quantity of fatty tissue and T1 values measured which may correlate with the values of the muscle measured.

Articular cartilage T1 readings appear to demonstrate the possible inclusion of small amounts of abnormal tissue within the ROIs measured. The morphological and pathophysiological changes in articular cartilage in OA have been described in many studies [264-268]. Degenerative articular cartilage displays decreased T1 values when compared to those of normal

tissue due to the reduction of glycosaminoglycans (GAGs) [269]. Therefore, the lower T1 readings of articular cartilage from the COSMOS study are likely to represent degenerative tissue within the ROI.

Synovial fluid, as expected, returned high T1 values due to the water content of the effusions. The range was 2738ms to 7942ms, with a mean value of 3915ms, SD 899ms. Synovial effusions do not just contain water however, but lymphocytes, hyaluronic fluid, debris from the joint and plasma proteins. The concentration of each will affect the T1 value recorded thus resulting in a wide range of values and a high standard deviation. It is notable however that the flip angles selected for the T1 mapping sequences were optimised to image synovitis, with an estimated T1 of 1100ms to 1500ms. Synovial fluid does have a considerably longer T1 than that of synovitis and as the T1 gets longer the change in signal gets smaller for each of the gradient echo acquisitions, thereby reducing the precision of the measurement for higher T1 values.

5.4.4.5 Conclusion

Plotting T1 MRI maps and calculation of T1 values is feasible when imaging the knee in patients with OA in an acceptable time for the patient (20 minutes). Manipulation of the data acquired by commercially available software allows for T1 maps to be generated providing a visual representation of the distribution of values within the knee.

Quantitative data can also be calculated from the images to produce data that can describe the quality of the tissue and can potentially be used to distinguish one tissue from another. Values from the COSMOS study provided a range of values that can be used to produce a reference tool for identifying the various tissues of the knee in patients with OA. The narrow range of T1 values for synovial tissue potentially provide a solution for imaging synovitis in one acquisition in a scanning time of time of less than ten minutes. This is explored and described further in Chapter 8.

5.4.5 Semi quantitative scoring of images

5.4.5.1 Introduction

The assessment of the presence, absence and severity of synovitis on MR images after the administration of intravenous gadolinium contrast agents can be performed using semi quantitative scoring methods [214, 270]. These scoring methods have been critiqued within the literature review of this thesis (Chapter 2). As a result of the literature review a modified scoring method based on Guermazi's [270] technique will be used to score synovitis on both the contrast enhanced and, for the first time, on non-contrast enhanced images to assess the severity of the synovitis on the MR images. By acquiring the reference standard in addition to the non-contrast COSMOS images it is possible to use concurrent validity to assess agreement of the novel imaging techniques.

5.4.5.2 Aims and objectives

The aim of this section of the project is to apply a modified semi quantitative scoring technique that has been used on post gadolinium contrast images and apply this to the non-contrast images acquired from the COSMOS protocol to allow for comparison of the techniques in determining the amount of synovitis present on the scans. With a particular interest in:

(a) Assessing the ability to modify this technique to non-contrast images of MT difference with fat overlay and T1 maps

(b) Comparing the non-contrast techniques with the reference standard of post gadolinium contrast images obtained from the suprapatellar pouch, infrapatellar pouch and Hoffa's fat pad.

5.4.5.3 Method

Images from fifty patients acquired in the COSMOS study were assessed by the author to compare the accuracy of the depiction of synovitis in patients with OA knee on MRI scans without the use of intravenous gadolinium contrast. T1 maps and MT difference images acquired as a result of the COSMOS non-contrast MRI protocol were scored and compared with matched post gadolinium images. The images from the first ten patients were not considered for review due to the technical issues that have been previously described when acquiring the T1 maps and MT data. The sequences used were sagittal SPGR ± MT to calculate MT difference images (TR 28ms, TE 2.46ms, Flip angle 15°, Time of acquisition 3.50 minutes), sagittal VIBE Dixon (TR 10ms, TE 2.45ms, Flip angle 10°, Time of acquisition 1.28 minutes), sagittal T1 SPGR mapping sequences (TR 11ms, TE 2.46ms, Flip angles 5°, 10°, 15°, 20° and 25°, Time of acquisition 4 minutes) and sagittal SPGR VIBE (TR9.8ms, TE4.9ms, Flip angle 30°, Time of acquisition 1.26 minutes). The images were selected from fifty consecutive patients that had post-contrast imaging as this is seen to be the reference standard with which the non-contrast images can be compared. The demographics of the patients are described in Table 5-14.

Gender	Number	Mean age (years)	Range of ages (years)
Female	n = 28	58	35 - 85
Male	n = 22	59.5	36 – 77

Table 5-14 Demographics of the patients whose data was used to compare semi quantifiable scoring to the reference standard of post gadolinium contrast VIBE imaging

All the images for the validation component were anonymised and separated from the corresponding full set of images to reduce bias in interpretation. Due to the quantity of images that were acquired for each patient, it was not practical to score all the images. It was decided to select a mid-volume slice that demonstrated the suprapatellar pouch, infrapatellar pouch and Hoffa's fat pad, thus providing three possible locations that synovitis could be demonstrated as described in the study performed by Guermazi in 2011 [202]. Sagittal MT difference with fat overlay, T1 map and post gadolinium contrast VIBE images were scored for the presence, absence and severity of synovitis. The scoring of the randomised images was performed over a period of three months using OsiriX® software to minimise any bias that may affect the observer.

Each potential region in which synovitis may have been present was scored by a modified method described by Guermazi [202] and described in the literature review. Three regions were scored with the following numerical outcomes: 0 = no synovitis, 1 = synovitis present less than 2mm in thickness, and 2 = synovitis present greater than 2mm in thickness. These values were combined to give a total score for each slice to investigate whether under or over visualisation of synovitis in a region affected the total burden scored.

5.4.5.4 Analysis

Visual assessment of the images was made to ensure that no artefacts were present on the images that may inhibit the ability of the observer in scoring the images to the best of their ability.

Comparison was made between the reference standard of post gadolinium contrast MR imaging and two novel non-contrast MR techniques (MT difference with fat and T1 mapping) to assess the presence or absence of synovitis within three compartments of the knee joint (suprapatellar, infrapatellar pouches and Hoffa's fat pad) in patients with OA knee from the COSMOS study.

Sensitivity and specificity were calculated for each imaging technique in each of the three compartments of the knee. Further interrogation of the results

was made to assess the combined effect of using both MT difference with fat images and T1 maps, using the equation described by Parikh et al in 2008 [271], on the accuracy of sensitivity for identifying synovitis by (Equation 5-1).

Combined sensitivity = 1 – [(1 – sensitivity of test 1) X (1 – sensitivity of test 2)]

Equation 5-1 Calculation of sensitivity using more than one diagnostic test [271]

However as the gold standard for detecting synovitis is histology and this was unavailable to use for comparing the non-contrast MRI results to, a conservative approach must be taken in interpreting these results. Because of this, agreement between the non-contrast imaging techniques and the post gadolinium images was assessed by the Spearman rho correlation coefficient and any possible systematic errors that may be present was determined by performing a Friedman test on the whole data set. If any systematic differences were demonstrated, the data would be further examined by using a Wilcoxon signed rank test to ascertain which imaging technique contributed to the error.

The median and IQR values were calculated for each of the imaging techniques in the three separate knee compartments (suprapatellar pouch, infrapatellar pouch and Hoffa's fat pad)

5.4.5.5 Results

(a) Assessing the ability to modify this technique to non-contrast images of MT difference with fat overlay and T1 maps:

The semi quantitative scoring of the COSMOS images has demonstrated that it is possible to visualise synovitis on the non-contrast MT difference with fat overlay and the T1 mapping MR images (Figure 5-16). Synovitis can be

visually delineated from synovial fluid, muscle and bone marrow within the knee of patients with OA knee.

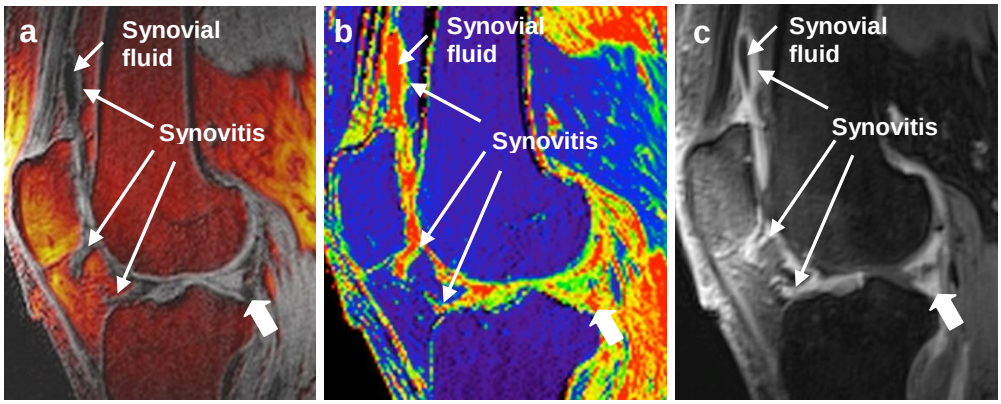

Figure 5-16 Comparison of non-contrast sagittal MR sequences with a post gadolinium contrast VIBE image for the visualisation of synovitis.

(a) MT difference with fat overlay image (b) T1 map image (c) Post contrast gadolinium VIBE image. All three sequences demonstrate synovitis in the suprapatellar pouch, infrapatellar pouch and Hoffa's fat pad regions as labelled. On the MT difference image with fat overlay, the synovitis is seen as pixels of grey signal intensity compared to the red pixels of fat and the hypointense synovial fluid signal. The T1 maps show the synovitis as a mixture of yellow and green pixels compared to the blue of tissue containing lipids and the high T1 values of synovial fluid (demonstrated as red). The post contrast gadolinium VIBE images demonstrate synovitis as hyperintense signal when compared to the isointense or hypointense signal of fatty tissue and synovial fluid. The area pointed to by the thick arrow suggests on the post contrast image that this represents synovitis whereas the non-contrast images indicate that this area is fluid.

(b) Comparing the non-contrast techniques with the reference standard of post gadolinium contrast images obtained from the suprapatellar pouch, infrapatellar pouch and Hoffa's fat pad:

The non-contrast images were scored for the presence of synovitis using the two non-contrast MRI techniques and the results are presented in Table 5-15.

	True +ve	False +ve	False -ve	True -ve
Suprapatellar pouch MT	26	1	9	16
Suprapatellar pouch T1	31	0	4	14
Infrapatellar pouch MT	21	0	7	22
Infrapatellar pouch T1	25	3	2	19
Hoffa's fat pad MT	19	0	7	24
Hoffa's fat pad T1	20	3	5	21

Table 5-15 Comparison of results for detecting synovitis in three compartments of the knee in patients from the COSMOS study using non-contrast MRI techniques of MT difference with fat overlay imaging and T1 maps.

Sensitivity and specificity of MT difference with fat and T1 mapping for detecting synovitis in patients with OA knee, were calculated for three compartments (suprapatellar pouch, infrapatellar pouch and Hoffa's fat pad). The results are presented in Table 5-16 and Table 5-17.

	MT difference with fat overlay	T1
Suprapatellar pouch	74 %	89 %
Infrapatellar pouch	75 %	93 %
Hoffa's fat pad	73 %	80 %

Table 5-16 Sensitivity of the non-contrast MR techniques of MT difference with fat overlay and T1 imaging for scoring synovitis in the suprapatellar, infrapatellar pouches and Hoffa's fat pad in the knees of patients with OA when compared to the reference standard of post gadolinium MR images.

	MT difference with fat overlay	T1
Suprapatellar pouch	95%	100 %
Infrapatellar pouch	100 %	86 %
Hoffa's fat pad	100 %	88 %

Table 5-17 Specificity of the non-contrast MR techniques of MT difference with fat overlay and T1 imaging for scoring synovitis in the suprapatellar, infrapatellar pouches and Hoffa's fat pad in the knees of patients with OA when compared to the reference standard of post gadolinium MR images.

T1 mapping was shown to be more sensitive in detecting synovitis when compared to MT difference with fat overlay imaging for the three compartments of the knee. However, MT difference with fat overlay imaging was more specific than T1 mapping when assessing for synovitis in the infrapatellar pouch and Hoffa's fat pad.

If however, the results from the two imaging techniques are combined, the sensitivity and specificity of detecting synovitis in the knee can be increased in comparison to the stand alone results of each technique. The sensitivity in detecting synovitis in the knee by using both novel techniques (MT difference with fat overlay and T1 mapping as a multiparametric technique) in combination is increased in all three compartments of the knee increasing the confidence of accurate detection of synovitis. While this reduces the specificity for identifying synovitis the ability to increase the sensitivity of synovitis detection outweighs the decrease in specificity because it is more important to rule out the presence of synovitis rather than rule it in.

	Combined sensitivity of detecting synovitis using MT difference with fat overlay imaging and T1 mapping
Suprapatellar pouch	97.1 %
Infrapatellar pouch	97.2 %
Hoffa's fat pad	94.6 %

Table 5-18 The results of increasing sensitivity as a consequence of combining the results of MT difference and fat overlay imaging and T1 maps using the method described by Parikh [271]

	Combined specificity of detecting synovitis using MT difference with fat overlay imaging and T1 mapping
Suprapatellar pouch	95 %
Infrapatellar pouch	86 %
Hoffa's fat pad	88 %

Table 5-19 The outcome of decreased specificity as a result of combining the results of MT difference and fat overlay imaging and T1 maps using the method described by Parikh [271]

Within the suprapatellar pouch, a good correlation of the results was demonstrated between the semi quantitative scoring of synovitis measured on the MT difference and post gadolinium images (ρ=7.40 p <0.0001). However a systematic difference was shown to be present: X^2 =12.082, df (2) p=0.002, which may reflect the variability of the presence of a synovial effusion within the suprapatellar pouch (Z=-0.3286 p = 0.001). T1 mapping showed moderate correlation when compared to the post gadolinium images (ρ = 0.539 p <0.0001) but demonstrated no systematic differences in results.

The median and interquartile ranges for the data obtained from the suprapatellar pouch are presented in Table 5-20.

Suprapatellar pouch	MT difference with fat overlay	T1 mapping sequence	Post gadolinium contrast
Median	0.5	1.0	2.0
IQR	2.0	2.0	2.0

Table 5-20 Comparison of the median and interquartile ranges of the semi quantitative scoring of synovitis in the suprapatellar pouch of the knee with non-contrast MRI techniques with the reference standard of post gadolinium images.

Within the infrapatellar pouch, a good correlation between the MT difference with fat overlay images and post gadolinium imaging ($\rho = 0.876$ $p < 0.001$) and poor correlation of the T1 maps and the post gadolinium images ($\rho = 0.242$ $p = 0.93$) was demonstrated. No systematic difference was identified within the results obtained from the infrapatellar pouch ($X^2 = 1.685$, df (2), $p=0.431$).

The median and interquartile ranges for the data obtained from the infrapatellar pouch are presented in Table 5-21.

Infrapatellar pouch	MT difference with fat overlay	T1 mapping sequence	Post gadolinium contrast
Median	0.0	1.0	1.0
IQR	2.0	2.0	2.0

Table 5-21 Comparison of the median and interquartile ranges of the semi quantitative scoring of synovitis in the infrapatellar pouch of the knee with non-contrast MRI techniques with the reference standard of post gadolinium images.

Within Hoffa's fat pad there was a very good correlation between the MT difference with fat overlay images and post gadolinium imaging ($\rho = 0.835$ $p < 0.001$) and the T1 maps with the post gadolinium imaging ($\rho = 0.770$ $p < 0.001$). No systematic difference was identified within the results obtained from Hoffa's fat pad ($X^2 = 4.000$, df (2), $p=0.135$).

The median and interquartile ranges for the data obtained from the Hoffa's fat pad are presented in Table 5-22.

Hoffa's fat pad	MT difference with fat overlay	T1 mapping sequence	Post gadolinium contrast
Median	0.0	0.0	0.5
IQR	2.0	2.0	2.0

Table 5-22 Comparison of the median and interquartile ranges of the semi quantitative scoring of synovitis in Hoffa's fat pad of the knee with non-contrast MRI techniques with the reference standard of post gadolinium images.

5.4.5.6 Discussion

The results from the COSMOS study have shown that it is feasible and practical to image and score for the presence of synovitis on knee MRI scans with a clinical diagnosis of OA knee without the need for intravenous gadolinium.

The acquisition time for producing the non-contrast images is approximately ten minutes for the MT difference with fat overlay images and twenty for the complete T1 mapping protocol.

Sensitivity and specificity and semi quantitative scoring can be used on the non-contrast images to identify and quantify synovitis within the knee. Calculating the sensitivity and specificity for both the MT difference with fat overlay images and T1 maps produced results that are better than those published in the literature for Hoffa's fat pad : sensitivity 71% and specificity 55% [272]. Unfortunately there are no other data sets to compare the results for the suprapatellar and infrapatellar pouches.

Whilst the results obtained for the sensitivity and specificity for the non-contrast MRI technique appear promising, these results could be improved

by combining the individual results. Parikh et al in 2008 proposed a method to increase the sensitivity or specificity of a diagnostic test by combining the results from two or more investigations but with a compromise resulting in a decrease to the factor that was not modified [271]. As it is more important in the assessment of synovitis within the knee to rule out its presence rather than rule it in, it was decided to use Parikh's method to increase the sensitivity of the test at a cost to specificity. This resulted in increasing the sensitivity of the non-contrast techniques in all three compartments of the knee to be over 94%. The resulting decrease in specificity calculated a value of over 86% for all three knee compartments. This decrease of specificity for detecting synovitis within Hoffa's fat pad is still greater than that reported by Crema et al in 2013, 55% [272]. This method supports the hypothesis that multiparametric imaging may be beneficial in identifying synovitis within the knee.

However, the results demonstrated by calculating sensitivity and specificity scores in the COSMOS study must be interpreted with care. Sensitivity and specificity assume that that the gold standard for measuring the quantity of synovitis in the knee is post contrast gadolinium imaging, where it is in fact histology. Unfortunately, histological samples were not available for comparing the results of the non-contrast MRI techniques and so pragmatism must be used when interpreting the sensitivity and specificity results.

As an alternative approach, the degree of accuracy of the non-contrast MRI sequences for assessing the quantity of synovitis present can be demonstrated by comparing the GBCA images to the novel techniques to look for agreement.

The semi quantitative scoring of synovitis within the suprapatellar pouch demonstrated that the MT difference with fat overlay imaging provided good correlation with that of the GBCA imaging by an experienced scorer. There was however a systematic difference in the MT difference with fat overlay results suggesting a constant over or under scoring of the amount of synovitis. T1 mapping showed moderate correlation but with no systematic errors present. The most probable cause for this is the variation of presence of a synovial effusion with synovitis within the suprapatellar pouch. On T1 maps the synovitis is assigned a pixel colour depending on the T1 value of the tissue and can be identified on the image by its tissue characteristics

despite the lack of fluid for use as a comparison. This is not the case with MT difference with fat overlay imaging, where the non-distended pouch provides no clear visual or empirical boundaries of synovitis resulting in the under scoring of quantity (Figure 5-17). This would also be true if MTR images instead of MT difference with fat overlay images were used, as the MTR technique, like that of T1 mapping, is a quantitative method of imaging which provides an empirical value.

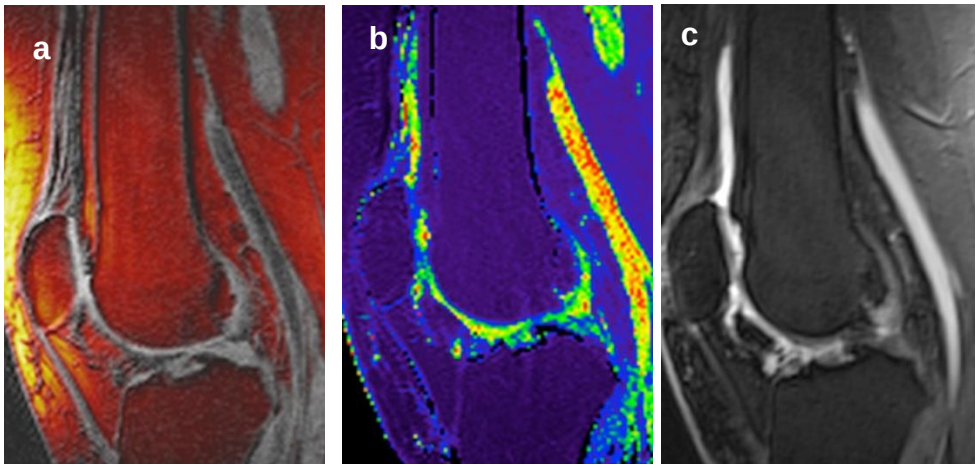

Figure 5-17 Comparison of non-contrast sagittal MR sequences with a post gadolinium contrast VIBE image showing the inability of the MT difference with fat overlay image to demonstrate synovitis without the presence of a synovial effusion in the suprapatellar pouch.

(a) MT difference with fat overlay image (b) T1 map (c) Post contrast gadolinium image

Within the infrapatellar pouch the MT difference with fat overlay images showed good correlation with the post contrast gadolinium images compared to a poor correlation calculated for the T1 maps. Unlike the suprapatellar pouch, there were no systematic differences demonstrated with the MT based imaging technique.

Both MT difference with fat overlay and T1 mapping showed good correlation with no systematic errors demonstrated, with the post contrast gadolinium imaging in Hoffa's fat pad. Within Hoffa's fat pad synovitis is an infiltrative

process of synovium within the fat. The conspicuity of synovitis within Hoffa's fat pad is due to the contrast between the synovitis and the lipid tissue which both of the non-contrast techniques are able to demonstrate without the presence of a synovial effusion.

The results of the semi quantitative scoring of synovitis within the suprapatellar and infrapatellar pouches of the knee suggest that if only one non-contrast imaging technique were to be employed, it would be that of the MT difference with fat overlay. However it must be remembered that systematic errors occur within the results obtained from the suprapatellar pouch and the MT based imaging technique. The scoring results from Hoffa's fat pad suggest that both novel imaging techniques show comparable results to those from the post contrast gadolinium imaging.

Both the MT difference with fat overlay and the T1 maps were able to exclude synovitis when it was not present, as determined by the post contrast reference standard imaging. Examples of non-contrast and post gadolinium images of a knee without synovitis are shown in Figure 5-18 where all three images agree with the non-depiction of synovitis within the knee joint.

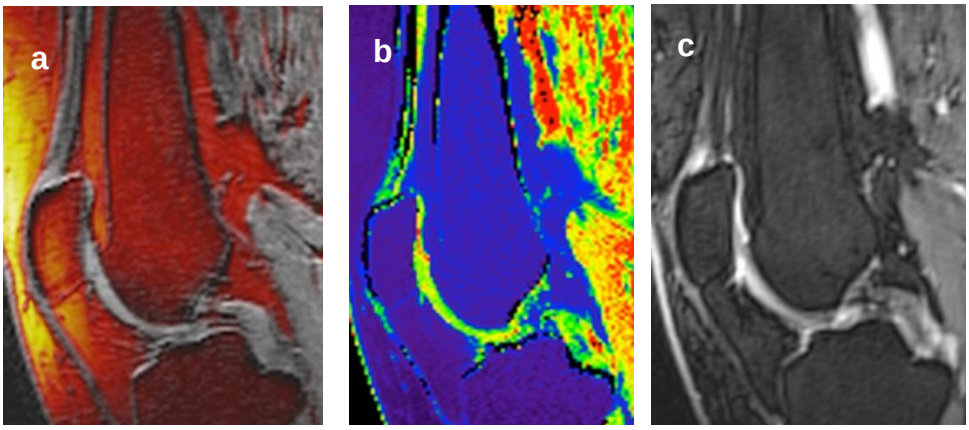

Figure 5-18 Comparison of non-contrast sagittal MR sequences with a post gadolinium contrast VIBE image showing a knee without synovitis in the suprapatellar pouch, infrapatellar pouch and Hoffa's fat pad.

(a) MT difference with fat overlay image (b) T1 map image (c) Post contrast gadolinium VIBE image.

The use of multiparametric approach for visually assessing the novel non-contrast images appears to suggest that the reference standard of the post gadolinium images does not reflect the gold standard of histology by over estimating the quantity of synovitis on the post gadolinium images. The non-contrast techniques of MT difference with fat overlay and T1 mapping appear to differentiate synovial fluid from purely synovitis as defined as synovitis on the post contrast gadolinium images. For example, in Figure 5-19 a series of non-contrast and post contrast gadolinium images are presented (Figure 5-19a, MT difference with fat overlay Figure 5-19b T1 map and Figure 5-19c post contrast gadolinium VIBE images). On the post contrast gadolinium image the areas highlighted with arrows appear to be synovitis on the post contrast image but are in fact synovial fluid when the non-contrast images are inspected. This disparity in tissue identification would lead to over estimation of the volume of synovitis in the patient and comparison with longitudinal scans may give false indication as to the progression or recession of the disease process.

Likewise this is again demonstrated on Figure 5-19d magnified MT difference with fat overlay, Figure 5-19e magnified T1 map and Figure 5-19f magnified post contrast gadolinium VIBE images. The thin arrows show an area which is confirmed as synovial fluid on all three sets of images whilst the thick arrows demonstrate areas of what would be considered as synovitis on the post gadolinium contrast images but again are shown to represent only synovial fluid on the non-contrast scans. This would again lead to an over estimation of synovitis volume on the reference standard post gadolinium images and could affect treatment plans or staging of the disease.

The possibility of the non-uniformity of the diffusion of contrast from the synovium into the synovial fluid could also affect the accuracy when comparing scans to assess the response to treatment. The overestimation of the volume of synovitis may be further compounded if the timing post injection were to be included as a variable. Variation in the timing of image acquisition post administration of gadolinium will influence the volume of synovial fluid shown as hyperintense signal despite being acquired in the recommended ten minute time frame by Østergaard in 2001 [188].

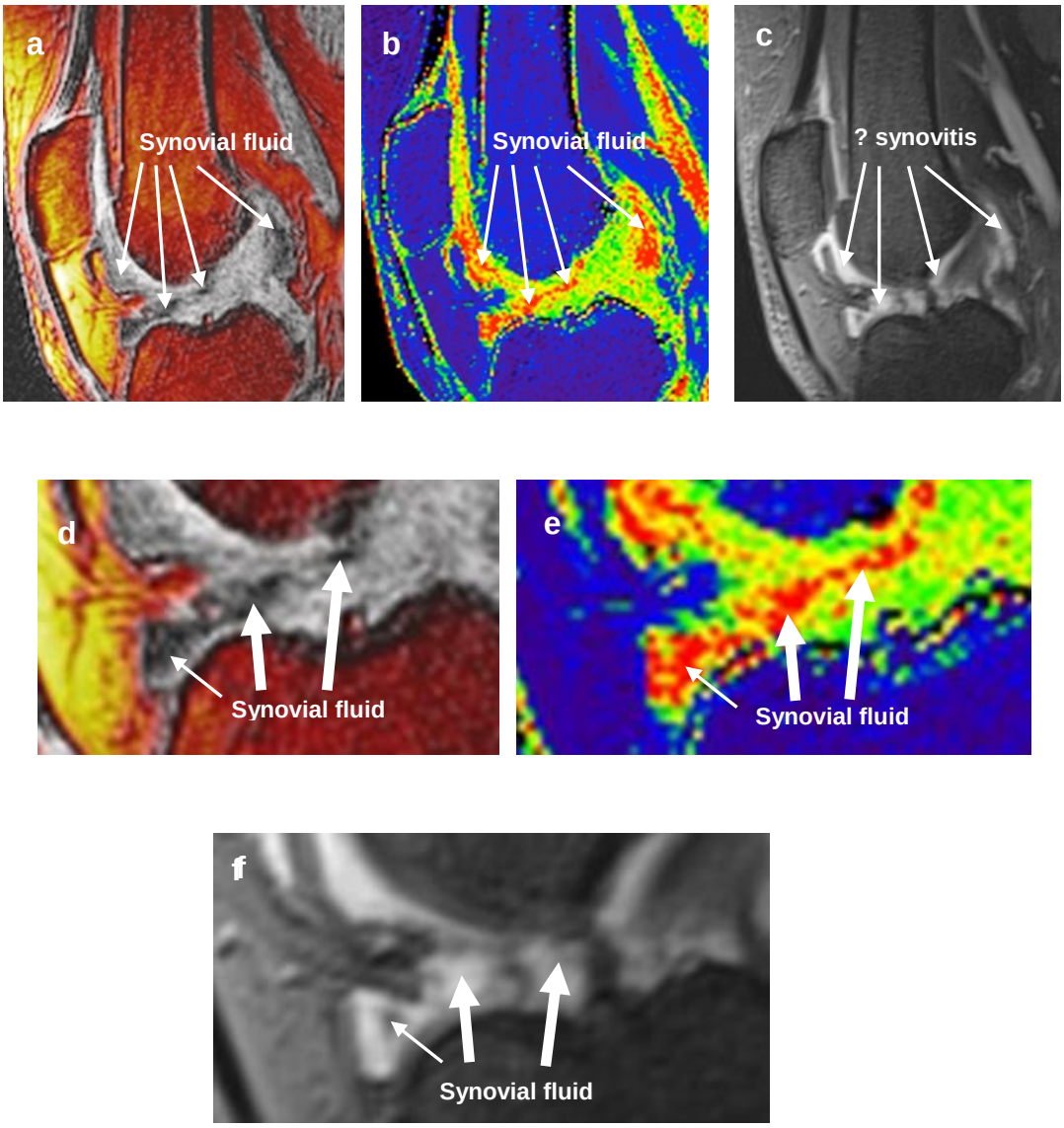

Figure 5-19 Sagittal MR images of the knee in patients with osteoarthritis depicting synovial fluid signal on MT difference with fat overlay, T1 maps and post contrast gadolinium images.

(a) MT difference with fat overlay, (b) T1 map, (c) post contrast gadolinium VIBE image, (d) magnified MT difference with fat overlay image, (e) magnified T1 map, (f) magnified post contrast gadolinium image. Comparison of the non-contrast images *d* and *e* with the post contrast gadolinium image *f* shows the ability of the new techniques to visualise synovial fluid where the post contrast image may be misinterpreted to visualise synovitis rather than synovial fluid.

5.4.5.7 Conclusion

The use of a modified Guermazi et al [202] semi-quantitative scoring technique developed by the author for assessing the volume of synovitis in the knee in patients with osteoarthritis is feasible and relatively quick to perform (assessing and scoring each scan takes approximately three to four minutes to achieve, depending on the volume of synovitis present on the image). Familiarity with the appearances of the MT difference with fat overlay images and T1 maps is essential so that normal and abnormal signal patterns can be recognised, as is necessary with any image interpretation. It proved possible to make measurements on the processed images using OsiriX® software which can also be saved as a JPEG or in DICOM format and used for comparison in longitudinal studies.

Measurements can be made within individual regions of the knee and these can be combined to provide a representative total volume of synovitis for the knee. This may provide a more accurate detection of the changes in volume of synovitis within the knee over a period of time, for example as the distribution of the disease may change; it may or may not alter the total volume. This could be applied further in future studies if a more accurate representation of the volume of the synovitis within the knee as a whole could be derived from multiple images.

In conclusion, the novel MRI techniques using MT difference with fat overlay and T1 mapping are able to be used to allow for semi quantitative scoring of synovitis within the suprapatellar pouch, infrapatellar pouch and Hoffa's fat pad in knees of patients with OA. The results show a good agreement with the reference standard of post contrast gadolinium imaging.

5.5 COSMOS protocol conclusion

The COSMOS study has shown that it is both feasible and practical to produce non-contrast MRI scans of synovitis within the knee in patients with OA in an acquisition time that is acceptable for patients.

The development of a protocol incorporating conventional and novel techniques has been compared with the reference standard of post gadolinium contrast imaging demonstrating favourable results.

The optimisation of SPGR sequences ± MT, producing MT difference and MTR images have provided a unique database of tissue characteristics that can be achieved in less than ten minutes per patient. Expansion of this database may allow for its use as a biomarker tool in the assessment of OA in the knee or other joints, or indeed other forms of arthritis. At the commencement of this project, it was thought that MT and derivatives of the raw data, would be the most robust and clinically suitable non-contrast parameters for assessing synovitis without contrast agents. Whilst MT does have its strengths in delineating fluid from other structures, the similarity of MTR values for muscle and synovitis limit its full potential.

Surprisingly, T1 mapping has shown the greatest potential for a non-contrast MRI protocol that may be able to identify synovitis in all compartments of the knee and potentially other joints. The distinct grouping of T1 values for synovitis and muscle has allowed for the separation of synovitis from muscle (by relaxation times) when the voxels are interrogated on a voxel to voxel basis or as a visual interpretation if a colour map is applied. The narrow range of T1 values demonstrated by the synovitis of the knee in patients with OA has been used successfully within the COSMOS study and a proof of concept study has subsequently been performed to investigate the use of an optimised inversion recovery protocol to better image synovitis without the use of GBCAs. The details of this work are described in Chapter 7 dedicated to the topic of inversion recovery imaging.

Both the data from the MTR and T1 measurements obtained in the COSMOS study provide a unique database of MRI characteristics of tissues within the knee joints in patients with OA knee. This data could provide:

1. Insight into the disease processes for different stages of disease presentation or progress and could be used as a diagnostic or therapeutic biomarker.
2. A reference databank to compare tissue reaction to therapeutic drugs
3. A prognostic tool as to possible progression of the disease

Semi-quantitative scoring of the non-contrast images is feasible and compares well with the reference standard of post gadolinium contrast imaging.

Findings from the COSMOS study may in future be applied to other forms of arthritis in an attempt to distinguish them from each other without the use of other invasive diagnostic tools. The characterisation of synovitis on MRI in different types of synovitis may change the management of disease in the future.

Chapter 6 Diffusion weighted imaging

6.1 Introduction

As described in the Chapter 2 of this thesis, axial single shot EPI (SS-EPI) diffusion weighted MRI has an established role in distinguishing between ischaemia and infarcts in patients presenting with cerebral vascular accidents [273]. This technique has recently been applied to other body regions in order to identify normal from malignant tissues e.g. prostate, uterus and breast [274, 275]. Results of DWI of the musculoskeletal system have been published concentrating on: bones to identify occult vertebral body fractures; muscles for tumour detection and articular cartilage to assess response post in-vivo transplant [276-278]. Whilst there has been some success in these studies, the images can be marred by artefacts leading to geometric distortion of the data, limited spatial resolution, poor SNR and the long scan times preclude them from becoming an ideal part of a clinical examination. Most of the published diffusion studies scan in the axial plane whilst the requirement of this study would be to scan in the sagittal plane to allow for direct comparison of the diffusion weighted images to the other non-contrast scans.

With new diffusion weighted imaging techniques being developed, there may be a possibility that these techniques decrease the artefacts when compared to conventional diffusion weighted imaging and allow for the visualisation of synovitis in the knee without contrast agents.

6.2 Aim and objectives

The aim of this chapter is to describe a proof of concept study that evaluated an alternative DWI technique to the conventional method utilising single shot fast spin echo imaging. The ability to produce DWI images that have reduced image distortion, increased spatial resolution and increased signal to noise ratio that could create sagittal diffusion weighted imaging scans and be able to calculate ADC values to identify synovitis from other structures of the knee in patients with osteoarthritis may provide an additional diagnostic tool when evaluating patients with OA.

The optimised DWI protocol was applied to a cohort of clinical patients to assess the practicality of and the diagnostic quality of the images produced.

6.3 Method

A Siemens® works in progress (WIP) Readout segmented EPI sequence (RS-EPI) was investigated to determine the possibility of imaging structures within the knee joint (WIP ref NA_544A_VB17A_PORTDA92_RESOLVE).

RS-EPI differs from SS-EPI in the following way:

1. SS-EPI acquires all the data for one slice within one repetition time (TR) whilst RS-EPI acquires a subset of data in each TR period. This results in the RS-EPI technique having a longer examination time but with the ability to acquire data at increased resolution. RS-EPI also employs a higher bandwidth (thus reducing the echo spacing) which should reduce any geometric distortion to the image.

2. T2 and T2* values for structures within the knee are shorter than those of the brain. SS-EPI uses relatively long TE values that result in low signal levels in the knee. The ability of RS-EPI to use shorter TE's within the knee should give a relative increase in the signal to noise ratio in the images produced.

3. SS-EPI is most often performed in the axial plane when used to image the brain and abdominal structures. Whilst this plane could be used in the knee joint, traditional imaging relies on sagittal imaging to demonstrate the structures within the knee. The ability to scan in conventional planes would allow for correlation with conventional imaging of the knee.

A 14 cm diameter polyethylene cylinder phantom containing tap water (to mimic the knee joint dimensions and provide loading of the coils) was used to optimise the imaging parameters of the RS-EPI sequence.

The water phantom was left in the MR scanning room for three hours to allow for the water temperature in the phantom to match the room temperature. Equalisation of temperatures of the phantom and the room, allowed a measurement of room temperature to be used as the temperature of the water within the phantom. Measured values of diffusion in this phantom could then be compared with analogous literature values to assess the accuracy of the diffusion measurement [279]. The scanning hardware was identical to that used in Chapter 5 so that if the developed diffusion protocol were successful it could be easily incorporated into human studies.

A qualitative assessment of the signal to noise ratio was made to calculate to optimal voxel size to produce an accurate ADC value. Using a slice thickness similar to that employed in some of the other non-contrast imaging techniques described in this thesis (2mm) proved inappropriate. The signal levels resulting from those of such relatively thin slices were too low. If the in plane resolution were to be decreased to recover signal, the resulting in-plane resolution was deemed to be inappropriate. The slice thickness was therefore increased to 4mm to increase the signal to noise ratio. Doubling the slice thickness employed also allows for a relatively simple superposition of the diffusion data with the data obtained using methods described elsewhere

in this thesis. In order to reduce the time of acquisition to allow for the scanning time to be clinically viable, parallel imaging (Grappa® with an acceleration factor of 2) was incorporated into the protocol.

In the RS-EPI sequence, ghosting can occur on the images if there is a time offset between the readout gradient and the analogue to digital converter sampling window and due to any readout gradient waveform imperfections. To minimise these potential artefacts, the sequence has two inbuilt parameters ('ADC delay' and 'RO amplitude') that were adjusted empirically to minimise the image artefacts.

Three b values were used: 50,100 and 500 s/mm^2. The justification for using a b value of 50 rather than 0 for the lowest value is because it will suppress any diffusion from any influence from vascular components that may appear on the images [280] and affect the ADC calculation. The imaging parameters used are described in Table 6-1.

	TR (ms)	TE (ms)	Averages	Bandwidth (Hz/pixel)	Imaging matrix	Slice thickness	Scan time
SS-EPI	6000	87	4	1012	130 x 130	4mm	8 minutes 22 seconds
RS-EPI	5000	47	3	558	128 x 128	4mm	13 minutes

Table 6-1 Key scanning parameters for the diffusion weighted imaging SS-EPI and RS-EPI sequences

ADC values of the water phantom were measured and compared to the literature to assess the measurement accuracy. An ADC value of $2.23*10^{-3}$ mm^2s^{-1} at a room temperature of 22.1°C was measured using the RS-EPI sequence which compared favourably to the literature value to $2.15*10^{-3}mm^2s^{-1}$ for water at the same temperature [279].

Comparison of the optimised RS-EPI sequence with the conventional SS-EPI diffusion sequence was performed in two healthy volunteers to assess patient acceptability and image quality.

A small pilot study including the optimised RS-EPI diffusion protocol was performed on three patients in the COSMOS study as per the inclusion criteria of the study. The demographics of the patients included into this arm of the study are presented in Table 6-2.

	Gender	Age (years)
COSMOS patient 73	Male	63
COSMOS patient 74	Female	57
COSMOS patient 75	Female	58

Table 6-2 Demographics of the patients included into the diffusion weighted imaging arm of the COSMOS study.

A limited non contrast scanning protocol was performed on the patients that had the diffusion weighted scans so that the scanning time was reduced to be acceptable to the patients. Post contrast imaging was performed to validate the presence or absence of synovitis on the images. The diffusion scanning volume was copied to that of the other sequences to allow for direct comparison of data and facilitate the possibility of superimposing the images if required at a later time.

6.4 Analysis

Images acquired were visually inspected for the presence or absence of any artefact. The DW images acquired on the phantoms were assessed for geometric distortion by comparing those obtained to a reference standard produced by a T2 TSE sequence.

In vivo images acquired using the optimised RS-EPI diffusion protocol were visually compared to those acquired with the conventional SS-EPI protocol for geometric distortion and anatomical clarity.

ADC values were measured in the medial head of the gastrocnemius muscle, synovial fluid and synovitis (if present) in two volunteers and three patients and compared to the literature.

6.5 Results

Evaluation of the initial images obtained with the non-contrast MRI protocol geometric parameters demonstrated that the voxel size was too small to produce diagnostic ADC values. The voxel size and signal to noise ratio were therefore increased by enlarging the slice thickness to 4mm from 2mm to allow for the production of diagnostic ADC maps.

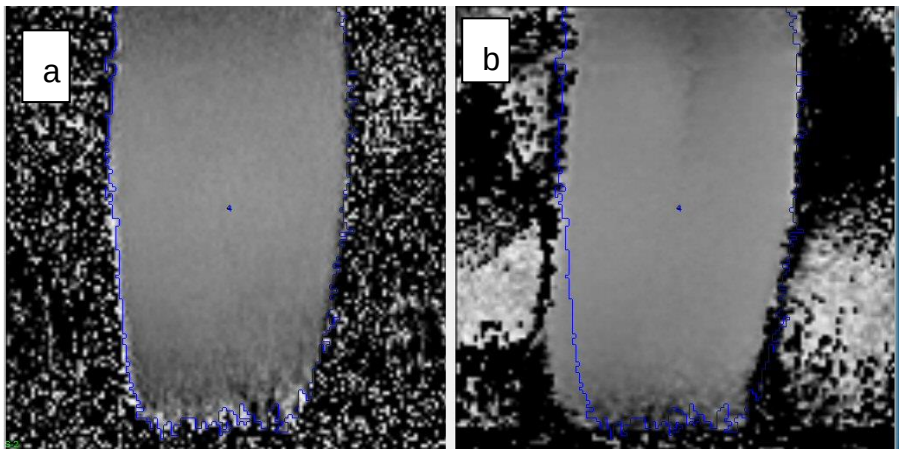

Figure 6-1 Sagittal ADC data obtained from the water phantom.
(a) RS-EPI sequence (b) SS-EPI sequence. The RS-EPI data has been acquired after empirical adjustment to the sequence delays ('RO' and 'ADC delay'. See text)

Figure 6-1 demonstrates sagittal images showing calculated ADC values acquired from the water phantom using the optimised RS-EPI and the SS-EPI sequences. Superimposed onto this data is a blue line depicting the edge of the phantom acquired using a T2 weighted imaging sequence with identical geometrical and locational values. The SS-EPI image demonstrates geometrical distortion of the phantom which has previously been stated to be a disadvantage when using this sequence. The distortion is either absent or is minimal in the RS-EPI image.

The effects of altering the ADC delay and RO values in the RS-EPI sequence are demonstrated in Figure 6-2. The increase in both ADC delay and RO value increases the geometrical distortion and introduces an artefact on the images. The combination of both renders the images un-diagnostic. The parameters that display the minimum amount of artefact on the RS-EPI sequence are ADC delay of 0μs and RO of 1.010.

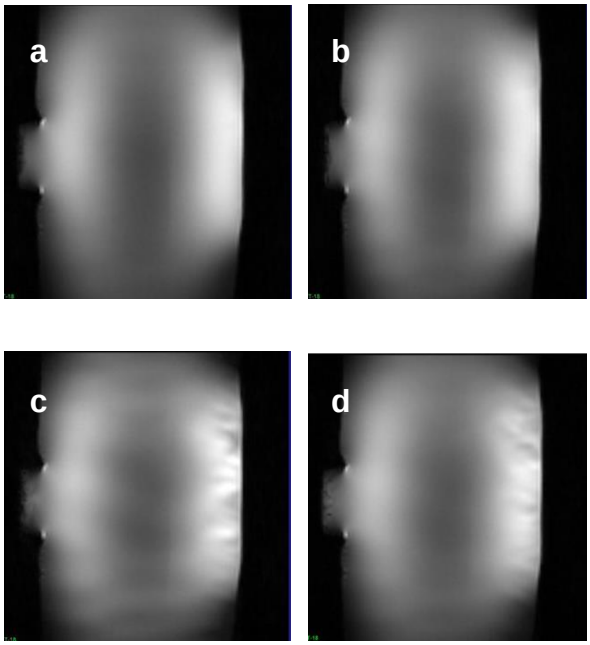

Figure 6-2 Sagittal diffusion weighted images of a water phantom acquired using the RS-EPI sequence with a b value =500 s/mm^2.
Scanning parameters were:

(a) ADC delay. RO=1.005 (b) ADC delay 0 µs. RO=1.025 (c) ADC delay 0 µs. RO=1.045 (d) ADC delay 1 µs. RO=1.025

Prior to imaging patients with the new RS-EPI diffusion scan, the knees of two healthy volunteers were scanned. The images were compared to those obtained using the conventional SS-EPI diffusion scan.

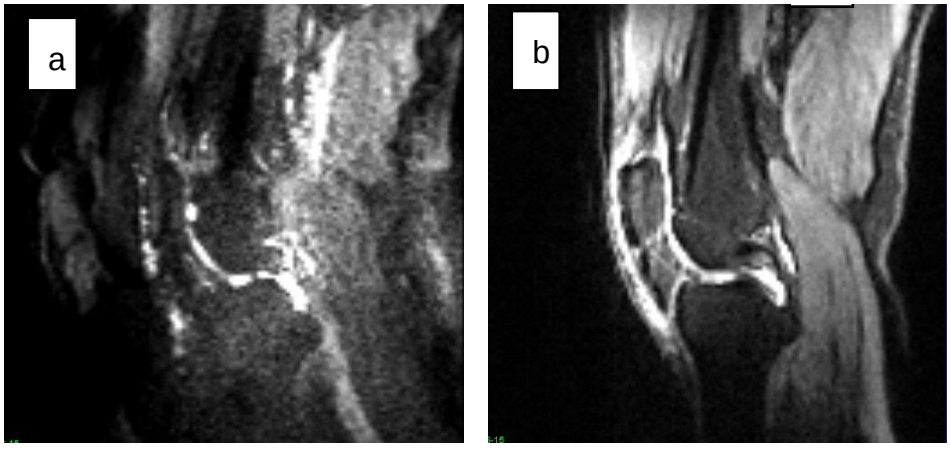

Figure 6-3 Diffusion weighted images obtained from (a) SS-EPI and (b) RS-EPI sequences of a knee in a healthy volunteer using a b value of 500s/mm^2

Figure 6-3 shows the raw diffusion data acquired in the knee of a healthy volunteer using SS-EPI (Figure 6-3a) and RS-EPI (Figure 6-3b). A b value of 500s/mm^2 was used. As can be seen on the images, the geometrical distortion of the images acquired using the RS-EPI is reduced when compared to those using SS-EPI and the signal to noise ratio has also increased.

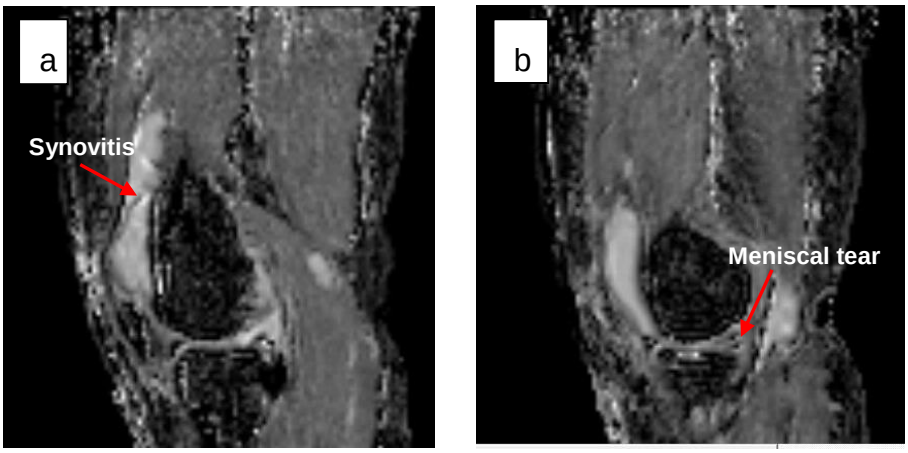

Figure 6-4 Sagittal ADC images using RS-EPI sequence of a knee in a patient with osteoarthritis.
(a) Shows synovitis within the supra-patellar pouch, (b) Shows fluid within a horizontal oblique tear of the medial meniscus

Figure 6-4 depicts images acquired using the RS-EPI sequence in a patient with osteoarthritis of the knee. In Figure 6-4a the arrow points to an area of synovitis sitting within the suprapatellar pouch surrounded by synovial fluid. In Figure 6-4b the arrow points to fluid within a horizontal oblique meniscal tear of the posterior horn of the medial meniscus.

ADC values were also taken of muscle, fluid and synovitis in the volunteers and patients scanned. 50 regions of interest were taken in each patient and volunteer in the head of the gastrocnemius muscle and synovial fluid and synovitis if present. These were averaged and the standard deviation calculated. These values are shown in Table 6-3 alongside documented literature values.

	Muscle (mm^2s^{-1}) (SD)	Synovial Fluid (mm^2s^{-1}) (SD)	Synovitis (mm^2s^{-1}) (SD)
Volunteer 1	$1.5*10^{-3}$ (0.1)	*	*
Volunteer 2	$1.6*10^{-3}$ (0.1)	$2.9*10^{-3}$(0.2)	*
Patient 1	$1.8*10^{-3}$ (0.2)	$3.0*10^{-3}$(0.1)	$2.2*10^{-3}$(0.7)
Patient 2	$1.6*10^{-3}$(0.1)	$3.0*10^{-3}$(0.5)	*
Patient 3	$1.6*10^{-3}$(0.2)	$2.1*10^{-3}$(0.5)	$1.9*10^{-3}$(0.5)
Literature value 1 [281]	$1.62*10^{-3}$(0.14)	*	*
Literature value 2 [282]	$1.21*10^{-3}$(0.07)	*	*
Literature value 3 [283]	*	*	$2.12*10^{-3}$+/- 0.45

Table 6-3 ADC values measured in the knee using RS-EPI diffusion sequence. Standard deviation values are shown in brackets.

6.6 Discussion

The optimised RS-EPI scan has produced apparent diffusion coefficient values which agree with those in the published literature [279]. The amount of artefact and geometrical distortion is less than that of the conventional SS-EPI sequence Figure 6-3 in the sagittal plane.

This pilot study has shown that RS-EPI has potential in demonstrating synovitis in the knee without the use of contrast agents. By manipulating parameters associated with this pulse sequence, ‘ADC delay’ and ‘RO’, images can be produced with minimal artefacts. The optimisation of ‘ADC delay’ and ‘RO’ are dependent on the other imaging parameters used, (e.g. parallel imaging accelerator factors) and may need to be changed if they were altered.

As demonstrated in Figure 6-4a, the difference in ADC values allows synovitis to be differentiated from fluid and muscle. Figure 6-4b shows that other pathologies of the knee can also be demonstrated such as torn menisci with fluid infiltration. The geometric distortion is greatly reduced when compared to images produced from the SS-EPI sequence. This allows for greater delineation of one structure from another thus increasing the sensitivity of identifying synovitis. ADC values recorded are comparable to those in the literature but there are differences which could be due to the following:

(a) The differences in diffusion time selected. If longer diffusion times were selected then the ADC values will increase. As the diffusion time approximates the time required for the water molecules to diffuse a distance similar to the spacing between the barriers, the number of water molecules encountering the barrier increases and the average displacement and hence the water diffusivity decreases [282].

(b) Variations may also be due to the population imaged. The populations imaged in the literature and in this study were different. The average age for the subjects in the literature was a mean of 33 years whilst in this study was 57 years.

(c) The muscle groups measured were different. In the literature, the thigh muscle groups had ADC measurements whilst in this study it was the head of the gastrocnemius. The muscle groups have different roles in the movement of the leg and will have different muscle ultra-structures within them.

(d) Patients with osteoarthritis tend to have more atrophy of the muscles with greater fat content. This is due to the lack of muscle conditioning of the joint due to pain or lack of function. Fat would give a different ADC value when compared to that of muscle.

Despite the apparent potential for this sequence there are major disadvantages to this sequence:

(a) The length of time for the sequence to be acquired. Thirteen minutes is a very long time to ask a patient to remain perfectly still. Any movement during this time would result in the images being un-diagnostic.

(b) The resolution of the scans is not adequate for imaging small structures and subtle areas of synovitis. The lack of resolution leads to partial volume of structures and the inability of direct comparison with other sequences, whether conventional or novel. Increasing the resolution would decrease the signal to noise ratio rendering the images un-diagnostic. Compensating for the lack of signal to noise would need the number of averages to be increased. The number of

averages is proportional to the length of time of the scan and thus increasing them would also increase the already unacceptable scan time.

6.7 Conclusion

The results of this pilot study show promise but currently deem this protocol unacceptable for imaging synovitis at this moment of time due to the lack of image resolution and long acquisition time. However, with evolving scanner and coil technology this protocol could be revisited in the future with beneficial results to patients in the imaging of synovitis using non-contrast MRI.

Chapter 7 Inversion recovery

7.1 Introduction

As previously described in Chapter 2, Jahng et al had previously carried out a study investigating the use of the inversion recovery imaging (IR) technique to image synovitis in the knee without the use of intravenous contrast agents [197].Unfortunately due to limitations in the imaging parameters of the study: the length of the scan (33 minutes), flow artefact on the images and the inability to scan more than one slice at a time due to the constraints of the nulling pulse, Jahng's method was not considered appropriate for clinical imaging.

Jahng's technique relied on the nulling of two tissue types (fat and synovial fluid) with two different inversion times to provide a representation of synovitis without actually optimising the sequence to directly image synovitis: i.e. the volume of synovitis was shown as a result of suppression of the two tissues (fat and synovial fluid) from the acquired image.

However, the large difference in T1 values of fat and synovial fluid that Jahng selected for his protocol could affect the accuracy, type and quantity of tissue suppression with similar T1 values. Therefore, if incorrect inversion times were selected, the images may not reflect the true synovial burden but a combination of synovitis and unsuppressed fat and synovial fluid.

As described in Chapter 5, the T1 values for synovitis in patients of the COSMOS study has been seen to fall in a narrow range (849ms-1277ms). The range of T1 values for fat, synovial fluid and muscle are distinct from that of synovitis. Fat, muscle and synovial fluid have discrete ranges of T1 values in patients with OA knee. However there is a broad spectrum of T1 values within these ranges: fat ranged from 358ms to 609ms, synovial fluid from 2738ms to 7942ms and muscle from 1305ms to 2638ms.

Initially, IR imaging was not a technique that was to be considered within this thesis due to the evidence from the literature review. However when considering the results of the T1 measurements (as described in Chapter 5), it was decided to investigate the feasibility of using the IR method to assess synovial tissue volume with an optimised inversion time to suppress synovitis in patients with OA of the knee. A subset of patients in the COSMOS study therefore underwent imaging using an optimised inversion recovery sequence.

7.2 Aim and objectives

The aim of the work described in this chapter was to assess the potential of the inversion recovery sequence to depict synovitis in OA patients. This study required artefact free images to be acquired without using contrast agents in a time that is acceptable to patients. Chapter 5 has allowed the reinvestigation of an inversion recovery sequence to image synovitis in knees without the use of intravenous gadolinium contrast agents.

7.3 Method

An MRI inversion recovery scanning protocol was developed to assess the presence of synovitis in the knee using results derived from T1 mapping study described in Chapter 5.

Twenty consecutive patients from the COSMOS study were scanned using a sagittal inversion recovery sequence. The demographics of the patients are presented in Table 7-1.

Gender	Mean age (years)	Range of ages (years)	Number of patients
Female	54.1	40 – 79	7
Male	63.7	47-87	13

Table 7-1 Demographics of the patients included into the inversion recovery arm of the COSMOS study

The scanning volume was copied from the other non-contrast sequences (e.g. MT) to replicate the geometrical and locational values thereby allowing for direct comparison and potential fusion of all the data.

In order to allow for the inclusion of the IR sequence in the patient scanning protocol and to minimise the time the patient was in the MRI scanner, the COSMOS MRI scanning protocol was modified by omitting the DESS and T2 TSE sequences due to the lack of additional information gained by them when compared to the other sequences.

Sequence	TR (ms)	TE (ms)	Flip angle (degree)	Inversion time (ms)	Voxel size (mm)	Scan Time (s)
2D PD fs	5000	42	*	*	1 x 1 x 2	3.22
2D IR	4000	12	*	705	1 x 1 x 2	5.30
3D SPGR + MT	28	2.46	15	*	1 x 1 x 1	3.50
3D SPGR – MT	28	2.46	15	*	1 x 1 x 1	3.50
3D VIBE Dixon	10	2.45/3.68	10	*	1 x 1 x 1	1.28
Sagittal T1 mapping sequences comprising of: 3D T1 map 5° 3D T1 map 10 ° 3D T1 map 15° 3D T1 map 20° 3D T1 map 25°	 11 11 11 11 11	 2.46 2.46 2.46 2.46 2.46	 5 10 15 20 25	 * * * * *	 1 x 1 x 1 1 x 1 x 1 1 x 1 x 1 1 x 1 x 1 1 x 1 x 1	 3.56 3.56 3.56 3.56 3.56
3D VIBE pre gad	9.84	4.9	30	*	1 x 1 x 1	1.26
3D VIBE post gad x 5	9.84	4.9	30	*	1 x 1 x 1	1.26

Table 7-2 Inversion recovery non-contrast protocol imaging parameters.

The 2D turbo spin echo based inversion recovery sequence had a slice thickness of 2 mm to replicate the geometry of the other conventional sequence (PD fs) in the non-contrast scanning protocol (voxel size equal to 1x1x2 mm). The 2D turbo spin echo based inversion recovery sequence employed a TR of 4000ms, a TE of 12ms and a TI of 705ms.

The value of TI was calculated using the equation presented in Equation 7-1:

$$TI = \ln(2) \times T1$$

Equation 7-1 Equation to calculate the inversion time required for an inversion recovery MRI sequence

TI is inversion time, T1 is T1 value of the tissue [116]

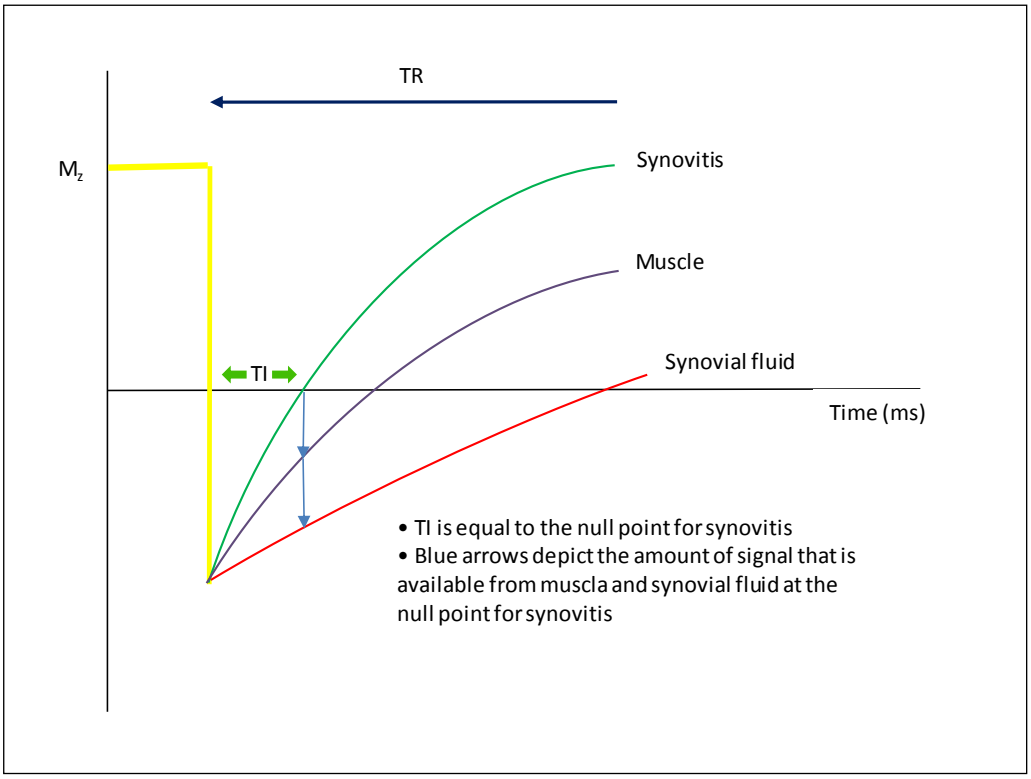

Figure 7-1 Following the 180° inversion pulse the z magnetisation for all tissues is inverted. When the pulse sequence is applied after a delay of TI (693ms), the tissue for which its z magnetisation has recovered and passes through zero returns no signal, suppressing the contribution of that tissue to the image. [284].

The initial 80 patients scanned gave synovitis a mean T1 value of 1005ms (SD 91ms) and this was used to calculate the inversion time for synovitis to be used in the IR sequence (Figure 7-1) as shown in Equation 7-2:

$$1005\text{ms} \times 0.69 = 693\text{ms}$$

Equation 7-2 Calculation of inversion time for the inversion recovery scans to suppress signal from synovitis in the COSMOS study using Equation 7-1.

However a TI of 705ms was used in the IR sequence due to the constraints of the MRI scanner and its tolerance of combined, selected compatible imaging conditions. The selection of 693ms prevented the other scanning parameters selected to match the other sequences within the protocol. It was decided to keep the geometry of the scan to match the other 2D sequences and select a slightly shorter T1.

Likewise, a pragmatic decision was taken in the selection of the TR value. A TR of 5000ms would be needed to allow for the tissue to approach complete relaxation. The TR was chosen to be 4000ms, approximately 4 times the TI of synovitis [115] which would allow for the acquisition time to be acceptable for the patient.

In the reconstruction of the IR data, there are two possible methods available: real (phase sensitive) or magnitude images. In the real (phase sensitive) images, the phase of the value of the signal which reflects the sign of the magnetisation before the 90° pulse is used in the reconstruction of the data (+/-). Signal from the tissue which is nulled by the inversion time is displayed as mid-grey on the pixel intensity scale and the other tissue types will be displayed as either higher or lower pixel intensity. Tissue with a longer relaxation time when compared to synovitis (e.g. synovial fluid) will have relatively lower pixel intensity and those with lower relaxation times (e.g. fat) will have a higher signal (Figure 7-2).

In magnitude reconstruction, the polarity of the signal is not used to calculate the image. The selected tissue will be nulled and have a pixel value of zero

and all other tissues will have higher signal intensities regardless of their relaxation times (Figure 7-2).

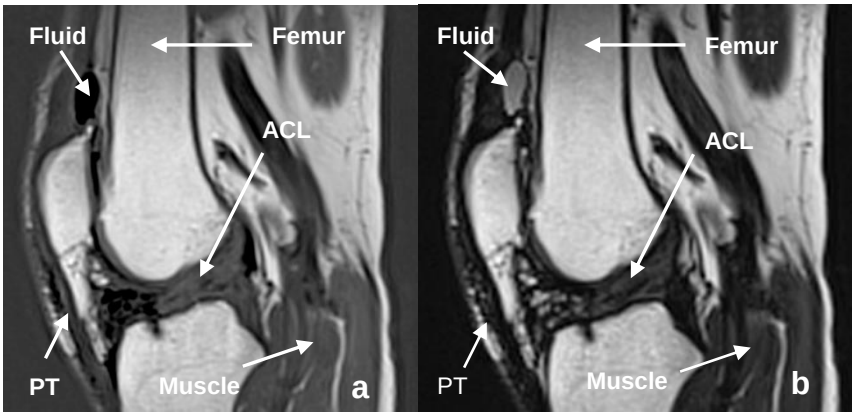

Figure 7-2 (a) Sagittal knee MRI IR Real image reconstruction (b) Sagittal knee MRI IR magnitude reconstruction showing anatomical features of an osteoarthritic knee joint.
PT is patellar tendon

The patient was scanned in the identical position as the main study with the two small flex coils wrapped around the knee, in the Siemens® Verio 3T MRI scanner.

In order to validate that the correct inversion time had been selected and synovial tissue was being suppressed on the IR images, regions of interest were drawn on the post contrast images and these were copied to the corresponding inversion recovery scans. If the inversion time for suppressing the synovial tissue had been correctly calculated, the synovial tissue should return a signal of zero.

7.4 Analysis

The images acquired with the optimised inversion recovery protocol were visually inspected for artefacts.

Signal intensities on the magnitude reconstructed images in areas of synovitis, as confirmed on the post contrast images, were measured. Signal intensities of a zero value were considered to be areas of complete inversion of tissue with a T1 of 1005ms.

7.5 Results

In this arm of this study, twenty patients of the COSMOS study had an inversion recovery scan. Post gadolinium imaging (as per the main study) was performed in thirteen patients of those twenty. Seven patients had contraindications to the administration of gadolinium, had no accessible venous access or refused the injection.

The presence or absence of synovitis in these patients is presented in Table 7-3. Whilst it was not possible to validate the presence of synovitis on the six patients that demonstrated synovitis on the IR scans but did not have post gadolinium imaging the experience gained by the author at identifying synovitis on the images indicated that synovitis was present. In the IR magnitude reconstructed images where the synovitis was thought to be present, the signal intensity returned a value of zero when a region of interest (ROI) was placed on them.

	Post gadolinium	Inversion Recovery
Number of patients imaged	13	20
Synovitis present	9	15
Synovitis absent	4	5

Table 7-3 Results of Magnitude reconstruction inversion recovery images versus post gadolinium imaging for 20 patients of the COSMOS study to identify synovitis in the knee joint

Figure 7-3 shows two inversion recovery images acquired from a patient suffering from OA of their knee. Figure 7-3a depicts the *'real'* image reconstruction whilst Figure 7-3b shows the '*magnitude'* reconstruction. In Figure 7-3a, the synovial fluid is dark in relation to the other structures of the knee and the synovitis is not clearly visible. However in Figure 7-3b the synovial fluid is seen as hyperintense signal with the synovium depicted as a hypointense line around it (as labelled on the images).

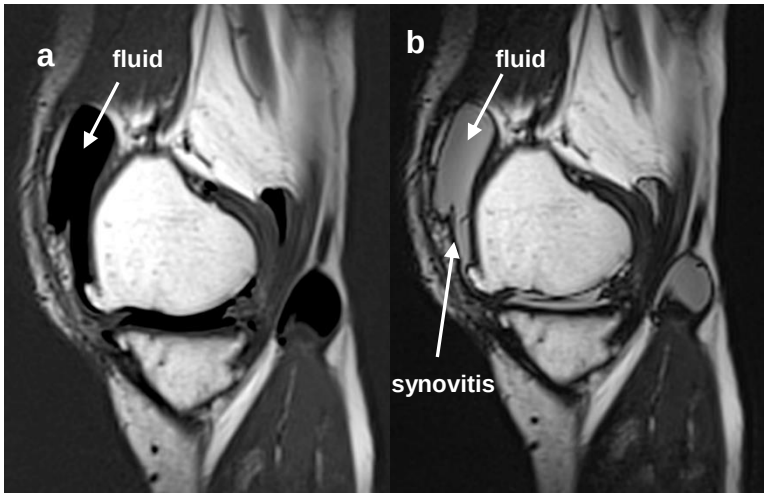

Figure 7-3 Sagittal inversion recovery MR images of a knee in a patient with osteoarthritis.
(a) Real image reconstruction. Hypointense signal depicts synovial fluid within the joint. The synovitis present does not return a signal that can be easily visualised. (b) Magnitude image reconstruction. The hyperintense signal depicts synovial fluid within the joint. The hypointense signal surrounding the fluid depicts synovitis and if a region of interest is placed in it, the mean pixel value returned is zero (see Figure 7-5).

In Figure 7-4a, an inversion recovery magnitude image of another patient with OA of the knee again shows the synovial fluid as hyperintense with the hypointense synovium surrounding it. This is compared to Figure 7-4b, a post contrast SPGR image of the same patient at the same positional location showing the synovitis as hyperintense signal (as labelled on the images). On visual inspection, both techniques in Figure 7-4 show similar results in depicting the distribution of synovitis within the knee.

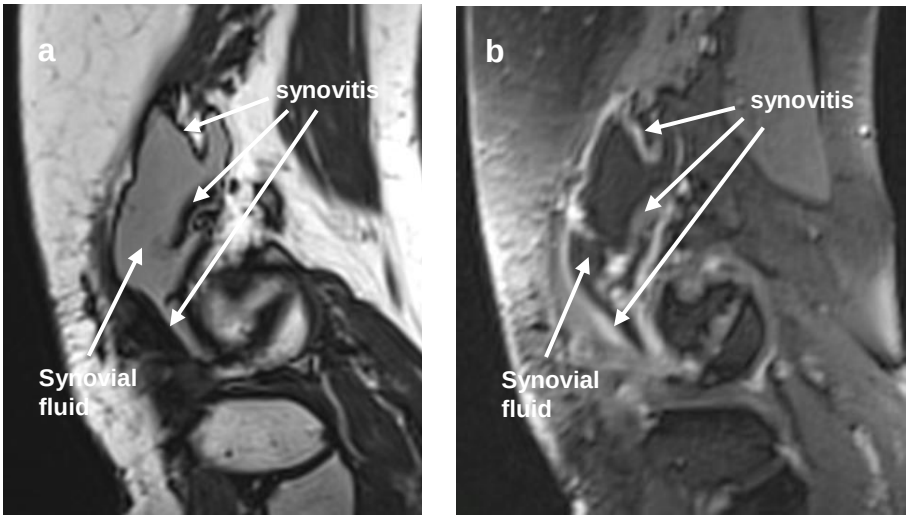

Figure 7-4 Sagittal MRI knee scans depicting synovitis in the lateral compartment. (a) Sagittal inversion recovery magnitude image showing synovitis as hypointense signal surrounding the hyperintense signal of the synovial fluid (b) Sagittal post gadolinium SPGR image showing synovitis as hyperintense signal surrounding the hypointense signal of the synovial fluid.

7.6 Discussion

Because of the limitations of segmentation methods (as previously described in Chapter 2), the images were scored using the modified semi-quantitative system as described in Chapter 5. Due to the small sample size (n=20), the range of disease presentation was limited and a number of scans did not show any synovitis (n=4 for post gadolinium images and n= 5 for inversion recovery scans).

On Figure 7-5a, a ROI has been defined on an area of synovitis on the post contrast images (green circle). This ROI was then copied to a matching IR magnitude image (Figure 7-5b). The value for the signal intensity recorded for the ROI on the IR image is zero as depicted in the text on the image (Figure 7-5b) highlighted by the red circle. The suppression of the synovial tissue has therefore been achieved by the selection of the appropriate inversion time.

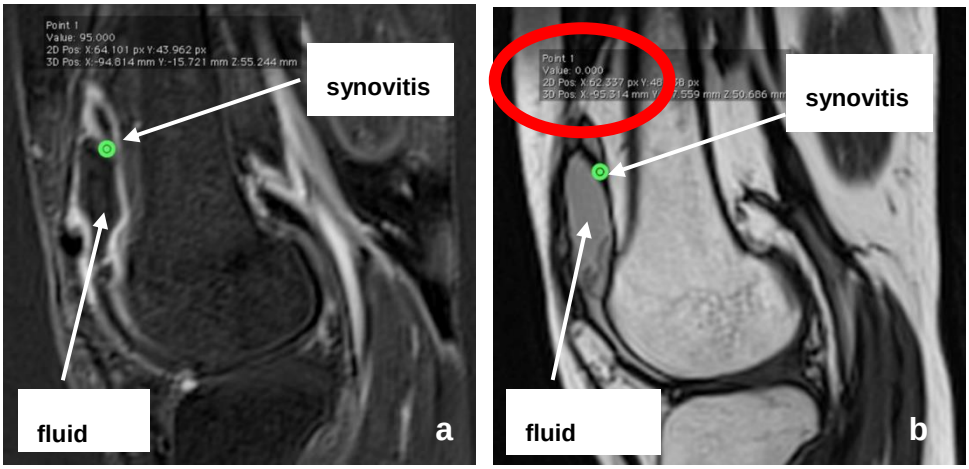

Figure 7-5 Sagittal knee MRI scans of a patient depicting synovitis with a synovial effusion.

(a) Post gadolinium enhanced SPGR MRI scan (b) Inversion Recovery Magnitude image.

The ROI located on synovitis on the post contrast image (green circle) has been copied to the IR scan.

The ROI of the IR scan returns a value of zero confirming that the correct inversion time has been selected for inverting the signal from synovitis and the signal from the synovitis has been suppressed.

The results of the inversion recovery sequence were surprising as this was not a sequence that was initially thought to be appropriate to image synovitis due to previous results reported in the literature. The discovery that the values for T1 of synovitis in knee OA in such a narrow range allowed for the inversion recovery time to be tailored to specifically suppress tissues within the range of T1s between 849ms and 1277ms. These values are such that there is a distinction between synovitis and muscle T1 values (muscle: 1305ms to 2638ms) allowing for synovitis signal on the inversion recovery images to be separated from muscle tissue. Whilst visual inspection and semi quantitative scoring of the inversion recovery images suggest that there is a similarity in the depiction of the synovial volume within the knee joint, it has not been possible to do a direct comparison of this with the reference standard of contrast enhanced imaging. Unfortunately, the contrast images were acquired in a 3D volume and the IR images in a 2D format. Whilst the

volumes were copied to each other and manipulated by software to represent the same positional and geometric locations, an exact match was not obtained. Because the acquisitions were not acquired consecutively to each other there is a possibility that the patients may move between the IR and post contrast sequences resulting in miss matching of anatomical landmarks and therefore potentially pathology. Even if the IR and post gadolinium sequences were acquired back to back to each other there is always a possibility that the patient may move despite being adequately immobilised when the contrast injection was administered. The actual physical process of administering the injection, the act of the operator talking to the patient to warn the patient of the impending injection, the break in the continuity of the soporific scanner noise or a combination of them all, may result in some movement of the joint being imaged and miss registration of the pre and post contrast images. Thus, the exact direct comparison of the pre and post contrast images is challenging but is similar to the approach taken in other imaging studies seeking an alternative to intravenous contrast agents.

However, the IR technique appears to potentially distinguish between types of arthritis all be it in one case. The only one clear outlier (out of the study, n=100) of muscle T1 value in the synovitis range was found to be from a patient that has had a second diagnosis of gout made since his MRI scan (Figure 7-6). At the time of consent for the COSMOS study, the patient had not experienced any symptoms of gout and this second form of inflammatory arthritis had not been diagnosed.

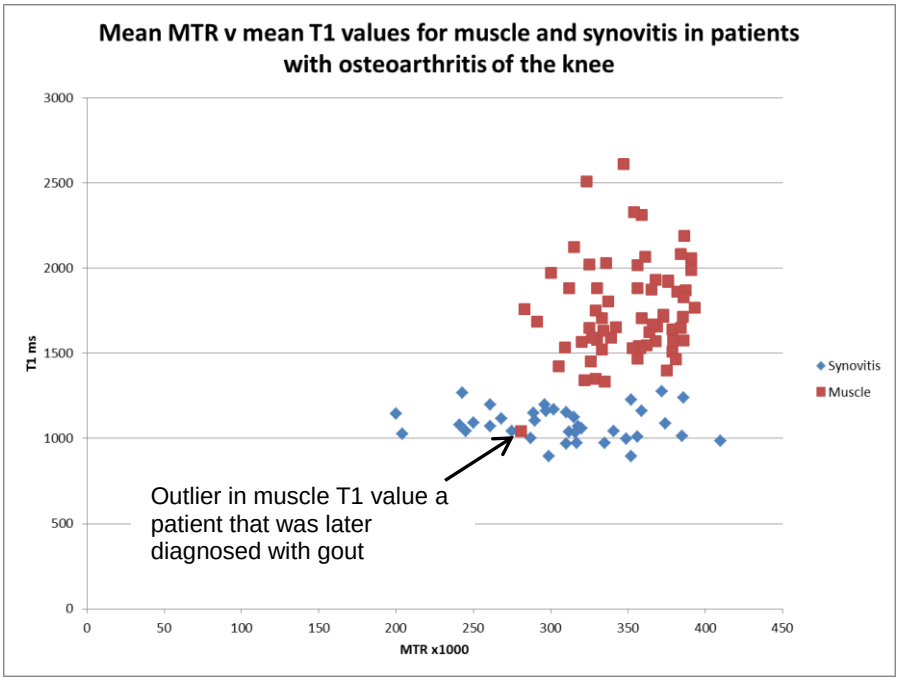

Figure 7-6 Graph showing mean T1 values of muscle and synovitis in patients with OA knee. The graph shows one outlier of muscle T1 signal (arrow) lying in the synovitis range, which is a patient that was later diagnosed with gout.

Despite only having a small sample size (n=20) the inversion recovery technique with an optimised inversion time for synovitis, appears promising in providing a non-contrast MRI technique to assess the synovial burden in patients with osteoarthritis of the knee. The relatively short acquisition time (5 minutes 30 seconds) which is acceptable to patients produces good quality images free from artefact that suppresses the signal from synovitis unlike the previous study implementing the IR technique [197]. Due to the small number of participants, the diversity and range of disease presentation was limited for this technique to be tested on.

T1 values measured from 80 patients with OA knee from the COSMOS study demonstrated a narrow range for synovitis. Further to this, the T1 values for synovial fluid, fat and muscle are very different from that of synovitis. The range of T1 values for muscle varies considerably (mean T1 values of 1041ms to 2638ms) and synovial fluid has a greater variation (mean T1 values 2738ms to 7942ms) (Figure 7-7). The difference in mean values for T1 measurements of structures and synovitis of the osteoarthritic knee allows

the IR novel technique to be a robust method for good delineation of synovitis.

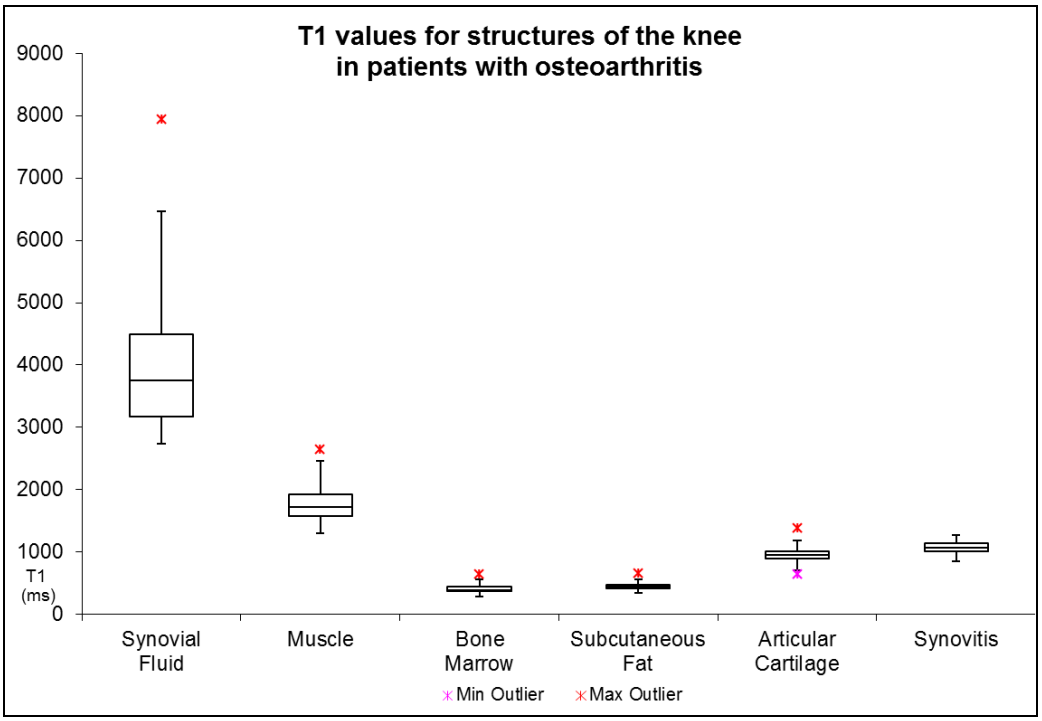

Figure 7-7 Box and whisker plot demonstrating the T1 values for structures of the knee in patients with osteoarthritis.

The figure shows the ranges and the median T1 values of the structures demonstrating that T1 measured values of synovitis, muscle, synovial fluid and fat based structures are distinct from each other. Articular cartilage has a similar range in values to synovitis but the location of articular cartilage is easy to define on other MRI sequences allowing it to be distinguished from the synovitis.

The advantages of using an IR sequence are firstly that no intravenous contrast is required to demonstrate the synovitis and secondly data is acquired using a single acquisition. This contrasts with the MTR and T1 mapping techniques which require multiple image acquisitions and are therefore relatively more prone to artefact arising from patient movement

when calculating the relevant images. Additionally, possible variations in the magnetic field or scanner conditions that may occur between concurrent acquisitions and may affect the calculated maps are irrelevant in the IR technique as only one acquisition is made (unlike the T1 and MTR map calculations).

This technique appears favourable when compared to the previous study of Jahng et al [197] in that it does not display some of the reported issues associated with their study. Unlike Jahng's study, the inversion time selected in this thesis was optimised to suppress only *one* specific tissue, i.e. synovitis and the value was calculated using a large body of data acquired in the COSMOS study (n=80). Because the T1 values for fat and synovial fluid have a wide range (Figure 7-7) from this study, calculating two accurate inversion times to suppress them independently from other tissues would be very difficult.

Jahng et al used an inversion time of 2830ms for fluid and 254ms for fat. Based on the T1 values recorded in the COSMOS study, the T1 values for fat ranged from 358ms to 609ms (calculates an inversion time of 247ms to 420ms) and for synovial fluid T1 values 2738ms to 7942ms (calculates an inversion time of 1889ms to 5480ms). If the readings recorded in the COSMOS study are representative of those to be found in the population of the OA community, then the inversion times chosen by Jahng et al will not demonstrate the burden of synovitis accurately. This may also be true when looking at individual patients longitudinally as alterations in the fluid or fat composition may alter the inversion times and hence affect the tissue's ability to be suppressed with the identified inversion times.

The variation in T1 readings of the structures recorded in the COSMOS study may be due to a number of factors; for example, the duration of the disease and therapeutic adjunct treatments that have been delivered in the past. Specifically, it is possible to speculate on the reasons for the differences in T1 times of synovial fluid and muscle:

Variations in the T1 values for synovial fluid could be due to the proportion of its constituents. Synovial fluid is comprised of phagocytes, interstitial fluid and hyaluronic acid [285]. The amount of these plus any by-products from the inflamed osteoarthritic joint will change the T1 of the fluid. These

constituents may vary over the period of the disease process depending on the inflammatory status of the disease.

Variations in muscle T1 values in patients with osteoarthritis are probably due to the ‘condition’ of the muscles. Patients with myopathies and dystrophies have been seen to have a high fat atrophy in the muscle groups which are reflected in the MR imaging of them [286]. Patients with painful knee joints may guard the joint to prevent excess pain and as a result, decondition the muscles. Fat atrophy or infiltration may occur exacerbating the cycle of deconditioning the muscles of the knee joint (Figure 7-9). Conversely, some patients take the advice from their clinicians and physiotherapists and perform regular exercises to strengthen and maintain the condition of the muscles of the knee, increasing the T1 when compared to atrophic muscles (Figure 7-8). When assessing the muscles of the patients within the COSMOS study, there was a large range of muscle quality and bulk muscle volume.

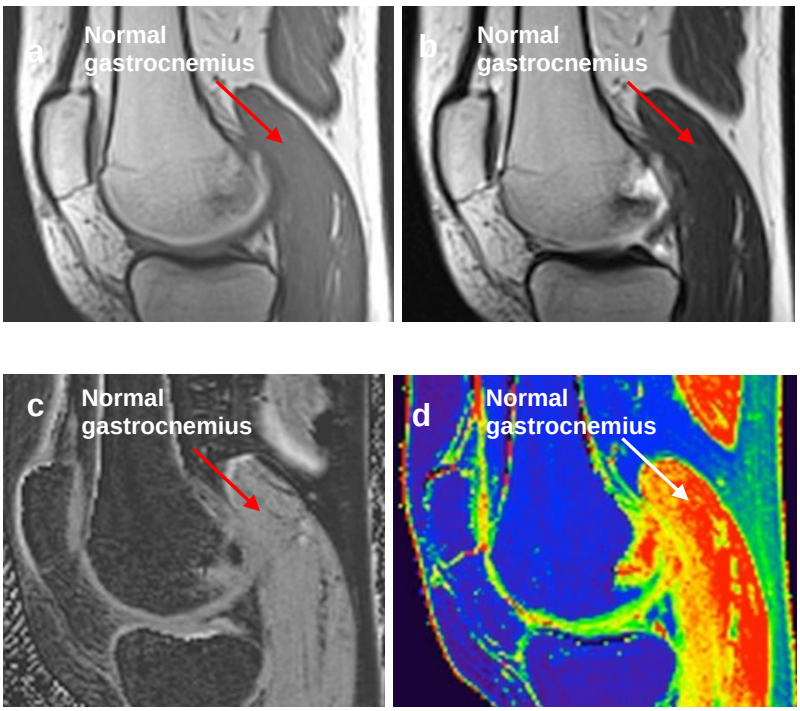

Figure 7-8 Sagittal MR images of the knee demonstrating normal gastrocnemius muscle signal characteristics
(a) T1 TSE (b) T2 TSE (c) MTR (d) T1 mapping

If the T1 characteristics of fat and muscle were to change, this would not affect the volume of synovitis shown on the single inversion time sequence as it is synovitis we are truly imaging and not a subtraction image relying on the characteristics of other tissues to produce the image as in Jahng's study.

Unlike the published study using IR, the inversion time selected in the COSMOS study was able to be applied to all the slices imaged allowing for suppression of the signal throughout the entire scanned volume without any artefacts due to the suboptimal suppression of the synovial tissue.

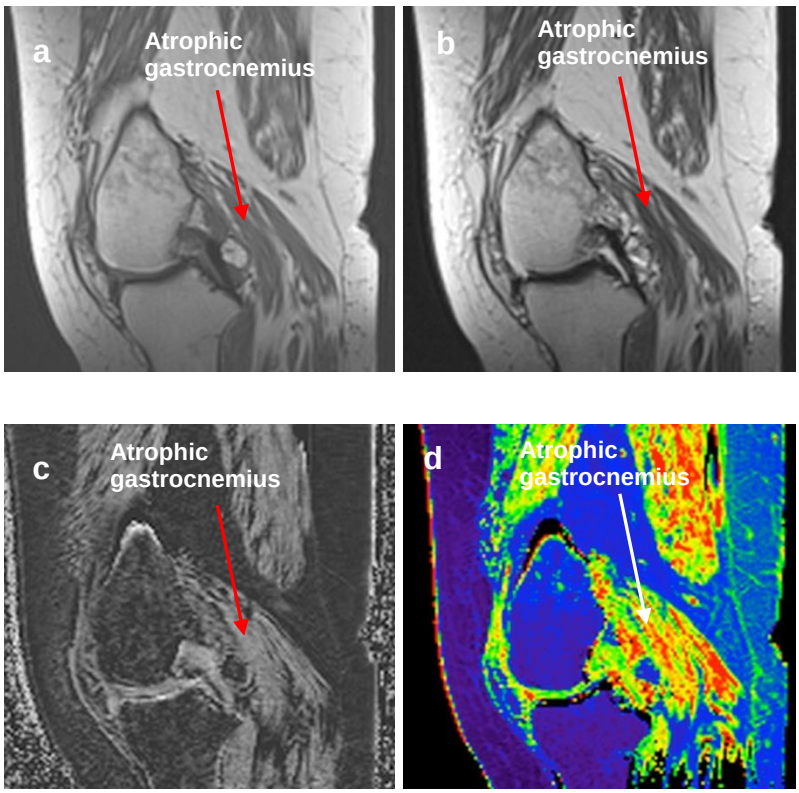

Figure 7-9 Sagittal MR images of an osteoarthritic knee demonstrating an atrophic gastrocnemius muscle signal characteristics.
The body of the muscle is smaller than that in the normal subject and the atrophy of the muscle is demonstrated by the fat infiltration within it.
(a) T1 TSE (b) T2 TSE (c) MTR (d) T1 mapping

There are limitations to this study which need to be acknowledged and addressed if this technique is to be applied in follow up studies.

One possible limitation that was identified prior to the conclusion of the study and therefore the resultant effect could be assessed, was the possible effect of MT on the images. A possible limitation in using 2D TSE based IR sequence is the unintentional MT effects on adjoining slices. The effect of MT

on the volume acquired and its influence on the results of the scan were tested in one patient:

A multi slice volume and single slice inversion recovery acquisition with identical imaging parameters to the IR non-contrast COSMOS protocol were acquired and the ROI signal intensity measurements of tissues in the OA knee were obtained and compared with each other [287]. Readings from the ROIs of the data from the single and multi-slice acquisitions recorded the same signal intensity measurements for identical ROIs. The suppression of the synovitis and thus the same inversion time for both single and multi-slice imaging techniques was not affected by the MT effects of multi-slice imaging.

In addition to the above, another limitation of this study was the discrepancy in geometric similarity of the IR and the post contrast images. Unfortunately it was not possible to perform a 3D IR protocol with identical imaging parameters to the post contrast sequences. Instead a compromise was made in the IR parameters so that they matched the other 2D pre contrast scans and were a 'multiple' of the post contrast images that could allow for comparison and fusion of the images if necessary. Ideally, the geometry of the two imaging sequences should be identical to allow for direct comparison but due to the constraints of the scanner this was not possible and a pragmatic solution sought. If this technique were to be further assessed in the future and applied to a larger sample size, compromises will have to be made to the protocol, resulting in altering the post contrast sequences to a 2D acquisition to allow for direct comparison of the IR and post contrast images. Future studies may include a 3D inversion recovery sequence such as SPACE® (Siemens Medical) or CUBE® (GE Healthcare) to allow direct comparison of the images with respect to slice location and geometry.

Despite there being only one outlier in T1 measurements, the disparity of the results with the rest of the population imaged and the only distinguishable factor from them to the group is the diagnosis of gout, this requires some exploration. It may be possible to use T1 measurements as a diagnostic biomarker of different forms of arthritis as well as a tool to assess response to treatment. In this study, there was one outlier of muscle signal in the synovitis range with a T1 measurement of 1041ms (range of muscle tissue 1305ms to 2638ms for other patients), with the literature recording a T1 value for skeletal muscle at 3T of 1412ms ±13ms [123]. This ROI reading of the

muscle from this patient infers that the muscle in those affected with gout has a higher fat content than patients suffering from osteoarthritis. As the patient had not been diagnosed prior to the MRI scan they were not on any disease modifying drugs and therefore this could not have influenced the results of the muscle readings. The patients with OA knees did display a limited range of muscle atrophy, which was to be expected to be as a result of the lack of use and conditioning of the muscles but not to the extent of the patient with gout. Whether this result for muscle T1 readings is a one off or is a trend for patients who have gout needs further exploration.

It would also be interesting to measure the T1 measurements of the same components of the knee in patients with other types of arthritis; psoriatic or rheumatoid arthritis. It has been assumed in this and previous studies that synovitis in all arthritidies interacts in the same way to intravenous contrast agents (the imaging reference standard). If there are differences in T1 values this may reflect significant variations in the structure and physiology of synovitis and other structures in patients with a range of arthritidies. Comparison of these findings and the possible results of this protocol on non-weight bearing joints in patients with OA looking at the influence of ‘weight’ on the characteristics and T1 values of the synovitis would be interesting.

Only one paper has been published in 1996 looking at enhancement of structures within the normal knee joint [182]. Whilst fat saturation was not used on the post contrast T1 images, the paper concludes that structures do enhance within the normal knee, stating that care should be taken in interpreting ‘mild’ enhancement patterns. Differentiating between the normal and abnormal synovitis on post gadolinium images may not be as clear cut as initially thought.

This thesis and other related and referenced studies, presume that there is a difference in MRI scanning and contrast enhancement between normal synovium and synovitis. If there is a difference in contrast enhancement in synovitis it would be expected that there would be a difference in T1 measurements between synovitis and normal synovium. Histology studies have shown microscopic differences in healthy and diseased synovium and it is expected that these would affect the T1 values of them [66, 69, 265, 288-291].

In order to explore this method further, the results of this pilot study could be the basis for a future study to validate the inversion recovery technique using a larger sample size against the reference standard of contrast enhanced MRI for the detection of synovitis in patients with OA without the use of contrast agents.

Running in parallel to the clinical validation study using inversion recovery imaging, future development that could increase the acceptability of clinicians to this technique and allow for transfer into the clinical environment, would be the development of a computer based method to automatically isolate the synovial volume based on the null signal returned from the synovitis on the inversion recovery images. If a programme were to be written that could apply a colour scale to the voxels of no signal, i.e. the synovitis nulled voxels, it would therefore be possible to produce an easy visual representation of the synovitis burden of the knee in OA that may appeal to clinicians and increase the acceptability of this technique.

7.7 Conclusion

In summary, inversion recovery MRI techniques appeared to work when imaging synovitis in the osteoarthritic knee. This technique is relatively quick (less than ten minutes) and is acceptable to patients. The technique is not influenced by fluctuations in the homogeneity of the magnetic field and only requires one scanning acquisition. A further study is required with a larger population of patients with OA to validate the results of this pilot study. It would also be interesting to compare the results from the OA study with other types of arthritis (rheumatoid and psoriatic) to investigate whether the synovitis in these diseases had a similar T1 value to that in OA. If a computer programme could be developed to visualise the nulled signal as a colour on the images or mask, this may allow for clinician acceptability of the technique and translation into the clinical environment.

Chapter 8 Discussion, major findings and future developments

8.1 Overview

The development of a novel, non-contrast imaging protocol to identify synovitis in osteoarthritis of the knee has been described in this thesis. Multiple methodological approaches have been used to develop and test this protocol systematically.

The initial hypothesis of this thesis was: *'MRI can detect with high sensitivity synovitis in the knee of patients with OA knee without the use of intravenous gadolinium based contrast agents.'* The work undertaken in this thesis supports this hypothesis and a synopsis of the stages of the work is presented as follows:

A review of the literature provided a foundation of knowledge regarding possible MRI techniques that had previously been used to demonstrate synovitis without contrast agents. This combined with appraising existing data held within the LMBRU provided information that allowed for the selection of sequences to be incorporated within a draft COSMOS study protocol. An in-depth assessment of protocols used previously within the unit highlighted some technical issues that if not rectified prior to the commencement of the COSMOS study would have rendered a high proportion of the data acquired invalid.

In Chapter 4, potential candidate sequences that had been selected as a result of chapter three were optimised and validated using phantoms and volunteers. The quantitative sequences of T1 mapping and MTR were tested rigorously and the sequences optimised to provide results that were comparable with the literature and test tools of known values.

The geometry and imaging parameters were selected and modified so that the images produced were geometrically matched for a given patients data set and could accommodate all sizes of patient without further modification.

The output of the work described in Chapter 4 was a non-contrast MRI protocol that had the potential for imaging synovitis in knees of patients with a clinical diagnosis of OA in an acquisition time that would be acceptable for patients.

The resulting non-contrast MRI protocol was applied to a clinical cohort of patients with a clinical diagnosis of OA knee. Initially a pilot study (n=10) was performed using the new non-contrast scanning protocol to ensure that there were no unforeseen issues with the protocol and that the procedure was tolerable for patients. It was noted in the pilot work that the scanning volume for the T1 and MT sequences was not adequate to accommodate 'large' knees. Minor adjustments were made therefore to increase the scanning volume to prevent this from occurring in subsequent patients. The modified protocol was then applied to all successive patients within the COSMOS main study.

The modified COSMOS non-contrast MRI protocol was successfully employed to scan 89 patients out of the 91 consented. Data acquired from the COSMOS study demonstrated that it was both feasible and practical to image synovitis in knees of patients with a clinical diagnosis of OA. It was possible to score the resulting MR images to measure the amount of synovitis using a modified semi quantitative scoring tool and these provided comparable results from non-contrast imaging to those of the reference standard of GBCA enhanced images.

An additional result of this study culminated in a unique database of MTR and T1 values that suggests different tissue types within the knee can be uniquely characterised by quantitative values.

Despite involving a small cohort (n=5) with limited results, it was deemed appropriate to dedicate a chapter to diffusion weighted imaging of synovitis. The optimisation of a new DWI sequence provided relatively diagnostic images demonstrating synovitis within the knee of patients with OA. The rate limiting factors for improving these results are the spatial and temporal resolution of the images. However, when compared to conventional EPI-SE

DWI the images are superior and anatomy and pathology can be identified. With constant improvement in computer hardware and software, the limitations of the sequence currently observed may be rectified in the near future allowing for the use of this technique to scan clinical patients.

The inclusion of an extra chapter dedicated to inversion recovery imaging of synovitis came as a result of the findings from the T1 mapping sequences from the main COSMOS study. The unexpected identification of a narrow range of T1 values for synovitis in OA knees prompted the exploration of using an inversion recovery sequence to image synovitis despite the results published in the literature review [197]. This unanticipated finding came quite late into the COSMOS study (n=80) as the ability to demonstrate this result required a significant volume of data to validate the finding. Despite this however, 20 patients were scanned using the inversion recovery sequence producing promising results.

8.2 Major findings

8.2.1 Feasibility of producing a novel non-contrast MRI protocol to image synovitis

It has been shown within this body of work that it is possible to image synovitis on MRI scans in knees of patients with a clinical diagnosis of OA without the use of intravenous contrast agents in a relatively short acquisition time (40 minutes). Previous studies have suffered from artefacts or limitations [142, 195, 197] that the COSMOS study was able to eliminate.

The COSMOS study has also shown that with the correct imaging parameters selected, MR sequences that were initially intended to be used for alternative anatomy can be used successfully in novel ways to image other anatomical structures and pathologies. The use of MT imaging is such an example. Originally designed to be used in brain imaging [292], the COSMOS study has shown that MT can be utilised in the musculoskeletal system to differentiate pathological indicators (for example synovitis) from

normal anatomy. The ability for MT based imaging to provide two types of image (MT difference and MTR images) allows for two different imaging techniques to be produced from the same raw data set.

8.2.2 The absence of a gold standard

Although the COSMOS study shows an agreement between the non-contrast and GBCA images in depicting synovitis, a degree of caution must be used when interpreting the results; the under estimation of the amount of synovitis by the COSMOS study may not be solely as a result of the inaccuracy of the new novel non-contrast imaging techniques but as a result of errors, probably over estimation of volume, associated with the shortcomings in the reference standard of post contrast gadolinium imaging.

Although post contrast gadolinium images are widely held as the gold standard for measuring the amount of synovitis within the knee this is not the case, as histology provides the only definitive measure [8]. GBCA MR imaging is purely a convenient reference standard utilised for radiological assessment of the quantity of synovitis. With this being the case, the GBCA images cannot be held to represent a gold standard ‘truth’ and it must be acknowledged that any variance between the non-contrast imaging and the GBCA imaging may arise from either approach.

The ability to acquire a ‘synovium only’ high resolution post contrast gadolinium image has proved elusive [293]. It is possible to perform low resolution dynamic contrast enhanced imaging to delineate the distribution of synovitis but this technique may not be resolved enough and can result in partial volume imaging which will affect the volume of synovitis visualised on the images.

Obtaining a true gold standard of histology and comparing with the MRI scans presents its own problems. Obtaining the true gold standards for assessing synovitis requires the invasive procedures of biopsy and/or arthroscopy, although these too have their limitations: Biopsy will demonstrate whether an inflammatory process is present in the synovium but correlating this with the exact position on a MRI scan is impossible.

Arthroscopy does not allow visualisation of synovitis in all areas of the knee again providing an inaccurate representation of the synovitis within the joint [294].

Whilst it would be ideal to have a true gold standard to compare the new non-contrast technique with, this may not be of such importance if any potential errors resulting from the non-contrast techniques are reproducible between individuals and over a longitudinal study. It is usually assumed that the GBCA images produce reproducible results within subjects and between groups of subjects and at various visit time points, while this is not probably correct. Variations between individuals (for example of cardiac output, height and weight) and those between imaging techniques (size of the venflon used, the location of placement of the venflon, the flow rate of contrast and exact post contrast imaging timing) are more likely to cause intra and inter participant variation of the volume of synovitis detected on post contrast gadolinium MRI scans [295].

The importance of inter-test agreement may not be essential providing the errors associated with the investigation experienced are kept the same [296]. Longitudinal assessment of the volume of synovitis in an individual using the COSMOS non-contrast technique would provide an accurate indicator of the phase of the disease process as the individual's base line scan is the reference standard to which all subsequent imaging is compared to. The omission of IV contrast in the COSMOS protocol would reduce some of the potential variables in the technique.

8.2.3 Timing of acquiring images after the administration of gadolinium

A major variable that will affect the amount of synovitis depicted on post contrast gadolinium images is that of the timing of the image acquisition after the administration of the agent. Despite the recommendations by Østergaard [188] with regards to acquisition timing after the administration of intravenous gadolinium, there is still ambiguity when defining the commencement of image acquisition and with no standardisation of MR technique, this results in difficulty when comparing the results between different studies.

Data from the COSMOS study was acquired in accordance with the recommendations of Østergaard et al, where five post contrast image sets were acquired within the first ten minutes after the commencement of administration of contrast agent. Despite conforming to the recommendations, each of the five phases showed a different amount of synovitis present. The precise phase of post contrast images used as the reference for the new method would therefore affect the apparent validity of the new imaging technique.

Whilst it was not within the remit of this work to undertake a full and exhaustive assessment of the post gadolinium sequences discrete times of acquisition after the administration of contrast within the recommended ten minutes, the raw data has been collected and may be interrogated at a later date to explore the precise effects of timing of imaging has on the volume of synovitis demonstrated on the MRI scans.

8.2.4 Multiparametric imaging

The application of a multiparametric approach to identifying synovitis has produced promising results in the COSMOS study and has shown an ability to distinguish different anatomical and tissue types. As has been demonstrated in previous studies with different anatomical structures such as the prostate gland [297, 298], it appears that a multiparametric approach to the imaging of synovitis improves the ability to distinguish pathology from anatomy.

Within the COSMOS study the MT difference, fat images from the VIBE Dixon sequence and T1 maps were used in conjunction, either as directly combined images or as individual elements assessed in parallel with each other, to define the distribution and amount of synovitis within the knee.

The ability of MRI images to characterise and identify tissues due to their intrinsic T1 and T2 relaxation properties allows for accurate detection of different tissue types and by combining the sequences results in greater visual accuracy of disease detection. This can be taken one step further to

provide empirical demarcation of tissue structures by a pixel by pixel interrogation of the values attributed to the T1 relaxation times or MT ratio. The quantitative sequences utilising MT and T1 have been shown in the COSMOS study to identify synovitis within the knee. From the data acquired it appears that MT difference with fat overlay sequences show greater agreement with the GBCA reference standard imaging than T1 maps when studied in isolation (presuming the reference standard equates to the gold standard of histology). Use of the two sequences in conjunction with each other also increases the sensitivity of the technique. The ability to visualise synovitis without intravenous GBCA's using quantitative MR imaging methods that provide further tissue characterisation in addition to the distribution in a time of approximately 30 minutes is achievable but the additional information obtained from this process may not benefit every patient.

For the purpose of a simple diagnostic map showing the distribution of synovitis within the knee, the inclusion of additional tissue characterisation would probably not be of any clinical benefit to the patient but if the COSMOS protocol were to be incorporated into a raft of diagnostic tools within a longitudinal study the diagnostic information obtained could be of great value. The ability to monitor the progression or remission of a disease process or its reaction to therapy using a non-invasive technique far outweighs the length of time needed to acquire the data.

Conversely, a quick (less than ten minute) scan demonstrating the distribution of synovitis may be appropriate for another cohort of patients. The use of an inversion recovery sequence of approximately six minutes duration may be helpful for clinicians who only require a diagnostic image demonstrating the amount and distribution of synovitis without any detailed tissue characterisation required.

Despite the sample being small in the COSMOS study (n=20), it appears that it is feasible to image synovitis without intravenous gadolinium in under ten minutes. The recognition of the small range in T1 values for synovitis within the COSMOS study allowed for an accurate inversion time to be calculated in order to supress synovial tissue. Only 20 patients were scanned with this technique and application of this technique within a larger cohort will be

required to further validate the ability of this sequence to image synovitis without the use of intravenous GBCA's.

8.2.5 Differentiating types of arthritis

Within the COSMOS study, it appeared that distinguishing between different types of arthritis may warrant further consideration. The MTR values of muscle from one patient were an outlier in the COSMOS study and on further investigation this subject was found to have been diagnosed with gout subsequent to participating in the COSMOS study. The MTR values could be a simple rogue outlier but it is noteworthy that out of 89 patients, the only obvious outlier was attributed to a patient who transpired to have an additional diagnosis of gout. The possibility of subclinical cellular processes that occur in the muscle in patients with gout which could account for this anomaly and be identified using quantitative MRI could, if confirmed in subsequent studies, provide an additional purpose for the COSMOS protocol as a diagnostic tool to differentiate between types of arthritis. Likewise, combined MTR and T1 imaging of muscle could provide additional information in diagnosing and assessing other muscle centric diseases.

In the initial review of existing data held within the LMBRU to identify potential candidate MRI sequences, it was assumed that synovitis was the same and had similar imaging characteristics, regardless of the type of arthritis associated with it. Whilst this has not been explored within the body of work forming this thesis, the possibility of this being untrue should be considered. Conventional imaging techniques may demonstrate no difference in synovitis distribution and appearance however quantitative differences may be apparent when T1 and MTR measurements are recorded.

8.2.6 Quantitative MRI of different tissue types

Quantitative multiparametric MR may also be able to provide a biomarker for longitudinal assessment of the response of the osteoarthritic disease process to therapies. Whilst the COSMOS study has focused on the values for

synovitis, it has also resulted in a database of T1 and MTR values for other structures of the knee that may be beneficial in assessing disease response. Whilst not all structures of the knee were measured to obtain T1 and MTR values (for example ligaments and menisci), the raw data could be further interrogated retrospectively to calculate those values.

Qualitative MRI is routine in the clinical environment and whilst identifying visually locational information is currently necessary for disease identification and treatment, the advent of new therapeutic processes that employ computer based empirical solutions used in combination with techniques such as multiparametric MRI may have a significant effect on medical diagnosis and treatment.

The prospect of reproducing and adapting the work of Ma et al [155] in producing a ‘MR fingerprint’ for anatomical structures other than the brain must be seen as a possibility if the preliminary results of the COSMOS study can be taken forward. COSMOS has provided a data bank of quantitative values for the structures of the OA knee using T1 and MT based sequences; this could potentially be the beginning of the development of a ‘MR fingerprint’ for diagnosing, monitoring and ultimately predicting the osteoarthritic disease process. It has been shown in the COSMOS study that tissue identification can be achieved by two quantitative MR methods. If this theory were to be expanded, it should theoretically be possible to either measure and store an individual’s ‘MR fingerprint’ to use for comparison with the results of a subsequent scan when pathology is suspected, or to use other normal tissues of the individual to compare with (such as contralateral knee) if appropriate.

8.3 Limitations of the thesis

Although the aim of this thesis has been achieved and it has been shown that synovitis can be visualised on non-contrast MRI scans there are a number of limitations to this study. The limitations apply both to the design of the study and to the MRI technique and may have practical implications for translating the COSMOS protocol into clinical practice and in other institutions.

In spite of the relatively large number of patients scanned in the main COSMOS study (n=89) compared to other published studies assessing non-contrast synovitis visualisation (n=27 [142], n=unknown [197] and n = 50 [195]) the cohort of this study still may not provide a wide enough range of OA severity to fully test the accuracy of the new techniques for imaging synovitis.

Patients were invited to participate in the COSMOS study if their consultant had made a diagnosis of OA but no attempt was made to quantify or control for the severity. From the literature, we know that patients referred to tertiary care for OA are likely to be moderate to severe, with most cases of OA being seen in primary care. In order to ensure that a representative sample of disease severity were to be included in any future studies assessing the use of non-contrast MRI techniques, it may be prudent to have a defined classification of diagnosis that uses other imaging techniques (X-rays for KL classification and ultrasound to assess the presence or absence of synovitis) and duration of the disease, and construct a representative cohort of patients for every phase of the disease.

Validation of the non-contrast techniques against the reference standard of post gadolinium contrast VIBE imaging was not possible for all patients. Patients with an allergic history or who had an eGFR < 40 $mL/min/1.73\ m^2$ were excluded from gadolinium administration. Despite rigorous examination of their allergic history four patients attended for the MRI scan and at that time declared an allergy that contraindicated the use of gadolinium that they had not admitted to at prior interviews. In addition to these, other patients that did not receive gadolinium were: the initial three patients of the study, one patient that was selected for reliability testing of the MT and T1 imaging, three patients who were recruited specifically for the DWI arm of the study and nine patients in whom venous access was impossible. The consented patients that were unable to have the gadolinium administered (due to contraindications or lack of venous access) represented 13% of the potential cohort of the study adding further weight to the justification of this thesis of the merits in developing an imaging technique that does not require injection of intravenous gadolinium.

No controls were imaged to explore whether the findings of the various imaging techniques were only seen in pathological tissue within the knee

joints of patients with OA. It was not within the scope of this work to examine the synovium of healthy subjects with both the novel imaging techniques and that of the reference standard to investigate whether healthy synovium displayed different imaging characteristics to the COSMOS cohort. If it can be assumed however, that the use of GBCA imaging enhances only pathological synovium, the COSMOS study demonstrated patients whose synovium did not enhance and was also negative on the non-contrast images.

The COSMOS study was performed on a 3T MRI scanner and whilst there are definite advantages for this (possible increased resolution, decreased time of acquisition and increased signal to noise ratio), there are also disadvantages (SAR implications and non-compatibility of surgical implants) which may have impacted on the COSMOS study.

Most surgical implants are safe to be exposed to and scanned with a magnetic field of 1.5T but there are many that are contraindicated for scanning within a 3T scanner. If a patient had an implant such as a cardiac stent they did not meet the inclusion criteria for the COSMOS study but may have been included in the study if it were performed on a 1.5T scanner. Patients with OA are likely to have co-morbidities, including cardiovascular disease [27]. Exclusion of patients with cardiac stents may have an impact on the severity of the disease examined in the COSMOS study. If the study had been performed on a 1.5T MRI scanner there is a possibility that these patients may have been included as the implant was deemed safe at 1.5T. This may however be less of an issue in the future as more passive implants are tested and deemed safe at 3T.

The COSMOS protocol has only been used at a single centre. The short term reproducibility of this protocol has been assessed using the same MRI scanner but has not been implemented at another site. In theory, the COSMOS protocol could be directly transferred to a different 3T scanner that uses receive only coils to image the knee. The successful translation of the COSMOS protocol is reliant on the manufacturer of the second scanner to be used to allow for manipulation of parameters so that they can be matched. If however the protocol is to be implemented on a 1.5T, the parameters for all of the sequences will need to be modified, in particular the choice of flip angles for the T1 mapping sequences. Conversely, a possible benefit of

scanning on a lower strength magnet (such as 1.5T) would be the reduction of SAR issues that were problematic at 3T. SAR implications are negligible at 1.5T and would allow for the reduction of the TR and therefore might reduce the scanning time.

Validation of the inversion recovery series has only been performed on a small cohort of patients (n=20). Whilst the data achieved so far appears promising a formal study is required to validate the results with the reference standard of post gadolinium contrast MRI scans.

Quantifying the volume of synovitis is a time consuming process using either segmentation or semi-quantitative scoring. Both techniques described in this thesis are feasible and can produce results that are comparable to the reference standard but there is potential for error in both techniques. Within the main COSMOS study the decision was made to use a modified semi quantitative scoring method based on Guermazi et al [270] paper of 2013. This method, whilst able to give a representative assessment of the synovial burden within the knee does not give a total for the whole joint. It does however provide more information than the study published by Rhodes et al in 2005 [204] in which the scoring of only one MR slice provides the observer with an indication of the disease process that is occurring within the joint but not the complete picture. If the observer wishes to know whether synovitis is present within the joint and observe the response in volume of synovitis to treatment, the inspection of one slice may be acceptable, assuming that the burden of synovitis alters uniformly in a joint as a response to treatment. However if this assumption cannot be made, then the entire synovial volume within the knee needs to be assessed. Calculation of the volume of synovitis within a joint is time consuming when using segmentation and is subject to a number of sources of variability. However, the potential of the inversion recovery imaging method to produce an image where synovitis is represented by a pixel with a value of zero may allow for the technique of ‘thresholding’ to be reinvestigated. Unlike ‘thresholding’ with a positive signal intensity value on the post contrast gadolinium images (which may incorporate vascular structures and therefore over estimate the amount of synovitis present) ‘thresholding’ with a zero value will only incorporate structures with that precise empirical range of T1 values (as calculated for synovitis) rather than a structure that exhibits similar visual appearance.

Despite these limitations, the COSMOS protocol has demonstrated the ability to image synovitis in OA knees without the use of intravenous GBCA. The use of T1 mapping was a significant success in this project as the range of T1 values for synovitis lay within a narrow range and was distinct from those of muscle. This may not be true for other types of arthritis however and whether the quantitative data can be applied to other types of synovitis requires further work. If though, the T1 of synovitis is found to be of a similar well defined range of values in other forms of arthritis then the COSMOS protocol could potentially be used to image and monitor those as well.

8.4 Future research and directions

The results of this thesis have suggested several potential pathways for further research to be undertaken using the non-contrast COSMOS MRI technique. They broadly fall into three categories and are described below:

8.4.1 Validation and future applications of the COSMOS protocol

The initial findings of the COSMOS study, suggest that the inversion recovery technique is able to produce images of synovitis without the use of contrast agents in a single acquisition of six minutes but further exploration is required to validate this technique with a larger cohort and complete range of disease presentation.

The final COSMOS protocol incorporating the inversion recovery sequence requires no further modifications in order to apply it to a larger cohort for further validation. However, the addition of a proton density sequence into the protocol would allow for subtraction of an inversion recovery image from the proton density image. The resultant images could potentially produce an image in which the highest pixel intensities would represent synovitis and

would obviate the need for any further post processing of the data. This would aid in the acceptability of this technique so that it may be accepted by clinicians and be translated into the clinical environment.

If a further validation study is performed using the inversion recovery sequence, it would be advised to ensure that the full range of the OA disease phases are included in the patient cohort.

If it is presumed that synovitis as a result of OA is the same in all joints and will therefore have similar tissue characteristics, then the COSMOS protocol could be applied to image other joints with minimal adjustments in the imaging parameters. There may need to be some modification in the geometry of the sequence, e.g. to increase field of view if the hip is being imaged or decrease it if the finger is of interest, but the imaging factors that allow the synovitis to be visualised with T1 mapping have been optimised for a range of T1 values centred on 1400ms and it might be expected that they could be appropriate for other OA joints. By imaging other joints that are affected by OA, comparisons can be made with regards to disease involvement and the response of disease progress to medical intervention. As no contrast agents are used in the COSMOS protocol, it is possible to image more than one joint at each attendance if the patient is compliant, something not possible with gadolinium enhanced imaging. Comparison of tissue characteristics of synovitis in weight bearing and non-weight bearing joints would be interesting using the COSMOS protocol to understand whether stresses on joints and the weight they carry affects the amount of synovitis, the characteristics of the tissue and therefore its possible response to treatment and the role synovitis has on joint degeneration.

A key development with the COSMOS protocol would be the ability to assess treatment response in longitudinal studies: with a progressive disease such as OA to assess response to treatment. The T1 maps may show alteration in tissue characteristics that may allow for a greater understanding of synovitis and its role in OA.

With the continual improvement in computer power and development of new MRI technology the ability to use DWI to image synovitis may be become clinically feasible in the near future. The modification of the imaging parameters of the diffusion weighted sequence which allow for higher

resolution images to be acquired within an acceptable acquisition time may soon be possible. The possibility of acquiring diffusion tensor data could again allow for additional knowledge of the OA process by probing the tissue structural properties.

Whilst the work described in this thesis employed five flip angles for the production of accurate T1 maps to visualise synovitis (for T1 value of approximately 1200ms), it may be possible to produce T1 maps with almost equivalent accuracy and reproducibility for the T1 range of interest with fewer flip angles and therefore in a shorter acquisition time. If this were thought to be important, retrospective calculations using different combinations of the flip angles acquired could be performed and the results of these compared to those achieved by utilising five.

8.4.2 Non-contrast MR imaging of synovitis in different types of arthritis

The initial assumption at the commencement of this project is that synovitis is the same regardless of the initial disease process. The tissue MR characteristics, particularly the narrow range of T1 values, of synovitis in patients with OA was found to be such that it was easily possible to separate synovitis from other tissues. It would be interesting to apply the COSMOS non-contrast MRI protocol in patients with other types of arthritis to see if the findings within the OA group are reflected in other types of arthritis.

An unexpected discovery from this thesis was that other forms of arthritis result in different MR characteristics in the tissues involved. One patient that was seen to be an outlier in MTR values measured in muscle recorded in the COSMOS study and who was later diagnosed with gout raises that the possibility of distinguishing between different types of arthritis may be feasible. Subtle changes may occur in tissues that affect the relaxation properties that would allow for identification of one type of arthritis from another. The ability to recognise and categorise subclinical disease could potentially change the treatment pathway for arthritis.

There are known diagnostic patterns that can be identified on images from patients with clinically suspected types of arthritis; for example erosions in RA [299], enthesitis in psoriatic arthritis [300, 301] and spondylitis in ankylosing spondylitis [302] but if there were a means of identifying these prior to the physical manifestation of these signs, it may allow for earlier intervention thus preventing or limiting the effect of the disease on the individual.

In order to assess the ability of the COSMOS study to image other types of arthritis, the COSMOS protocol would have to be tested in a cohort of patients with the appropriate disease, and the study repeated as was done in the main COSMOS study. It would be interesting to see how the tissue characterisation of anatomical structures in patients with different types of arthritis compared to those in patients with OA.

8.4.3 Software development to aid the translation of the COSMOS protocol into the clinical environment

The acceptance and translation of the novel non-contrast MRI techniques into clinical practice would be greatly enhanced if it were possible to develop a computer programme that had the ability to easily define and enhance visually the synovitis on the images. If, as suspected from the initial results obtained from the inversion recovery sequence, this technique was able to demonstrate synovitis on a single scan which takes less than ten minutes, reduction in the time required to interpret the images would possibly allow for clinicians to use this technique. If a colour could be attributed on a pixel by pixel basis to tissues with a signal intensity of zero, the distribution of the synovitis could be readily visualised. Currently, the images need to be interpreted on a pixel by pixel basis by a human operator using ROIs to identify those that have a zero value which is both a time consuming process and introduces the potential for human error. If this process can be automated it could allow for a fast error free interpretation of the data thus making the usage of intravenous gadolinium contrast redundant in the imaging of synovitis within the knee.

8.5 Summary

The work presented in this thesis has, for the first time, demonstrated the ability to depict synovitis in knees in patients with a clinical diagnosis of OA, using MT based and T1 mapping sequences without the use of intravenous gadolinium contrast agents. The images produced allow for the semi quantification of synovitic burden and depict the distribution of the synovitis present. Additionally it has been demonstrated that synovitis can also be depicted on images acquired using diffusion weighted and inversion recovery techniques.

The potential for a one-sequence inversion recovery acquisition technique which takes less than ten minutes, to replace the current reference standard of contrast enhanced imaging warrants further validation in order to benefit patients.

References

1. Smith, S., *OA nation 2012*. 2012, Arthritis Care: London.
2. Wang, Y.C., et al., *Health and economic burden of the projected obesity trends in the USA and the UK.* The Lancet, 2011. **378**(9793): p. 815-825.
3. National Institute for Health and Care Excellence., *Osteoarthritis. Care and management in adults*. 2014: England. p. 1 - 37.
4. Bieleman, H.J., *Work loss in osteoarthritis.* Rheumatology, 2014. **53**(3): p. 387-8.
5. Arthritis Research Campaign., *UK arthritis facts - at a glance*. 2008.
6. Chen, A., et al., *The Global Economic Cost of Osteoarthritis: How the UK Compares.* Arthritis, 2012. **2012**: p. 698709.
7. Menashe, L., et al., *The diagnostic performance of MRI in osteoarthritis: a systematic review and meta-analysis.* Osteoarthritis and cartilage / OARS, Osteoarthritis Research Society, 2012. **20**(1): p. 13-21.
8. Wenham, C.Y.J. and P.G. Conaghan, *The role of synovitis in osteoarthritis.* Therapeutic Advances in Musculoskeletal Disease, 2010. **2**(6): p. 349-359.
9. Benito, M.J., et al., *Synovial tissue inflammation in early and late osteoarthritis.* Annals of the rheumatic diseases, 2005. **64**(9): p. 1263-7.
10. Berenbaum, F., *Osteoarthritis as an inflammatory disease (osteoarthritis is not osteoarthrosis!).* Osteoarthritis and cartilage / OARS, Osteoarthritis Research Society, 2013. **21**(1): p. 16-21.
11. Thomsen, H.S., *Is NSF only the tip of the "gadolinium toxicity" iceberg?* Journal of magnetic resonance imaging : JMRI, 2008. **28**(2): p. 284-6.
12. Gray, H., *Gray's anatomy*. 1982: The Promotional Reprint Company Limited.
13. Fenn, S., A. Datir, and A. Saifuddin, *Synovial recesses of the knee: MR imaging review of anatomical and pathological features.* Skeletal radiology, 2009. **38**(4): p. 317-28.
14. Lee, S.H., *Extrasynovial spaces of the cruciate ligaments: Anatomy, MR imaging and diagnostic implications.* American Journal of Roentology, 1996. **166**: p. 1433-1437.
15. Connelly, L.B., A. Woolf, and P. Brooks. *Cost-effectiveness of interventions for musculoskeletal conditions.* . Available from: www.dcp2.org/pubs/DCP/51/Section/7643.
16. Wollf, A.D., *Understanding the burden of musculoskeletal conditions: The burden is huge and not reflected in national health priorities.* British Medical Journal, 2001. **322**: p. 1079-1080.

17. Watt, I., *Osteoarthritis revisited---again!* Skeletal radiology, 2009. **38**(5): p. 419-23.
18. Teichtahl, A.J., et al., *Imaging of knee osteoarthritis.* Best practice & research. Clinical rheumatology, 2008. **22**(6): p. 1061-74.
19. Lawrence, R.C., et al., *Estimates of the prevalence of arthritis and other rheumatic conditions in the United States. Part II.* Arthritis and rheumatism, 2008. **58**(1): p. 26-35.
20. Reginster, J., *The prevalence and burden of osteoarthritis.* Rheumatology 2002. **41**(Suppl 1): p. 3-6.
21. Blagojevic, M., et al., *Risk factors for onset of osteoarthritis of the knee in older adults: a systematic review and meta-analysis.* Osteoarthritis and cartilage / OARS, Osteoarthritis Research Society, 2010. **18**(1): p. 24-33.
22. Oxford Economics., *The economic costs of arthritis for the UK economy*. 2010.
23. Culliford, D., et al., *Future projections of total hip and knee arthroplasty in the UK: results from the UK Clinical Practice Research Datalink.* Osteoarthritis Cartilage, 2015. **23**(4): p. 594-600.
24. Black, C., *Working for a healthier tomorrow*. 2008: London.
25. Ellams, D., et al., *National Joint Registry 8th annual report 2011*. 2011.
26. Wilkie, R., et al., *Frequency and predictors of premature work loss in primary care consulters for osteoarthritis: prospective cohort study.* Rheumatology, 2014. **53**(3): p. 459-64.
27. Keenan, A.M., et al., *Impact of multiple joint problems on daily living tasks in people in the community over age fifty-five.* Arthritis and rheumatism, 2006. **55**(5): p. 757-64.
28. Lin, E.H., *Depression and osteoarthritis.* Am J Med, 2008. **121**(11 Suppl 2): p. S16-9.
29. Pallant, J.F., et al., *Measuring the impact and distress of osteoarthritis from the patients' perspective.* Health Qual Life Outcomes, 2009. **7**: p. 37.
30. Kingsbury, S.R., et al., *Osteoarthritis in Europe: impact on health status, work productivity and use of pharmacotherapies in five European countries.* Rheumatology, 2014.
31. Felson, D.T. and T. Neogi, *Osteoarthritis: is it a disease of cartilage or of bone?* Arthritis and rheumatism, 2004. **50**(2): p. 341-4.
32. Felson, D., et al., *Osteoarthritis: New Insights Part 1: The Disease and Its Risk Factors.* Annals of Internal Medicine., 2000. **133**: p. 635-6646.
33. Arden, N. and M.C. Nevitt, *Osteoarthritis: epidemiology.* Best practice & research. Clinical rheumatology, 2006. **20**(1): p. 3-25.
34. Bremner, J.M., J.S. Lawrence, and W.E. Miall, *Degenerative joint disease in a Jamaican rural population.* Annals in Rheumatic Diseases, 1968. **27**: p. 326-332.
35. Anderson, J.J. and D.T. Felson, *Factors associated with osteoarthritis of the knee in the first national health and nutrition examination survey (HANES I).* American Journal of Epidemiology, 1988. **128**(1): p. 179-189.

36. Zhang, Y., et al., *Comparison of the prevalence of knee osteoarthritis between the elderly chinese population in Beijing and whites in the United States. The Beijing osteoarthritis study.* Arthritis & Rheumatism, 2001. **44**(9): p. 2065-2071.
37. Lachance, L., et al., *The experience of pain and emergent osteoarthritis of the knee.* Osteoarthritis and cartilage / OARS, Osteoarthritis Research Society, 2001. **9**(6): p. 527-32.
38. Blumberg, B.S., et al., *A Study of the prevalence of arthritis in Alaskan Eskimos* Arthritis and Rheumatism, 1961. **4**(4): p. 325-341.
39. Hart, D.J., *Incidence and risk factors for radiographic knee osteoarthritis in middle aged women.* Arthritis & Rheumatism, 1999. **42**: p. 17-24.
40. Srikanth, V.K., et al., *A meta-analysis of sex differences prevalence, incidence and severity of osteoarthritis.* Osteoarthritis and cartilage / OARS, Osteoarthritis Research Society, 2005. **13**(9): p. 769-81.
41. Oliveria, S.A., et al., *Incidence of symptomatic hand, hip and knee osteoarthritis among patients in a health maintenance organisation.* Arthritis and rheumatism, 1995. **38**(8): p. 1134-1141.
42. Buckwalter, J.A. and J.A. Martin, *Osteoarthritis.* Adv Drug Deliv Rev, 2006. **58**(2): p. 150-67.
43. Felson, D.T., et al., *The prevelence of knee osteoarthritis in the elderly. The Framingham Osteoarthritis Study.* Arthritis & Rheumatism, 1987. **30**: p. 914-918.
44. Szoeke, C.E., et al., *Factors affecting the prevalence of osteoarthritis in healthy middle-aged women: data from the longitudinal Melbourne Women's Midlife Health Project.* Bone, 2006. **39**(5): p. 1149-55.
45. Sandmark, H.H., C. Lewold, S and Vingård, E., *Osteoarthrosis of the knee in men and women in association with overweight, smoking, and hormone therapy.* Annals in Rheumatic Diseases, 1999. **58**: p. 151-5.
46. Spector, T.D., et al., *Genetic influences on osteoarthritis in women: a twin study.* British Medical Journal, 1996. **312**: p. 940-943.
47. Wright, G.H., A.E. Regan, M and Doherty, M., *Association of two loci on chromosome 2q with nodal osteoarthritis.* Annals in Rheumatic Diseases, 1996. **55**: p. 317-319.
48. Sarzi-Puttini, P., et al., *Osteoarthritis: an overview of the disease and its treatment strategies.* Seminars in arthritis and rheumatism, 2005. **35**(1 Suppl 1): p. 1-10.
49. Wluka, A.E., C.B. Lombard, and F.M. Cicuttini, *Tackling obesity in knee osteoarthritis.* Nature reviews. Rheumatology, 2013. **9**(4): p. 225-35.
50. Hinman, R.S. and K.M. Crossley, *Patellofemoral joint osteoarthritis: an important subgroup of knee osteoarthritis.* Rheumatology, 2007. **46**(7): p. 1057-62.
51. Cooper, C.M., T. Coggon, D. Egger, P and Dieppe, P., *Occupational activity and osteoarthritis of the knee.* Annals in Rheumatic Diseases, 1994. **53**: p. 90-93.

52. Buckwalter, J., *Athletics and osteoarthritis.* American Journal of Sports Medicine, 1997. **25**: p. 873-881.
53. Kujala, U.M.K., J. and Sarna, S. , *Osteoarthritis of weight bearing joints of lower limbs in former elite male athletes.* British Medical Journal, 1994. **308**: p. 231-234.
54. Hill, C.L., et al., *Synovitis detected on magnetic resonance imaging and its relation to pain and cartilage loss in knee osteoarthritis.* Annals of the rheumatic diseases, 2007. **66**(12): p. 1599-603.
55. Van de Laar, M., et al., *Pain Treatment in Arthritis-Related Pain: Beyond NSAIDs* The Open Rheumatology Journal, 2012. **6**: p. 320-330.
56. Felson, D.T., et al., *The Association of Bone Marrow Lesions with Pain in Knee Osteoarthritis.* Annals of Internal Medicine., 2001. **134**: p. 541-549.
57. Baker, K., et al., *Relation of synovitis to knee pain using contrast-enhanced MRIs.* Annals of the rheumatic diseases, 2010. **69**(10): p. 1779-83.
58. Szebenyi, B., et al., *Associations between pain, function, and radiographic features in osteoarthritis of the knee.* Arthritis and rheumatism, 2006. **54**(1): p. 230-5.
59. Ip, S., et al., *Frequency of bone marrow lesions and association with pain severity: results from a population-based symptomatic knee cohort.* The Journal of rheumatology, 2011. **38**(6): p. 1079-85.
60. Hernandez-Molina, G., et al., *The association of bone attrition with knee pain and other MRI features of osteoarthritis.* Annals of the rheumatic diseases, 2008. **67**(1): p. 43-47.
61. Haugen, I.K., et al., *Associations between MRI-defined synovitis, bone marrow lesions and structural features and measures of pain and physical function in hand osteoarthritis.* Annals of the rheumatic diseases, 2012. **71**(6): p. 899-904.
62. Finan, P.H., et al., *Discordance between pain and radiographic severity in knee osteoarthritis: findings from quantitative sensory testing of central sensitization.* Arthritis and rheumatism, 2013. **65**(2): p. 363-72.
63. Sharma, L., et al., *The Role of Knee Alignment in Disease Progression and Functional Decline in Knee Osteoarthritis.* Journal of American Medical Association, 2001. **286**(2): p. 188-195.
64. Altman, R., et al., *Development of criteria for the classification and reporting of osteoarthritis. Classification of Osteoarthritis of the Knee.* Arthritis & Rheumatism, 1986. **29**(8): p. 1039-1049.
65. Zhang, W., et al., *EULAR evidence based recommendations for the diagnosis of knee osteoarthritis.* Annals in Rheumatic Diseases, 2009. **69**(3): p. 483 - 489.
66. Smith, M.D., *The Normal Synovium* The Open Rheumatology Journal, 2011. **5**(Suppl 1:M2): p. 100-106.

67. Hayashi, D., et al., *Imaging of Synovitis in Osteoarthritis: Current Status and Outlook.* Seminars in arthritis and rheumatism, 2011. **41**(2): p. 116-130.
68. Aigner, T., et al., *Osteoarthritis: pathobiology-targets and ways for therapeutic intervention.* Adv Drug Deliv Rev, 2006. **58**(2): p. 128-49.
69. Loeuille, D., et al., *Macroscopic and microscopic features of synovial membrane inflammation in the osteoarthritic knee: correlating magnetic resonance imaging findings with disease severity.* Arthritis and rheumatism, 2005. **52**(11): p. 3492-501.
70. Haraoui, B., et al., *Synovial membrane histology and immunopathology in rheumatoid arthritis and osteoarthritis. In Vivo Effects of Antirheumatic Drugs.* Arthritis and Rheumatism, 1991. **34**(2).
71. Pelletier, J.P.M.-P., J and Abramson, S.A. , *Osteoarthritis, an inflammatory disease: potential implication for the selection of new therapeutic targets.* Arthritis & Rheumatism, 2001. **44**: p. 1237-47.
72. Loeuille, D., et al., *Magnetic resonance imaging in osteoarthritis: which method best reflects synovial membrane inflammation? Correlations with clinical, macroscopic and microscopic features.* Osteoarthritis and cartilage / OARS, Osteoarthritis Research Society, 2009. **17**(9): p. 1186-92.
73. Rhodes, L.A., et al., *The relationship between limited MRI section analyses and volumetric assessment of synovitis in knee osteoarthritis.* Clinical radiology, 2005. **60**(12): p. 1295-9.
74. Ayral, X., et al., *Synovitis: a potential predictive factor of structural progression of medial tibiofemoral knee osteoarthritis -- results of a 1 year longitudinal arthroscopic study in 422 patients.* Osteoarthritis and cartilage / OARS, Osteoarthritis Research Society, 2005. **13**(5): p. 361-7.
75. Sellam, J. and F. Berenbaum, *The role of synovitis in pathophysiology and clinical symptoms of osteoarthritis.* Nature reviews. Rheumatology, 2010. **6**(11): p. 625-35.
76. Krasnokutsky, S., et al., *Quantitative magnetic resonance imaging evidence of synovial proliferation is associated with radiographic severity of knee osteoarthritis.* Arthritis and rheumatism, 2011. **63**(10): p. 2983-91.
77. Krasnokutsky, S., et al., *Current concepts in the pathogenesis of osteoarthritis.* Osteoarthritis and cartilage / OARS, Osteoarthritis Research Society, 2008. **16 Suppl 3**: p. S1-3.
78. Belo, J.N., et al., *Prognostic factors of progression of osteoarthritis of the knee: a systematic review of observational studies.* Arthritis and rheumatism, 2007. **57**(1): p. 13-26.
79. Vlad, S.C., et al., *No association between markers of inflammation and osteoarthritis of the hands and knees.* The Journal of rheumatology, 2011. **38**(8): p. 1665-70.
80. Felson, D.T., *Osteoarthritis as a disease of mechanics.* Osteoarthritis and cartilage / OARS, Osteoarthritis Research Society, 2013. **21**(1): p. 10-5.

81. Loeser, R.F., et al., *Osteoarthritis: a disease of the joint as an organ.* Arthritis and rheumatism, 2012. **64**(6): p. 1697-707.
82. Burstein, D. and D.J. Hunter, *"Why aren't we there yet?" Re-examining standard paradigms in imaging of OA: summary of the 2nd annual workshop on imaging based measures of osteoarthritis.* Osteoarthritis and cartilage / OARS, Osteoarthritis Research Society, 2009. **17**(5): p. 571-8.
83. Braun, H.J. and G.E. Gold, *Diagnosis of osteoarthritis: imaging.* Bone, 2012. **51**(2): p. 278-88.
84. Iagnocco, A., et al., *Imaging Modalities in Osteoarthritis.* European Musculoskeletal Review, 2011. **6**(2): p. 74–8.
85. Ferrnandez-Madrid, F., et al., *Synovial thickening detected by MR imaging in osteoarthritis of the knee confirmed by biopsy as synovitis.* Magnetic Resonance Imaging, 1995. **13**(2): p. 177-183.
86. Felson, D.T., et al., *Bone Marrow Edema and Its Relation to Progression of Knee Osteoarthritis.* Annals of Internal Medicine., 2003. **139**: p. 330-336.
87. Guermazi, A., et al., *MR findings in knee osteoarthritis.* European radiology, 2003. **13**(6): p. 1370-86.
88. Spector, T.D., et al., *Definition of osteoarthritis of the knee for epidemiological studies.* Annals in Rheumatic Diseases, 1993. **52**: p. 790-4.
89. Sharma, L., et al., *Significance of pre-radiographic MRI lesions in persons at higher risk for knee osteoarthritis.* Arthritis & Rheumatology, 2014: p. n/a-n/a.
90. Kellgren, J.H. and J.S. Lawrence, *Radiological assessment of Osteo-arthrosis.* Annals of Rheumatic. Diseases , , 1957. **16**: p. 494 -502.
91. Cibere, J., *Do we need radiographs to diagnose osteoarthritis?* Best practice & research. Clinical rheumatology, 2006. **20**(1): p. 27-38.
92. Tack, D., V. De Maertelaer, and G. P.A., *Dose reduction in multidetector CT using attenuation-based online tube current modulation.* American Journal of Roentology, 2003. **181**: p. 331-334.
93. Nicolaou, S., et al., *Dual-energy CT as a potential new diagnostic tool in the management of gout in the acute setting.* AJR. American journal of roentgenology, 2010. **194**(4): p. 1072-8.
94. Johnson, T.R., et al., *Material differentiation by dual energy CT: initial experience.* European radiology, 2007. **17**(6): p. 1510-7.
95. Wang, Y., et al., *Metal artifacts reduction using monochromatic images from spectral CT: evaluation of pedicle screws in patients with scoliosis.* European journal of radiology, 2013. **82**(8): p. e360-6.
96. Polster, J.M., et al., *Rheumatoid Arthritis: Evaluation with Contrast-enhanced CT with Digital Bone Masking.* Radiology, 2009. **252**(1): p. 225 -231.
97. Brenner, W., *18 F-FDG PET in rheumatoid arthritis: There still Is a long way to go* Journal of nuclear medicine, 2004. **45**: p. 927-929.

98. Boegård, T., et al., *Bone scintigraphy in chronic knee pain: comparison with magnetic resonance imaging.* Annals in Rheumatic Diseases, 1999. **58**: p. 20–26.
99. Hutton, C.W., et al., *99mTc HMDP bone scanning in generalised nodal osteoarthritis. II. The four hour bone scan image predicts radiographic change.* Annals in Rheumatic Diseases, 1986. **45**: p. 622-626.
100. de Bois, M., et al., *Joint scintigraphy for quantification of synovitis with 99m Tc-labelled human immunoglobulin G compared to late phase scintigraphy with 99mTc-labelled diphosphonate.* British Journal of Rheumatology, 1994. **33**: p. 67-73.
101. Polison, R.P., et al., *Use of magnetic resonance imaging and positron emission tomography in the assessment of synovial volume and glucose metabolismin pattients with rheumatoid arthritis.* Arthritis & Rheumatism, 1995. **38**(6): p. 819-825.
102. Wandler, E., et al., *Diffuse FDG shoulder uptake on PET is associated with clinical findings of osteoarthritis.* American Journal of Roentology, 2005. **185**: p. 797-803.
103. Nakamura, H., et al., *Positron emission tomography with 18F-FDG in osteoarthritic knee.* Osteoarthritis and cartilage / OARS, Osteoarthritis Research Society, 2007. **15**(6): p. 673-81.
104. Drzezga, A., et al., *First clinical experience with integrated whole-body PET/MR: comparison to PET/CT in patients with oncologic diagnoses.* J Nucl Med, 2012. **53**(6): p. 845-55.
105. Wakefield, R.J., W.W. Gibbon, and P. Emery, *The current status of ultrasonography in rheumatology.* Rheumatology, 1999. **38**(3): p. 195-8.
106. Sahn, D., *Instrumentation and physical factors related to visualization of stenotic and regurgitant jets by doppler color flow mapping* Journal of American College of Cardiology, 1988. **12**: p. 1354-65.
107. Walther, M., et al., *Correlation of power Doppler sonography with vascularity of the synovial tissue of the knee joint in patients with osteoarthritis and rheumatoid arthritis.* Arthritis & Rheumatism, 2001. **44**: p. 331-8.
108. Martinoli, C., et al., *Power Doppler sonography: clinical applications.* European Journal of Radiology, 1998. **28**: p. S133-140.
109. Dougados, M., et al., *The ability of synovitis to predict structural damage in rheumatoid arthritis: a comparative study between clinical examination and ultrasound.* Annals of the rheumatic diseases, 2012.
110. Rowbotham, E.L. and A.J. Grainger, *Rheumatoid arthritis: ultrasound versus MRI.* AJR. American journal of roentgenology, 2011. **197**(3): p. 541-6.
111. Smith, J. and J.T. Finnoff, *Diagnostic and interventional musculoskeletal ultrasound: part 1. Fundamentals.* PM R, 2009. **1**(1): p. 64-75.
112. Østergaard, M., S.J. Pedersen, and U.M. Dohn, *Imaging in rheumatoid arthritis--status and recent advances for magnetic resonance imaging,*

ultrasonography, computed tomography and conventional radiography. Best practice & research. Clinical rheumatology, 2008. **22**(6): p. 1019-44.
113. Conaghan, P., *Is MRI useful in osteoarthritis?* Best practice & research. Clinical rheumatology, 2006. **20**(1): p. 57-68.
114. Ridgway, J.P., *Cardiovascular magnetic resonance physics for clinicians: part I.* Journal of cardiovascular magnetic resonance : official journal of the Society for Cardiovascular Magnetic Resonance, 2010. **12**: p. 71.
115. McRobbie, D.W., et al., *MRI from proton to picture.* 2003: Cambridge University Press.
116. Hashemi, R., H and W.G. Bradley, Jr, *MRI the basics*. 1997, Baltimore: Williams & Wilkins.
117. Cosmus, T.C. and M. Parizh, *Advances in Whole-Body MRI Magnets.* IEEE Transactions on applied superconductivity, 2011. **21**(3): p. 2104-2109.
118. Kijowski, R. and G.E. Gold, *Routine 3D magnetic resonance imaging of joints.* Journal of magnetic resonance imaging : JMRI, 2011. **33**(4): p. 758-71.
119. Peterfy, C.G., E. Schneider, and M. Nevitt, *The osteoarthritis initiative: report on the design rationale for the magnetic resonance imaging protocol for the knee.* Osteoarthritis and Cartilage, 2008. **16**(12): p. 1433-1441.
120. Roemer, F.W., et al., *Short tau inversion recovery and proton density-weighted fat suppressed sequences for the evaluation of osteoarthritis of the knee with a 1.0 T dedicated extremity MRI: development of a time-efficient sequence protocol.* European radiology, 2005. **15**(5): p. 978-87.
121. Schraa, B., *T1 weighted phase sensitive inversion recovery for imaging multiple sclerosis lesions in the cervical spinal cord.* MAGNETOM Flash ·, 2013. **5**: p. 64 - 68.
122. Simon, B., et al., *Improved in vivo detection of cortical lesions in multiple sclerosis using double inversion recovery MR imaging at 3 Tesla.* European radiology, 2010. **20**(7): p. 1675-83.
123. Stanisz, G.J., et al., *T1, T2 relaxation and magnetization transfer in tissue at 3T.* Magnetic resonance in medicine : official journal of the Society of Magnetic Resonance in Medicine / Society of Magnetic Resonance in Medicine, 2005. **54**(3): p. 507-12.
124. Gold, G.E., et al., *Musculoskeletal MRI at 3.0 T: Relaxation Times and Image Contrast.* American Journal of Radiology, 2004;. **183**: p. 343–351.
125. Jordan, C.D., et al., *Musculoskeletal MRI at 3.0T and 7.0T: A comparison of relaxation times and image contrast.* European journal of radiology, 2011.
126. Wright, P.J., et al., *Water proton T1 measurements in brain tissue at 7, 3, and 1.5 T using IR-EPI, IR-TSE, and MPRAGE: results and optimization.* Magma, 2008. **21**(1-2): p. 121-30.

127. Barral, J.K., et al., *A robust methodology for in vivo T1 mapping.* Magnetic resonance in medicine : official journal of the Society of Magnetic Resonance in Medicine / Society of Magnetic Resonance in Medicine, 2010. **64**(4): p. 1057-67.
128. Maestrini., V., et al., *New generation cardiac parametric mapping: the clinical role of T1 and T2 mapping.* MAGNETOM Flash ·, 2013. **5**: p. 104-107.
129. Hauger, O., et al., *Water excitation as an alternative to fat saturation in MR imaging: Preliminary results in musculoskeletal Imaging.* Radiology, 2002. **224**(3): p. 657- 663.
130. Horger, W. and B. Kiefer, *Fat Suppression Techniques – a Short Overview.* MAGNETOM Flash ·, 2001. **1**: p. 57-59.
131. Glover, G.H. and E. Schneider, *Three-point Dixon technique for true water/fat decomposition with B0 inhomogeneity correction.* Magnetic resonance in medicine : official journal of the Society of Magnetic Resonance in Medicine / Society of Magnetic Resonance in Medicine, 1991. **18**(2): p. 371-83.
132. Dixon, W.T., *Simple proton spectroscopic imaging.* Radiology. , 1984. **153**(1): p. 189-94
133. Reeder, S.B., et al., *Multicoil Dixon chemical species separation with an iterative least-squares estimation method.* Magnetic resonance in medicine : official journal of the Society of Magnetic Resonance in Medicine / Society of Magnetic Resonance in Medicine, 2004. **51**(1): p. 35-45.
134. Thomas, S.D., et al., *Application of magnetization transfer at 3.0 T in three-dimensional time-of-flight magnetic resonance angiography of the intracranial arteries.* Journal of magnetic resonance imaging : JMRI, 2002. **15**(4): p. 479-83.
135. de Boer, R.W., *Magnetization transfer contrast Part 1: Physics.* MedicaMundi, 1995. **40**(2): p. 64 -73.
136. Qiu, H., et al., *Progression of a focal ischemic lesion in rat brain during treatment with a novel glycine/NMDA antagonist: an in vivo three-dimensional diffusion-weighted MR microscopy study.* Journal of magnetic resonance imaging : JMRI, 1997. **7**(4): p. 739-44.
137. Agarwal, V., et al., *Diffusion tensor anisotropy magnetic resonance imaging: a new tool to assess synovial inflammation.* Rheumatology, 2009. **48**(4): p. 378-82.
138. Wang, X., et al., *Association between MRI-detected knee joint regional effusion-synovitis and structural changes in older adults: a cohort study.* Ann Rheum Dis, 2014.
139. Atukorala, I., et al., *Synovitis in knee osteoarthritis: a precursor of disease?* Ann Rheum Dis, 2014.
140. Eckstein, F., *Double echo steady state magnetic resonance imaging of knee articular cartilage at 3 Tesla: a pilot study for the Osteoarthritis Initiative.* Annals of the rheumatic diseases, 2006. **65**(4): p. 433-441.

141. Moriya, S., et al., *Three-dimensional double-echo steady-state (3D-DESS) magnetic resonance imaging of the knee: contrast optimization by adjusting flip angle.* Acta radiologica, 2009. **50**(5): p. 507-11.
142. Pelletier, J.P., et al., *A new non-invasive method to assess synovitis severity in relation to symptoms and cartilage volume loss in knee osteoarthritis patients using MRI.* Osteoarthritis and cartilage / OARS, Osteoarthritis Research Society, 2008. **16 Suppl 3**: p. S8-13.
143. Forslind, K., et al., *Detection of joint pathology by magnetic resonance imaging in patients with early rheumatoid arthritis.* British Journal of Rheumatology, 1997. **36**(6): p. 683-8.
144. Østergaard, M., et al., *Magnetic resonance imaging determined synovial membrane and loint effusion volumes in rheumatoid and ostearthritis. Comparison with the macroscopic and microscopic appearance of the Synovium.* Arthritis and Rheumatism, 1997. **40**(10): p. 1856-1867.
145. Jackson, D.W.L., L.D. Maywood, R.M. and Berger B.E., *Magnetic resonance imaging of the knee.* The American journal of sports medicine, 1988. **16**(1): p. 29-38.
146. Frahm, J., *Rapid NMR imaging of dynamic processes using the FLASH technique* Magnetic Resonance in Medicine, 1986. **3**: p. 321-327.
147. Mirowitz, S.A., *Fast scaning and fat-supresion MR Imaging of musculoskeletal disorders.* American Journal of Roentology, 1993. **161**: p. 1147-1157.
148. Erickson, S.J., R.W. Prost, and M.E. Timins, *The "Magic Angle" effect: Background physics and clinical relevance'.* Radiology, 1993. **188**: p. 23-25.
149. Hayes, C.W. and J. Parellada, *The magic angle effect in musculoskeletal MR imaging.* Topics in Magnetic Resonance Imaging, 1996. **8**(1): p. 51-56.
150. Bydder, M., et al., *The magic angle effect: a source of artifact, determinant of image contrast, and technique for imaging.* Journal of magnetic resonance imaging : JMRI, 2007. **25**(2): p. 290-300.
151. Peh, W.C.G. and J.H.M. Chan, *Artifacts in musculoskeletal magnetic resonance imaging: identification and correction.* Skeletal Radiology :, 2001. **30**: p. 179–191.
152. Lin, P.C., D.A. Reiter, and R.G. Spencer, *Classification of degraded cartilage through multiparametric MRI analysis.* J Magn Reson, 2009. **201**(1): p. 61-71.
153. de Boer, R.W., *Magnetization transfer contrast Part 2: Clinical applications.* MedicaMundi, 1995. **40**(2): p. 74 -83.
154. Henkelman, R.M., G.J. Stanisz, and S.J. Graham, *Magnetization transfer in MRI: a review.* NMR in biomedicine, 2001. **14**(2): p. 57-64.
155. Ma, D., et al., *Magnetic resonance fingerprinting.* Nature, 2013. **495**(7440): p. 187-92.
156. Østergaard, M., et al., *Reducing invasiveness, duration, and cost of magnetic resonance imaging in rheumatoid arthritis by omitting*

intravenous contrast injection -- Does it change the assessment of inflammatory and destructive joint changes by the OMERACT RAMRIS? The Journal of rheumatology, 2009. **36**(8): p. 1806-10.
157. Jans, L., et al., *3 T DCE-MRI assessment of synovitis of the interphalangeal joints in patients with erosive osteoarthritis for treatment response monitoring.* Skeletal radiology, 2012.
158. Cimmino, M.A., et al., *Dynamic gadolinium-enhanced magnetic resonance imaging of the wrist in patients with rheumatoid arthritis can discriminate active from inactive disease.* Arthritis and rheumatism, 2003. **48**(5): p. 1207-13.
159. Agarwal, R., et al., *Gadolinium-based contrast agents and nephrogenic systemic fibrosis: a systematic review and meta-analysis.* Nephrology, dialysis, transplantation : official publication of the European Dialysis and Transplant Association - European Renal Association, 2009. **24**(3): p. 856-63.
160. Adam, G., et al., *Rheumatoid arthritis of the knee: value of gadopentetate dimeglumine-enhanced MR imaging.* AJR. American journal of roentgenology, 1991. **156**(1): p. 125-9.
161. Østergaard, M., et al., *The Accuracy of MRI determined Synovial Membrane and Joint Effusion Volumes in Arthritis. A comparison of pre- and post-aspiration volumes.* Scandanavian Journal of Rheumatology, 1995. **24**: p. 305-31 1.
162. Rand, T., et al., *Discrimination between fluid, synovium, and cartilage in patients with rheumatoid arthritis: contrast enhanced Spin Echo versus non-contrast-enhanced fat-suppressed Gradient Echo MR imaging.* Clinical radiology, 1999. **54**(2): p. 107-10.
163. Østergaard, M., et al., *Synovial volume--a marker of disease severity in rheumatoid arthritis? Quantification by MRI.* Scandinavian journal of rheumatology, 1994. **23**(4): p. 197-202.
164. Østergaard, M., et al., *Quantification of synovitis by MRI: correlation between dynamic and static gadolinium-enhanced magnetic resonance imaging and microscopic and macroscopic signs of synovial inflammation.* Magnetic Resonance Imaging, 1998. **16**(7): p. 743–754.
165. Oliver, C. and I. Watt, *Intravenous MRI contrast enhancement of inflammatory synovium: a dose study.* British Journal of Rheumatology, 1996. **35 Suppl 3**: p. 31-5.
166. Hodgson, R.J., et al., *Changes underlying the dynamic contrast-enhanced MRI response to treatment in rheumatoid arthritis.* Skeletal radiology, 2008. **37**(3): p. 201-7.
167. Gaffney, K., et al., *Quantitative assessment of the rheumatoid synovial microvascular bed by gadolinium-DTPA enhanced magnetic resonance imaging.* Annals of the rheumatic diseases, 1998. **57**(3): p. 152-7.
168. McQueen, F.M., *The use of MRI in early RA.* Rheumatology, 2008. **47**(11): p. 1597-9.

169. Hayashi, D., et al., *Imaging of synovitis in osteoarthritis: current status and outlook.* Seminars in arthritis and rheumatism, 2011. **41**(2): p. 116-30.
170. Shellock, F.G. and A. Spinazzi, *MRI safety update 2008: part 1, MRI contrast agents and nephrogenic systemic fibrosis.* AJR. American journal of roentgenology, 2008. **191**(4): p. 1129-39.
171. Yerram, P., et al., *Nephrogenic systemic fibrosis: a mysterious disease in patients with renal failure--role of gadolinium-based contrast media in causation and the beneficial effect of intravenous sodium thiosulfate.* Clinical journal of the American Society of Nephrology : CJASN, 2007. **2**(2): p. 258-63.
172. Grobner, T., *Gadolinium--a specific trigger for the development of nephrogenic fibrosing dermopathy and nephrogenic systemic fibrosis?* Nephrology, dialysis, transplantation : official publication of the European Dialysis and Transplant Association - European Renal Association, 2006. **21**(4): p. 1104-8.
173. Boyd, A.S., J.A. Zic, and J.L. Abraham, *Gadolinium deposition in nephrogenic fibrosing dermopathy.* J Am Acad Dermatol, 2007. **56**(1): p. 27-30.
174. Joffe, P.T., H.S. and Meusel,M., *Pharmacokinetics of Gadodiamide Injection in Patients with Severe Renal Insufficiency and Patients Undergoing Hemodialysis or Continuous Ambulatory Peritoneal Dialysis'.* Academic Radiology, 1998. **5**(7): p. 491-502.
175. Davenport, M.S., R.H. Cohan, and J.H. Ellis, *Contrast Media Controversies in 2015: Imaging Patients With Renal Impairment or Risk of Contrast Reaction.* AJR Am J Roentgenol, 2015: p. 1-8.
176. Kanda, T., et al., *High signal intensity in the dentate nucleus and globus pallidus on unenhanced T1-weighted MR images: Relationship with increasing cumulative dose of a gadoliniumbased contrast material.* Radiology, 2014. **270**(3): p. 834-841.
177. McDonald, R.J., et al., *Intracranial Gadolinium Deposition after Contrast-enhanced MR Imaging.* Radiology, 2015.
178. Bjorkengren, A.G., et al., *MR Imaging of the Knee in Acute Rheumatoid Arthritis: Synovial Uptake of Gadolinium-DOTA.* AJR 1990. **155**: p. 329-332.
179. Chung, C.B., R. Boucher, and D. Resnick, *MR imaging of synovial disorders of the knee.* Seminars in musculoskeletal radiology, 2009. **13**(4): p. 303-25.
180. Evangelisto, A., R. Wakefield, and P. Emery, *Imaging in early arthritis.* Best practice & research. Clinical rheumatology, 2004. **18**(6): p. 927-43.
181. Østergaard, M., et al., *Quantitative assessment of the synovial membrane in the rheumatoid wrist: An easily obtained MRI score reflects the synovial volume.* British Journal of Rheumatology, 1996. **35**: p. 965-971.
182. Boegard, T., et al., *Gadolinium-DTPA-enhanced MR imaging in asymptomatic knees.* Acta Radiologica 1996. **37**: p. 877-882.

183. Partik, B., et al., *Patterns of Gadopentetate-Enhanced MR Imaging of Radiocarpal Joints of Healthy Subjects.* American Journal of Radiology, 2002. **179**: p. 193–197.
184. McQueen, F., et al., *Pitfalls in scoring MR images of rheumatoid arthritis wrist and metacarpophalangeal joints.* Annals of the rheumatic diseases, 2005. **64 Suppl 1**: p. i48-55.
185. Peterfy, C.G., *Magnetic resonance imaging of rheumatoid arthritis: the evolution of clinical applications through clinical trials.* Seminars in arthritis and rheumatism, 2001. **30**(6): p. 375-96.
186. Yamato, M., et al., *MRI of the knee in Rheumatoid arthritis. Gd-DTPA perfusion dynamics.* Journal of Computer Assisted Tomography, 1993. **17**(5): p. 781 -785.
187. Hodgson, R.J., P. O'Connor, and R. Moots, *MRI of rheumatoid arthritis image quantitation for the assessment of disease activity, progression and response to therapy.* Rheumatology, 2008. **47**(1): p. 13-21.
188. Østergaard, M. and M. Klarlund, *Importance of timing of post-contrast MRI in rheumatoid arthritis: what happens during the first 60 minutes after IV gadolinium-DTPA?* Annals of the rheumatic diseases, 2001. **60**(11): p. 1050-4.
189. Østergaard, M., et al., *Significant improvement in synovitis, osteitis, and bone erosion following golimumab and methotrexate combination therapy as compared with methotrexate alone: a magnetic resonance imaging study of 318 methotrexate-naive rheumatoid arthritis patients.* Arthritis and rheumatism, 2011. **63**(12): p. 3712-22.
190. McQueen, F.M., et al., *Magnetic resonance imaging of the wrist in early rheumatoid arthritis reveals progression of erosions despite clinical improvement.* Annals of the rheumatic diseases, 1999. **58**(3): p. 156-63.
191. Prince, M.R., et al., *Incidence of Nephrogenic Systemic Fibrosis at Two Large Medical Centers.* Radiology, 2008. **248**(3): p. 807- 816.
192. Roemer, F.W., D.J. Hunter, and A. Guermazi, *Semiquantitative assessment of synovitis in osteoarthritis on non contrast-enhanced MRI.* Osteoarthritis and cartilage / OARS, Osteoarthritis Research Society, 2009. **17**(6): p. 820-1; author reply 822-824.
193. Roemer, F.W., et al., *Anatomical distribution of synovitis in knee osteoarthritis and its association with joint effusion assessed on non-enhanced and contrast-enhanced MRI.* Osteoarthritis and cartilage / OARS, Osteoarthritis Research Society, 2010. **18**(10): p. 1269-74.
194. Singson, R.D. and F.M. Zalduondo, *Value of unenhanced spin-echo MR imaging in distinguishing between synovitis and effusion of the knee.* AJR. American journal of roentgenology, 1992. **159**(3): p. 569-71.
195. Roemer, F.W., et al., *Hoffa's Fat Pad: Evaluation on Unenhanced MR Images as a Measure of Patellofemoral Synovitis in Osteoarthritis.* AJR. American journal of roentgenology, 2009. **192**(6): p. 1696-700.
196. Santyr, G.E. and R.V. Mulkern, *Magnetization Transfer in MR Imaging.* Journal of Magnetic Resonance Imaging 1996. **5**: p. 121-124.

197. Jahng, G.-H., et al., *Optimization of a double inversion recovery sequence for noninvasive synovium imaging of joint effusion in the knee.* Medical Physics, 2011. **38**(5): p. 2579.
198. Aoki, T., et al., *Diagnosis of early-stage rheumatoid arthritis: usefulness of unenhanced and gadolinium-enhanced MR images at 3 T.* Clinical Imaging., 2012.
199. Basser, P.J. and D.K. Jones, *Diffusion-tensor MRI: theory, experimental design and data analysis- a technical review.* NMR in biomedicine, 2002. **15**: p. 456 - 467.
200. Beaulieu, C., *The basis of anisotropic water diffusion in the nervous system - a technical review.* NMR in biomedicine, 2002. **15**(7-8): p. 435-55.
201. Saupe, N., et al., *Diffusion Tensor Magnetic Resonance Imaging of the Human Calf. Comparison Between 1.5 T and 3.0 T —Preliminary Results.* Investigative Radiology, 2008. **43**(9).
202. Guermazi, A., et al., *Assessment of synovitis with contrast-enhanced MRI using a whole-joint semiquantitative scoring system in people with, or at high risk of, knee osteoarthritis: the MOST study.* Annals of the rheumatic diseases, 2011. **70**(5): p. 805-11.
203. Hunter, D.J., et al., *The reliability of a new scoring system for knee osteoarthritis MRI and the validity of bone marrow lesion assessment: BLOKS (Boston Leeds Osteoarthritis Knee Score).* Annals of the rheumatic diseases, 2008. **67**(2): p. 206-11.
204. Rhodes, L.A., et al., *The validation of simple scoring methods for evaluating compartment-specific synovitis detected by MRI in knee osteoarthritis.* Rheumatology, 2005. **44**(12): p. 1569-73.
205. Østergaard, M., et al., *Quantitative assessment of synovial inflammation by dynamic Gadolinium enhanced magnetic resonance imaging.A study of the effect of intra-articular methylprednisolone on thre rate of early synovial enhancement.* British Journal of Rheumatology, 1996. **35**: p. 50-59.
206. Conaghan, P., *The EULAR-OMERACT rheumatoid arthritis MRI reference image atlas: the metacarpophalangeal joints.* Annals of the rheumatic diseases, 2005. **64**(suppl_1): p. i11-i21.
207. McQueen, F., *Pitfalls in scoring MR images of rheumatoid arthritis wrist and metacarpophalangeal joints.* Annals of the rheumatic diseases, 2005. **64**(suppl_1): p. i48-i55.
208. Østergaard, M., et al., *An introduction to the EULAR-OMERACT rheumatoid arthritis MRI reference image atlas.* Annals of the rheumatic diseases, 2005. **64 Suppl 1**: p. i3-7.
209. Østergaard, M., *Different Approaches to synovial membrane volume determination by magnetic resonance imaging : Manual versus automated segmentation.* British Journal of Rheumatology, 1997. **36**.
210. Creamer, P., et al., *Quantitative magnetic resonance imaging of the knee: a method of measuring response to intra-articular treatments.* Annals in Rheumatic Diseases, 1997. **56**: p. 378-81.

211. Lee, S.H., et al., *MR evaluation of radiation synovectomy of the knee by means of intra-articular injection of holmium-166-chitosan complex in patients with rheumatoid arthritis: Results at 4-month follow-up.* Korean Journal of Radiology, 2003. **4**(3): p. 170-178.
212. Argyropoulou, M.I., et al., *Magnetic resonance imaging quantification of hand synovitis in patients with rheumatoid arthritis treated with infliximab.* Joint Bone Spine, 2005. **72**(6): p. 557-61.
213. Fotinos-Hoyer, A.K., et al., *Assessment of synovitis in the osteoarthritic knee: Comparison between manual segmentation, semiautomated segmentation, and semiquantitative assessment using contrast-enhanced fat-suppressed T1-weighted MRI.* Magnetic resonance in medicine : official journal of the Society of Magnetic Resonance in Medicine / Society of Magnetic Resonance in Medicine, 2010. **64**(2): p. 604-9.
214. Hunter, D.J., et al., *Evolution of semi-quantitative whole joint assessment of knee OA: MOAKS (MRI Osteoarthritis Knee Score).* Osteoarthritis and cartilage / OARS, Osteoarthritis Research Society, 2011. **19**(8): p. 990-1002.
215. Peterfy, C.G., et al., *Whole-Organ Magnetic Resonance Imaging Score (WORMS) of the knee in osteoarthritis.* Osteoarthritis and cartilage / OARS, Osteoarthritis Research Society, 2004. **12**(3): p. 177-90.
216. Kornaat, P.R., et al., *MRI assessment of knee osteoarthritis: Knee Osteoarthritis Scoring System (KOSS)--inter-observer and intra-observer reproducibility of a compartment-based scoring system.* Skeletal radiology, 2005. **34**(2): p. 95-102.
217. Hill, C.L., et al., *Cruciate ligament integrity in osteoarthritis of the knee.* Arthritis and rheumatism, 2005. **52**(3): p. 794-9.
218. Roemer, F.W., et al., *MRI-detected subchondral bone marrow signal alterations of the knee joint: terminology, imaging appearance, relevance and radiological differential diagnosis.* Osteoarthritis and cartilage / OARS, Osteoarthritis Research Society, 2009. **17**(9): p. 1115-31.
219. Krabben, A., et al., *MRI-detected subclinical joint inflammation is associated with radiographic progression.* Annals of the rheumatic diseases, 2014.
220. Loeuille, D., et al., *Comparing non-enhanced and enhanced sequences in the assessment of effusion and synovitis in knee OA: associations with clinical, macroscopic and microscopic features.* Osteoarthritis and cartilage / OARS, Osteoarthritis Research Society, 2011. **19**(12): p. 1433-9.
221. Habib, S., et al., *MRI-based volumetric assessment of joint effusion in knee osteoarthritis using proton density-weighted fat-suppressed and T1-weighted contrast-enhanced fat-suppressed sequences.* Skeletal radiology, 2011. **40**(12): p. 1581-5.

222. Ejbjerg, B., et al., *The EULAR-OMERACT rheumatoid arthritis MRI reference image atlas: the wrist joint.* Annals of the rheumatic diseases, 2005. **64 Suppl 1**: p. i23-47.
223. Burnett, C., et al., *The use of multi-parametric MRI to identify synovitis in patients with osteoarthritis of the knee without the use of a contrast agent.* Annals in Rheumatic Diseases, 2014. **73**(Suppl 2): p. 1059.
224. Liu, L., et al., *Correlation between synovitis detected on enhanced-magnetic resonance imaging and a histological analysis with a patient-oriented outcome measure for Japanese patients with end-stage knee osteoarthritis receiving joint replacement surgery.* Clinical rheumatology, 2010. **29**(10): p. 1185-90.
225. Harvill, L.M., *Standard Error of Measurement.* Educational Measurement: Issues and Practice 1991: p. 33-41.
226. Sinclair, C.D., et al., *Quantitative magnetization transfer in in vivo healthy human skeletal muscle at 3 T.* Magnetic resonance in medicine : official journal of the Society of Magnetic Resonance in Medicine / Society of Magnetic Resonance in Medicine, 2010. **64**(6): p. 1739-48.
227. Stevenson, V.L., et al., *Variations in T1 and T2 relaxation times of normal appearing white matter and lesions in multiple sclerosis.* Journal of neurological sciences, 2000. **178**: p. 81-87.
228. Gibbs P, et al., *Comparison of quantitative T2 Mmpping and diffusionweighted imaging in the normal and pathologic prostate.* Magnetic Resonance in Medicine, 2001. **46**: p. 1054-1058.
229. Buchbender, C., et al., *Cartilage quality in rheumatoid arthritis: comparison of T2* mapping, native T1 mapping, dGEMRIC, DeltaR1 and value of pre-contrast imaging.* Skeletal radiology, 2012. **41**(6): p. 685-92.
230. Liney, G.P., *Comparison of conventional single echo and multi-echo sequences with a fast spin-echo sequence for quantitative T2 mapping: Application to the prostate* Journal of Magnetic Resonance Imaging, 2005. **6**(4): p. 603-607.
231. Watrin-Pinzano, A., et al., *T2 mapping: an efficient MR quantitative technique to evaluate spontaneous cartilage repair in rat patella.* Osteoarthritis and Cartilage, 2004. **12**: p. 191-200.
232. Li, X., et al., *Spatial distribution and relationship of T1rho and T2 relaxation times in knee cartilage with osteoarthritis.* Magnetic resonance in medicine : official journal of the Society of Magnetic Resonance in Medicine / Society of Magnetic Resonance in Medicine, 2009. **61**(6): p. 1310-8.
233. Tofts, P., *Quantitative MRI of the Brain: Measuring Changes Caused by Disease*. 2003, Chichester, United Kingdom: Wiley.
234. Hollak, C., et al., *Dixon quantitative chemical shift imaging is a sensitive tool for the evaluation of bone marrow responses to individualized doses of enzyme supplementation therapy in type 1 Gaucher disease.* Blood Cells Mol Dis, 2001. **27**(6): p. 1005-12.

235. Kellman, P., et al., *Multi-echo Dixon fat and water separation method for detecting fibro-fatty Infiltration in the myocardium.* Magnetic Resonance in Medicine, 2009. **61**(1): p. 215-221.
236. Fishbein, K.W., et al., *Introduction of fast MR imaging in the assessment of hepatic steatosis.* Magnetic Resonance Imaging 1997. **15**(3): p. 287-293.
237. Shellock, F.G. and E. Kanal, *Magnetic resonance: Bioeffects, safety and patient managemet*. 1996, Pennsylvania, United States of America: Lippincott-Raven.
238. Collins, C.M. and Z. Wang, *Calculation of radiofrequency electromagnetic fields and their effects in MRI of human subjects.* Magnetic resonance in medicine : official journal of the Society of Magnetic Resonance in Medicine / Society of Magnetic Resonance in Medicine, 2011. **65**(5): p. 1470-82.
239. Burnett, C., et al., *Magnetisation transfer contrast of bone marrow oedema in arthritis*, in *International Society of Magnetic Resonance Imaging*. 2010: Stockholm.
240. Burnett, C., et al., *The use of magnetisation transfer contrast in imaging bone marrow oedema in patients with arthritis.* Annals in Rheumatic Diseases, 2010. **69**(Suppl 3): p. 304.
241. Ballester, M.A.G.Z., AP. and Brady, M., *Estimation of the partial volume effect in MRI.* Medical image analysis, 2002. **6**: p. 389-405.
242. Lenk, S., et al., *3.0 T high-resolution MR imaging of carpal ligaments and TFCC.* RoFo : Fortschritte auf dem Gebiete der Rontgenstrahlen und der Nuklearmedizin, 2004. **176**(5): p. 664-7.
243. Schmid, M.R., et al., *Imaging of patellar cartilage with a 2D Multiple-Echo Data Image Combination sequence.* American Journal of Roentology, 2005. **184**: p. 1744-1748.
244. Duc, S.R., et al., *Diagnosis of articular cartilage abnormalities of the knee: Prospective clinical evaluation of a 3D water-excitation true FISP sequence.* Radiology, 2007. **243**(2): p. 475 - 482.
245. Eckstein, F., et al., *Magnetic resonance imaging (MRI) of articular cartilage in knee osteoarthritis (OA): morphological assessment.* Osteoarthritis Cartilage, 2006. **14 Suppl A**: p. A46-75.
246. Schabel, M.C. and G.R. Morrell, *Uncertainty in T(1) mapping using the variable flip angle method with two flip angles.* Physics in medicine and biology, 2009. **54**(1): p. N1-8.
247. Brookes, J.A., et al., *Accuracy of T1 measurement in dynamic contrast-enhanced breast MRI using two-and three-dimensional variable flip angle fast low-angle shot.* Journal of Magnetic Resonance Imaging, 1999. **9**: p. 163-71.
248. Deoni, S.C., B.K. Rutt, and T.M. Peters, *Rapid combined T1 and T2 mapping using gradient recalled acquisition in the steady state.* Magn Reson Med, 2003. **49**(3): p. 515-26.
249. Tofts, P., *Methods for quantitative relaxation parameter mapping: measuring T1 and T2*, in *ISMRM*. 2009: Hawaii, United States of America.

250. Marques, J.P., et al., *MP2RAGE, a self bias-field corrected sequence for improved segmentation and T1-mapping at high field.* NeuroImage, 2010. **49**(2): p. 1271-81.
251. Reddick, E.R.O., RJ. Steen, RG. and Taylor, JS., *Statistical Error Mapping for Reliable Quantitative T 1 Imaging.* Journal of Magnetic Resonance Imaging, 1996(1): p. 244-249.
252. Lind Ramskov, K. and H.S. Thomsen, *Nephrogenic systemic fibrosis and contrast medium-induced nephropathy: a choice between the devil and the deep blue sea for patients with reduced renal function?* Acta radiologica, 2009. **50**(9): p. 965-7.
253. Dekker, J., et al., *Pain and disability in osteoarthritis: a review of biobehavioral mechanisms.* Journal of behavioural medicine, 1992. **15**(2): p. 189-214.
254. Elias, I., et al., *A specific bone marrow edema around the foot and ankle following trauma and immobilization therapy: pattern description and potential clinical relevance.* Foot & ankle international / American Orthopaedic Foot and Ankle Society [and] Swiss Foot and Ankle Society, 2007. **28**(4): p. 463-71.
255. Lohmander, L.S., *Articular cartilage and osteoarthritis. the role of molecular markers to monitor breakdown, repair and disease.* Journal of anatomy, 1994. **184**: p. 477-492.
256. Laurent, D., et al., *In vivo MRI of cartilage pathogenesis in surgical models of osteoarthritis.* Skeletal Radiol, 2006. **35**(8): p. 555-64.
257. Nolte-Ernsting, C., et al., *MRI of degenerative bone marrow lesions in experimental osteoarthritis of canine knee joints.* Skeletal Radiology :, 1996. **25**: p. 413-420.
258. Hodgson, R., et al., *Dynamic contrast enhanced MRI of bone marrow oedema in rheumatoid arthritis.* Ann Rheum Dis, 2008. **67**(2): p. 270-2.
259. Li, X., et al., *Quantitative assessment of bone marrow edema-like lesion and overlying cartilage in knees with osteoarthritis and anterior cruciate ligament tear using MR imaging and spectroscopic imaging at 3 Tesla.* Journal of Magnetic Resonance Imaging, 2008. **28**(2): p. 453-461.
260. Ruhdorfer, A., et al., *Association of Thigh Muscle Strength With Knee Symptoms and Radiographic Disease Stage of Osteoarthritis: Data From the Osteoarthritis Initiative.* Arthritis care & research, 2014. **66**(9): p. 1344-1353.
261. Fink, B., et al., *Morphologic changes in the vastus medialis muscle in patients with osteoarthritis of the knee.* Arthritis and rheumatism, 2007. **56**(11): p. 3626-33.
262. Varghese, J., et al., *Integrated treadmill stress testing and MR relaxometry (T1, T2, T2*): response in healthy calf muscles.* Journal of Cardiovascular Magnetic Resonance, 2014. **16**(Suppl 1): p. P68.
263. Huang, Y., et al., *Quantitative MR relaxometry study of muscle composition and function in Duchenne Muscular Dystrophy.* Journal of Magnetic Resonance Imaging, 1994. **4**(1): p. 59-64.

264. Eckstein, F., D. Burstein, and T.M. Link, *Quantitative MRI of cartilage and bone: degenerative changes in osteoarthritis.* NMR in biomedicine, 2006. **19**(7): p. 822-54.
265. Freemont, A.J., *The pathophysiology of cartilage and synovium.* British Journal of Rheumatology, 1996. **35 Suppl 3**: p. 10-3.
266. Choi, J. and G. Gold, *MR Imaging of Articular Cartilage Physiology.* Magnetic Resonance Clinics of North America, 2011. **19**(2): p. 249-282.
267. Kim, D.K., et al., *Analysis of Water-Macromolecule Proton Magnetization Transfer in Articular Cartilage.* Magnetic Resonance in Medicine 1993. **29**: p. 211-215
268. Lin, P.C., D.A. Reiter, and R.G. Spencer, *Classification of degraded cartilage through multiparametric MRI analysis.* Journal of magnetic resonance, 2009. **201**(1): p. 61-71.
269. Zuo, H., et al., *Quantitative evaluation in combination with nonquantitative evaluation in early patellar cartilage osteoarthritis at 3.0 T.* Clin Interv Aging, 2014. **9**: p. 1133-43.
270. Guermazi, A., et al., *MRI-based semiquantitative scoring of joint pathology in osteoarthritis.* Nature reviews. Rheumatology, 2013. **9**(4): p. 236-51.
271. Parikh, R., et al., *Understanding and using sensitivity, specificity and predictive values.* Indian Journal of Opthalmology, 2008. **56**(1): p. 45 - 50.
272. Crema, M.D., et al., *Peripatellar synovitis: comparison between non-contrast-enhanced and contrast-enhanced MRI and association with pain. The MOST study.* Osteoarthritis and cartilage / OARS, Osteoarthritis Research Society, 2013. **21**(3): p. 413-8.
273. Lansberg, M.G., et al., *Advantages of adding Diffusion-weighted magnetic resonance imaging to converntional magnetic resonance imaging for evaluating acute stroke.* Archives of Neurology, 2000. **57**: p. 1311-1316.
274. Qi, L.P., et al., *Using diffusion-weighted MR imaging for tumor detection in the collapsed lung: a preliminary study.* European radiology, 2009. **19**(2): p. 333-41.
275. Long-Hua, Q., et al., *Diffusion-weighted MRI evaluation of breast cancer extension.* Clinical Imaging, 2010. **34**(2): p. 89-96.
276. Baur, A. and M.F. Reiser, *Diffusion-weighted imaging of the musculoskeletal system in humans.* Skeletal Radiology :, 2000. **29**: p. 555–562.
277. Khoo, M.M., et al., *Diffusion-weighted imaging (DWI) in musculoskeletal MRI: a critical review.* Skeletal radiology, 2011. **40**(6): p. 665-81.
278. Friedrich, K.M., et al., *Diffusion-weighted imaging for the follow-up of patients after matrix-associated autologous chondrocyte transplantation.* European journal of radiology, 2010. **73**(3): p. 622-8.
279. Mills, R., *Self-diffusion in normal and heavy water in the range of 1-45 degrees.* The journal of physical chemistry, 1973. **77**: p. 685-688.

280. Taouli, B., *Diffusion-weighted MR imaging of the liver.* Radiology, 2010. **254**(1): p. 47-66.
281. Qi, J., et al., *Diffusion-weighted imaging of inflammatory myopathies: polymyositis and dermatomyositis.* Journal of magnetic resonance imaging : JMRI, 2008. **27**(1): p. 212-7.
282. Sigmund, E.E., et al., *Stimulated echo diffusion tensor imaging and SPAIR T2 -weighted imaging in chronic exertional compartment syndrome of the lower leg muscles.* Journal of magnetic resonance imaging : JMRI, 2013. **38**(5): p. 1073-82.
283. Neubauer, H., et al., *Diffusion-weighted MRI of bone marrow oedema,soft tissue oedema and synovitis in paediatric patients: feasibility and initial experience.* Paediatric Rheumatology, 2012. **10:20**.
284. Biglands, J.D., A. Radjenovic, and J.P. Ridgway, *Cardiovascular magnetic resonance physics for clinicians: part II.* Journal of cardiovascular magnetic resonance 2012. **14**(66).
285. Tortora, G.J. and N.P. Anagnostakos, *Principles of anatomy and physiology*. 1990, New York: Harper and Row.
286. Wattjes, M.P., R.A. Kley, and D. Fischer, *Neuromuscular imaging in inherited muscle diseases.* European radiology, 2010. **20**(10): p. 2447-60.
287. Meara, S.J. and G.J. Barker, *Impact of incidental magnetization transfer effects on inversion-recovery sequences that use a fast spin-echo readout.* Magnetic resonance in medicine : official journal of the Society of Magnetic Resonance in Medicine / Society of Magnetic Resonance in Medicine, 2007. **58**(4): p. 825-9.
288. Pessler, F., et al., *The synovitis of "non-inflammatory" orthopaedic arthropathies: a quantitative histological and immunohistochemical analysis.* Annals of the rheumatic diseases, 2008. **67**(8): p. 1184-7.
289. de Hair, M.J.H., et al., *Features of the Synovium of Individuals at Risk of Developing Rheumatoid Arthritis: Implications for Understanding Preclinical Rheumatoid Arthritis.* Arthritis & Rheumatology, 2014. **66**(3): p. 513-522.
290. O'Connell, J., *Pathology of the Synovium.* American Journal of Clinical Pathology 2000. **114**: p. 773-784.
291. Simkin, P.A., *Physiology of Normal and Abnormal Synovium.* Semmars in Arthritis and Rheumatism, 1991. **21**(3): p. 179-183.
292. Helms, G., H. Dathe, and P. Dechent, *Modeling the influence of TR and excitation flip angle on the magnetization transfer ratio (MTR) in human brain obtained from 3D spoiled gradient echo MRI.* Magnetic resonance in medicine : official journal of the Society of Magnetic Resonance in Medicine / Society of Magnetic Resonance in Medicine, 2010. **64**(1): p. 177-85.
293. Gaffney, K., et al., *Quantification of rheumatoid synovitis by magnetic resonance imaging.* Arthritis and rheumatism, 1995. **38**(11): p. 1610-7.

294. Karim, Z., et al., *Validation and reproducibility of ultrasonography in the detection of synovitis in the knee: a comparison with arthroscopy and clinical examination.* Arthritis Rheum, 2004. **50**(2): p. 387-94.
295. Jackson, A., D. Buckley, and G.J.M. Parker, *Dynamic contrast enhanced magnetic resonance imaging in oncology.* . 2003, Berlin: Springer.
296. Rutjes, A., et al., *Evaluation of diagnostic tests when there is no gold standard. A review of methods.* Health Technology Assessment, 2007. **11**(50).
297. Peng, Y., et al., *Validation of Quantitative analysis of Multiparametric Prostate Mr images for Prostate cancer Detection and aggressiveness assessment: A Cross-Imager Study.* Radiology 2014. **271**(2): p. 461-471.
298. Yu, J., et al., *Prostate cancer and its mimics at multiparametric prostate MRI.* The British journal of radiology, 2014. **87**(1037): p. 20130659.
299. Farrant, J.M., P.J. O'Connor, and A.J. Grainger, *Advanced imaging in rheumatoid arthritis. Part 2: erosions.* Skeletal radiology, 2007. **36**(4): p. 269-79.
300. McGonagle, D., *Imaging the joint and enthesis: insights into pathogenesis of psoriatic arthritis.* Annals of the rheumatic diseases, 2005. **64 Suppl 2**: p. ii58-60.
301. Ory, P.A., D.D. Gladman, and P.J. Mease, *Psoriatic arthritis and imaging.* Annals of the rheumatic diseases, 2005. **64 Suppl 2**: p. ii55-7.
302. Rudwaleit, M., et al., *MRI in predicting a major clinical response to anti-tumour necrosis factor treatment in ankylosing spondylitis.* Ann Rheum Dis, 2008. **67**(9): p. 1276-81.